Size and Shape control mechanism of Nucleus

By

Abira Ganguly
[LIFE 09201004025]

Tata Memorial Centre
Mumbai

A thesis submitted to the
Board of Studies in Life Sciences
In partial fulfillment of requirements
For the Degree of

DOCTOR OF PHILOSOPHY

Of

HOMI BHABHA NATIONAL INSTITUTE

October, 2016

HOMI BHABHA NATIONAL INSTITUTE

Recommendations of the Viva Voce Board

As members of the Viva Voce Board, we certify that we have read the dissertation prepared by Ms. Abira Ganguly entitled 'Size and Shape Control Mechanism of Nucleus' and recommend that it may be accepted as fulfilling the dissertation requirements for the Degree of Doctor of Philosophy.

S.N. Dalal 24/10/16
---------- Date: ----------

Chairperson: -- Dr. Sorab N. Dalal

Dibyendu Bhattacharyya 24/10/16
---------- Date: ----------

Convenor -- Dr. Dibyendu Bhattacharyya

M. M. Vaidya
---------- Date: ----------

Member 1: -- Dr. Milind M. Vaidya

Sanjay Gupta 24/10/16
---------- Date: ----------

Member 2: -- Dr. Sanjay Gupta

Suman Kumar Dhar 24/10/2016
---------- Date: ----------

External Examiner: -- Dr. Suman K. Dhar

Final approval and acceptance of this dissertation is contingent upon the candidate's submission of the final copies of the dissertation to HBNI.

I hereby certify that I have read this dissertation prepared under my direction and recommend that it may be accepted as fulfilling the dissertation requirement.

Date: 24.10.16

Place: Navi Mumbai

Dibyendu Bhattacharyya 24/10/16
Dr. Dibyendu Bhattacharyya

(Guide)

STATEMENT BY AUTHOR

This dissertation has been submitted in partial fulfillment of requirements for an advanced degree at Homi Bhabha National Institute (HBNI) and is deposited in the Library to be made available to borrowers under rules of the HBNI.

Brief quotations from this dissertation are allowable without special permission, provided that accurate acknowledgement of source is made. Requests for permission for extended quotation from or reproduction of this manuscript in whole or in part may be granted by the Competent Authority of HBNI when in his or her judgment the proposed use of the material is in the interests of scholarship. In all other instances, however, permission must be obtained from the author.

Place: Navi Mumbai

Date:
24th October 2016

Abira Ganguly
Abira Ganguly

DECLARATION

I, hereby declare that the investigation presented in the thesis has been carried out by me. This work is original and has not been submitted earlier as a whole or in part for a degree / diploma at this or any other Institution / University.

Place: Navi Mumbai

Date:
24th October 2016

Abira Ganguly
Abira Ganguly

List of Publications arising from thesis

1. Febs Letters, Ganguly A, Bhattacherjee C, Bhave M, Kailaje V, Sengupta I, Jain B, Rangarajan A and Bhattacharyya D. Perturbation of nucleolcytoplasmic transport affect the size of nucleus and nucleolus. Febs Letters, Mar;590(5):631-43; PMID:26813731

2. To be submitted:

Ganguly A. Bhattacharyya D. Nuclear kinesins Kar3, Cin8 and splicing protein prp45 ts mutants control nuclear shape and size in budding yeast *Sacharomycescerevisiae (Manuscript under preparation)*

Chapters in books and Lecture notes: Not Applicable

Conferences:

1. "7th Bangalore Microscopy course", at NCBS, Bangalore, India in September 2015 [Poster presentation: Attenuation of Nuclear import Affects Nucleus and Nucleolus Size in Human cells]

2. "18th International Microscopy Congress'', at Prague, Czech Republic in September 2014 [Poster presentation: Nucleus Size and Shape Mystery]

3. "The All India Cell Biology Conference on Cell Dynamics and Cell Fate", at inSTEM-Bangalore, India in December, **2013 [Stage Presentation: Study to investigate nuclear size control mechanism]**

4. "Society for Biological Chemists'' at CIMAP-Lucknow, India in November 2011 [**Poster** presentation: To develop an assay system to study the Size and Shape control mechanism of Nucleus]

Other Publications

1. Bhattacharjya S#, Roy KS#, **Ganguly A,** Sarkar S, Panda CK, Bhattacharyya D, Bhattacharyya NP, RoychoudhuryS. Inhibition of nucleoporin member Nup214 expression by miR-133b perturbs mitotic timing and leads to cell death. Mol Cancer. 2015 Feb 15;14(1):42. PMID: 25743594

2. Nath S#, Chowdhury A#, Dey S, Roychoudhury A, **Ganguly A,** Bhattacharyya D, Roychoudhury S. Deregulation of Rb-E2F1 axis causes chromosomal instability by engaging the transactivation function of Cdc20-anaphase-promoting complex/cyclosome. Mol Cell Biol. 2015 Jan;35(2):356-69. PMID: 25368385

3. Bhave M#, Papanikou E#, Iyer P, Pandya K, Jain BK, **Ganguly A**, Sharma C, Pawar K, Austin J 2nd, Day KJ, Rossanese OW, Glick BS, Bhattacharyya D. Golgi enlargement in Arf-depleted yeast cells is due to altered dynamics of cisternal maturation. J Cell Sci. 2014 Jan 1;127(Pt 1):250-7. PMID: 24190882

……

Signature: Abira Ganguly …… Signature: ……

Student: Ms. Abira Ganguly Guide: Dr. Dibyendu Bhattacharyya

List of Conference presentations

Participation in Conferences:

“7th Bangalore Microscopy course”, at NCBS, Bangalore, India in September 2015 [**Poster** presentation]

“18th International Microscopy Congress’’, at Prague, Czech Republic in September 2014 [**Poster presentation**]

"The All India Cell Biology Conference on Cell Dynamics and Cell Fate", at inSTEM-Bangalore, India in December, 2013 [**Stage Presentation**]

“Society for Biological Chemists’’ at CIMAP-Lucknow, India in November 2011 [**Poster** presentation]

“7th Graduate students’ Meet’’, at ACTREC-Mumbai, India in December 2011 [**Poster** presentation]

Participation in Workshops:

Extensive microscopy workshop from basics to recent advances of microscopy in “7th Bangalore Microscopy course”, at NCBS, Bangalore, India in September 2015

“Writing Research Article” by Prof. Tony Wilson, *University of Oxford, UKand editor of* Journal of Microscopy at IMC-Prague, Czech Republic in September 2014

SERB School on "Introduction to Systems and Synthetic Biology for Scientists and Engineers" at IIT, Mumbai, India in April 2013

Dedicated

To

Maa *(Mrs. Gauri Ganguly) &*

Baba *(Mr. Amit Kumar Ganguly)*

Acknowledgements

PhD is a great long journey. I wish to take this opportunity to thank everyone who had been instrumental in making this long journey a rewarding and truly an indelible one. First and foremost, I would like to express my sincere gratitude to my mentor Dr. Dibyendu Bhattacharyya, for taking me to the world of organelle biology, his constant support throughout my PhD tenure, his continuous guidance, critical analysis, and encouragement to make this thesis a better one. All his food treats was a bonus during the PhD.

I am thankful to Dr. S. V. Chiplunkar (Director, ACTREC), Dr. Rajiv Sarin (Ex-Director, ACTREC) and Dr. Surekha Zingde (Ex-Deputy Director, ACTREC) for providing the excellent infrastructure. I am honor-bound to ACTREC-DAE, India for my PhD fellowship. I am thankful to TMC for funding my project. My sincere thanks to the funding agencies, Sam-mystery and HBNI for supporting the international travel to present my work at an international conference.

I am grateful to all my Doctoral Committee Chairpersons, Dr. G. B. Maru (Ex.Chairperson), Dr. Sorab N Dalal (Chairperson), and members Dr. Sanjay Gupta, Dr. Milind M Vaidya, for their important suggestions, encouragement, and cooperation towards the progress of my work. A special thanks to Dr. Sanjeev Galande who gave very good suggestions in the beginning of my PhD.

Thanks are also extended to all the members of our Bhattacharyya Lab cohort. I am thankful to Sanjay and Mansi for their excellent technical help. I thank all my colleagues, Madhura, Prasanna, Bhawik, Kaushal, Chumki Di, Ketakee, Pravin, Naini, Sudeshna. I thank one of my trainee Durmi for her huge help. I sincerely thank to all my trainees, especially Edlyn, Asha and Durmi for their help when it was mostly needed.

I would like to thank Dandekar sir, Aruna, Seema, Maya, Vaishali, Tanuja, Shyamal, for untiring support, whenever needed.

Thanks to the special group of people whom I consider as members of my extended family, Pooja, Rupa, Sushmita, Bhanu, Tanmay, Kedar, Madhura, Snehal, and Srikanta for the fun times we shared will be cherished always. I also thank my entire batch 2010. I extend my thanks to all the members of our doctoral cohort, the ACTREC student community for their support in either organizing any scientific event or towards any other sort of scientific help. I especially thank many of my seniors from whom I learned a lot.

Gratitude is extended to few more important persons Dr. Hunain Alam, Dr. Ajit Chande, Dr. Dimpu Gogoi, Dr. Ratika Kunder, Dr. Cheryl Travasso, Dr. Gaurav Arora, and Dr. Amitabha Mukhopadhyay for their unconditional support in many scientific problems during my PhD tenure in ACTREC.

Finally, special recognition goes out to my parents, my sisters *Oindrila* (Didi) and *Sreela,* and my whole big family for their encouragement, support, and patience during my pursuit of the doctorate in educational leadership. I thank all of you for your patience and love you more than you will ever know. I would like to end this by thanking Almighty God for everything. Thank you.

Abira Ganguly

Table of Contents

Synopsis

Homi Bhabha National Institute

Ph. D. PROGRAMME

Synopsis Report:

1. Name of the Student: Abira Ganguly

2. Name of the Constituent Institution: TMC-ACTREC

3. Enrolment No.: LIFE 09201004025

4. Title of the Thesis: Size and Shape control mechanism of Nucleus

5. Board of Studies: Life Sciences

1. Introduction:

One of the fundamental properties of eukaryotic cell is their ability to maintain organelle size, number, dynamics that are appropriate for different growth and differentiation states (1). Organelles are specialized organization to perform different regulatory or biochemical processes with distinct morphologies (1, 2). For example, single spherical nucleus, reticulated networks of endoplasmic reticulam, mitochondria, Golgi etc. Cell possesses an active mechanism to build and maintain such structures. Moreover, altered organelle size and shape leads to improper cell function. It is likely that metabolism and/ or signaling get affected by organelle size. One approach of reprogramming organelle size can result into reprogramming cellular state or behavior. Here comes the concept of organelle directed medicine to cure diseased cells (1, 3). Nucleus, is the largest cellular organelle, yet surprisingly very little is known about its size and shape controlling factors. From the very onset of cell birth Nucleus size increases slowly until it reaches to its final volume. This expansion is surprisingly well regulated as we observe a constant nuclear to cell volume ratio or

karyoplasmic ratio throughout cell cycle. Not only has that, N/C ratio remained constant in cells with widely different DNA contents (4). However, N/C ratio alteration is very prominent in cancer cells (5). In fact, the pathologists look for aberrant nuclear morphology, altered N/C ratio and nucleolar morphology to detect cancer cells (6, 7, 8). Despite being 100 years of known fact, it remains poorly understood how size and shape of Nucleus is regulated in normal cells.

2. Objectives:

I. To study the control mechanism of nucleus size and shape in mammalian system

II. To study the control mechanism of nucleus size and shape in yeast system

3. Work Plan:

I. To study the control mechanism of nucleus size and shape in mammalian system:-

A. **To develop different tools to monitor size and shape of nucleus in live cell condition.**

B. **Comparative analysis of nucleus and nucleolus size and shapes in immortalized and corresponding transformed cells.**

C. **To study the effect of nuclear transport blockage in size and shape of nucleus and nucleolus.**

II. To study the control mechanism of nucleus size and shape in yeast system:-

A. **To develop an assay system to monitor size and shape of nucleus in live cell condition.**

B. **Directed mutagenesis to find out genes responsible for nuclear size and shape.**

<u>I. To study the control mechanism of nucleus size and shape in mammalian system:-</u>

A. To develop different tools to monitor size and shape of nucleus in mammalian cells

To study the nucleus size and shape in live cell condition under high end microscopes, the first necessity was to develop proper nuclear and cell membrane marker tagged with different fluorescent proteins. For this purpose Lamin as nuclear membrane marker and Farnesylation signal as cell membrane marker were selected. Different Fluorescent proteins were tagged with either of them to make the final construct. To study Nucleolus, Fibrillarin was selected. Different constructs used in this study are listed below.

Nucleus Membrane Marker	Nucleus Core Marker	Cell Membrane Marker
pmGFPC1-LaminA	pmGFPC1-H4	pEGFP-F
Lamin-RFP	pmGFPN1-H4	pmCherryc1-F
Lamin-CFP	--	pLvx-GFPC1-F

To measure nuclear to cell volume ratio, pmGFPC1-Lamin and pmCherryC1-F were used. To measure nucleolus to nucleus ratio, Fibrillarin-GFP and Lamin-RFP were used.

B. Comparative analysis of nucleus and nucleolus size and shapes in immortalized and corresponding transformed cells.

Nucleus size and shape as well as cell size are very heterogeneous in culture for different tissue. We determined the range of variation of N/C ratio in different immortalized and transformed cell lines of same tissue origin. We have selected four pairs of immortalized and transformed cell lines of similar tissue origins, namely skin, colon-intestine, breast and liver for comparative measurements of N/C ratio.

Immortalized	Transformed	Origin
HaCaT	A431	Skin
Int407	HCT116	Intestine/Colon
MCF10 A	MCF7	Breast
HHL 5	HepG2	Liver

We have transfected each of the cell lines with constructs expressing GFP-Lamin and F-mCherry for subsequent measurements of nuclear volume and cell volume respectively. Using 3D reconstruction of confocal images, we have calculated the

nuclear-to-cell volume (N/C) ratio for each cell line. Our analysis showed that N/C ratio is significantly higher ($p<0.001$) in transformed cell lines (A431, HCT116, MCF7 and HepG2) compared to their respective immortalized counterparts (HaCaT, INT 407, MCF10A and HHL5). N/C ratio is approximately 80% higher in transformed cell lines from colon-intestine, approximately 45% higher in breast cell lines, 40% higher in skin cell lines and 30% higher in liver cell lines. The N/C ratio varies widely in all the transformed cell lines compared to their immortalized counterparts in which it maintains primarily a constant value of (0.10±0.04) which is similar in range to the highly constant value of N/C ratio of budding yeast (0.09±0.01). It is evident from these observations that increase in N/C ratio is variable in different transformed cell lines. All measurements were done in an unsynchronized condition. We have repeated the measurements in G1/S enriched conditions and found similar results.

The nucleolus number and volume alters in transformed cells

The nucleus is host of several other sub nuclear compartments. An intriguing question to solve was whether the size and number of such compartments also changes as the nuclear size changes in transformed cell lines. We quantified the nucleolus number and volume with respect to nucleus volume in all four pair of immortalized and transformed cell lines used in this study. Quantitative measurements for nucleolar spots and nuclear volumes were done by the 3D reconstruction of confocal images.

Depending on tissue origin, we found that size and number of nucleolus spots altered differently from immortalized cell line to corresponding transformed cell lines. To address this complexity in quantitative manner, we have measured two parameters, ‘average volume’ and ‘total volume’ of nucleolus. For the first parameter the average volume of all nucleolus spot’s per nucleus was calculated and for the second parameter, the volume of all nucleolus spots per nucleus was summed. In most of the cases, the first parameter alters in incremental fashion; if it does not alter then always the second parameter increases. To be precise, the average nucleolar spot volume mostly increases in transformed cells; when average nucleolus spot volume remained unchanged then the total nucleolar volume increases. In the former case, nucleolar spot number decreases while the same increases for the latter case. For example in case of skin, colon-intestine and liver cell lines (A431, HCT116, and HepG2 respectively) average volume of nucleolus spots were found to be significantly higher

($p<0.001$) and numbers of nucleolus spots were significantly reduced compared to their immortalized counterparts (HaCaT, INT407, HHL5 respectively. On the other hand, in breast cell lines, both number and total volume of nucleolus spots were increased significantly in transformed cell lines (MCF7) compared to immortalized cell line (MCF10A) although average volume of nucleolus spots remained unchanged. We have also observed, in transformed cells lines, average volume of nucleolus spots per nucleus varies greatly compared to their immortalized counterparts. Although the N/C ratio was invariably found to be increased in all the transformed cell lines, but to address consistent nucleolus size alteration in transformed cells, we calculated another parameter, the total nucleolus volume to nucleus volume (Nu/N) ratio by dividing total volume of nucleolus spots per nucleus and volume of the nucleus. We found Nu/N ratio to be significantly increased in all the transformed cell lines except that of colon-intestine origin in which the increase was not statistically significant. Increase in Nu/N ratio (in most of the transformed cell lines) certainly indicate that the nucleolus size also scale with respect to nucleus in transformed cells.

C. To study the effect of nuclear transport blockage in nuclear size and shape

We have validated the phenomenon of the N/C ratio increase in transformed cells, we wanted to further investigate whether the N/C ratio could be altered by perturbation of any physiological or cellular process in immortalized cell lines. For this reason, we decided to attenuate the nuclear transport in immortalized cells and study the effect of this on the N/C ratio. We used an over expression of dominant negative forms of Importin beta and Ran to create such attenuation of nuclear transport (9, 10, 11, 12)[1-3]. Nucleo-cytoplasmic transport attenuation was first confirmed by co-transfecting NLS-YFP along with dominant negative form of importin beta or Ran^{Q69L} in which NLS-YFP is restricted in the cytoplasm compared to vector control cells.

Effect of overexpression of Importin beta 1-364

The dominant negative form of Importin beta blocks multiple pathways of nucleo-cytoplasmic transport. We over expressed Importin beta 1-364 fragment along with GFP-Lamin and F-mCherry in HaCaT and Int 407 (immortalized) cells. 3D reconstruction of confocal images results quantitative measurement of N/C ratio as described earlier. N/C ratio was increased significantly ($p<0.0001$) (almost 50%),

when we over expressed Importin beta 1-364, in the immortalized cell line HaCaT and Int 407.

Effect of Overexpression of Ran ^{T24N} and Ran ^{Q69L} on immortalized cell

An over expression of any of the two mutant forms, Ran^{T24N} or Ran^{Q69L}, can effectively perturb the nucleo-cytoplasmic transport pathway. Once again we over expressed dominant negative pCMV 3X Flag- Ran^{T24N} or pCMV 3X Flag- Ran^{Q69L} in HaCaT and Int 407 cells along with GFP-Lamin and F-mCherry as described earlier. Dominant negative Ran^{T24N} or Ran^{Q69L} over expression also increased N/C ratio significantly ($p<0.0001$, $p<0.0027$ respectively) (almost 30% and 20% respectively) in immortalized cells compared to vector control transfected cells.

We conclude that perturbation of nuclear transport pathway by overexpressing dominant negative Importin beta and Ran leads to increase in N/C ratio in immortalized cells. Such perturbation of nucleo-cytoplasmic transport does not affect the transformed cells though.

Next obvious question was to check if there is any property associated with malignancy such as invasiveness is changed when N/C ratio is increased in immortalized cell lines. To test this we performed invasion assay in immortalized cell line (HaCaT) after overexpressing either Importin beta 1-364 or Ran^{T24N} or Ran^{Q69L}. We found that there was no significant change in invasiveness compared to control cells. As a control experiment, invasiveness was also checked between A431 (transformed) and HaCaT (immortalized) and found to be significantly more in case of A431. What is also fascinating is when wild type Importin beta or Ran is overexpressed in skin transformed cell line (A431); the N/C ratio remains unchanged.

The nucleolus number and volume alters upon blockade of nucleo-cytoplasmic transport

It is evident from the data shown in section B, that the size of nucleus and the nucleolus are correlated. This prompted us to explore whether the nucleolus size is also controlled by nuclear transport perturbation. To test that, we transfected the same dominant negative constructs (used earlier) along with GFP-Fibrillarin and RFP-Lamin. Over expression of Importin beta 1-364 in immortalized cell line Int 407 causes an increase of the average & total nucleolus spot volumes significantly ($p<0.001$); while number of nucleolar spots were decreased in this condition($p<0.05$). The Nu/N ratio is significantly higher in Importin beta 1-364 over expressed cells

compare to vector control transfected cells. We conclude that the overexpression of Flag-importin beta 1-364 not only increases the N/C ratio, it also increases the size of nucleolus and Nu/N ratio as compared to vector control cell. We over expressed Flag-Ran^{T24N}or Flag-Ran^{Q69L} in the same way as described above. When we over expressed Flag-Ran^{T24N}, no significant difference was observed in nucleolus size or in Nu/N ratio but number of nucleolus spots increased significantly. Interestingly upon over expression of Flag-Ran^{Q69L} the average volume of nucleolar spots did not increase significantly, the total nucleolus volume and Nu/N ratio increased significantly. We found similar results of nucleolus volume and number in over expression studies of dominant negative Importin beta and Ran performed in another immortalized cell line HaCaT.

Cytosolic component determines the size of nucleolus

It is now evident that Importin beta 1-364 over expression leads to increase in nucleus size as well as nucleolus size. To study this in detail, we have developed an '*in vitro'* assay system in which intact nucleus isolated was incubated with cytosolic fraction isolated from a cell with different expression background. We incubated the isolated pure nuclei with different cytosolic fractions in 1:2 ratios at 22°C for 30 minutes. Confocal imaging was done in different conditions; and volume of nucleolus and numbers were calculated from 3d reconstruction images. When Cytosolic fraction of vector control transfected cells was incubated with pure nucleus population of Importin beta 1-364 transfected cells, nucleoli volume was scaled back to its normal size and vice versa whereas the number of nucleoli of Importin beta 1-364 transfected cells were increased although not significantly. When the cytosolic fraction of two different sources (vector control transfected cells and that for importin beta 1-364 transfected cells) were combined in a 50-50 ratio approximately 50% scaling of nucleolus size was observed.

These results suggest the following conclusions:

1. Cytosol of vector control transfected cell can scale down the increased size of nucleolus in a nucleus isolated from cells in which nucleo-cytoplasmic import is blocked.

2. Cytosol of cells in which nucleo-cytoplasmic import is blocked can scale up the smaller size of nucleolus in a nucleus isolated from a vector control transfected cell.

The results also indicate the importance of nuclear transport for size regulation of nucleus and nucleolus and underlay the possible role of unknown cytosolic factors in such regulation.

II. To study the control mechanism of nucleus size and shape in yeast system

A. To develop different tools to monitor size and shape of nucleus in yeast

To monitor the size and shape of the yeast nucleus in live cell condition under the microscope, we have developed an assay system, in which nuclear pore complex protein Nup116 and cell membrane proteins Ras2 were selected. By PCR mediated epitope tagging NUP116 GFP is incorporated at the endogenous gene locus in JK9 strain. Cell membrane marker mherry Ras2 is linearized and integrated in the leu locus of the same JK9 strain.

B. Directed mutagenesis to find out genes responsible for nuclear size and shape

In a database known as "*Mitocheck*" enlists all the genes for defective cellular phenotypes responsible for mitosys by screening 22,000 human genes during mitosis using siRNA & high-throughput live cell imaging (13). In the *mitocheck primary screen*, there are more than 200 genes showed phenotypes for strange nuclear shape, in which some of the genes are reported to have yeast homologue. In this part of our study, we intended to see if the genes listed for mammalian nucleus are equally responsible for yeast nucleus size and shape. Nucleus size and shape regulation is one of the very primary processes inside cell and any organelle size and shape regulation is strongly selected during evolution. So, it is expected that the control mechanism for nucleus size and shape must be conserved from single cell eukaryote or Yeast to Mammalian system. Genes responsible for strange nuclear shape from the *mitocheck* database were listed. Next, yeast orthologues of all those genes were searched through *Ensemble Genome browser* and listed. Finally yeast genes were searched in *Saccharomyces Genome Database* (SGD) and listed in two categories essential genes and non essential genes. Null mutation of any gene if viable makes that particular gene as nonessential and vice e versa. Next all the nonessential genes' genomic loci were collected from *SGD* in FASTA format and simulated in *Snapgene database*. For

making null mutants, a very well-known strategy is available in which the gene of interest is removed by homologous recombination through a PCR selection cassette. Using two different vectors, namely pUG6 (G418) and pUG72 (URA3) different genes' deletion cassettes were PCR amplified and transformed individually in the assay system strain. Null mutants were first confirmed by PCR using two primers in which one primer is 500bp upstream of the gene of interest and another primer is in the PCR deletion cassette. Next, null mutants were imaged in confocal microscope. Nuclear surface area and volumes were quantified using *imaris-bitplane* software. In this way, null mutant were created, two mutants showed altered nuclear morphology. Although in mammalian system all these genes showed altered nuclear shape but in yeast system very few showed the same. One plausible explanation could be in the mammalian system, transformed cell line HeLa was used, which cannot be considered as a normal mammalian system to study nucleus size and shape as already many genes, pathways in the same are distorted. Secondly, the genes which are showing strange nuclear shape in yeast system considered being important factors, as control mechanism of nucleus size and shape is a conserved phenomenon.

Null mutants of Kar3 and Cin8, which are minus end and plus end motor proteins respectively, showed abnormal nuclear shape:-

Kar3 and Cin8 both the mutants showed altered nuclear morphology. Three dimensional reconstruction of confocal images revealed that nuclear shape as well as nuclear volume are increased in both the strains. However, nuclear to cell volume ratio did not change. Kar3p and Cin8p code for evolutionarily conserved motor proteins, kar3 is a minus end motor protein while cin8 is a plus end motor protein. To confirm that null mutant of kar3 and cin8 caused the altered nuclear phenotype; wildtype kar3 and cin8 are cloned in yCplac33 vector and transformed in the mutant strains. Single copy of kar3 and cin8 rescued the altered nuclear phenotype. Electron micrographs also showed the same. To further check the chromatin distribution in these mutants, histone H2B tagged with mCherry was expressed in wild type and cin8 and kar3 null mutants. Histone distribution was found to be unchanged in wild type as well as null mutants. This indicates that chromatin did not detach from the nuclear envelope. These null mutants were able to grow and divide but their growth is slower compare to wild type cells.

Temperature sensitive mutant of prp45 1-169, a pre m RNA splicing protein showed abnormal nuclear shape:

PRP45 is reported to play important role in pre-mRNA splicing. Since PRP45 is an essential gene, we used temperature sensitive mutant prp45 1-168 ts mutant to check nucleus size and shape alteration. Three dimensional reconstruction of confocal images revealed that nuclear shape as well as nuclear volume are increased in both the strains. Surprisingly, nuclear to cell volume ratio also altered in prp45 1-169 mutant. We expect this change in nucleus size and shape is due to global splicing defect.

Nuclear shape mutants showed abnormal nuclear morphology throughout cell cycle:

Budding yeast have a closed mitosis and during cell division yeast nucleus goes through altered nuclear shape. We asked alteration in nuclear shape in kar3, cin8 are they dependent or independent of cell division cycle. We captured images in different stage of cell cycle based on the bud structure and nucleus structure. 3d reconstruction of confocal images showed that nucleus shape and size are altered throughout the cell cycle in kar3 and cin8 mutants. Electron microscopy is also done to show that nuclear shape is altered in all stages of cell cycle.

4. Summary & Conclusion:

In this study, we studied two model organisms for understanding nucleus size and shape control mechanism. We have demonstrated alteration in N/C ratio and size of nucleolus in different transformed cell lines compared to the immortalized cell lines of same tissue origin. For the first time we showed perturbation of nucleo cytoplasmic transport can alter both N/C ratio and nucleolus size and number in immortalized cells, although this increased N/C ratio could not change the invasion potential further of the same immortalized cells. Using an in vitro assay system, it has been demonstrated that cytosolic factors control size of nucleolus. All these results indicate the importance of nuclear transport for size regulation of nucleus and nucleolus. We conclude that in mammalian system, communication between nucleus and cytoplasm is very important to maintain the N/C ratio in immortalized cells. In yeast system, we found that motor proteins control nuclear size and shape and alteration in nucleus size and shape is observed in all stages of cell cycle as shown by light microscopy and electron microscopy. We found another novel protein PRP45 which is a pre-mRNA

splicing protein that controls nuclear size and shape. We conclude that in yeast, nucleus size and shape alteration phenotype can be achieved by many different factors. Alteration in nuclear surface area or volume does not necessarily alter the chromatin inside the nucleus.

5. References:

1. Marshall, W. (2002) Size control in dynamic organelles, *Trends in cell biology.* 12, 414-9.

2. Marshall, W. F. (2008) Engineering design principles for organelle size control systems, *Seminars in cell & developmental biology.* 19, 520-4.

3. Handwerger, K. E. & Gall, J. G. (2006) Subnuclear organelles: new insights into form and function, *Trends in cell biology.* 16, 19-26.

4. Neumann, F. R. & Nurse, P. (2007) Nuclear size control in fission yeast, *The Journal of cell biology.* 179, 593-600.

5. Zink, D., Fischer, A. H. & Nickerson, J. A. (2004) Nuclear structure in cancer cells, *Nature reviews Cancer.* 4, 677-87

6. Lever, E. & Sheer, D. (2010) The role of nuclear organization in cancer, *The Journal of pathology.* 220, 114-25.

7. Nickerson, J. A. (1998) Nuclear dreams: the malignant alteration of nuclear architecture, *Journal of cellular biochemistry.* 70, 172-80.

8. Busch, H., Byvoet, P. & Smetana, K. (1963) The nucleolus of the cancer cell: a review, *Cancer research.* 23, 313-39.

9. Kutay, U., Izaurralde, E., Bischoff, F. R., Mattaj, I. W. & Gorlich, D. (1997) Dominant-negative mutants of importin-beta block multiple pathways of import and export through the nuclear pore complex, *The EMBO journal.* 16, 1153-63.

10. Ribbeck, K., Lipowsky, G., Kent, H. M., Stewart, M. & Gorlich, D. (1998) NTF2 mediates nuclear import of Ran, *The EMBO journal.* 17, 6587-98.

11. Klebe, C., Bischoff, F. R., Ponstingl, H. & Wittinghofer, A. (1995) Interaction of the nuclear GTP-binding protein Ran with its regulatory proteins RCC1 and RanGAP1, *Biochemistry.* 34, 639-47.

12. Hutchins, J. R., Moore, W. J. & Clarke, P. R. (2009) Dynamic localisation of Ran GTPase during the cell cycle, *BMC cell biology.* 10, 66.

13. Neumann B, Ellenberg, J., (2010) Phenotypic profiling of the humna genome by time-lapse microscopy reveals cell division genes, *Nature*. 464 (7289), 721-727

6. Publications in Refereed Journal:

A. Published:

Ganguly A, Bhattacherjee C, Bhave M, Kailaje V, Sengupta I, Jain B, Rangarajan A and Bhattacharyya D. Perturbation of nucleolcytoplasmic transport affects the size of nucleus and nucleolus. Febs Letters, doi: 10.1002/1873-3468.12077; PMID:26813731

B. To be submitted:

Ganguly A. Bhattacharyya D. Nuclear kinesins Kar3, Cin8 and splicing protein prp45 ts mutants control nuclear shape and size in budding yeast *Sacharomyces cerevisiae (Manuscript under preparation)*

C. Other Publications:

1. Bhattacharjya S[#], Roy KS[#], **Ganguly A,** Sarkar S, Panda CK, Bhattacharyya D, Bhattacharyya NP, RoychoudhuryS. Inhibition of nucleoporin member Nup214 expression by miR-133b perturbs mitotic timing and leads to cell death. Mol Cancer. 2015 Feb 15;14(1):42. PMID: 25743594

2. Nath S[#], Chowdhury A[#], Dey S, Roychoudhury A, **Ganguly A,** Bhattacharyya D, Roychoudhury S. Deregulation of Rb-E2F1 axis causes chromosomal instability by engaging the transactivation function of Cdc20-anaphase-promoting complex/cyclosome. Mol Cell Biol. 2015 Jan;35(2):356-69. PMID: 25368385

3. Bhave M[#], Papanikou E[#], Iyer P, Pandya K, Jain BK, **Ganguly A**, Sharma C, Pawar K, Austin J 2nd, Day KJ, Rossanese OW, Glick BS, Bhattacharyya D. Golgi enlargement in Arf-depleted yeast cells is due to altered dynamics of cisternal maturation. J Cell Sci. 2014 Jan 1;127(Pt 1):250-7. PMID: 24190882

Signature of Student: Abir Ganguly
Date: 26.02.16

Doctoral Committee:

S.	Name	Designation	Signature	Date
1	Dr. S. N. Dalal	Chairperson	S.N Dalal	28.02.16
2	Dr. D. Bhattacharyya	Guide & Convenor		28.02.16
3	Dr. S. Gupta	Member		28.02.16
4	Dr. M.M.Vaidya	Member	M M Vaidya	28/02/16

Forwarded through:

S.V. Chiplunkar 9/3/16

Dr. S.V. Chiplunkar
Director, ACTREC
Chairperson, Academic &
Training Programme
ACTREC

Dr. S. V. Chiplunkar
Director
Advanced Centre for Treatment, Research & Education in Cancer (ACTREC)
Tata Memorial Centre
Kharghar, Navi Mumbai 410210.

Dean-Academic
Dr. K. Sharma,
Director, Academics,
T.M.C.

Prof. K.S. Sharma
DIRECTOR - ACADEMICS, TMC
Mumbai - 400 012

List of Figures

List of Tables:

Chapter 1:

Introduction

1.1: Background of the work:

The fundamental features such as number, polarity, size, shape and dynamics of intracellular organelles are precisely controlled by a mostly unknown complex mechanisms [1]. Very little is known about how the overall sizes & shapes of the organelles are maintained or regulated. The mechanisms are possibly different for different organelles. The Nucleus is a good candidate to study such mechanism, mostly single in number, primarily it is the largest organelle and easy to visualize accurately [2-4]. Size and shape of the Nucleus vary from cell to cell in the same organism. Nucleus size changes from the very onset of cell birth and continues until next cell division. It has been also observed that nucleus size or shape changes in different cellular conditions in a very dynamic manner [2, 5]. Moreover, alterations in size & shape of the nucleus are observed during different normal physiological conditions as well in diseases [6, 7]**.** Nuclear size or shape varies from cell to cell from species to species. Nucleus size also changes in different physiological conditions; for example during liver regeneration nuclear size is increased in the most abundant liver cells, the hepatocytes [8]. Specific tumor types are associated with characteristic alterations of nucleus shape and size which in turn provide an important diagnostic feature [7]. Despite being years of cancer research it remains poorly understood how nuclear size and shape is regulated. Although almost all major cancerous cells have the hallmark of aberrant nuclear architecture, it has been conceived for a long time that such change of nuclear size in cancerous cells is an indirect effect; primarily caused by aneuploidy. However, recent studies show that when genetic and growth conditions were altered, nuclear size varied with cell size but not with ploidy, suggesting the existence of a regulatory mechanism of nuclear size control [9]. These revolutionary findings opened up the possibility to initiate the

study of nuclear size control in normal cells which in turn will provide insight to the aberrant nuclear architecture of any diseased cells.

1.2: Layout of the thesis:

The thesis starts with the review of literature, chapter 2, describing a brief introduction of organelles, general features of nucleus, size and shape of nucleus, Nucleus size and shape association with different diseases, sub compartments of the nucleus, especially detailed description of nucleolus, its association with different disease and size control mechanism of nucleolus. 'Aims and Objectives' are described in chapter 3. A description of various methodologies and reagents used are described in chapter 4 as 'Materials and Methods'. The findings of the work are presented and discussed in chapter 5 and chapter 6, each chapter is further divided into 'An Introduction, Results and Discussion'. Chapter 5 deals with our findings on nucleus and nucleolus size control mechanism in mammalian cell lines. Chapter 6 shows that different genetic alteration leads to nuclear shape alteration in the single cell yeast system. The 'Summary' of the thesis is presented in chapter 7. The references are compiled towards the end as 'Bibliography' in chapter 8.

Chapter 2:

Review of Literature

2.1: Cell Complexity

In 1665, English microscopist Robert Hooke discovered and thereby coined the term "Cell'[10]. Following this, in 1889, Schleiden and Schwann, a German zoologist, proposed the first two aspects of the cell theory [11]:

- All organisms are composed of one or more cells.
- The cell is the structural unit of life.

Rudolf Virchow, a German pathologist, in 1885 proposed the third aspect:

- Cells can arise only by division from a pre-existing cell.

-------"With the discovery of cell, biology discovered its atom. To characterize life, it was henceforth essential to study the cell and analyze its structure: to single out the common denominators, necessary for the life of every cell; alternatively, to identify differences associated with the performance of special functions." —François Jacob, La logique du vivant: une histoire de l'hérédité (The Logic of Life: A History of Heredity), 1972.

Further curiosity led to more research which includes the components and functions of the cell. Each of the thousands of different molecules in a cell has a well-defined function and their interactions with other molecules are well regulated [12]. A wide range of chemical reactions occurs inside the cell with the help of such molecules which are spread across the different organelles in the cell [13]. Using such molecules, the cell has developed the ability to sense changes in its surroundings and also to respond towards it. All these are undoubtedly indicative of the high level of complexity in a cell. Yet, the cell as a unit is so organized in structure and function [1, 12]. The cell had developed an intelligent complex regulatory mechanism/ s which enables a single cell to sense and maintains very fundamental features for example

number, polarity, size and shape of intracellular objects ranging from macromolecules to organelles [1, 13].

2.2: Organelle Introduced

2.2.1: Brief introduction of an organelle

The idea behind the name organelle is, these structures are to the cells what an organ is to the body (hence the name organelle). In 1884, German zoologist Karl August Möbius used the term "organula". It took several years for the organelle to be accepted and expanded in meaning to include subcellular structures in multicellular organisms. Later, the widely used definition of organelle emerged, that is cellular structures with surrounding membrane. An organelle is one of the several structures with specialized functions, suspended in the cytoplasm of a eukaryotic cell [1]. Eukaryotes are the most structurally complex cell type and consist of many smaller interior compartments, which are also enclosed by lipid membranes that resemble the outermost cell membrane [1]. The examples of organelles are Nucleus, Mitochondria, Golgi apparatus, Lysosome, Endoplasmic reticulum, chloroplast etc.

Organelles make an additional level of organization inside the cell. Organelles always optimize their structures to their functions (**Table 2.1**). Different biochemical and regulatory functions are performed by different organelles. Inside Endoplasmic reticulum (ER) fatty acid chain elongation takes place but beta-oxidation of fatty acids occurs inside mitochondria [1, 13]. The size, shape and number also vary for different organelle, while nucleus is mostly single in number, mitochondria occurrence is much more. The nucleus is mostly spherical while ER is reticulated network. Size, shape, and numbers are very well maintained in all the organelles and alterations of those are often associated with different pathophysiological conditions [13]. For example, The

enlarged vacuole in *fab1* mutants of budding yeast leads to improper karyogamy and fitness defects [13]. Mitotic spindle length defects can result in faulty chromosome separation [13]. Cilia and flagella that are too long or short result in defective motility [1, 13].

	Shape	Number	Functions	Transport	Capacity
Nucleus	Single compartment, central	One	Storage of genetic information (only one/ two copies normally), transcription	Nuclear pores mediate transport of mRNA, ribosomes, etc.	DNA storage and transcription in lumen, transport through membrane
ER	Many: distributed tubular network, large sheets, nuclear envelope	One network	Protein/membrane synthesis, translocation, trafficking	Deliver proteins/lipids via budding vesicles into the secretory pathway or via diffusion	Ca^{2+} storage in lumen, protein translation and lipid synthesis in membrane
Golgi	Multiple disc-like cisternae, sometimes arranged in a stack	One to multiple	Trafficking/sorting of proteins, posttranslational modification, lipid synthesis	Proteins enter and exit by secretory vesicle delivery and budding	Modification of proteins in lumen and membrane, vesicle fusion/budding at membrane
Vacuole/ Lysosome	Clustered or distributed spherical compartment(s)	One to multiple individuals	Waste degradation, storage and recycling, stress response, autophagy	Membrane channels and vesicle fusion deliver membrane, cytoplasm, proteins, etc.	Lumen is where much of processing, storage and buffering occurs
Mitochondria	Varies: distributed linear network common, sometimes clumped	One network containing many individuals	Respiration, lipid synthesis	Metabolites and products of respiration transferred across membrane	Length and amount are related to respiratory capacity
Peroxisome	Individual small spherical structures	Multiple individuals	Waste processing	Individual organelles are carried along cytoskeleton	Increases with number and individual size
Flagella/ Cilia	Elongated and tubular	One or multiple individuals	Movement, chemical sensing	Cell-cilium transport occurs through a membrane pore, intraciliary transport along central microtubules	Length affects stroke/ beating pattern, cell motility

Table 2.1: Summary & characterization of different organelle[7]

2.2.2: Biological importance of organelle size control mechanism

Most of the organelles are separated by a membrane. Organelle membranes separate reactions from each other and store intermediates and products, hence termed as ‘‘reaction vessels’’[13]. For an effective manufacturing process, size and shape of the reaction vessel are equally important as reactants and products. Likewise, organelle size inside the cell would influence the rates of biochemical reactions [13]. Two main parameters of an organelle are surface area and volume, in which surface area can

limit the rate of import and export of intermediates or products while the volume determines the quantity of intermediates that can be accommodated inside [13, 14].

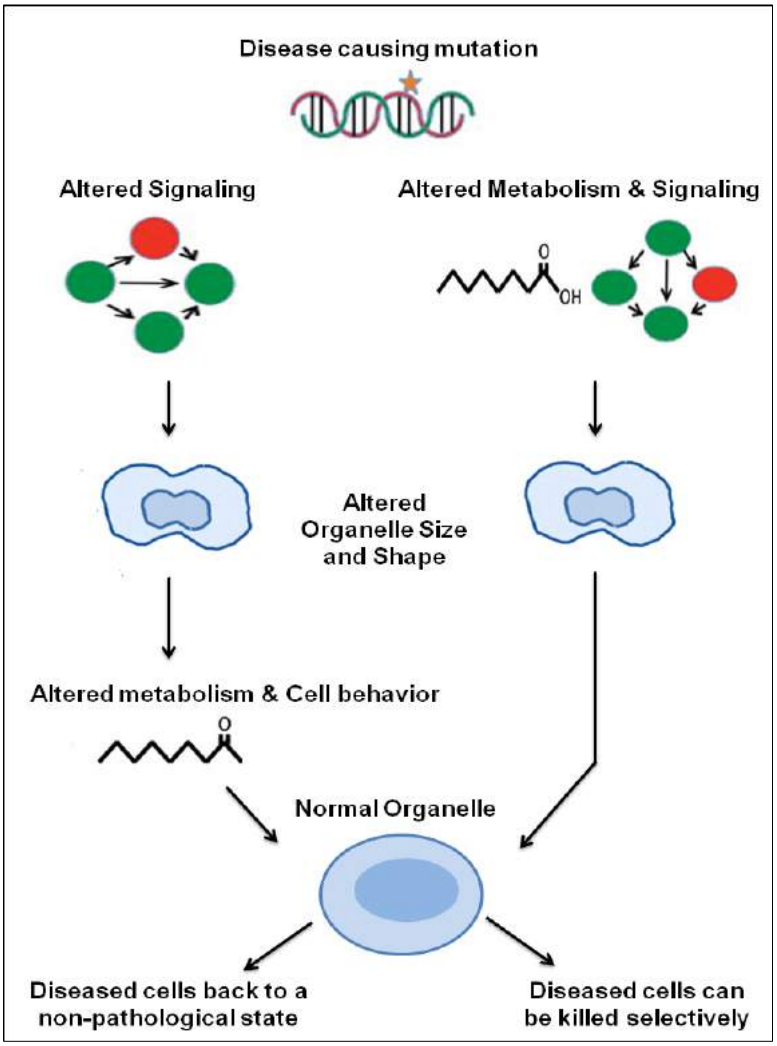

Figure 2.1: Organelle Directed Medicine to Cure Diseased Cells [13]

Disease causing mutations (for example, loss of tumor suppressor genes or activation of oncogenes) cause organelle size changes. This can happen in two ways. In the right scheme, the disease mutation causes alterations in cellular signaling and metabolism, and organelle size changes as a consequence. If organelle size could be reverted, disease cells might die due to mismatch between metabolic requirements and organelles supporting those metabolic pathways. In the left scheme, disease mutation causes alterations in cellular signaling pathways, which impinge on organelle size, and this size change itself is a direct contributor to alterations in metabolism and cell behavior. In this case, if organelle size could be reverted to wild-type, it might be possible to push the diseased cells back to a non-pathological state [13]

It can be speculated that metabolism is also influenced by size of organelles, as in certain cells size of organelles are enlarged compared to other cell types, for example

in secretory cells, the requirement for a high rate of flux of secreted proteins is met by a massive over proliferation of ER and Golgi apparatus, enlarged lipid droplets in adipose cells, proliferation of microvilli on the surface of cells lining the intestine, increment in the surface area and volume of rhodopsin containing vesicles in rods versus cones, and also increase number of mitochondria as a function of respiratory state [1, 13, 14]. If we hypothesize that organelle size affects metabolism and signaling, then reprogramming of organelle size could scale back the altered organelle and can be used as a novel strategy for reprogramming metabolism and signaling pathway as a function of cellular state and behavior, with direct applications in medicine (**Figure 2.1**) [13].

2.2.3: Size and Shape regulation of an organelle

The cell organelles are important to study. Organelle is complex yet organized not only in terms of the variety of its components and the reactions within it but also in terms of its ability to maintain its own size and also of its organelles. D'Arcy Wentworth Thompson rightly said, "Everywhere Nature works true to scale, and everything has its proper size accordingly" [14]. Cell biologists therefore always like to unravel the size control mechanisms of various organelles.

Organelle size regulation can be considered by three factors,

1. The ratio of organelle size versus number,
2. Organelle Scaling
3. Organelle Surface area or volume [1, 14, 15].

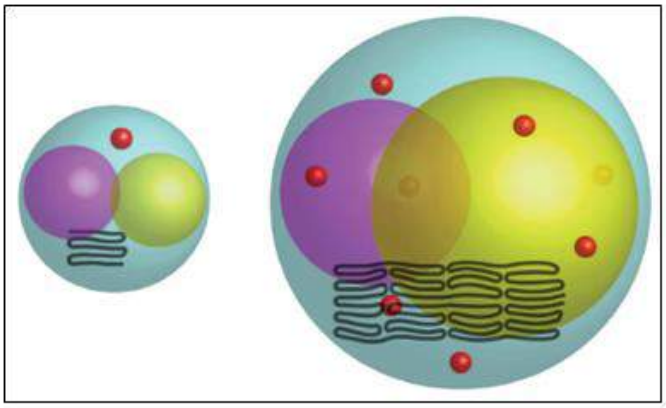

Figure 2.2: Schematic Representation of Organelle Size Scaling [14]

The cell on the right is twice the diameter of the left. The eight-fold increase in cell volume is correlated to a proportionate increase in: (I) volume for a centralized organelle (purple), (II) total network length of tubular organelles (black lines), (III) copy number for organelles with multiple copies (red). The yellow organelle shows the effect of an eight-fold increase in surface area rather than volume for a centralized organelle.[14]

Organelle size can increase in many different ways [16], for example,

- Isotropic, 3D expansion – example Nucleus (Round, Large)
- Increasing the linear length of the network, keeping the cross-sectional dimensions roughly constant –example ER, Mitochondria (Distributed Network)
- Increasing in number—example Peroxisomes (Multiple copies)
- Combination of all- example Fungal Vacuole (single, round morphology /fragmented collection of smaller vesicles)

At least, the cell must in some way ensure that the size of its organelles is greater than zero [16]. It can be hypothesized that larger organelles contain larger quantities of metabolic enzymes and thus mediate higher fluxes through their biochemical pathways. Mostly, organelle size should be suited to cellular needs, including functional, distribution, and transport requirements, or other factors [13, 15]. The size of organelles will influence the rates of biochemical pathways contained within them.

Organelle surface area can limit the rate of import of substrates and efflux of products while the volume of the organelle can dictate the quantity of intermediates that can build up [15]. Many key metabolic enzymes are organelle membrane proteins, and in such cases increased surface area could allow larger numbers of molecules into the membrane to increase metabolic flux. The influence of organelle size on metabolism is indicated by the fact that in cells specialized for certain pathways; the organelles that contain these pathways are enlarged compared to other cell types [1, 13, 14]. Evidently, organelle size optimizes in cells with specialized roles. For examples, in secretory cells with greatly expanded ER and in rod and cone photoreceptors whose outer segment size correlates to their light sensitivity [1, 13]. Cells have developed ways to sense and control the size of their organelles. Size-sensing mechanisms range from direct measurements provided by dedicated reporters to indirect functional readouts and they are used to modify organelle size under both normal and stress conditions. Organelle size can also be controlled in the absence of an identifiable size sensor.

Clearly, our understanding of organelle size control systems is still at a primitive level. Although progress has been made in understanding the biochemical mechanisms underlying how membranes are formed and shaped, little is known about how the overall sizes of these organelles are determined [1]. Recently different groups are focused in studying size control mechanisms of different organelles like the nucleus, Golgi apparatus, mitochondria. Of particular interest, size control mechanism of the nucleus, one of the important organelle, has emerged in last decade.

2.3: Nucleus – a brief introduction

The Nucleus is the most prominent, spherical or oval structure at the center of the cell (**Figure 2.3**) [3]. The Nucleus is also known as the controlling unit of the cell as it controls all cell activities. In 1710, Leeuwenhoek in noted a centrally placed "clear area" which was almost certainly the structure as the nucleus in living blood cells of amphibians and birds. But credit for the discovery of the nucleus is usually given to Fontana (1781), who examined isolated epidermal cells from eel skin and observed in each an ovoid structure; the nucleus [3, 4].

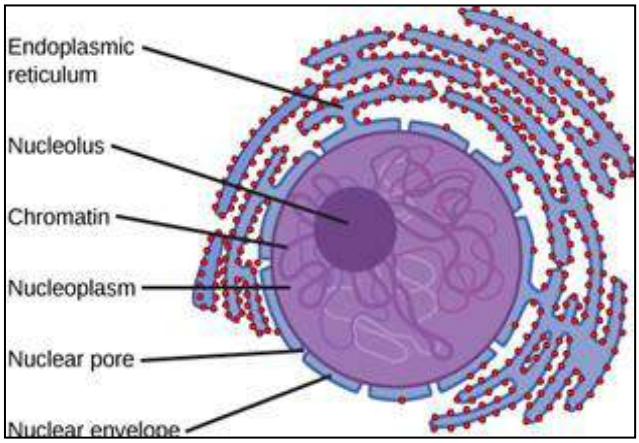

Figure 2.3: The Schematic Diagram of Nucleus

The nucleoplasm is enclosed by the nuclear envelope (NE) containing the inner nuclear membrane (INM), the outer nuclear membrane (ONM), the nuclear pore complex (NPC), and the lamina. The Chromatin and the nucleolus are present in the nucleoplasm.

Brown (1831) recognized the constant occurrence of a nucleus in botanical material and first enunciated the concept of the nucleated cell as the unit of structure in plants, a concept soon extended to animals.

2.3.1: General features of Nucleus

Eukaryotic cells are characterized by the presence of the nucleus. However, it is absent in erythrocytes. Generally, a nucleus is unitary in a cell. But, in few cases, it is observed that nucleus is present in more numbers. Based on the number of nucleus,

the cells are classified into the following types: anucleate cell (nucleus is absent, examples mammalian erythrocytes, blood platelets, core fibers of the lens erythrocytes of human etc), mononucleate cell (single nucleus; example Amoeba), binucleate cell (two nuclei are present; example Paramecium, Tetrahymena thermophila [17]) and multinucleate cell (many nuclei; example Opalina [18]). The position of nucleus varies from cell to cell. Mostly it is situated in the cell center, sometimes it is situated near the periphery (adipose cells or egg rich in the yolk), in some cells, nucleus lies in the basal region (Acetabularia).

2.3.2: Nucleus –the organization

The nucleus structure and its functional organization remains a subject of debate. At one extreme, it has been proposed that the nucleus has its own nucleoskeleton [5, 19]. At another extreme, it is considered as a largely disordered, containing DNA, RNA, and other macromolecules. All these "structures" are no more than transient complexes that form and disperse as a result of transcription, replication, and RNA processing activities in various regions of the genome [19, 20]. One of the major goals of cell biology is to understand the molecular detailing of the organizing principles of the nucleus.

2.3.4: Compartments within the Nucleus

The Nucleus itself contains many levels of organization as depicted in the **figure 2.4**. It is enclosed by a double membrane lipid bilayer membrane which is also known as the nuclear envelope. The outer nuclear membrane (ONM) is in continuous with general ER and the inner nuclear membrane is lined by lamin and many other proteins [3, 4, 19]. The nuclear envelope is embedded with many nuclear pore complexes

(NPC). NPCs are transmembrane, multiprotein complexes, which allow transport of molecules between cytoplasm and nucleus [21].

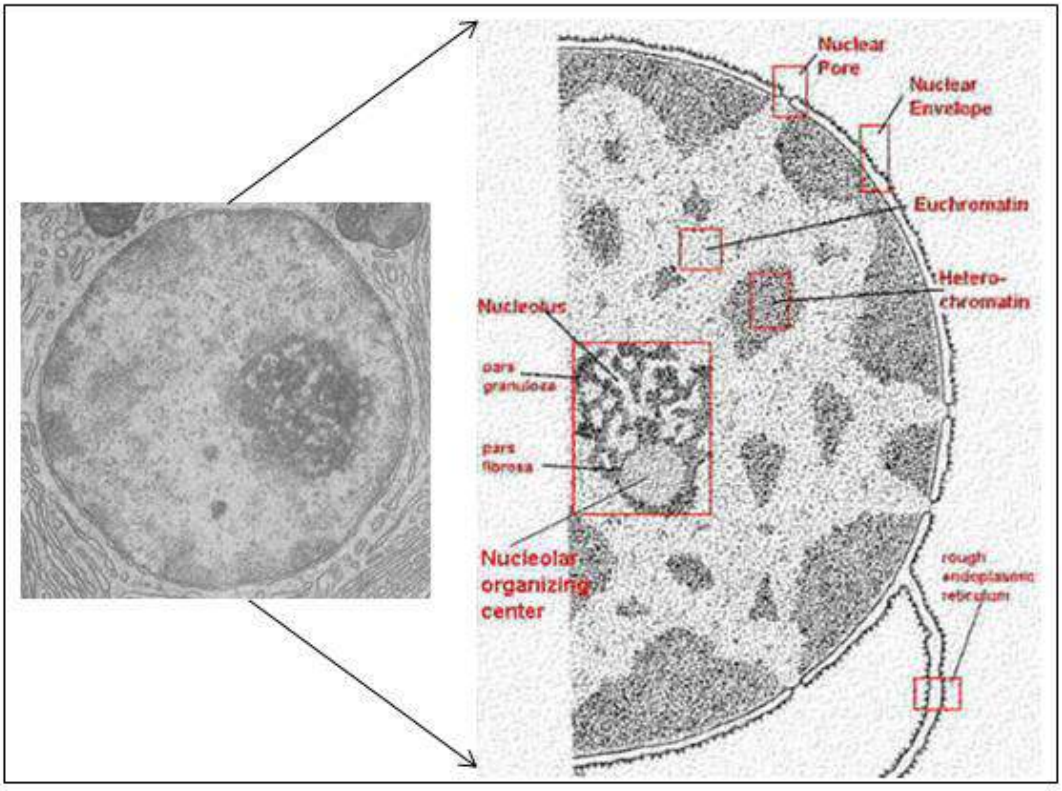

Figure 2.4: Compartments within the nucleus

Electron micrograph of mammalian nucleus. The left image is showing the entire nucleus and cross section of the nucleus is shown in the right with detailed sub nuclear structures

Interior of the nucleus is known as nucleoplasm which contains many different domains that include chromatin, nucleolus, Cajal body, nuclear speckles etc. and also contain nuclear matrix proteins [20]. Individual chromosomes form discrete patches which are known as chromosomal territories. In the periphery of CTs, active genes are preferably present. All these domains inside the nucleus are also functionally specialized which lack membranes [20].

2.3.5: Nucleus size and shape control mechanism

Size and shape are two different characteristics of nucleus. Nuclei do have a characteristic shape and also a typical size in a given tissue. The size and shape of the nucleus are controlled by either same or different mechanisms.

Nucleus, the largest of all the organelle inside a cell, varies in size from about 3µm to 20µm in diameter, depending on cell type. Nucleus size changes from the very onset of cell birth and continues until next cell division [2, 5]. This raises a question; what is responsible for controlling this nucleus size? Is it just a consequence of increasing the volume over time or are there any dedicated factors which regulate and limit this nuclear expansion? Based on available theories of organelle size and shape control mechanisms, it can be speculated that nucleus size and shape is very well regulated in normal cells. Richard Hertwig, in the year 1903, based on his work on sea urchin embryos and algae formulated the first quantitative hypothesis about this phenomenon [3]. He proposed the "karyoplasmic ratio" also known as "Kern-Plasma-Relation", as a constant characteristic for every cell type. It suggests that nuclear and cytoplasmic volumes are somehow related to each other. This volume relationship is found in cells with widely different DNA contents, ranging from single-celled eukaryotes to mammalian cells. Moreover, it was observed that in both budding and fission yeast, the ratio of nuclear volume to cytoplasmic volume (N/C) remains constant throughout the cell cycle even if there is an increase in the cell volume [9, 22].

2.3.6: The Nucleus SIZE

One of the fundamental properties of eukaryotes is their ability to maintain the size of their organelle that is appropriate for different growth and differentiation states. Nucleus size or volume changes in different physiological conditions; for example

nuclear size is increased in the most abundant liver cells, the hepatocytes, during liver regeneration [8]. Two conflicting hypothesis for nucleus size control mechanism exists. One hypothesis talks about nucleo-skeletal theory, which says that higher the DNA content, and extent of compactness, greater the nucleus size and in turn the increased cell size [15, 19, 23]. This theory is supported by the fact that larger genomes have larger nuclear and cellular volumes among different species. It has been shown in mouse embryo nuclei, tetraploid is twofold larger than diploid. However, the drawback in this hypothesis is, differently shaped and sized nucleus from cells of different tissues exists in a given organism. The other hypothesis promotes nuclear scaling mechanism [24, 25]. It says nuclear volume is proportional to cellular factor/(s). Evidence to support this hypothesis also exist, HeLa cell nucleus expanded when small hen erythrocyte nucleus was implanted in it, provided the fact that DNA content did not affect [26].

In last decade, several researchers studied control mechanism of nuclear size in different model organisms. To start with the single-celled eukaryotes, yeast, cellular scaling was investigated by Jorgensen et al. In budding yeast *Saccharomyces cerevisiae*, larger cells contains a large nucleus and it always maintains a constant N/C ratio [22]. The fission yeast *Schizosaccharomyces pombe* also maintains a constant N/C ratio over a 35-fold range of cell size [9]. Nucleus size is shown to increase concomitantly when cell proceeds through the cell cycle from G1 to G2 in either budding yeast, fission yeast or in Hela cells. However, nucleus size does not increase steadily in S phase when only DNA content increases in the same [15]. Consistent with results in yeast, nucleus size also alters in *Caenorhabditis elegans* and *Drosophila melanogaster*, when cell growth and size related genes are mutated. [15, 27]. It is noteworthy that, nucleus size did not alter when DNA content is increased by

16 fold by genetic manipulation in *S. pombe* cells [9]. Multinucleated cells can be generated by a cytokinesis mutation in *S. pombe* cells. In such mutants, nuclei surrounded by a higher proportional amount of cytoplasm were larger than nuclei exposed to smaller cytoplasmic volumes [9]. Moreover, when nuclei were artificially displaced by centrifugation those nuclei exposed to a larger cytoplasmic volume grew faster [9]. These lines of evidences delineate that the content of DNA does not influence the size of the nucleus or N/C ratio. Rather it is the cytoplasmic volume which controls nucleus size or N/C ratio. Similar results also observed in HeLa nuclei when injected in Xenopus oocytes or in sea snail *Crepidula plana* embryos [15]. Precisely, nuclear size is determined by diffusion limited cytoplasmic factors.

Different cellular processes could also be responsible for nuclear size control mechanism such as nucleo-cytoplasmic transport, ribosome biosynthesis, lipid biosynthesis etc [9, 22]. It is of importance that when nuclear export is blocked in *S. pombe* cells, there is a significant increase in the size of nucleus and N/C ratio [9]. This supports the fact that cytoplasmic components or nucleo-cytoplasmic transport might be responsible for controlling nuclear size in yeast. Nuclear import was shown to regulate nucleus size in two related but different sized frog species namely *Xenopus laevis* and *Xenopus tropicalis* [25]. In cell-free extracts of *Xenopus* oocytes, an intact ER is required for nuclear volume to increase after NE assembly which might be due to the fact that membrane components are supplied from ER [28]. The limiting factor here is thus membrane availability.

Tetrahymena thermophila, a ciliated protozoan that possesses two morphologically and functionally distinct nuclei, offers a unique system to investigate mechanisms of nuclear size control within the same cell [15, 17, 29]. The macronucleus (MAC) is much larger and is generated by programmed DNA rearrangements and

amplifications. Different linker histone H1 isoforms are specifically targeted to each nucleus, and deleting one nucleus-specific H1 isoform enlarged that nucleus without affecting the size of the other [15]. How H1 itself affects nuclear size is an open question. Is it through chromatin structure or gene expression? However, many questions remain. For example, how do yeast – which lack lamins and lamin-associated proteins – adjust nuclear volume in response to changes in cytoplasmic volume?

2.3.6.1: Does nuclear size matters for its function?

The existence of karyoplasmic ration (KR) suggests that nuclear size is important for biological function [2, 4-7, 15]. Any alteration in this ratio is associated with certain types of cancers [7, 30]. Some reports suggest that cell cycle progression is dependent on the size of the nucleus. The KR is continuously monitored to determine the proper time to enter the cell cycle. Nuclear size is also correlated with RNA transcript level as well as cell size [9]. Most likely, the size of nucleus might play a role to maintain nuclear compartments such as nucleolus, different enzymes activity, such as DNA polymerase and RNA polymerase [9, 22]. Cajal bodies are examples of self-organization through stochastic interaction between the units of which they are composed of. Nucleus size might be important for such self-organization processes as well [20].

2.3.7: The Nucleus SHAPE

The cell nucleus in most of the cells is either oval or spherical or ellipsoid [5]. The shape of the nucleus is very striking and alters in certain diseased cases. An abnormal nuclear shape is important for cell function in certain normal cell types. During aging, it is found that mutation in lamin protein is responsible for altered nuclear shape

(**Figure 2.5B**) [5, 31]. In some cases, altered nuclear shape is observed due to forces from the cytoplasm. But the surprising part is how altered nuclear shape affects cell function?

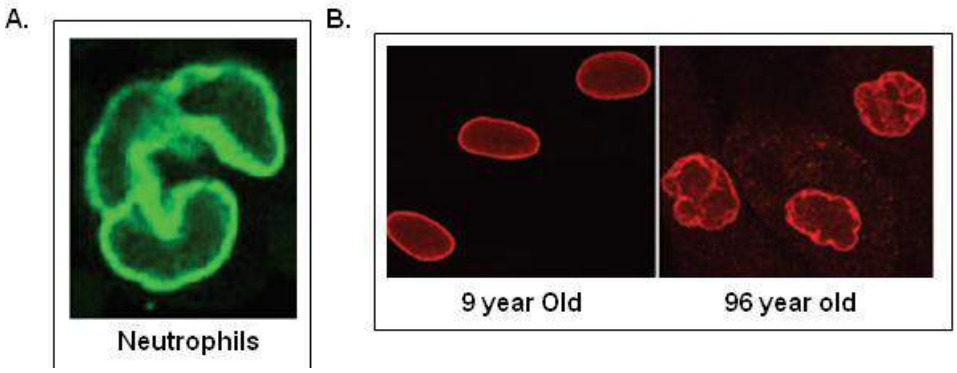

Figure 2.5: Variation of Nuclear shapes in different physiological conditions.

A. Non rounded Multi-lobulated Neutrophils visualized by antibody against Lamin B [32].B. Nuclear shape changes with aging as shown in nuclei from a 96- year-old compared with nuclei of cells from a 9- year-old individual (human fibroblast cells). Nuclei are visualized by antibody specific for lamin A and C respectively[31] . Nuclei are not shown to scale.

Two mutually non-exclusive hypothesis exist; first one proposes, changes in nuclear shape alter the rigidity of the nucleus, which could be beneficial for cells that need to squeeze through tight spaces, but deleterious to cells that are under mechanical stress. The second hypothesis is that changes in nuclear shape result in chromatin reorganization and thereby affect gene expression [5]. Some cells (Spermatids) also undergo dramatic changes in nuclear shape during differentiation and maturation. One prominent example, human embryonic stem cells have large, round nuclei, with roving chromatin and express no A-type lamins. The shape of the nucleus and it's rigidity changes when such cell differentiates with less mobile chromatin and highly expressed lamin A [5]. These changes can happen due to remodeling of chromatin structure. This increases the accessibility of specialized genes necessary for differentiation. An example of normal cells with abnormal nuclei is the most studied

immune system cell, multi-lobed neutrophil (**Figure 2.5A**) [5]. Neutrophils have to travel through the tissue towards the site of infection. Hypolobulated neutrophils are associated with cellular dysfunction. They are unable to migrate through small openings [5, 33]. Such evidence helps to understand, nuclear lobulations is an adaptation for cell function.

Lamins, various nuclear lamina proteins, and microtubules are shown to be responsible for such lobulations. Thus, both nuclear and cytoplasmic proteins are affecting nuclear shape in neutrophils [5]. During cellularization in the Drosophila embryo, when nuclei change shape from spherical to ellipsoid, microtubules play a significant role, which is achieved by again both nuclear and cytoplasmic proteins, kugelkern or charleston, and microtubules respectively [5, 27, 34]. In the above example, microtubule generated forces help to alter the nuclear shape. In some cells, interphase fission yeast nuclei, microtubule generated forces in the cytoplasm can alter the nuclear shape only if any inner nuclear membrane protein is inactive. Here, counteracting forces are required for microtubule generated forces [35]. Changes in nuclear shape also observed in the case of cancer. It has been speculated that changes in nuclear shape lead to changes in chromosome organization, which in turn can affect gene expression. Others have proposed that the altered nuclear shape in cancer cells facilitates the formation of metastases because of reduced nuclear stiffness. This reduced nuclear stiffness could increase the ability of transformed cells to penetrate tissue [36].

There are many different mutations in different proteins to abnormal nuclear shape and size, but the mechanisms are unknown. The relationship between protein inactivation and altered nuclear shape might be indirect. Proteins, associated with ER, when inactivated showed abnormal nuclear shape [37, 38]. Lipid synthesis is also

reported to affect nuclear shape in *C. elegans* and yeast [39-41] . Inactivation of a lipid phosphatase, homologous to the mammalian lipin has also been shown to cause both alterations of ER and nucleus shape.

2.3.8: Size and shape alteration of nucleus in cancer

An abnormal nuclear size and shape is often associated with cancer (**Figure 2.6**) [7]. The functional relationship between altered nuclear shape and cellular transformation – or even the underlying cause of altered nuclear morphology – is often not known. One of the most complex diseases is cancer which is linked to various alterations of different biochemical pathways. Being studied so much, almost more than 100 years, still today the diagnosis of cancer requires the use of light microscopy to assess a biopsy sample.

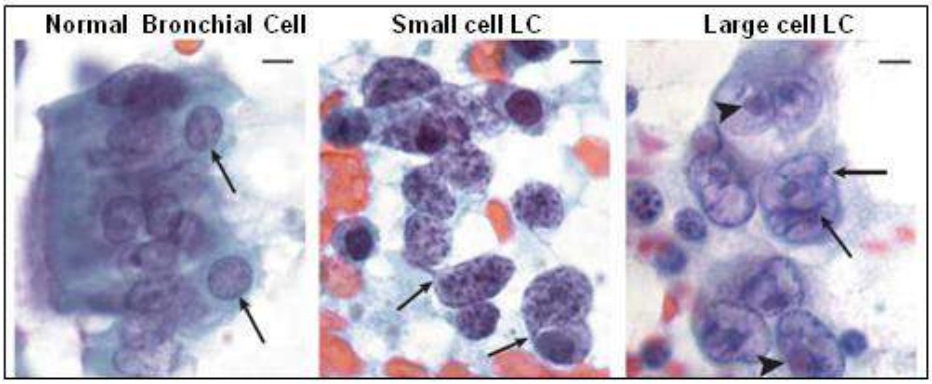

Figure 2.6: Nuclear size and shape alteration in cancer [7]

Normal bronchial epithelium contains basal cells (arrows point to two nuclei of basal cells with round to oval nuclei. Small-cell lung carcinoma shows aberrant nucleus, scant cytoplasm. Large-cell lung carcinoma is distinguished from small-cell lung carcinoma on the basis of nuclear enlargement and a more irregular nuclear contour. Scale bars represent 5 µm. Tissues were stained using the Papanicolaou technique.

In this biopsy sample, a pathologist looks for primarily altered nuclear size and shape (**Table 2.2**) [7]. One of the first descriptions of these changes was by Lionel S. Beale

of King's College Hospital, London, in 1860, examined unstained sputum from a patient with cancer of the pharynx and observed the nuclear size and shape variations in cancer cell [7].

Nuclear Characteristics	Cancer type	
Changes in Nuclear Shape	Malleable nuclei with frequent crush artifacts	Small-cell lung carcinoma
	Grooves and long clefts	Papillary thyroid carcinoma urothelial tumours, including Brenner tumour of the ovary, granulosa-cell tumour of ovary, follicular lymphomas
	Polylobulation	Some adenocarcinoma
	Indentations, undulations, folds	Many types of cancers
Chromatin Changes	Coarse aggregates of heterochromatin	Many types of cancers
	Assymetric aggregates of heterochromatin	Wide range of Cancers
	Dispersed heterochromatin	Small Cell Lung carcinoma
	Loss of heterochromatin aggregates	Papillary thyroid carcinoma, wide range of other carcinomas

Table 2.2: Nuclear Characteristics in Different Cancers[7]

In the 1930s and 1940s George Papanicolaou developed a stain that simultaneously displays a broad range of cytoplasmic and nuclear structural features of cells, and applied the stain to exfoliated cervical cells to test for cancer As a result of this 'Pap

test', in women cervical cancer mortality has decreased from the leading cause to the eighth most common cause of death from cancer [7]. The nuclear matrix participates in the spatial organization of the genome and other nuclear components. The protein composition of the nuclear matrix is altered in tumour cells and these changes might be useful tumour markers. Characteristic changes of nuclear shape and of chromatin texture can be induced in normal cells in vitro by oncogene activation. Chromosome territories and gene loci display characteristic spatial arrangements inside nuclei, and these have an important role in the generation of diagnostically significant translocations associated with human malignancies[42, 43]. Structural alterations in tumor cells also include changes in nucleoli and the appearance of the perinucleolar compartment. High-throughput nuclear-structure-based assays to screen drugs for their ability to revert malignancy-associated nuclear changes might identify new therapeutics.

2.4: Nucleolus Introduced

2.4.1: Nucleolus structure and function

The nucleolus, the unique membrane less organelle, was first identified by F. Fontana in 1781 as an ovoid body inside the nucleus of the slime of an eel [44, 45]. In 1898, Montgomery wrote a review after reviewing 700 references post nucleolus discovery and also based on his own work on nucleolus of 175 different oocytes species. Three remarkable conclusions, which are still valid today, were 1) There is no constant number of nucleoli per cell; 2) cells that are actively growing typically have more and larger nucleoli, and 3) generally, the larger the cell the larger its nucleolus [45] With the help of light microscopy, nucleolar morphology was described by different cytologists [44]. Nucleolus structure is composed of mainly three components,

fibrillar centers (FCs), which are mostly surrounded by a highly contrasted region, the dense fibrillar component (DFC), and Granular component (GC) in which FC and DFC are embedded (**Figure 2.7**) [44, 46-48]. In nucleolus, this special organization is maintained strictly in a membrane-less compartment [46]. In 1934, Mc Clintock proposed nucleolus organization occurs in the telomere with the help of nucleolus organizing bodies.

In 1960, rDNA was discovered in the nucleolar organizing areas. The Nucleolus is the place where ribosomes are synthesized and assembled [49]. It is long believed that the rRNA synthesis is the main important phenomenon occurring in the nucleolus [49].

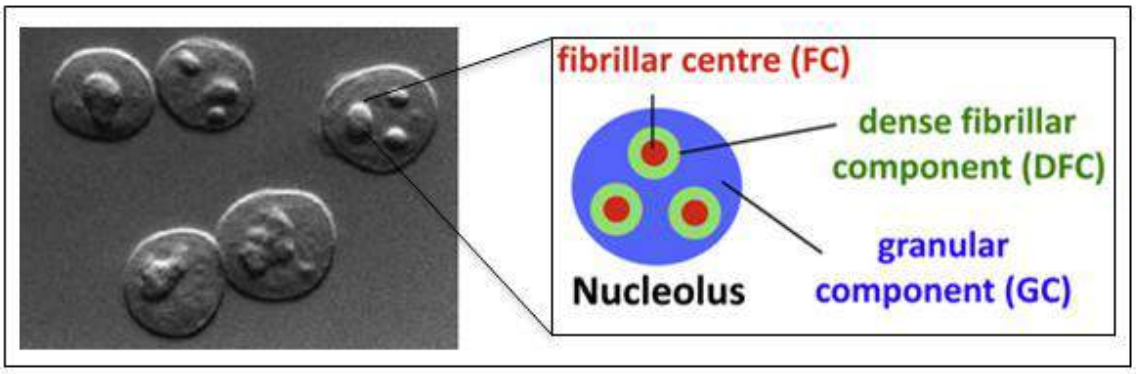

Figure 2.7: The Nucleolus Structure

Isolated HeLa cells nucleoli (left) and schematic representation of nucleolar structure (Right)[19]

However, the impetus of congregation of all rDNA transcription units into one or few nucleoli in a nucleus remains elusive. During the cell cycle, mammalian nucleoli disappear during mitosis and form de novo in early G1 around rDNA [50]. Ribosome assembly begins in the nucleolus, followed by in nucleoplasm and ends in the cytoplasm. This process is extensively studied in *Saccharomyces cerevisiae* [51].

A recent study indicated the presence of noncoding RNAs in the nucleolus and their role in the rRNA process [50]. With the help of microscopy and RNA deep sequencing, it is demonstrated that Pol II dependent intronic Alu RNAs regulate the structure of nucleolus [50]. Other than ribosomal genes and noncoding RNAs nucleolus also contains a collection of other DNA regions. Satellite DNA of the centromere is one of the common components of the interior of nucleoli [52]. DNA sequence analysis of nucleolus associated domains (NADs) revealed the presence of human chromosomal territories of chromosome 1, 9, Y and acrocentric chromosomes as well as telomeres within or very close to nucleoli. Nucleolus constitutes about 4% of the genome and includes sequences from almost all chromosomes. Surprisingly, NADs contain mostly inactive chromosomal regions. Heterochromatin formation is correlated with NADs localization in the nucleolus or more precisely perinucleolar regions. In the same context, X chromosome inactivation center is also demonstrated in the nucleolus [52]. The nucleolus along with nuclear periphery plays an important role in the dynamic organization of the genome by rearranging segments of the chromatin [53].

Nucleolar mass spectrometric coupled with proteomic analysis identified more than 700 nucleolar proteins. To the surprise, only 30% of these are involved in rRNA transcription, assembly and modification. Some of the remaining proteins functions are still unknown and some carry out roles in other established pathways [54]. The nucleolus is also reported to play several other roles, for example, p53 management, ribonucleoprotein biogenesis, stress response, cell cycle regulation [51]. It is believed that the dynamic structure of nucleolus is important for its various functions.

2.4.2: Nucleolus and diseases

Nucleolus dysfunction often associated with pathological implications. Growing appreciation of this provides new insights into nucleolus' role as a multifunctional signaling hub. Nucleolus is thought to play a key role in the preservation of cellular homeostasis. Nucleolar proteins have been implicated in cardiac physiology [55]. In different neurodegenerative diseases, for example in Parkinson's disease, Alzheimer's disease, Huntington's disease, and in spinocerebellar ataxia, nucleolar stress is reported [55-57]. The size of the nucleolus is reduced in Alzheimer's and Parkinson's diseases [57].

Size changes of nucleolus with respect to the nucleus are one of the major cytological changes observed in different malignant cells regardless of the type or origin of neoplasm (**Figure 2.8**) [58]. Although an exception of large nucleoli is observed in neurocytes and oocytes in normal human cells [59]. In last century, many studies had been done to find out nucleolus hypertrophy as a diagnostic for cancer cells, but with the help of light or electron microscopy, no constant general difference in nucleolar morphology could be demonstrated [60]. However, the introduction of silver staining of nucleolus structure helped tumor pathologists to quantitatively address the difference between tumor and nontumor cells. In fact, those earlier studies gave an insight to the high heterogeneity of nucleolar morphology in human tumor cells [7, 59].

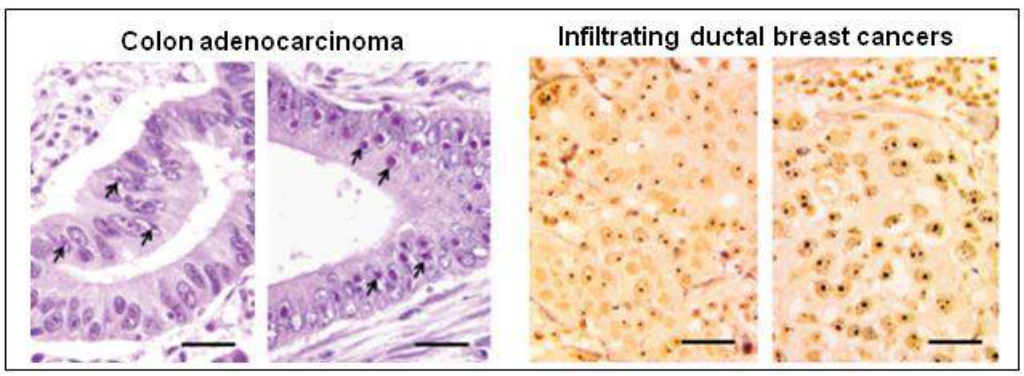

Figure 2.8: Alteration of Nucleolar Structure in Different Cancer

Left panel is histological sections from two routinely processed colon adenocarcinomas stained with hematoxylin and eosin (H&E). The nucleolus frequently appears as a roundish body mainly stained with eosin, due to its high protein content. Arrows indicate nucleoli. Right panel is histological sections from two routinely processed infiltrating ductal breast cancers, specifically silver-stained for the argyrophilic nucleolar proteins. Nucleoli are very darkly stained by silver[61]. Scale bar is 25 μm.

For this reason, a selective visualization of the nucleolar structure within the cell nucleus is mandatory [62]. Malignant tumors of different origin such as breast, liver, large-cell lung carcinoma and Hodgkin's disease often shows increased number and size of nucleoli [63]. One school of thought explains up regulation of ribosome biogenesis enhances translational capacity for rapid and sustained growth and division of malignant cells. In contrast to this, small nucleoli are observed in some of the most rapidly proliferative human tumors such as small-cell anaplastic lung cancer and certain types of hematological malignancies. So, nucleolar size is not always positively correlated with proliferative activity and aggressiveness [63, 64]. One example is intra epithelial prostate cancer, in which cell proliferation is dramatically high but nucleoli size is much enlarged than some other type of intra epithelial cancer. Not only size of nucleolus alters in different cancers, it becomes very irregular shaped (**Table 2.3**).

Nucleolar Characteristics	Cancer type
Enlarged Nucleoli	Wide Range of Cancers
Inconspicuous Nucleoli	Pre cancerous squamous lesions of cervix; Small-cell anaplastic lung carcinoma
Number of nucleolus variation	Wide Range of cancers

Table 2.3: Nucleolar Characteristics in different Cancers [7]

How this different size and shapes of nucleoli are altered in malignant cells still remains elusive [63]. A different representation of size and shape of nucleolus alteration in different cancer could be due to dysregulation of nucleolar functions that might be unrelated to ribosome biogenesis [47].

2.4.3: Nucleolus associated signaling and drug target

One of the important aspects of the nucleolus is it is a multifunctional organelle; many of its functions are still unknown. Proteomic analysis revealed 4500 proteins associated with nucleolus of which only 30 % are directly involved in ribosome biosynthesis. The same study and few other recent studies enlightened the role of the nucleolus in different pathways, for example, cell cycle regulation, DNA repair and replication, viral infection, stress signaling, cell survival, induction of apoptosis etc. Nucleolus controls such diverse cellular processes are through sequestering and releasing the important key regulatory proteins involved in those processes. The nucleolus serves as a stress response center, where RNA and protein content constantly changes in response to various cellular stresses, such as genotoxic, chemotherapeutic agent, UV radiation, hypoxia, inhibitors of nucleotide synthesis, growth factor deprivation, loss of tumor suppressor etc. inhibit or hyperactivate different steps of ribosome biosynthesis which is basically termed as nucleolar stress . Diverse cellular stresses increase p53 stability and disruption of nucleolar integrity. Nucleolar structure integrity disruption is not always same, for example, UV light mediated DNA damage causes p53 stabilization and nucleolar segregation and formation of cap structure while ionizing radiation mediated DNA damage also leads to p53 stabilization but complete nucleolar disruption. Several such studies linked

nucleolus as stress sensor responsible for p53 level suppression. In perturbation of ribosome synthesis pathway triggers nucleolar stress pathway and subsequent disruption of nucleolar integrity. P53 stress pathway downstream target is the oncoprotein MDM2, which either directly binds p53 making it inactive from transactivating basal polII transcription, or alters p53 stability through its E3 ubiquitin ligase activity and thus targets p53 for nuclear export.

Now we understand, out of many non ribosomal functions, nucleolus' critical function is to control different tumor suppressor and oncogenes. Rational behind cell proliferation and stress signaling pathway coupling with ribosome biogenesis is a cell must ensure enough protein synthesis capacity prior to commit cell cycle progression (activates p53 in ribosome biogenesis impairment) while in another case, cell should reduce expended huge energy used in making ribosome if not going for cell division (inactivation of p53 in response to excess ribosome biogenesis driven by survival or oncogenic signals).

Nucleolar stress and RNA transcription can also be affected by pRb or retinoblastoma pathway. Another pathway Myc and PI3KAKT-mTOR are also shown to be involved ribosome biosynthesis [65]. When all these pathways are very active, they are more likely give rise to a more aggressive form of a tumor [65].

Nucleolus can be a potential drug target as it is involved in all these pathways discussed above [65]. But nucleolus has the housekeeping function in sustaining growth of normal cells. However, it has been controversial for a long that how to differentiate ribosome biogenesis in highly proliferating normal cells versus cancer cells drug targeting. Recent advancement in drug screening identified some specific drugs that specifically targets different levels of ribosome biogenesis coupled with disrupted nucleolar phenotype [64]. Actinomycin D, Cisplatin are of good examples

of impairing rDNA transcription specifically while 5 FU disrupts rRNA processing. Different inhibitor of protein kinases also impairs ribosome synthesis. Recently, specific inhibitors are designed (CX-5461, CX-3543) which specifically inhibits ribosome biosynthesis at rDNA transcription level and nucleolar disintegration [64]. The question still remains how selectivity and sensitivity of drugs are conferred when targeted to nucleolus?

2.4.4: Size control mechanism of nucleolus

Nucleolus size, number, dynamics are important for cell function [51]. Alteration in nucleolus size is often associated with pathophysiological conditions as described earlier [7, 56, 59, 62]. To understand nucleolus size regulation, one must not misconstrue the nucleolus size increase or decrease with nucleolus structure disintegration. For its association with ribosome biosynthesis, the size of nucleolus mostly studied in terms of nucleolus segregation.

One of the major questions is how nucleolus size is being maintained even in normal cells? Earlier studies showed nucleolus have a low density sponge like structure. The nucleolus then was demonstrated in amphibians oocytes nucleus, to behave like liquid like droplets [66]. This kind of structure is sufficient to maintain the size and shape of the nucleolus [66]. The surface tension is important for the spherical shape of the nucleolus. The authors talked about the volume of nucleoli follow a power law distribution characteristic of aggregation process of the nucleolus in amphibian oocytes [66]. Because of the nucleolus structure, one hypothesis exists about nucleolar size distribution, which says it must depend on two factors, the rate of production of amplified rDNA mini-chromosomes and the rate at which nucleoli contact one another [66]. However, the functional significance of nucleolar fusion remains elusive.

Nucleolus size scales with cell size in fission yeast and in *C. elegans*, [9, 67]. However, it is not known whether nucleolus size scales with nucleus size [68]. Several intracellular proteins that control transcription of ribosomal genes are important for maintaining the nucleolus structure. Some of the protein involved in NAD localization such as CTCF, NCL, NPMI and Ki67 are those candidate proteins. Ki-67 depletion in human cells makes nucleoli smaller and fewer. In flies, NCL depletion showed altered the nucleolar structure.

The cohesin (regulate sister chromatid separation during cell division) binds to ribosomal DNA from bacteria to human cells. In yeast, it is demonstrated that mutations in any subunit of the cohesin ring are associated with defects in ribosome biogenesis and disrupted nucleolar morphology [69]. However, alteration in the nucleolar organization due to loss of cohesion can be directly attributed to the defects at the rDNA is still not known [69].

In another study, the actin family protein ARP6, which is also a part of chromatin remodeling complex, has been shown to control nucleolus architecture [70]. ARP6 knockdown in HeLa cells showed reduced and condensed nucleolus size in DFC and FC regions respectively [70]. However, ARP6 depletion in mammalian cells had small or no effect on the expression of ribosomal genes [70]. Thus, the nucleolus size control by ARP6 is a direct effect or through regulation of rDNA transcription is not very clear [70].

One of the comprehensive studies focused on identifying genetic networks combined with mass spectrometry-proteomic analysis that might influence the regulation of overall the nucleolus size not nucleolus disintegration performed in two different species simultaneously, *Saccharomyces cerevisiae* and *Drosophila melanogaster* [71]. This study identifies a direct role of the histone information regulator (HIR) complex

in controlling nucleolar size and repressing rDNA transcription in yeast. Deletion of HIR1 and /hir2 resulted in an increase in nucleolar size [71]. As described earlier, nucleolus contains different long noncoding RNAs (lncRNAs) and they are also important for regulation of perinucleolar structures [52].

Size and number of nucleolus vary greatly in human cells; rapidly proliferating small cell anaplastic lung cancer cells have a small nucleolar area per nucleus while slower-growing large cell lung carcinoma cells have a much larger nucleolar area per nucleus [7]. However, most human cells have far fewer active nucleoli. Many questions remain about the mechanisms controlling nucleolar number [51].

In a recent study nucleolar number variation is examined in multiple cell lines. A number of nucleoli even varies within a population of same cell line [51]. Nucleolus number has no correlation with the ploidy of the same cell [51]. Amongst different mammalian species, like a hamster, dog, human, an average number of nucleoli per cell is same [51]. However, the average nucleoli per nucleus vary in different cell lines. For example, U2OS (human bone osteosarcoma) contains six nucleoli per nucleus while T98G (human glioblastoma multiforme) cells have eight nucleoli per nucleus. In the 1960s, it was shown in different mouse tissue sections, nucleoli average number is two to three [51].

The mechanism that controls nucleolus number is still not known. Some studies indicate genetic factor to determine nucleolus number. Another school of thought is the protein-protein interaction between heterochromatin regions of different chromosomes gives rise to coalesce of nucleolus [72].

It is of utmost importance to shed some light on the nucleolus size, shape, and number control mechanism. We must be careful with the fact that inhibition of different steps of ribosome biogenesis although results in disintegrated nucleolus structure and

function but that might not be related to ribosome biogenesis which includes genome stability maintenance. The same reason can promote tumorigenesis as well. Hence, the molecular detailing of signaling networks controlling nucleolus size should be very thoroughly determined.

2.5: Nucleo cytoplasmic transport introduced

2.5.1: The outline of nucleo cytoplasmic transport

The site of exchange of macromolecules between the nucleus and cytoplasm are the nuclear pore complexes (NPCs) [73, 74]. They allow diffusion of small molecules (40 to 60 KD) and active transport of particles with several million Daltons in molecular weight. Active transport is mostly carrier-mediated and bidirectional across the NPCs. The Nuclear Localization Signal (NLS) are one or more clusters of basic amino acids which are responsible for nuclear import of proteins [75]. The import of these proteins containing NLS is one of the most characterized nucleo cytoplasmic pathways. On re-addition of the cytosolic factors into the nuclei of digitonin-permeabilized cells, it was observed that there were four soluble factors which had implications in the nuclear import- Ran GTPase/TC4, Importin α, Importin β and NTF2 [75].

For import of the desired protein, the NLS-protein complex binds to the importin α/β heterodimer in the cytoplasm. Importin α has on one side the NLS binding site and on the other end the importin β binding (IBB) domain. IBB domain is known as the nuclear targeting signal of importin α. Binding of importin β to this IBB domain is enough for efficient nuclear entry. The trimetric complex i.e. the importin α/β-NLS, docks to the cytoplasmic periphery of the NPC via importin β and helps in translocation as a single entity through the NPC. Translocation of this complex terminates by disassembly of the importin α/β-NLS at the nucleo cytoplasmic side of

the NPC followed by the release of importin α and the NLS-protein into the nucleoplasm [75]. This importin heterodimer dissociation occurs due to direct binding of importin β to RanGTPase.

Inactivation of Ran binding site in the importin β leads to failure in termination. The transport intermediates translocate and accumulates in the NPCs nuclear baskets but are not released into the nucleoplasm. That is why Ran GTP to Ran GDP gradient across nucleus to cytoplasm is very crucial for the direction of nuclear transport [76, 77]. Importin β binds to Ran only in its GTP bound state. This Ran-GTP is only generated in the nucleus because of the availability of its guanine exchange factor thereby releasing the NLS cargo and Importin α. This ensures unidirectional import of the protein into the nucleus [76, 77]. Nucleotide hydrolysis takes place in the cytoplasm where the Importin β is dissociated from Ran-GTP and Ran-GDP is formed which in turn is then imported back inside the nucleoplasm by the NTF2; a dedicated transport factor for Ran-GDP, thus encouraging another round of Ran-GTP production & cargo release [76, 77].

In a study in *Xenopus laevis* and *Xenopus tropicalis* involving nuclear scaling, it was shown that nuclear size regulation is affected by nucleo cytoplasmic transport and various cytoplasmic factors. On the other hand, some of these nucleo cytoplasmic factors are expressed in different forms of cancers. Importin beta is observed over expressed in colon, breast, and lung cancers while importin alpha expression is altered in breast cancer and in melanoma [78]. Even truncated form of importin alpha (without NLS binding domain) over expression is associated with p53 accumulation in the cytoplasm in breast cancer cell line [74, 78]. Nucleocytoplasmic transport and cytoplasmic factors are thought to be involved in nucleus size regulation and maintaining homeostasis inside the cell.

Chapter 3:

Aims and Objective

3.1: Statement of the problem

The nucleus size increases from the time of its formation until it reaches its final size in interphase. Moreover, in both budding and fission yeasts, the N/C ratio or KR remains constant throughout the cell cycle. Strong association of nuclear volume and cytoplasmic volumes were observed for many years, this phenomenon is referred to as the karyoplasmic ratio (KR). KR remains constant in widely different DNA content, different growth conditions etc. Existence of karyoplasmic ratio suggests that nuclear size is important for cell function. Alteration in this ratio is associated with certain types of cancer. Importance of nuclear transport to control nuclear size had been shown to be important in yeast and *Xenopus*. On the other hand, nuclear shape alteration is associated with different pathophysiological conditions. Different yeast mutants are documented to be responsible for altered nuclear shape. Different mammalian genes, (other than Lamin) are also reported to be involved in maintaining nuclear shape.

3.2: Hypothesis

This information suggests the existence of an active mechanism that controls the nucleus size that links nuclear and cellular volumes. If indeed such a mechanism exists, does cytoplasmic volume dictate nuclear volume, or does nuclear volume determine cell volume? What cellular factors determine nuclear volume? And finally, why is nuclear volume important? Another important aspect is nuclear size and nuclear shape is controlled by same or different mechanisms? Nuclear shape alteration is always associated with nuclear size alteration or vice e versa?

3.3: Objectives

I. To study the control mechanism of nucleus size and shape in mammalian system

II. To study the control mechanism of nucleus size and shape in yeast system

3.3.1: Detailed Objectives

I. To study the control mechanism of nucleus size and shape in mammalian system

A. To develop an assay system to monitor size and shape of nucleus in live cell condition.

B. Comparative analysis of 3D reconstruction of nucleus and nucleolus size in normal immortalized and corresponding cancer cells.

C. To study the effect of nuclear transport blockage in nuclear and nucleolus size.

II. To study the control mechanism of nucleus size and shape in yeast system

A. To develop an assay system to monitor size and shape of nucleus in live cell condition.

B. Directed mutagenesis in yeast genome to find out genes responsible for nuclear size and shape.

3.4 Work Done

The results and discussion of the work carried out under above mentioned objectives are presented as two chapters with following headings:

Chapter 5: Nucleo cytoplasmic transport perturbation affects size of nucleus and nucleolus in human cells.

Chapter 6: Study to investigate size and shape control mechanism of nucleus in budding yeast system

Each chapter is composed of an introduction, results and discussion.

Chapter 4:

Materials and Methods

4.1: Molecular cloning and bacterial culture

Host strain: E. coli DH5α

Luria-Bertani (LB) (HiMedia) medium: Powdered Luria Broth (20g) was dissolved in 800 ml deionized milliQ (D/W) and the volume was adjusted to 1 liter with milliQ and sterilized by autoclaving. For making LB-agar plates, 20g bacteriological grade agar powder was dissolved/ L sterilized by autoclaving and poured in 90 mm sterile plates.
Antibiotics:
Final Concentrations for ampicillin and kanamycin are 50μg/ml and 30μg/ml respectively.

4.1.1: Preparation of ultra-competent E. coli

Higher competency is very important to ensure high transformation efficiency that often helps in cloning. DH5α was made ultra-competent for the transformation of recombinant/routine plasmid vectors.

Super optimal broth (SOB): Dissolve all the following ingredients in millQ, 2% Bactopeptone (Himedia), 0.5% yeast extract(Himedia), 10mM NaCl(Merck), 2.5mM KCL(Merck), 10mM MgCl2, 10mM MgSO4 and autoclave to sterilize.

SOC media: To 98ml of sterile SOB, add filter sterilized 2M glucose and autoclaved 2M Mg.

Transformation buffer (TB): 100 ml of D/W; 10 mM PIPES(Sigma), 15 mM $CaCl_2$, 250 mM KCl, adjusted pH to 6.7 with 5N KOH, 55 mM $MnCl_2$, filter sterilized through 0.2 μ membrane filter.

Method:

E. coli DH5α cells are streaked on LB agar plate and incubated overnight at 37^0C. Single colony is inoculate in 250 ml SOB medium and incubated on refrigerated shaker incubator with 200 RPM at 18^oC until OD_{600} reaches to 0.6. Incubate the flask on ice for 10 minutes and spin the culture at 2500g (3500 RPM) for 10 minutes at 4^oC. Resuspend the cells very gently in 80 ml of ice cold transformation buffer and again keep on ice for another 10 minutes. Spin the mixture at 2500 x g (3500 RPM) for 10 minutes at 4^oC. Resuspend the cells gently in 20 ml of ice cold transformation buffer. Incubate on ice for 10 minutes. Add DMSO to a final concentration of 7% (1.4

ml) and mix by pipetting up and down. Aliquot100µL of cells in a tube and freeze the vial in liquid nitrogen and store at -80^{o}C.

4.1.2: Bacterial Transformation[79]

Take out 100µL aliquots of ultra-competent cells from -80˚C and thaw in ice. Add 10 µl (50-100 ng) of DNA to 100µl thawed competent cells (avoid disturbing cells by pipetting rather tap the tube gently). Incubate on ice for 30 minutes. Give heat shock to the vial by keeping in 42^{o}C water-bath for 45 seconds. Place on ice immediately for 5 minutes. Add 200µl of ice cold SOC medium to the vial aseptically. Incubate 37^{o}C with shaking at180 RPM for 60 minutes. Plate the cells on appropriate antibiotic containing LB agar plate. Incubated at 37^{0}C for 12-16 hours to appear colony.

4.1.3: Plasmid DNA isolation

Plasmid DNA was isolated by various methods.

4.1.3.1: QIAprep Spin Miniprep method

Reagent- Qiagen miniprep kit, as per manufacturer's protocol.

QIAprep Spin Columns contain a unique silica membrane that binds up to 20 µg DNA in the presence of a high concentration of chaotropic salt and allows elution in a small volume of low-salt buffer.

Inoculate a single colony in10ml of LB-amp/ LB-kan media and incubate at 37^{o}C for 12-16 hours at 180 RPM bacterial shaker incubator. Transfer the bacterial culture in a 15 ml tube and spin at room temperature for 5 minutes at 5000 RPM. Vortex the pellet briefly and then resuspend in 250µl of Buffer P1 and transfer to a micro centrifuge tube (Ensure RNase A has been added to Buffer P1). Add 250µl of buffer P2 and invert the tube 4–6 times. Immediately add 350µl of buffer N3 and again

invert the tube 4–6 times. Spin the lysate at 13,000RPM for 10 minutes. Add the clear supernatant very carefully to the QIAprep spin column. Spin the column for 30–60 seconds and discard the flow-through. Add 600µl of buffer PE to wash the QIAprep spin column and again spin for 30–60 seconds. Discard the flow through. Wipe the column from outside so as to remove any residual buffer PE. Then place the column in a dry tube and spin at 13000 RPM for 2 minutes to remove any residual wash buffer. Now, place the QIAprep column in a clean 1.5 ml microcentrifuge tube. Add 50µl Buffer EB (pre warmed at 50˚C) to the centre of QIAprep spin column, let it stand for 2 minutes. Centrifuge for 2 minutes at 14000 RPM to elute Plasmid DNA.

4.1.3.2: Plasmid DNA isolation using TELT buffer

This is a quick and cost effective protocol for preparing plasmid DNA which was mainly used during regular screening for positive clones in all the cloning experiments.

TELT buffer [50mM TrisCL (Sigma) pH7.5, 62.5mM EDTA(Fischer Scientific) pH8, 0.4% Triton X100(Sigma), 2.5M LiCl (Sigma)], Lysozyme (Sigma) (50mg/ml), 70% ethanol, Absolute alcohol (Merck), TE buffer.

Inoculate bacterial culture in 1.5ml LB-antibiotic (Amp/ Kan) media and incubate at 37^{o}C, for 12-16 hours at 200 RPM. Spin cells at 14000 RPM for 1 minute at 4^{o}C to pellet down cells. Discard the supernatant; resuspend the pellet in 150µl TELT buffer and vortex briefly. Add 5.7µl lysozyme (Stock 50mg/ml) to the same and mix well. Incubate the vial on ice for 1 minute. Incubate the vial in boiling water bath for 1 minute. Immediately place the vial on ice for 10 minutes. Spin at 4^{o}C at 15000 RPM for 10 minutes and collect supernatant in a new vial. Add 330µl chilled absolute alcohol and incubate at -80^{o}C for 30 minutes. Spin at 4^{o}C at 15000 RPM for 10

minutes. Add 200µl chilled 70% ethanol for washing the DNA pellet and again centrifuge at 15000 RPM at 4^{o}C for 5min.

Dry the pellet so as to remove all remaining alcohol and re-suspend in 20µl TE buffer.

4.1.3.3: Plasmid DNA isolation by Cesium Chloride (CsCl) equilibrium density gradient centrifugation:-

It is very important to get high quality plasmid DNA to transfect the mammalian cells with high efficiency. CsCl equilibrium density gradient centrifugation yields very pure plasmid DNA preparation which is completely free from salts, broken fragments.

Materials:

Solution I: 50 mM Glucose (Sigma), 25 mM Tris.Cl (pH 8.0), 10 mM EDTA.2H2O; D/W to make up the total volume;

Solution II: freshly prepare 0.2 N NaOH (Sigma), 1% SDS (Sigma); D/W to make up the total volume;

Solution III: 5M Potassium Acetate (Sigma) 60 ml, Glacial acetic acid (Merck)11.5 ml, D/W 28.5 ml; Tris/EDTA (TE) pH 8.0; Cesium chloride (Himedia): 1 g/ml in TE buffer; isopropanol (Merck),

Ethidium bromide (Himedia): 10 mg/ml in D/W

Method:

Spin 500 ml culture at 5000 rpm for 10 minutes in a sorvall centrifuge GS-3 at 4^{0}C.

Discard the supernatant and re-suspend the pellet in 18 ml of solution I, keep vortexing. Add 2 ml of lysozyme solution and mix properly. Add 40 ml of freshly prepared solution II, mix by inverting slowly followed by incubation at room temperature for 10 minutes. Add40 ml of ice chilled solution III, mix by inversion and store on ice for 10 minutes. Spin the tubes at 5000 RPM for 15 minutes at 4^{0}C in (rotor- sorvall SS-34). In the meantime, prepare TE buffer. Filter the supernatant into HS 50 tubes by passing through gauze (4 fold). Add 0.8X volume of isopropanol to each tube. Incubate at room temperature for 10 minutes, then spin at 8000 RPM for 15 minutes (rotor-SS-34 sorvall). Wash the pellet with 70 % alcohol (5 ml in each tube).

Spin at 8000 RPM for 10 minutes at 4^0C. Dissolve the properly in 8.5 ml of 1X TE buffer. Add 8.5 grams of cesium chloride (CsCl) to each tube. (Dissolve CsCl properly). Add 0.25 ml (Stock 10mg/ ml) of ethidium bromide mix properly. Spin at 8000 RPM for 5 minutes at 4^0C. Load the mixture in ultracentrifuge tubes, sealed and balanced and then centrifuged at 60, 000 RPM for 22 hours in an ultracentrifuge. After the run ends, prick the tube on top of the tube by 23 G needle very carefully. Using 18 G needle, pull the band of covalently closed circular DNA. Release the band from in a 15 ml tube. Add Equal volume of water saturated butanol and vortex briefly. Spin at 3000 RPM for 2 minutes. Repeat this step, until pink color completely goes away, also both layers should be completely colorless. Add 2 volume of sterile dH_2O and 6 volume of 100% alcohol to DNA solution (2ml DNA solution + 4ml dH_2O + 12ml 100 % ethanol) in new T50. Incubate at 4^oC for 30 minutes to 1 hour followed by Spin at 8000 RPM for 20 minutes at 4^oC. Wash the DNA pellet with 70% alcohol and spin at 8000 RPM for 15 minutes at 4^oC. Discard the supernatant and invert the tube on tissue paper. (Dry the pellet completely until no alcohol smell remains). Dissolve the DNA pellet in ~500µl of TE.

4.1.4: Agarose gel electrophoresis

Agarose gel electrophoresis is routinely used method for the analysis and preparation of DNA molecules. Various size DNA fragments can be separated on agarose gels using different concentrations of agarose.

Ethidium bromide 0.5 µg/ml

6X Gel loading dye**:** 1.2ml glycerol, 1.2ml 0.3mM EDTA, 300µl of 20% SDS, 160 µl of 0.5% Bromophenol blue stock, nuclease free water to make volume to 10ml

Sodium Borate (SB) buffer: 10mM NaOH pH 8.5 adjusted with boric acid for 1X SB buffer.

Weigh agarose powder as per requirement of percentage of gels (depends on the size of DNA fragments), for example to make a 0.8% agarose gel, add 0.48g of agarose powder in a glass flask, to which add 60ml of 1X sodium borate (SB) buffer. Microwave the mixture for 2 minutes so that agarose powder melts and get dissolves. Allow the boiling mixture to cool down so as to add ethidium bromide (to visualize DNA) at a final concentration of 1µg/ml (stock 10mg/ml). Mix well without creating bubbles and pour the mixture to the gel tray, place comb to create wells. Once the gel is solidified, remove comb. Pour 1X SB buffer (running buffer) to the tank containing agarose gel. Dilute DNA sample (Plasmid DNA, PCR fragments, restriction digestion fragments, ligated DNA) with 6X gel loading dye (to make a final concentration 1X). Standard 1Kb or 100bp ladders were run in parallel to understand the size of DNA fragments being analyzed. DNA bands were visualized using gel documentation system.

4.1.5: cDNA synthesis

For cloning Human Ran, Importin beta in pCMV-3x-Flag vector, Exons of the then were amplified from cDNA made from total human RNA (Sigma) using cDNA synthesis kit of Invitrogen.

Add the following components to a nuclease free micro-centrifuge tube.

	Reagent	**Amount**
1	Oligo $(dT)_{20}$ (50µM)	1µL
2	Total RNA (10pg to 5 ug)	1µL
3	10mM dNTP mix	1µL
4	DEPC treated water	13 µL

Table 4.1: Contents of cDNA synthesis step I

Heat the mixture to 65C for 5 minutes followed by incubation on ice for 1 minute. Briefly centrifuge the content and add following components

	Reagent	Amount
1	5X first strand synthesis buffer	4 µL
2	0.1M DTT	1 µL
3	RNase OUT(recombinant RNase inhibitor)	1 µL
4	Superscript III Reverse Transcriptase (200 Units)	1 µL

Table 4.2: Contents of cDNA synthesis reaction step II

Mix by pipetting gently up and down, if using random primers incubate tube at 25˚C for 5 minutes. Incubate at 50˚C for 50 to 60 minutes. Inactivate the reaction by heating at 70˚C for 15 minutes. The cDNA can now be used for any PCR amplifications (either for cloning or expression analysis). To remove RNA complementary to the cDNA, add 1 of *E.coli* RNase H and incubate at 37˚C for 20 minutes.

4.1.6: Polymerase chain reaction (PCR)

The PCR technique provides specific DNA amplification of the sequence of interest from a template (yeast genomic DNA / plasmid DNA /cDNA) with the help of two oligo nucleotide primers that bind to opposite strands in a sequence specific manner. A thermostable DNA polymerase is used for extension of the primers at 3’ end. Phusion high fidelity DNA polymerase was used for PCR amplifications.

1. A typical mixture of a PCR reaction includes following additives:

	Components	Final concentration
1	H_2O	To make up volume
2	5X buffer HF/GC	1X
3	10mM dNTP mixture	200µM
4	Forward primer	0.5µM
5	Reverse primer	0.5µM
6	Template DNA	50ng (Plasmid DNA) 100ng (Genomic DNA or cDNA)
7	DNA polymerases	0.02 U/µl

Table 4.3: Contents of a PCR reaction

Thaw all the samples on ice and add all the reagents as per the order stated in the table above followed by short spin the PCR tube after addition of all the components. Transfer quickly to the thermo cycler preheated to the denaturation temperature (98°C) so as to start the reaction.

Typical PCR cycle:

Cycle step	Temperature	Time	Cycles
Initial denaturation	*98°C*	*3 minutes*	*1*
Denaturation	*98°C*	*30 seconds*	
Annealing	*Lower Tm+3*	*30seconds*	*30-34*
Extension	*72°C*	*60 seconds /Kb*	
Final extension	*72°C*	*8 minutes*	*1*
Final hold	*4°C*	*Forever*	

Table 4.4: Cycling conditions for PCR using Phusion DNA polymerase

Check the PCR product on agarose gel.

4.1.7: Quick change mutagenesis[80]

Quick change mutagenesis was used to introduce either point mutation or insertion or deletion of few bases in a gene of interest with the help of high fidelity Pfu Turbo polymerase. Prepare a oligo mix by mixing 5µl of each forward and reverse primer (from 100µM stock) and 40µl of ddH_2O (1:10 dilution). Template concentration should be between 40-60 ng/µl.

The reaction was set up as follows:

Components	Volume (µl)
H_2O	15.3
10X buffer for Pfu Turbo	2
10mM dNTPs	0.4
Primer mix (1:10 dilution)	0.4
Template DNA (40ng/µl)	1
Pfu Turbo polymerases	0.4 (20U)

Table 4.5: Contents of PCR reaction for site directed mutagenesis

Cycling conditions for quick change mutagenesis:

Cycle step	Temperature	Time	Cycles
Initial denaturation	*95^oC*	*30s*	*1*
Denaturation	*95^oC*	*30s*	
Annealing	*55^oC*	*60s*	*18*
Extension	*68^oC*	*2min/Kb*	

Final extension	*68^{o}C*	*8min*	*1*

Table 4.6: Cycling conditions for PCR for site directed mutagenesis

4.1.8: Gene Cloning[81]

In gene cloning, plasmid DNA is cleaved with one or more RE in order to get blunt/cohesive ends and then foreign DNA fragment of variable sizes with compatible ends are ligated. The ligated heterogeneous mix is then transformed into a suitable bacterial host to propagate the clones. The resulting transformed recombinant clones are then screened by RE digestion to confirm the recombinant clone. Different strategies are used to clone fragment of DNA in a plasmid vector, for example PCR based cloning, sticky end based directional cloning etc.

4.1.8.1: Restriction Digestion

Restriction enzymes or restriction endonucleases cut at a specific site in the template DNA. The components of preparative and analytical restriction digestion reaction were as follows:

Components	Preparative	Analytical
Plasmid DNA	1 µg	100ng
H_2O	To make up volume to 50µl	To make up volume to 10µl
10X buffer	5µl	1µl
BSA	If required	If required
Enzyme	5U (1µl)	1U (0.2µl)

Table 4.7: Reaction mix for restriction digestion

1. Add all the components in a micro centrifuge tube.

2. Add the enzyme in the end.

3. Briefly vortex the tube followed by short spinning the tube.

4. Incubate the tube at 37˚C for 2-4 hours in a water bath (or, at any other temperature if mentioned specifically for a particular enzyme).

5. For any vector preparation in a cloning method, add 1 µl alkaline phosphatase (FastAP) (NEB) in the reaction tube and incubate for another 1 hour (Alkaline Phosphatase removes the 5'-phosphate groups of DNA from both the termini of digested vector so as to avoid the self-ligation of the vector).

6. Analyse the digested DNA fragment on agarose gel.

4.1.8.2: Purification of restriction digested DNA or PCR product

For cloning of digested DNA fragments (either vector or insert), it is very important to purify them to remove nucleotides, primers, enzymes, mineral oil, salts, agarose, ethidium bromide, and other impurities from DNA samples before setting up ligation reaction.

Nucleotide removal kit (Qiagen), Gel extraction kit (Sigma)

QIAquick Nucleotide Removal Kit was used to remove DNA impurities during all cloning procedures. Columns contain a silica membrane assembly for binding of DNA in high-salt buffer and elution with prewarmed water. The protocol is as follows-

Add 5 volumes of Buffer PN to 1 volume of the reaction sample and mix them homogeneously. Transfer the mixture in a QIA quick spin column, placed in 2 ml

collection tube. Centrifuge the tube for 1 min at 6000 RPM, discard the flow-through. Add 600µl of buffer PE to the column and centrifuge for 1 min at 6000 RPM. Discard the flow through. Wipe the column from outside so as to remove any residual buffer PE. Then place the column in a dry tube and spin at 13000 RPM for 2 minutes to remove any residual wash buffer. Now, place the column in a clean 1.5 ml micro centrifuge tube. Add 50µl pre warmed (at 50˚C) autoclaved water to the centre of the column, let it stand for 2 minutes, and centrifuge for 2 minutes at 14000 RPM to elute pure DNA. To increase the concentration of the pure DNA, freeze the DNA by keeping the eppendorf tube at -80˚C for 20 minutes, once frozen, then concentrate the DNA in a Speed Vac at 4˚C until the volume reduces]

4.1.8.3: Purification of DNA fragments from agarose gel

For cloning of digested DNA fragments (either vector or insert) or to get any pure PCR product, sometimes DNA bands of specific size had to be cut from agarose gel followed by removal of agarose from DNA samples before setting up ligation reaction. GenElute Gel Extraction Kit (Sigma) was used to purify DNA fragment from agarose gels. Place the agarose gel containing DNA band of interest in a gel doc machine under UV light to visualize DNA. Cut the DNA band from the gel using sharp scalpel pre sterilized with 70% alcohol (Remove as much as excess agarose to increase the yield). Make small pieces of the DNA band and place them in an eppendorf. Add 3 volume of the Gel Solubilisation Solution to the gel slice. (For every 100mg of agarose gel, added 300 ml of Gel Solubilisation Solution). Incubate the gel mixture at 60°C for 10-15 minutes with intermittent vortexing. In the meantime, add 500 ml of the column preparation solution to the binding column and centrifuged for 1 minute. Discard the flow through. Add 1 gel volume of 100%

isopropanol and mix homogenously. The solubilized gel solution mixture was then added to binding column and centrifuged for 1 minute at 6000rpm. The flow through liquid was discarded. Add 600µl of buffer PE to the column and centrifuge for 1 min at 6000 RPM. Discard the flow through, Wipe the column from outside so as to remove any residual buffer PE. Place the column in a dry tube and spin at 13000 RPM for 2 minutes to remove any residual wash buffer. Now, place the QIAprep column in a clean 1.5 ml micro centrifuge tube. Add 50µl pre warmed (at 50˚C) autoclaved water to the centre of the column, let it stand for 2 minutes, and centrifuge for 2 minutes at 14000 RPM to elute pure DNA. [To increase the concentration of the pure DNA, freeze the DNA by keeping the eppendorf tube at -80˚C for 20 minutes, once frozen, then concentrate the DNA in a SpeedVac at 4˚C until the volume reduces]

4.1.8.4: Ligation reaction

DNA ligase enzyme creates a phoshphodiester bond between a 5'- phosphate termini and a 3'- hydroxyl group of two different DNA fragments and ligates the vector and insert DNA.

Method-

Components	Molar ratio	Concentration (µg/µL)	Length (in base pair)	Max Volume
Vector	1	x µg/µL	Size in bp	Available vol
Insert	3	y µg/µL	Size in bp	Available vol

Table 4.8: Typical Ligation Reaction Calculation

Measure the concentration of purified vector and insert DNA fragments. The typical ratio of vector: insert used was 1:3 which can vary depends on the size of either vector

or insert. Calculate the amount of vector and insert fragment required to achieve 1:3 molar ratio as per the following table in any insilico ligation calculator.

Add the components of ligation reaction as mentioned in the following table-

Components of ligation reaction	**Total volume (10 µL)**
Nuclease free water	To make up volume
10X T4 DNA ligase buffer	1 µL
Vector	As calculated from the above table
Insert	As calculated from the above table
T4 DNA Ligase	200U

Table 4.9: The Components of Ligation Reaction

Always set up a positive control (any plasmid DNA of same concentration without vector and insert, to check if transformation worked) and a negative control (another ligation mixture without insert fragment). Incubate the reactions at 22°C for 2-4 hours or at 16°C for overnight. Transform all the three reaction mixture in E. coli cells and check for positive clones

4.1.8.5: Screening of recombinant bacterial clones

Clones have to be screened for presence of the specific insert. If the test plate contains more colonies compare to the negative control plate, then only proceed for clone screening. Ideally, in negative control plate, there should not be any colonies.

Method-

Replica plate transformants on LB-Amp or LB-Kan plates and inoculate in 1.5ml antibiotic containing LB broth. Incubate eppendorf tubes at 37^0C for 12-16 hours at

200 RPM. (Each clone was given a specific miniprep number for documentation). Following day, isolate plasmid DNA using TELT buffer protocol. Set up restriction digestion for the clones along with vector control DNA in which one restriction enzyme present in the vector DNA and another enzyme is present in the insert DNA to confirm presence of insert in the final clone. Analyze the digested fragment in agarose gel electrophoresis.

4.2: Mammalian Cell Culture Techniques

4.2. Methods used in mammalian cell line studies:

4.2.1.1: Daily Observations of Cell Culture of following

Cell morphology
pH of the media
Incubator setting and levels of CO_2 and temperature
Water level in the tank inside incubator

When to Subculture Cells?

Cells covered the entire surface available for growth
Color of media if became yellow (pH became acidic)
Cells are saturated the buffering capacity of media with the by-products of their metabolism
Sometimes change of medium is enough if they used nutrients but did not outgrow the surface area; Cell morphology changes in such conditions.

Cell cultures are described based on two parameters**:-**

Origin of the cells – All are established cell lines (No primary culture)
Manner of growth– All are epithelial cells and adherent growth

Do's and Don'ts for Cell Culture**:-**

Never culture two cell types at the same time.

Keep the media clearly labeled with the – Name, Date and if specific for any particular cell line. Pre-warm all media in 37^{o}C water bath.

Wipe all surfaces and bottles with 70% alcohol before starting.

UV sterilize laminar hood every time before and after use of cell culture.

Always wear gloves.

Name	Tissue origin	Medium
HeLa	Human Cervical epithelial transformed	DMEM
HaCaT	Human skin epidermoid immortalized	DMEM
A431	Human Skin epithelial transformed	DMEM
Int407	Human Intestine epithelial immortalized	DMEM
HCT116	Human colon epithelial transformed	DMEM
HHL5	Human liver epithelial immortalized	DMEM
HepG2	Human epithelial Transformed	RPMI
MCF10A	Human mammary epithelial immortalized	DMEM+ F12
MCF7	Human mammary epithelial Transformed	DMEM

Table 4.10: Cell lines

4.2.1.2: Reviving Cells from Frozen Stock

Dulbecco's Modified Eagle Medium (DMEM) :13.5gpowdered medium was dissolved in~900 ml autoclaved distilled water, supplemented further with 3.7 g sodium bicarbonate (NaHCO3). pH was adjusted to 7.1-7.2 with concentrated HCL or 0.5N NaOH and volume made up to 1 L. The medium was filtered through 0.22 µ sterile filter and stored at 4°C.
Complete medium (CM): DMEM supplemented with 10% FBS and 1% antibiotics [Anti-bacterial Anti-mycotic (Gibco)], was prepared as needed

Method-

Thawing and recovery of cells from liquid nitrogen must be done quickly. Media are pre-warmed by keeping at 37^{o}C.

Cryovial is removed from liquid nitrogen and immediately placed in 37°C water bath. (Note: Be very careful while removing cryovial from cylinder, box should be removed very slowly, remove individual vial by using forceps, wait until the fumes from vial are completely gone, then place the vial in incubator, otherwise vials sometimes burst). Transfer the vial into the laminar hood. Before opening, wipe outside of the vial with 70% ethanol. Transfer the thawed cell in pre-warmed 10ml medium (DMEM + 10% FBS + 1% Antibiotic) kept in 90mm petri dish. Gently add the cells (aliquot entire vial content in plate at high density to optimize recovery) and incubate at 37°C in a CO_2 incubator. After 12 hours, ensure cells are attached. Change culture media to remove non-adherent cells and replenish nutrients. Changing the culture media will also remove any DMSO residues.

4.2.1.3: Cell passaging

Phosphate buffered saline (PBS): NaCl-8.0g, KCl-0.2g, KH_2PO_4-0.24g, Na_2HPO_4. $2H_2O$-1.44g dissolved in 1L distilled water; pH was adjusted to 7.4 and sterilized by autoclaving.

Trypsin–EDTA: EDTA disodium salt-0.01g, D-glucose-0.1g, KCl-0.04g, NaCl-0.8g, $NaHCO_3$-0.058g, Trypsin-0.025g, pH was adjusted to 7.2 and volume made up to 100ml, Sterilized by passing through 0.22µ sterile filter and stored at 4°C.

Method-

Place plates or T25 flasks in hood from the incubator. Attach an aspirating pipet to the tube attached to vacuum. Turn on vacuum system by opening vacuum valve in hood. Using the aspirator, liquid media covering the cells, is sucked out. Add 5 ml of 1X PBS to cells and wash cells very gently by swirling the flask gently followed by aspirating PBS. Add 2 ml trypsin-EDTA to cells. Incubate flask at 37˚C incubator for 2-5 minutes. (Trypsin is highly active, relatively non-specific, used in concentration of 0.05 to 0.25 %, cleaves proteins on the cell surface and extracellular matrix,

removes adhesion molecules, EDTA is added to enhance the activity of trypsin, Ca 2+ chelator, removes calcium and causes cell rounding, cell adhesion through cadherins and selectins is calcium dependent, low calcium causes cells to internalize adhesion molecules, rounding or detachment). Check cells under microscope to confirm that cells are detached from the surface. Add 10 ml of complete media (Supplemented with serum) to deactivate trypsin. Carefully re-suspend cells. Transfer cell suspension in 15 ml centrifuge tube. (Important: Label tube). Centrifuge cells for 4 min at 500 RPM. In the meantime, pipet appropriate volume of fresh media into new T flasks or plates as needed. Label with name, date, cell type, passage number and passage dilution (Very important). After centrifugation, aspirate supernatant. Cell pellet should remain at base of tube. Resuspend cells in 1 ml media. Aliquot appropriate volume of cell suspension into freshly prepared T flasks with media. Swirl media and cells to mix and keep the flask/plates in 37˚C CO_2 incubator. Dispose of liquid and solid biohazards wastes properly. Clean hood with ethanol.

4.2.1.4: Freezing of cell line

Freezing Medium- 90% Serum + 10% DMSO

Method- Before starting with cell harvesting, label the cryovial properly and arrange in the hood.

Seed the cells in T75 flask and harvest when cells are 80% confluent. (Cells should be healthy and over 90% cells should be viable). Pellet down cells as mentioned in previous section at step 10. Remove supernatant and resuspend the cells in cold 2.7ml serum. Make single cell suspension ($1x10^6$ cells per ml). Just before adding to cryovial, add 300µl of DMSO to the cell suspension and pipette up and down gently to ensure single cell suspension. (DMSO is toxic to cells, so should not be exposed to

the cells at room temperature for any longer than necessary, from this step to step 6should be completed as soon as possible). Make aliquots of 1 ml of the cell suspension into each cryovial. From one T75 flask with 80% cell confluency, 3 cryovials should be made. Place the cryovials in an isopropanol chamber chiller and store them at –80°C for overnight. Next day, transfer frozen cells to liquid nitrogen cylinder in a properly labelled box. (Maintain a record of cryovials for each cell line, kept inside the liquid nitrogen cylinder)

4.2.2: Transfection of DNA in different cell lines

X-tremeGENE HP DNA Transfection Reagent (Roche)/ Lipofectamine 2000 reagent (Invitrogen) were used for all the transfection.

We seeded cells in 50-60% confluency so as to achieve healthy and well spreaded cells for imaging experiments.

Seed cells in glass bottom chamber (35mm dish) the day before, for all the imaging experiments. Dilute required DNA and transfection reagents in 2 different tubes containing 100 µl of incomplete media (DMEM medium without serum and antibiotic) each. (DNA concentrations, used in different experiments are enlisted in table 4.11; X-tremeGENE HP DNA Transfection Reagent/ Lipofectamine 2000 reagent were used in 1:2 DNA to transfection reagent ratio). Incubate two tubes separately for 5-10 min at room temperature. Mix both the diluted DNA and transfection reagent together from two different tubes and incubate for another 30 minutes. Add 200 µl of the mixture to the glass bottom chamber drop wise. Mix gently and incubate the dish in CO_2 incubator for 12 hours. Change the media of the

plate after 12 hours with complete DMEM media. Add 2 ml of pre warmed Phenol-red free DMEM media to 35mm glass bottom chamber petri dish just before imaging.

	DNA	Concentration used
1	GFP-Lamin	400ng
2	F-mCherry	100ng
3	RFP-Lamin	400ng
4	GFP Fibrillarin	100ng
6	Importin beta/ Ran	1000ng
7	Importin beta 1-364/ Ran T24N/Ran Q69L	1000ng

Table 4.11: Different DNA concentrations used in this study

4.2.3: Cell synchronization at G1/ S phase by double thymidine block [82]

Thymidine blocks DNA synthesis by inhibiting the synthesis of specific nucleotides resulting in a reversible arrest in S phase with partly synthesized DNA. Synchronizing cells using double thymidine involves two sequential exposures of high levels of thymidine, with each exposure separated by a time interval determined from the knowledge of the normal cell cycle distribution of the exponentially growing cells and the recovery time for the thymidine block. Cells were plated cells at 40-50% confluency in a 35mm tissue culture dish. Next day, add Thymidine to a final concentration of 2mM (Stock 100mM). Incubate cells for 16 hours in incubator (During this stage the G2/M cells will progress to G1 and then with the original G1 population acquire a biochemical state equivalent to G1/S border, cells already in S phase will be blocked in the same upon addition of thymidine). After 16 hours,

remove thymidine by washing with 1X PBS (wash twice gently to remove any trace amount of thymidine) and add fresh media. Incubate for 8 hours in incubator in thymidine free media (During this time, cells will progress through cell cycle and enter in G1 phase of the next cycle. Entry into G1 of the next cell will commence with the cells that were blocked at the end of S phase. Entry into G1 of the next cell cycle end with the lagging edge cells (those arrested at G1/S) progressing through the cell cycle and dividing between 16 hours) (Transfection can be done in this time interval if required). After 8 hours, add thymidine to final concentration of 2mM again and incubate for another 22 hours. At 22ndhour, cell will be ceased at G1/S stage. Release cells from this block by washing with 1X PBS and adding fresh DMEM. Imaging experiments were done in blocked condition.

4.2.4: FACS (Fluorescence activated cell sorter) analysis [83, 84]

The DNA-binding dye propidium iodide (PI) is very well used to stain DNA of mammalian cells, in which it binds to DNA in stoichiometric manner (bind in proportion to the amount of DNA present in the cell). Thus, cells that are in S phase will have more DNA than cells in G1 and cells in G2 will be approximately twice as brighter than cells in G1.

Cell are seeded for synchronization as described earlier, and harvested after last thymidine block ends. Wash cell pellet (From one 35mm plate) with 400µl of 1X PBS and spin at 2000 RPM for 5 minutes. Resuspend cells in 250µl of 1X PBS and make single cell suspension. Fix cells with 1ml 70% ethanol (While fixing cells, tube containing cells should be kept on vortex and ethanol should be added drop wise to ensure homogenous fixation). At this stage cells can be stored at -20ºC for 3-4 months or store at 4ºC overnight for immediate use. [Alcohol is a dehydrating fixative which

also permeabilizes]. Next day, spin cells or 5minute at 2000RPM. Wash with 1X PBS twice to remove all ethanol contents. Resuspend cells in 500 of 1X PBS, vortex to single cell suspension.Pass cells through needle to ensure single cell suspension. Add 0.1% Triton X-100 (500µl) [permeabilizes cell, at this stage cells cannot be stored for as long as fixed ones and should be processed within hours], resuspend. Add 10µg/mL RNase A. Incubate for 30 minutes at 37˚C. Add propidium iodide 25µg/mL final concentration (Stock 10mg/ml). Incubate another 10minutes at 37˚C in dark. Cell is ready to be analysed in FACS machines (Carry cells by wrapping tubes in foil paper).

4.2.5: Invasion Assay [85]

Invasion assay was performed for HaCaT and A431cells and upon dominant negative over expression on HaCaT cells. Standard in vitro invasion assay in which cells migrate through Matrigel towards 10% serum (chemo attractant) was used.

Before cell seeding, add Matrigel to inserts (Boyden chamber) and incubate in 37ºC incubator for an hour. Seed 50,000 cells; resuspended in DMEM with 0.2% FBS in rehydrated Matrigel-coated inserts (8µm pore size inserts). Place the inserts in 24-well companion plates with DMEM and 10% FBS in the bottom chamber. After 24 h, 4µg/ml calcein AM was added in the bottom chamber and incubated for 1 hour at 37°C, 5% CO_2. Remove the non-invading cells in the upper surface of the membrane using a cotton tip. Take reading of fluorescence of invaded cells at wavelengths of 494/517 nm (Excitation/ Emission) on a bottom-reading fluorescent plate reader. The graph was prepared by plotting absorbance at 494/517nm (Excitation /Emission). [Calcein AM is internalized by the cells, and intracellular esterases cleave the

acetomethylester (AM) moiety. Free Calcein fluoresces brightly and is used to quantitate the number of cells that have invaded or migrated.]

Or after step5, Stain the insert with DAPI and take images for DAPI filter under 20X objective for 5 different fields.

4.2.6: Isolation of pure nuclei from cells [86]

Lysis buffer for nuclei isolation:
0.25 M sucrose, 50 mM Tris-Cl pH7.5, 25 mM KCl, 5 mM MgCl2, 0.1% Triton X-100, 0.2 mM PMSF, 0.2 mM protease cocktail inhibitor

Nuclei buffer:
0.34 M sucrose, 15 mM Tris-Cl pH7.5, 60 mM KCL, 15 mM NaCl, 2 mM EDTA, 0.5 mM EGTA, 0.15 mM bME, 0.15 mM spermine, 0.15 mM spermidine)
Method-

Seed cells in 90 mm petridish in a confluency of 50-60%. Transfect cells with nucleolus marker and other gene of interests. 48 hours post transfection, harvest cells in 2 ml chilled 1X PBS. Spin cells at 2000 RPM for 10 minutes at 4°C. Discard the supernatant and resuspend the pellet again in 2 ml chilled 1X PBS.. Centrifuge at 2000 RPM for 10 minutes at 4 °C. Discard the supernatant and add 2 ml chilled lysis buffer to the pellet, incubate for 10-15 minutes on ice. Vortex cells intermittently. Check under microscope if cells are lysed properly. If cells are not lysed increase the incubation time in lysis buffer. (It takes almost 30 minutes for proper lysis). Add 1% NP40 and vortex at high speed for 15 seconds. Centrifuge at 10000 RPM for 10 minutes at 4 °C. Nuclei will be pelleted and supernatant contains the cytoplasmic fraction. Quantify the protein in the supernatant (cytoplasmic fraction). Resuspend the pellet in 200 µl of Nuclei Buffer. Pure nuclei can be checked with DAPI staining under microscope.

4.2.7: SDS PAGE and Western Blotting

4.2.7.1: Protein Estimation

Protein estimation was done using Bradford's reagent as per manufacturer's protocol using BSA (1mg/ml stock)

Add 1ml (1:4 diluted) Bradford reagent to each reaction. Incubate samples for 10 minutes at room temperature.Take reading of optical density of samples at 595nm along with blank and standard curve is plotted. Use 5µl of lysate for determination of protein concentration with reference to standards.

4.2.7.2: SDS-PAGE[87]

SDS-PAGE enables to separate proteins on the basis of their size and charge.

30% Acrlyamide solution: 29g Acrylamide and 1g Bis-acrylamide(USB) were dissolved in distilled water on a magnetic stirrer overnight (O/N) at room temperature; The volume was made up to 100 ml and filtered through 0.45 µm filter and stored in a dark bottle at 4^{o}C.

6X sample loading buffer: 50mM Tris.Cl (pH 6.8), 10% glycerol, 2% SDS, 1% β-mercapto-ethanol (BME) 0.1 % bromophenol blue.

Electrophoresis buffer: 25mM Tris base, 250 mM Glycine (pH 8.3) and 0.1% SDS

Method: The resolving gel of 10% and 18% was made according to following table:

Pour the resolving gel keeping space for the stacking gel. Add water gently over the resolving gel to avoid oxidation and allow the gel to solidify completely for ~20 min. Add the stacking mix over resolving gel after decanting the water layer and insert the comb. Remove the comb after gel polymerization; clean the wells with running buffer.

Component	Volume for 8 ml (10%)	Volume for 8 ml (18%)
H_2O	3.2 ml	1 ml

30% Acrylamide mix	2.67 ml	4.8 ml
1.5M Tris pH 8.8	2 ml	2 ml
10% SDS	80 µl	80 µl
10% APS	80 µl	80 µl
TEMED	8µl	

Table 4.12: Reaction mixture of resolving gel of SDS PAGE

Component	**Volume for 5 ml (4%)**
H_2O	3ml
30% Acrylamide mix	0.67 ml
1M Tris pH 6.8	1.25 ml
10% SDS	50µl
10% Ammonium per sulphate	50µl
TEMED	5µl

Table 4.13 Reaction mixture of a stacking SDS PAGE gel

Place the gel in the tank and add running buffer to the appropriate level. Dilute protein samples in a sample buffer according to the amount of protein to be loaded on to the gel. Boil the samples for 5 minutes, centrifuge and load on gel. Load pre-stained protein molecular weight marker along with the test samples in defined order. Run the gel at constant voltage of ~180V.

4.2.7.3: Wet transfer of proteins on PVDF membrane

Wet transfer method is used to transfer proteins separated on SDS-PAGE onto PVDF membrane for further analysis by immunoblotting.

High Glycine transfer buffer: 0.1M Tris, 0.19M Glycine, 20% methanol, 0.04% SDS.

Remove the resolving gel from the electrophoresis assembly, rinse gently in water to remove excess of SDS and immersed in transfer buffer for 10 min. Activate the Membrane (PVDF) by soaking for 1 minute in methanol and immersed in transfer buffer. Setup the transfer by placing the gel and membrane in between pieces of filter paper and fiber sheets in the transfer cassette and immerse this sandwich in the transfer apparatus, with the gel towards the negative electrode. Electro blotting at 300 mA was continued for 3 hrs at 4°C.

4.2.7.4: Western Blotting[88]

Western blotting is an analytical technique which detects presence of native or denatured proteins which are first electro-transferred onto a membrane and are then detected using protein specific antibody.

Tris buffered saline (TBS): 150/500 mM NaCl, 20 mM Tris (pH 7.4);

Tris buffered saline with Tween20 (TBS-T): 1X TBS + 0.1 % Tween 20;

Blocking agent: 5% or 3% BSA in 1X TBS;

Block the membrane with either 0.3% BSA in TBST (for β Tubulin) or in 0.5% BSA in TBST (for Histone 3) at room temperature for 2-3 hour. Incubate the membrane with primary antibody (diluted in 1% BSA, TBST) for 1 hour [for β Tubulin (1:1000 dilution)] at room temperature or for overnight [for Histone 3(1:3000 dilutions)] in the slow rocker. Give 3 washes in TBST for 10 minutes each in high speed rocker. Incubate the membrane with secondary antibody anti mouse HRP (horse radish peroxidise) of 1:5000 dilution in 0.5% BSA for 1 hr at room temperature. Give 3 washes in TBST for 10 minutes each in high speed rocker. Detect the signal by enhanced chemiluminescence (ECL+), by incubating the blot with detection reagent for 5 min, followed by exposure to X-ray film and development.

4.2.8: Immunofluorescence of intracellular proteins[89]

The purpose of immunefluorescence is to detect the localization and relative abundance of any protein for which one have an antibody. Most of the protocol involves harsh fixation and washing steps tend to damage the intracellular delicate structures. A modified immunofluorescence method (Reference) which makes use of fast dehydration using chilled organic solvent and rehydration in presence of a chemical cross-linker was used (For simple intracellular structure immunofluorescence, cross linking step is omitted).

Blocking solution: 20µl Normal Horse Serum in 1ml PBS,

Method-

Seed cells in a confluency of 50-60% (cells should spread nicely and well separated). Keep methanol in T50 tube at -20^{o}C (For each cover slip one T50 tube, for glass bottom plates, add methanol directly to plate). Freshly prepare blocking solution by adding 10µl NHS (Horse serum) to 1ml 1X PBS, brief vortex for homogenous solution. Prepare a humidified chamber by placing a moist paper towel (Thick tissue papers) in a glass tray covered with Saran wrap to avoid drying. Take out cover slip from media (at different time points based on experimental need), Soak excess media by inverting the cover slip on a tissue paper, Press gently on the bottom of the cover slip with forceps (For glass bottom plates, take out media with suction pump completely). Transfer the cover slip to -20^{o}C pre-chilled methanol and allow cells to be fixed for 4 min in methanol (Should be done within 30s of taking out from 37^{o}C, for glass bottom plates, directly add -20^{o}C pre-chilled methanol). Take out cover slips from methanol and allow excess methanol to evaporate by holding cover slip near air flow gratings (For glass bottom plate, take out methanol and allow excess methanol to

evaporate). Place cover slips (Glass bottom plate) in a clean tissue paper inside the humidified chamber. Add blocking solution (chilled), cover the entire area (At this stage can be stored overnight if required), incubate for 30 minutes to 1 hour at room temperature inside the incubation chamber. Prepare primary antibody dilutions (1:100 for Mouse Anti-Flag) in blocking solution. Take out blocking solution from cover slip or glass bottom plate and add 50µL of primary antibody solution, incubate for 30 minutes to 1 hour at room temperature inside incubation chamber. Wash very gently with 1X chilled PBS 3 to 4 times (use suction pump while taking out solution from cover slip, do simultaneously adding and taking out solutions, do not allow to dry the coverslip). Dilute Secondary antibodies (1:100 for Alexa Fluor 405 goat anti mouse) in blocking solution and keep in dark (wrap foil paper). Add 50µL of Secondary antibody solution; incubate for 30 minutes to 1 hour at room temperature inside incubation chamber. Wash 5 times (as described in step 14). Add PBS 1.5 ml to glass bottom plate for imaging, can be stored at -20ºC. For mounting of coverslip, aspirate the final drop of PBS completely, add 5µl of mounting solution, invert coverslip onto a glass slide and seal with clear nail polish.

4.2.9: Mammalian Live Cell Imaging [90]

DMEM without phenol Red, 1X PBS, 200mM glutamine

Preparation of Mammalian Sample-

Seed cells in glass bottom chamber plate or in coverslips (0.15 mm thickness is must as it is required for microscope objective and sample refractive index). After transfection live cell imaging can be done at different time points based on experimental need. In most of our experiments, we did imaging 48 hours post transfection. Before starting imaging, change media with phenol-red free DMEM media (transparent media will help to reduce the reflection while acquiring image).

Before starting imaging, turn on the microscope incubation chamber (37^0C and 5% CO_2).

4.2.10: Microscopy & Image Processing

Zeiss LSM 510, LSM 780 or Leica SP8-STED confocal microscopes were used for different experimental need.

Microscope setting involved

1. 63X 1.4NA oil immersion objective
2. 512 X 512 format
3. 1 airy-unit pinhole
4. Z step size 500µM (Nucleus and Cell), 300µM (Nucleolus, Cajal body)
5. 16-bit images

Special measures in Leica-STED

1. BrightR mode in Leica SP8 for nucleolus imaging (Gain is always 10 in this mode)
2. No averaging
3. HyD detectors
4. DAPI scan always in the end of sequencial scanning (DAPI laser is very powerful, which can damage other signals)
5. Bidirectional scans on
6. Galvo flow always on

Image Processing:

First, process the images through ImageJ software to remove background. Assemble the representative images (2D or 3D) using Adobe Photoshop. For volume measurement (Nucleus/ Nucleolus/ Cell), we used Bitplane Imaris software. View images in 'Surpass' mode and process images using surface fill option for all volume rendering. This software uses isosurface rendering. Use 'Slice' mode to view the 3D

image in all Z sections. The Z section of an image with largest diameter (Nucleus/ Nucleolus/ Cell) was always taken into consideration to set the threshold. Threshold for smoothing was kept $1/10^{th}$ of the diameter. Surface filling was done around fluorescent signal in the image by dragging the control line so as to exactly cover the fluorescent surface. To check appropriate surface filling, rotate the 3D rendering in all directions. Once the filling was complete, export the statistical values in a excel file.

4.3: Basic Yeast Techniques[91]

Yeast strain: Saccharomyces cerevisiae strain JK9-3d

Genotype: leu2-3,112 ura3-52 rme1 trp1 his4 [92]

Media preparation: Media were prepared as indicated on the bottles by dissolving powder in distilled water & autoclaved for sterilization. Drop out media were prepared for selection of clones after transformation. These were prepared by adding yeast nitrogen base, glucose, CSM without a particular amino acid for selection in a proportion as indicated on media bottles. They were sterilized by autoclaving. (YPD ready mix powder, synthetic complete media powder SD, Yeast nitrogen base, glucose, complete supplementary mixture, CSM without URA/ TRP/ LEU)

4.3.1: Retrieving strains from the yeast collection

UV sterilize the laminar hood and ready a YPD plate / auxotrophic dropout plate in hood. Identify the appropriate vial (Labelled location number) from -80°C. Remove vial from -80°C and place in ice. Using a sterile toothpick, take small amount of the frozen cell and streak on YPD plate or auxotrophic dropout plate (only for strains containing episomal plasmids). Incubate at 30°C (wild type) / 25°C (thermo-sensitive mutants) incubator.

4.3.2: Growing yeast log phase culture

Inoculate single colony from plates in 5 mL YPD medium/ auxotrophic dropout medium in a preculture tube (This tubes with loose lids allow proper aeration). Incubate cells at 30°C (wild type) / 25°C (thermo-sensitive mutants) at 200 RPM for 48 hours for a saturated preculture (Cells should be settled in the bottom of the tube, and whole bottom of the tube should be filled with cells). Inoculate 0.1% from saturated preculture for a log phase culture in baffled flask (No other than this flask so as to maintain proper aeration and further good results). For achieving a log culture the following formula can also be used.

$$\text{Required OD} * \text{total volume(ml)/OD preculture} * 2^{\underline{n}}$$

n= number of generations

OD_{600} of the culture should be 0.5 for any further experiment (if not mentioned otherwise).

4.3.3: Freezing Yeast

15% glycerol was prepared in distilled water & was sterilized by autoclaving

Method-

Inoculate yeast cells in pre-culture tube overnight until culture is saturated. Plate 400µl cell suspension from saturated pre-culture on 2 YPD plates or plates of selection medium. Plates were incubated at the appropriate temperature until lawn growth appeared. For each strain, two cryovials were prepared by placing 1.5ml sterile 15% Glycerol in each vial. A location number for freeze down of the strain was obtained by making new entry in Filemaker yeast database of lab. Each vial was labeled with this location number on the top. The details of the strain were written on the side of cryovials. Using a small sterilized tip, about a third of the lawn (YPD plates) or an entire lawn (selective plates) was scraped off and re-suspend in one of

the vials. Procedure was repeated for the second vial. The vials were placed in respective yeast freeze down box in the -80^{o}C freezer. One vial was placed in standard collection, and an identical vial was kept in the back up collection. Complete information about the strain was entered in the Filemaker yeast database of the lab.

4.3.4: Yeast transformation[93]

High Efficiency Yeast Transformation with LiAc was used for transforming integrating, centromeric, episomal plasmids as well as PCR products in yeast cells.

1M Lithium acetate: 10.2 g of lithium acetate dehydrate was dissolved in 100 ml sterile. Distilled H_2O & sterilized by filtration through 0.22 µ filter.

50% Polyethylene glycol: 50g of PEG 3350 was weighed & added in a 150-ml beaker. Distilled H_2O was added slowly to this beaker. Mixture was stirred with a magnetic stirrer until the PEG dissolved completely.The volume was adjusted to 100 ml with distilled H_2O. The solution was filter sterilized through 0.22µ filter and stored in a tightly capped bottle at room temperature.

Method-

From a saturated preculture inoculate cells in 50mI YPD media (grow as described earlier) to anOD_{600} of 0.5. Prepare a fresh 0.1 M LiAc solution (100µL 1M LiAc + 900µL sterile distilled H_2O). A fresh solution of PEG/LiAc was prepared by mixing (100µL 1M LiAc + 100µL sterile distilled H_2O+ 800µL sterile 50% PEG [Polyethylene glycol]), give a brief vortex to get uniform mixture. Check optical density at 600 and start when it reaches to 0.5, take the culture in T50 tube. Spin cells for 3 minutes at 3000 RPM at room temperature in a table top centrifuge. (If proper pellet is not forming or it is getting mixed, increase the time for centrifugation from 3 minutes to 10 minutes). Resuspend the pellet in 20 ml sterile distilled H_2O (To remove excess media). Spin again for 3 minutes at 3000 RPM at room temperature, discard the supernatant. Resuspend in 0.5 ml 0.1M LiAc and transfer cell suspension in microcentrifuge tube. Incubate the cell suspension for 15 min at 30ºC in a water

bath. Meanwhile, boil an aliquot of single-stranded carrier DNA at 99ºC for 10minutes in a thermo-mixer or boiling water, then cooled by placing vial on ice. Add 5 µl boiled carrier DNA and approximately 100ng transforming DNA (in 5 µl or less) for each transformation at room temperature inside hood. For each transformation, include a negative control (only carrier DNA) & a positive control (DNA of same auxotrophic marker as in test). Add 50 µl cells to each transformation tube, give a brief vortex. Add 300 µl PEG/LiAc solution and mix by repeated gentle pipetting with a 1ml pipette (to obtain a uniform mixture). Incubate cell suspension and DNA-PEG/ LiAc mixture for 30 min at 30ºC. Give heat shock for 15 minutes at 42ºC. (In case of temperature sensitive cells, first incubation is at 25ºC and heat shock is at 30ºC to avoid cell death). Spin the cells at high speed for 10 seconds in a micro centrifuge. Discard the PEG/LiAc supernatant. Resuspend cells gently in 200µl sterile distilled H_2O. Spread cells using sterile glass beads on a selective plate. Incubate plates at appropriate temperature until colonies appeared.

4.3.5: Replica plating for screening transformants

Grids and lines are made in a fresh plate and put numbers on the plate. Replica plate as much as colony from transformation plate (after colony appears) in a new plate to screen for positive transformants. Incubate at 30ºC incubator for 24 hours.

4.3.6: Genomic DNA isolation [94, 95]

Breaking buffer: 2 % (v/v) Triton X-100, 1% (v/v) SDS, 100 mM NaCl, 10 mM Tris-Cl, pH 8.0 1 mM EDTA, pH 8.0, Distilled H20(sterile)

Method-

Inoculate colony from replica plate in preculture tube (5-6 ml)/ Eppendorf tube (1ml).

Grow culture overnight at 30ºC 200 RPM. Spin for 5minute at 3000 RPM in room temperature. Remove supernatant and wash pellet (resuspend, spin and discard the supernatant) with 0.5mL MQ. Vortex pellet briefly, add 200µl of freshly prepared breaking buffer and resuspend cells. Add 0.3 g (200 µl in vol.) small glass beads and 200 µl phenol (cold)/chloroform. The mixture is vortexd at highest speed for 3min to achieve cell lysis. Add 200 µl 1X TE buffer and give a brief vortex. Centrifuge at highest speed for 5 min, at room temperature. Transfer aqueous layer to fresh tube and add 1ml 100% ethanol (ice cold), mix by inverting tubes. Incubate tubes at -20ºC for 1 hour for DNA precipitation. Centrifuge tubes for 5-10 minutes at highest speed at room temperature. Remove the supernatant and resuspend pellet in 0.4 ml in 1X TE Buffer. Add 3µl RNaseA (Stock l0 mg/ml), mix and incubate for 5 min at 37^{o}C to remove RNA contamination. Add 10 µl of 4M Ammonium acetate and 1ml of 100% ethanol, mix by inversion, and incubate at -20 º C for 1 hour. Centrifuge tube at room temperature for 10-15 min at 14000 RPM. Discard supernatant and air dry pellet. Resuspend DNA pellet in 20µl TE buffer. Store at -20ºC.

4.3.7: Checking fluorescence signal in upright microscope for screening

Take little amount of colony from replica plate and resuspend in 20µl of SD media. Clean the slides & cover slips with Colin& air-dried. Add 5µl of cell suspension on slide and place the cover slip from the top on this suspension. Press the inverted slide gently on tissue paper to remove excess cell suspension. Seal the cover slips with transparent nail polish. Add a drop of immersion oil on the cover slip and slide was placed on microscope stage for viewing. Cells were focused in bright field & then fluorescence was checked by selecting appropriate fluorescent filter.

4.3.8: Manipulating Yeast Genome

Gene targeting by homologous recombination is one of the most powerful and important techniques available for studies in yeast. A gene at its normal chromosomal location can be removed or replaced with an allele created in vitro, such that the only genetic difference between the initial strain and the final strain is that particular allele. Therefore, phenotypes conferred by null mutations or any other types of mutations can be analyzed. Genes can also be modified to be fused to the coding sequence for fluorescent proteins, such as green fluorescent protein (GFP). Because the epitope tag or fusion is made in the genomic context, the tagged gene is subject to native regulation. The properties of a strain containing the epitope tag or fusion can be compared to an isogenic wild-type strain that lacks the tag to study gene function, localization and regulation.

4.3.8.1: PCR based gene deletion strategy[96]

Principle

Deletion of an entire open-reading frame (ORF) of a gene deletion creates a null mutation, allowing for the analysis of loss-of-function phenotypes. To generate a deletion, the gene sequence from start to stop codon is removed and is generally replaced with a selectable marker (Kanmax/ URA3). The vectors used for gene deletion were pUG6 (KanMX marker) and pUG72 (URA3 marker).

PCR amplify the deletion casette using either pUG6 or pUG72 plasmids as template. (Primers would contain 5’ and 3’ flanking region homologous to the ORF of interest.) PCR mixture is same as described in 3.4. (Template concentration 50 ng). PCR cycle for creating deletion casettes is as described in table 4.14. Purify the amplicon using

Qiaquick nucleotide removal kit. Transform the purified amplicon in the background yeast strain. Check integration of the deletion casette in the tranformant strain.

Cycle step	Temperature	Time	Cycles
Initial denaturation	98^{o}C	3 minutes	1
Denaturation	98^{o}C	30s	
Annealing	Lower Tm+ 3	60s	30
Extension	72^{o}C	2 minutes	
Final extension	72 ^{o}C	8 minutes	1

Table 4.14: PCR cycling condition to prepare deletion cassette

4.3.8.2: PCR based epitope (GFP Fusion) protein tagging[97]

The ability to epitope tag or create fusion proteins with the endogenous wild-type or mutant copy of yeast genes makes yeast one of the most powerful systems for the study of multiple biological processes. Because the tag is engineered into the genomic locus, the tagged version of the gene is expressed and regulated like the wild-type gene. Furthermore, the parental strain serves as an important isogenic negative control. A plethora of C-terminal tagging modules have been developed for virtually every epitope and fluorescent protein variant. Using ~40-60 bp sequences immediately upstream and downstream of the stop codon as targeting sequences on the forward and reverse PCR primers the resulting PCR fragments from these modules are integrated into the genome by one-step gene replacement (Figure 4.1). Correct integration can be confirmed by PCR and/or by checking for expression of the tagged protein in the microscope

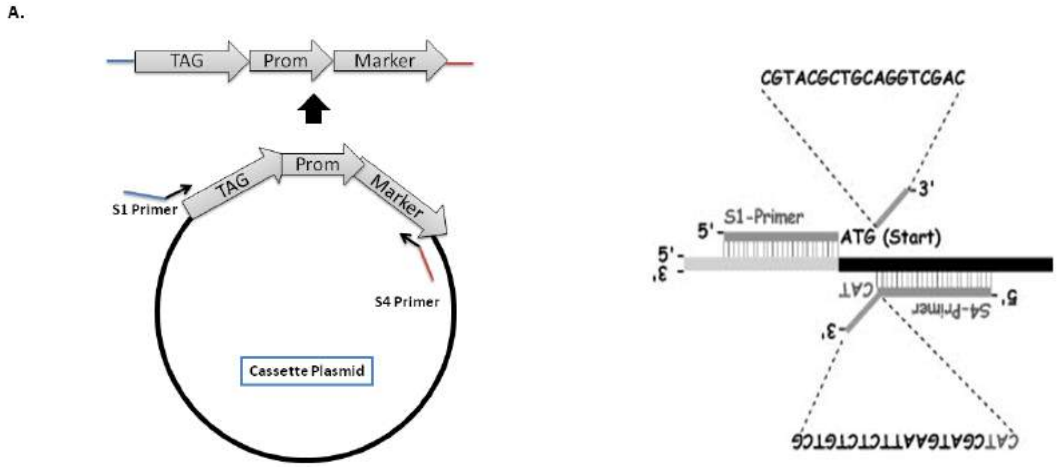

Figure 4.1: Vector for Epitope tagging and the strategy for Primer designing

The plasmid contains a cassette, which consists of a selection marker, and additional sequences, which can be promoter sequences and/or sequences that encode for a tag (e.g. GFP). The S1 and S4 primers allow amplification of cassettes and targeting of the respective PCR product to the desired genomic location, which becomes defined by the overhangs provided by the S1 and S4 primers. Upon transformation, an integration of the cassettes into the yeast genome occurs due to homologous recombination (C).

Primer design: The following rules should help to design the primers using specific software such as DNA Strider.

S1-primer- 45–55 bases upstream of the ATG (including ATG, start codon) of the gene, followed by 5-CGTACGCTGCAGGTCGAC-3;

S4-primer- the reverse complement of 45–55 bases downstream of the ATG (start-codon) of the gene (excluding ATG), followed by 5-CATCGATGAATTCTCTGTCG-3

Protocol is same as making deletion strains.

4.3.9: 5-FOA plates for popping out URA based plasmid[98]

Yeast cells expressing $URA3^+$ are unable to grow on media containing 5-Fluoro-orotic acid (5FOA) (a pyrimidine analog) but mutant yeast strains containing $ura3^-$ mutants grow normally [98]. This gives advantage of selecting yeast cells which lack wild type URA3 allele. By this method, it is possible to take out the URA3 expressing plasmid out of cells.

Preparation of FOA plates:

Contents for making 250ml SD media were mixed in 125ml distilled water; 250mg of 5FOA powder was added to this mixture & sterilized by filtering through 0.22µ filter. In 125ml distilled water, 5g agar was added & this was autoclaved for dissolving agar & for sterilization. Later this autoclaved agar solution & sterilized medium with 5FAO were mixed well & poured in plates. Final concentration of 5FOA was 1mg/ml.

4.3.10: Yeast Live Cell Imaging

For Yeast cell imaging: Concanavalin A was dissolved in distilled water to the concentration of 2mg/ml & 100µl aliquots were made & stored at -20°C

Method- Clean the glass bottom plate with Colin. Treat the glass bottom plate with 200µl aliquot of concanavalin-A for 30 minutes. Remove the concanavalin-A using pipette, and rinse the plate with milli-Q water. Air dry the plate completely. Add 200µl log phase yeast culture (OD_{600} 0.5-0.6) to Con-A coated glass surface and incubatefor12 minutes at room temperature. Remove the culture and wash gently with SD media so as to remove all unattached cells. Later 1.5 ml of SD media was added for imaging.

4.3.11: Alpha factor synchronization followed by nocodazole treatment of cells [99, 100]

Grow an overnight starter culture inoculated from one single colony (200 rpm, 30 °C). From the overnight culture inoculate into fresh media to get OD_{600}=0.2 in a baffled flask. Add 50 ng/ml α-factor to the media and grow them for 120 minutes. (G1 arrested cells have typical pear shape. Usually between 90 and 120 min ~100% synchrony can be observed.) To release the cells from the arrest, spin down the cells and wash them with water. Resuspend the cells in the working volume of fresh media. Grow the cells up to OD_{600}=0.4 and add nocodazole 10µg/ml for again 120 minutes.

7. Perform the imaging experiments as per requirement with or without nocodazole containing media.

4.3.12: Electron microscopy of yeast[101]

Grow a 50-ml yeast culture to an OD_{600} of about 0.5. Filter the cells slowly on a 0.22 µM bottle-top filter down to a volume of about 5 ml. Do not dry the cells completely. Rapidly add 40 ml of ice-cold 50 mM KPi (pH 6.8), 1 mM $MgCl_2$, 2% glutaraldehyde. (Use a fresh vial of EM-grade glutaraldehyde to prepare this fixative solution.) Allow the fixation to proceed for 1 hr on ice. [Note: Glutaraldehyde is toxic. Work in the hood, wear gloves and safety glasses, and dispose of all glutaraldehyde-containing solutions in the organic liquids waste.] Spin the fixed cells 3 min at 3000 rpm at 4°. Pour off the supernatant, and resuspend the pellet by vortexing in 25 ml ice-cold 50 mM KPi (pH 6.8). Repeat step #4 twice more, for a total of three washes. Spin again after the last resuspension. This time resuspend the pellet in 1 ml 50 mM KPi (pH 6.8), and transfer the cell mixture to an Eppendorf tube. The remaining steps until resin polymerization are all done at room temperature. Spin 1 min at 5000 rpm in a microfuge. Resuspend the cells in 0.75 ml freshly prepared 4% $KMnO_4$. Mix end-

over-end for 30 min. [Note: $KMnO_4$ takes a while to dissolve with vigorous vortexing. This solution is a potent oxidizing agent, so use caution: wear gloves and safety glasses, and dispose of the waste in the caustic liquids container. Spin 1 min at 5000 rpm. Resuspend the cells in 0.75 ml H_2O. Repeat twice more. Spin as above, and resuspend the cells in 0.75 ml 2% uranyl acetate. (Sterile filter the uranyl acetate solution and store it at room temperature in the dark. If a precipitate forms, discard the solution and prepare it fresh.) Mix end-over-end for 1 hr. Wash four times with H_2O as in step #8. Prepare normal spurrs resin according to the formula given in the kit instructions. Work in the hood and wear gloves, as these compounds are extremely toxic. It is convenient to mix the resin components in a disposable plastic beaker placed on a balance in the hood. Mixing can be done with a glass rod. Dehydrate the cells in the following graded series of EtOH solutions. After each spin (1 min at 5000 rpm) and resuspension, mix the cells end-over-end for 5 min. Start with a fresh, unopened bottle of water-free EtOH. 50%, 70%, 80%, 85%, 90%, 95%,100%, 100%,100%, 100%. Resuspend the cells in 0.75 ml of a 3:1 EtOH:Spurrs mixture. Mix end-over-end for 1 hour. Spin 1 min at 5000 rpm. Resuspend the cells in 0.75 ml of a 1:1 EtOH:Spurrs mixture. Mix end-over-end overnight. Spin 1 min at 5000 rpm. Resuspend the cells in 0.75 ml of a 1:3 EtOH:Spurrs mixture. Mix end-over-end for 1 hr. Spin 1 min at 14,000 rpm. Resuspend the cells in 0.75 ml of pure spurrs. Mix end-over-end for 1 hr. Repeat step #16. Spin 1 min at 14,000 rpm. Resuspend the cells in 300 µl fresh Spurrs. Transfer 100 µl of the cell suspension into each of three BEEM capsules sitting in a metal rack, making sure to avoid trapping any air at the bottom of the capsule. Fill each capsule to the brim with Spurrs. Insert a small square of paper containing a printed sample number. Leave the capsules uncapped throughout the

procedure, including during polymerization (see below). Place the rack with the capsules in a vacuum dessicator, and degas for 15 min. Place the rack on a block of styrofoam in an accurate temperature-controlled oven set at 68°C. Allow the resin to polymerize for 36-48 hrs. The samples are now ready for sectioning and staining with lead citrate. Ultrathin sections were cut on ultra-microtome (Leica UC7, Germany) and collected on copper grids. Finally, sections contrasted with uranyl acetate and lead citrate and micrographs were taken on Jeol 1400 plus Transmission Electron Microscopy (Japan) at 120 KeV to capture images in bright field mode.

4.3.13: Statistical tests:

For every experiment, datasets are incorporated in Graph Pad prism 6 software. Datasets are first checked for normal distribution by column statistics. If the distribution of the datasets were found to be not normal, then we performed non parametric test, which is Mann-Whitney test. (In all mammalian results, mostly we performed Mann-Whitney Tests, since the datasets were found to have a not normal distribution). Thus significance tests were performed. If the distribution of the datasets were found to be normal, then we performed unpaired student t test. Graphs were plotted in column type mean with standard error mean or with range.

Chapter 5:

Nucleo-cytoplasmic transport perturbation affects size of the nucleus and nucleolus in human cells

5.1: Introduction

The nuclear to cell volume ratio or "Karyoplasmic ratio" (KR) remains a roughly constant value in cells with widely different DNA contents, ranging from single-celled eukaryote to mammalian cells [9, 22]. Moreover, abnormal organelle architecture, primarily altered nuclear size or nucleolus morphology, has been considered for a long time a diagnostic hallmark for cancer [7, 102-105]. In spite of such an early knowledge of association with several forms of cancers, the regulation of nuclear or nucleolar size, especially in human cells, still remains a poorly understood field. However, a few groups have shown recent interests in the field and several studies in different model organisms have been reported over last few years [9, 25].

It was thought for a long time that nuclear size increases in cancer cells simply to accommodate the higher DNA content as a result of aneuploidy [106-108]. However, ploidy had been shown to have no direct effect on the nuclear size of both budding and fission yeast [9],[22] suggesting the existence of active regulation of nuclear size in synchrony with cell size. Disruption of the cytoskeleton did not affect N/C ratio in fission yeasts [9]. In fact, it exemplified that in yeast almost no genetic or physiological modification can alter the N/C ratio except a blockade in nucleo-cytoplasmic transport [9]. In metazoans, the nuclear envelope is perforated by the nuclear pore complex (NPC) which mediates nucleo-cytoplasmic transport [109]. In other organisms, namely *S. pombe*, mammalian cells, the NPC has shown to have no direct role in regulating nuclear size [110, 111]. Nuclear scaling acts mainly through the import pathway, with a much higher level of importin α and also of importin α1, importin α3, and importin β in *Xenopus* [25]. Different studies in *Tetrahymena*

thermophile , *Drosophila melanogaster*, and in *C. elegans*, showed that different import factors are what most likely play a role in controlling their respective nuclear size [15]. Altered nuclear transport is frequently observed in transformed cells [15, 109]. These coinciding results from different organisms suggest that nucleo-cytoplasmic transport most likely directly or indirectly controls nuclear size in human cells.

The nucleolus is present inside the nucleus [112]. Although many similar characteristics exist between the nucleus and nucleolus, it is unknown whether the sizes of the nucleus and the nucleolus are controlled by same or different active mechanisms. Nucleus size and cell size are shown to correlate with RNA transcription level [113] [114]. Genes regulating rRNA biosynthesis, ER-Golgi transport, nucleosome assembly are shown to be responsible for decreased nucleolar size in yeast and Drosophila while genes involved in cell cycle regulation are shown to be responsible for increased nucleolus size [71]. Considering these facts, we can postulate that the size and shape of the nucleus and nucleolus are carefully controlled by similar or different mechanisms, which are normally disrupted in transformed cells.

The size control mechanism of the nucleus and the nucleolus of human cells remains poorly understood. Barely studies on human cells to address the size control mechanism of either nucleus or nucleolus are available. In this part of the thesis, we have determined the range of variation of nuclear size in terms of N/C ratio and nucleolus size with respect to nucleus size in different immortalized and transformed cell lines of same tissue origin. Upon nuclear transport perturbation, it is found that N/C ratio and nucleolus size are increased significantly in immortalized cell lines. In

an in vitro assay system, combining intact nucleus and cytosolic fractions from different sources has been established to determine regulation of morphogenic changes of nucleolus. The analysis of the results from the nuclear transport perturbation has led to the conclusion that nucleolar size is indeed correlated with nucleus size.

5.2: Results

5.2.1: Development of assay system to visualize nucleus size and shape under the microscope in live cell condition

To study the size and shape control mechanism of nucleus, we developed an assay system to monitor the nucleus in live cell condition. The final system will be based on live cell imaging of nucleus and cell upon over expression of dominant negative proteins with nucleus and cell labeled with two different color fluorescent fusion proteins. For this purpose, we have selected lamin as nuclear membrane marker and farnesylation modification sequence of p21 (Ras) as cell membrane marker.

Serial No.	Name of Constructs	Labeling intracellular compartment
1	mGFP-Histone4	Histone 4 is tagged in C terminal
2	Histone4-mGFP	Histone 4 is tagged in N terminal
3	mGFP-Lamin	Lamin is tagged in C terminal of GFP
4	Lamin-RFP	Lamin is tagged in C terminal of RFP
5	F-EGFP	F is tagged in N terminal of GFP
6	F-mCherry	F is tagged in N terminal of mCherry

Table 5.1: Different nuclear and cell membrane fusion proteins

We have cloned the cell membrane protein 'F' with mCherry fluorescent protein and Lamin A with GFP fluorescent protein (Appendix 1.1 & 1.2). Both the constructs were confirmed by sequencing. Upon transfection in cell lines, we can see nuclear membrane as green and cell membrane as red under the confocal fluorescent microscope. Thus nuclear and cell membrane label enabled us to measure nuclear to cell volume ratio from live cell images.

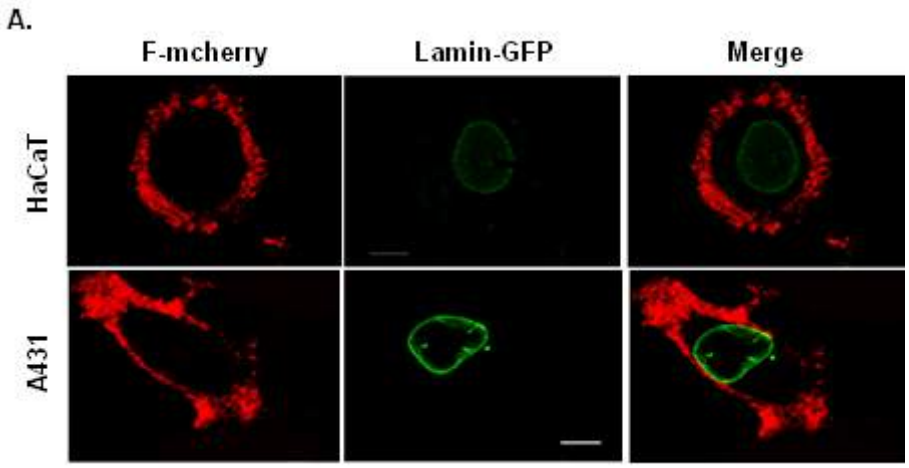

Figure 5.1: Assay System to Study Nucleus and Cell volume.

Live cell images of HaCaT and A431 cells transfected with nuclear and cell membrane marker, Lamin-GFP and F-mCherry respectively. Scale bar is 10µm.

In this study, we have also created different nuclear and cell membrane fusion proteins listed in table 5.1.

5.2.2: Comparative analysis of N/C Ratio in different immortalized and transformed cells of same tissue origin

At first, we wanted to determine the range of variation of N/C ratio in mammalian cell lines since the size and shape of both nucleus as well as cell from different tissue types are very heterogeneous. For comparative measurements of N/C ratio, we have

selected four pairs of immortalized and transformed cell lines of similar tissue origin (**Table 5.2**).

Tissue type	Immortalized	Transformed
Skin	HaCaT	A431
Colon-Intestine	Int407	HCT116
Breast	MCF10A	MCF7
Liver	HHL5	HepG2

Table 5.2: Cell lines used in the study

We have transfected each of the cell lines with constructs expressing GFP-Lamin and F-mCherry for subsequent measurements of nuclear volume and cell volume respectively. 3D reconstruction (**Figure 5.2A**) of confocal images of each cell as well as their corresponding nucleus resulted near accurate respective volume estimations. Using these volume estimation results, we have calculated the nuclear-to-cell volume (N/C) ratio for each cell line. Our analysis shows that N/C ratio is significantly higher ($p<0.001$; Mann-Whitney test) in transformed cell lines (A431, HCT116, MCF7 and HepG2) compared to their respective immortalized counterparts (HaCaT, INT 407, MCF10A and HHL5) (**Figure 5.2B**). N/C ratio is approximately 80% higher in transformed cell lines from colon-intestine, approximately 45% higher in breast cell lines, 40% higher in skin cell lines and 30% higher in liver cell lines (**Figure 5.2C**).

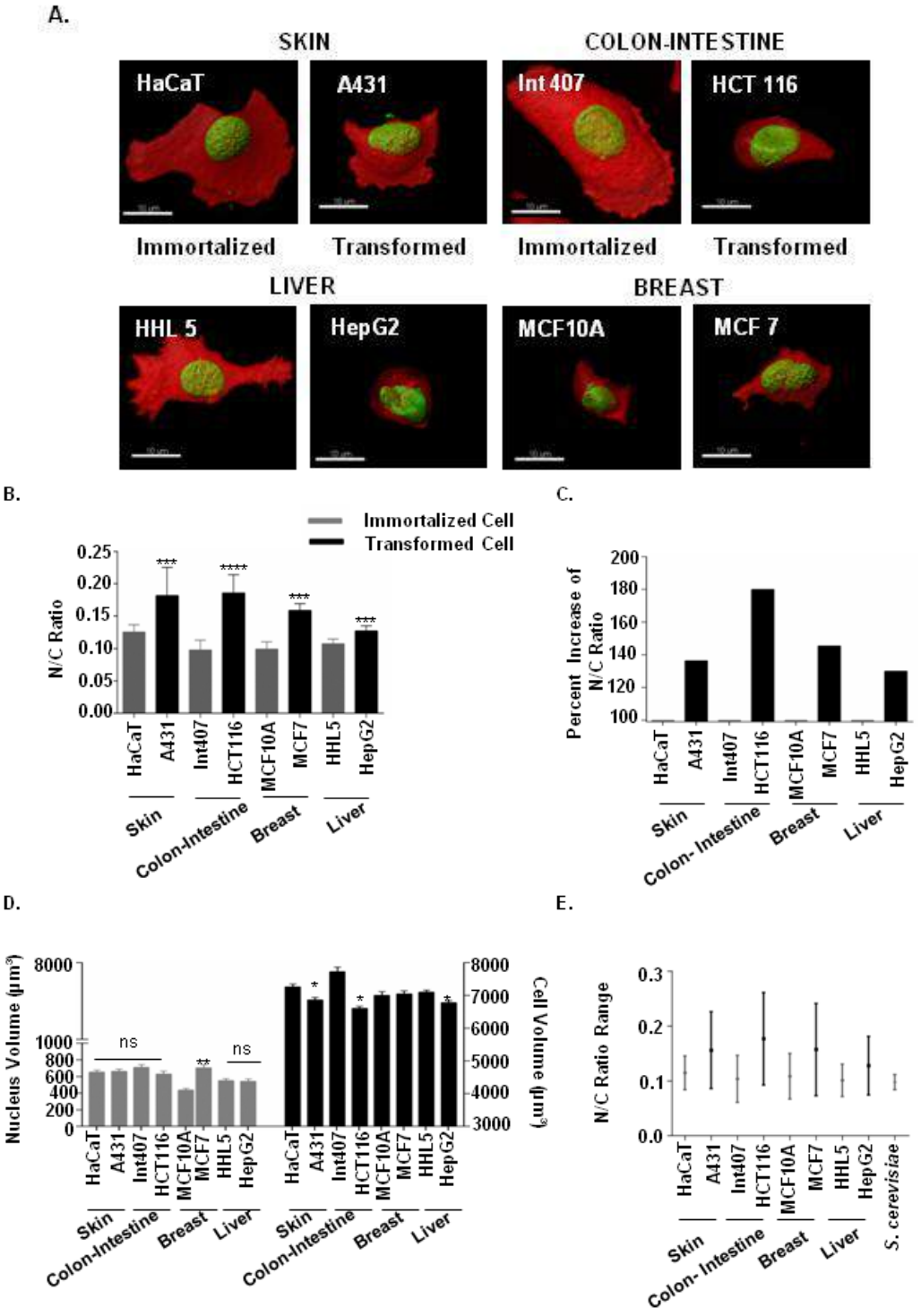

Figure 5.2: Transformed cell lines exhibit significant increase in N/C ratio compared to immortalized cell lines

(A) Overlay of 3D reconstruction images of live cells; cell membrane (F-mCherry) and nuclear envelope (GFP-Lamin). Scale bar is 10 lm. (B) N/C ratio is significantly higher ($P < 0.0001$, $P < 0.001$) in all transformed cell lines compared to the corresponding immortalized cell lines as represented in column graph. Error bars

*represent standard error mean (SEM). (C) 30–80%increase in N/C ratio in different transformed cell lines were observed compared to immortalized counterpart. (D) Column graph showing nucleus volumes and cell volumes was quantified from images (as represented in A) in IMARIS software for 100 cells in each case in five different experiments. (E). the range of N/C ratio varies more in all transformed cell lines compared to immortalized counterparts ***P≤ 0.001; ****P ≤ 0.0001.*

The N/C ratio varies widely (**Figure 5.2E**) in all the transformed cell lines compared to their immortalized counterparts in which it maintains primarily a constant value of (0.10±0.04) which is similar in range to the highly constant value of N/C ratio of budding yeast(0.09±0.01) (**Figure 5.2E**). Previous reports have shown that fission yeast also has a similar constant value of N/C ratio [9]. It was noted that nuclear volume may not have always increased in a transformed cell line. Rather the reduction of cell volume in transformed cell lines is what contributed to the effective increase of N/C ratio in the same (**Fig 5.2D**). However, in case of breast origin, cell volumes are comparable, but the nucleus volume is higher in the transformed cell line (MCF7) compared to its immortalized counterpart (MCF 10A) (**Figure 5.2D**).

Since all these measurements were performed in an unsynchronized condition, we have also checked N/C ratio alteration in synchronized condition in transformed cells. To check N/C ratio alteration in G1/S synchronized condition in transformed cell lines compare to immortalized cell lines, we have done synchronization using double thymidine block. Double thymidine block (2.5 mM) is used to arrest cells in G1/S phase.

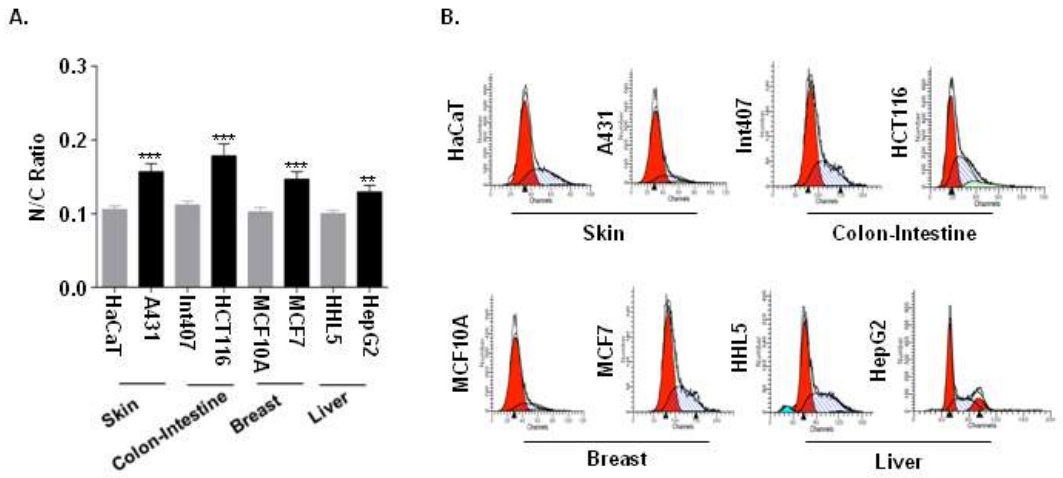

Figure 5.3: Transformed cells exhibit significantly increased N/C ratio compared to immortalized cells in G1/S synchronized condition

A. Cells were synchronized using double thymidine block and images were captured as described earlier. N/C ratios were measured from 3D reconstruction of confocal images. N/C ratio is significantly higher ($P < 0.0001$, $P < 0.001$) in all transformed cell lines compared to the corresponding immortalized cell lines as represented in column graph. Error bars represent standard error mean (SEM). B. G1/S phase cell enrichments are shown by cell cycle analysis of respective cells using FACS

During the first release, in between the two blocks, cells are transfected with Lamin-GFP and F-mcherry. 22Hrs post second thymidine block cells are imaged within 2 Hrs. We have confirmed the G1/S synchronization by fluorescence-activated cell sorting (FACS). Our result shows that N/C ratio is significantly increased in transformed cell lines compared to immortalized cell lines in G1/S synchronized condition (**Figure 5.3A and B**). Comparative analysis of N/C ratio in different immortalized and transformed cells of same tissue origin helped us to validate the phenomenon of the N/C ratio increase in transformed cells quantitatively.

5.2.3: Effect of Nuclear transport perturbation on N/C Ratio of immortalized cells:

Nucleo-cytoplasmic transport perturbation affects size of mammalian nucleus

Our result shows that across the immortalized cells N/C ratio value remains constant. We have decided to further investigate whether the N/C ratio could be altered by perturbation of any physiological or cellular process in immortalized cell lines. Previously it had been reported that nucleo-cytoplasmic transport played an important role in regulating nuclear size and nuclear scaling in yeast and *Xenopus* systems respectively [25]. However, to our knowledge no such studies have been reported in mammalian cells. For this reason, we decided to attenuate the nuclear transport in immortalized cells and study the effect of this on the N/C ratio. We used an over expression of dominant negative forms of Importin beta and Ran to create such attenuation of nuclear transport [115-117]

5.2.3.1: Effect of over expression of importin beta 1-364

The dominant negative form of Importin beta blocks multiple pathways of nucleo-cytoplasmic transport. Importin beta 1-364 truncated protein has been shown to block nuclear import. We have cloned Importin beta 1-364 in pCMV-3X-Flag vector and confirmed by sequencing (Appendix 1.3). First nucleo-cytoplasmic import attenuation by importin beta 1-364 was confirmed by co transfecting NLS-YFP along with dominant negative form of importin beta 1-364.

We observed that NLS-YFP is restricted in the cytoplasm compared to vector control cells in which NLS-YFP is localized inside the nucleus (**Figure 5.4A**) We over express Importin beta 1-364 fragment along with GFP-Lamin and F-mCherry in HaCaT (skin immortalized) cells. Live cell imaging was done for total of a hundred cells in five different experiments, after 48 hours of transfection. Post live cell imaging, Immunoflurescence against Flag-Imp-beta 1-364 was done to identify Importin beta 1-364 positive cells that showed nuclear pore localization and

cytoplasmic localization (**Figure 5.4C**). 3D reconstruction of confocal images (**Figure 5.4B**) results quantitative measurement of N/C ratio as described earlier. N/C ratio is increased significantly ($p<0.0001$; Mann-Whitney test), when we over express Importin beta 1-364, in the immortalized cell line HaCaT (**Figure 5.4B right panel**). The N/C ratio is increased by almost 50% **(Figure 5.4 B right panel**) as compared to the vector control transfected same cells.

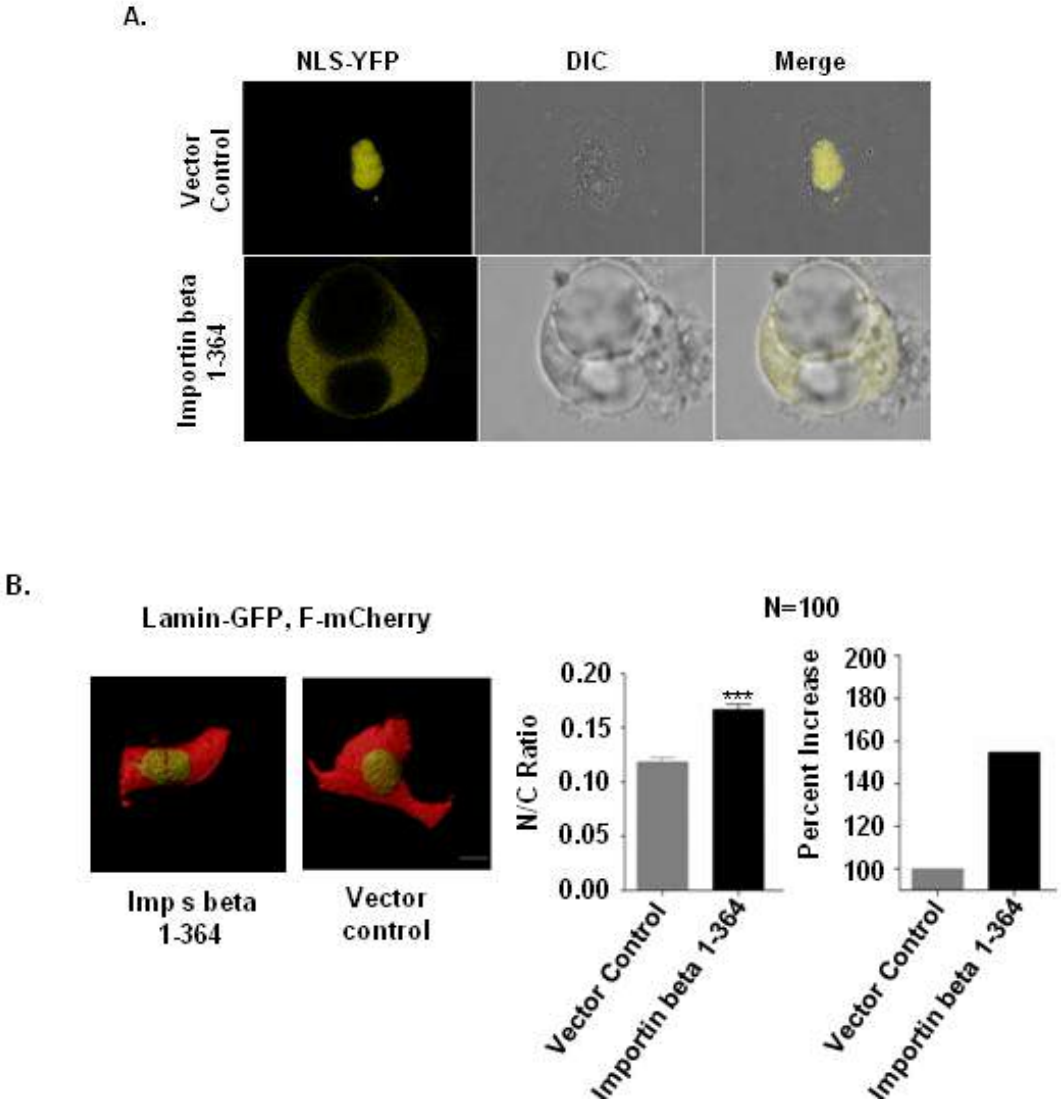

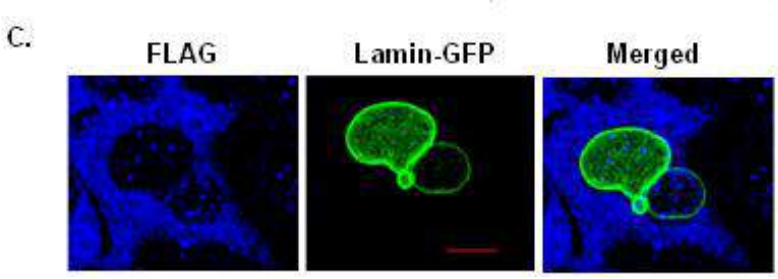

Figure 5.4: Over expression of dominant negative Importin subunit beta 1-364 causes (N/C) ratio to increase significantly in immortalized cells

(A) Live Cell images of HaCaT (Skin immortalized) cells transfected with NLS-YFP along with dominant negative proteins importin beta 1-364 and/ or vector control. (B) Overlay 3D reconstruction images of live cells transfected with importin beta 1-364 along with GFP-Lamin, F-mCherry in HaCaT (skin immortalized),Scale bar is 10 µm. N/C ratios were quantified from images (as represented in B) in IMARIS software for 100 cells from five different experiments. N/C ratio is significantly higher (P < 0.001) in Importin beta 1-364 transfected cells compared to vector control represented in column graph. Error bars represent standard error mean (SEM). (C) Dominant negative proteins in the cells were visualized by immunofluorescence against mAb Flag. GFP-Lamin images are live cell images. Scale bar is 5µm.

.

5.2.3.2: Effect of over expression of Ran^{T24N} and Ran^{Q69L} on immortalized cell

Ran is one of the key players of classical nuclear transport pathway [73, 76, 77, 118]. An over expression of any of the two mutant forms, Ran^{T24N} or Ran^{Q69L}, can effectively perturb the nucleo-cytoplasmic transport pathway [76, 116, 117, 119, 120]. From nucleus to cytoplasm Ran-GTP to Ran-GDP concentration gradient is strongly maintained and disturbance in this concentration gradient is associated with many cellular dysfunctions. Ran ^{T24N} - Reduced affinity for nucleotides and forms a stable complex with RCC1. Ran ^{Q69L} - It's a GDP locked form, but still can't bind to NTF2, defective in GTP hydrolysis. First we have cloned Wild type Ran in pCMV-3X-Flag vector. In that construct mutagenesis is performed to make T24N and Q69L mutants (Appendix 1.5).

In this case also, nucleo-cytoplasmic transport attenuation by Ran^{Q69L} or Ran^{T24N} was confirmed by co transfecting NLS-YFP along with Ran^{Q69L} and NES GFP along Ran^{T24N} respectively.

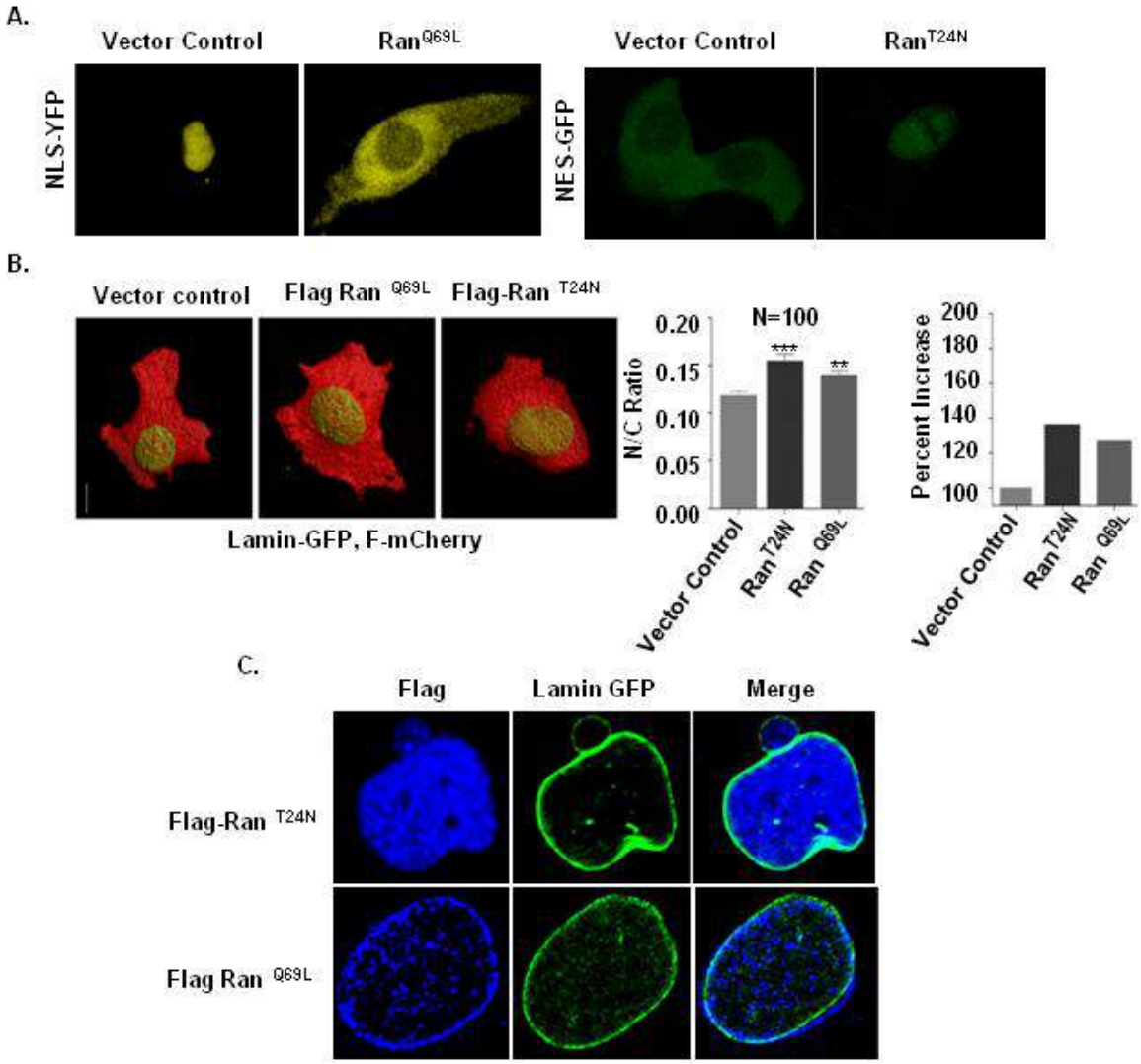

Figure 5.5: Over expression of dominant negative Ran^{T24N} and Ran^{Q69L} causes (N/C) ratio to increase significantly in immortalized cells

(A) Live Cell images of HaCaT (Skin immortalized) cells transfected with NLS-YFP along with dominant negative protein Ran^{Q69L} and NES-GFP along with Ran^{T24N} and/ or vector control.(B) Overlay 3D reconstruction images of live cells transfected with either Ran^{T24N} or Ran^{Q69L} along with GFP-Lamin, F-mCherry in HaCaT (skin immortalized). Scale bar is 10 µm. N/C ratios were quantified from images (as represented in B) in IMARIS software for 100 cells from five different experiments. N/C ratio is significantly higher ($P < 0.001$, $p< 0.05$) in Ran^{T24N} or Ran^{Q69L} transfected cells compared to vector control represented in column graph. Error bars represent standard error mean (SEM) (C) Dominant negative proteins in the cells

were visualized by immunofluorescence against mAb Flag. GFP-Lamin images are live cell images. Scale bar is 5µm.

We observed that upon Ran^{Q69L} over expression, NLS-YFP is restricted in the cytoplasm compared to vector control cells in which NLS-YFP is localized inside the nucleus while upon Ran^{T24N} over expression, NES-GFP is localized inside the nucleus compared to vector control cells in which NES-GFP is localized all over cytoplasm except nucleus (**Figure 5.5A**). Once again we over expressed dominant negative pCMV-3XFlag-Ran^{T24N} or pCMV-3XFlag-Ran^{Q69L} in HaCaT cells along with GFP-Lamin and F-mCherry as described earlier. Post live cell imaging, immunofluorescence against Flag- RanT24N showed overall nuclear localization (**Figure 5.5C top**) while Flag- Ran^{Q69L} showed localization on nuclear pore complex (**Figure 5.5C bottom**) suggesting successful nuclear transport perturbation. 3D reconstruction of live cell images (**Figure 5.5B left panel**) results in quantitative measurements. Dominant negative Ran^{T24N} or Ran^{Q69L} over expression also increased N/C ratio significantly ($p<0.0001$, $p<0.0027$ respectively; Mann-Whitney test) in immortalized cells compared to vector control transfected cells (**Figure 5.5B right panel**) by approximately 30% and 20% respectively (**Figure 5.5B right panel**).

We found similar results in the over expression studies of dominant negative importin subunit beta and ran performed in another immortalized cell line **Int407**. We conclude that perturbation of nuclear transport pathway by overexpressing dominant negative importin beta and ran results in the increase of N/C ratio in immortalized cells.

5.2.4: Effect of dominant negative Importin beta and Ran on invasion property of immortalized cells:

Cellular transformation is associated with altered N/C ratio. Transformed cells mostly known to have higher migration and invasion properties. To correlate higher N/C ratio

with different transformation phenomenon of transformed cells, we have done invasion assay using boyden chamber in HaCaT (immortalized) and A431 (transformed) cells. Our results showed that transformed cell line A431 showed higher N/C ratio compared to immortalized cell line HaCaT. Invasion assay showed A431 is significantly more invasive compare to HaCaT cells (**Figure 5.6A**). We asked the obvious question if invasion is changed when N/C ratio is increased in immortalized cell lines.

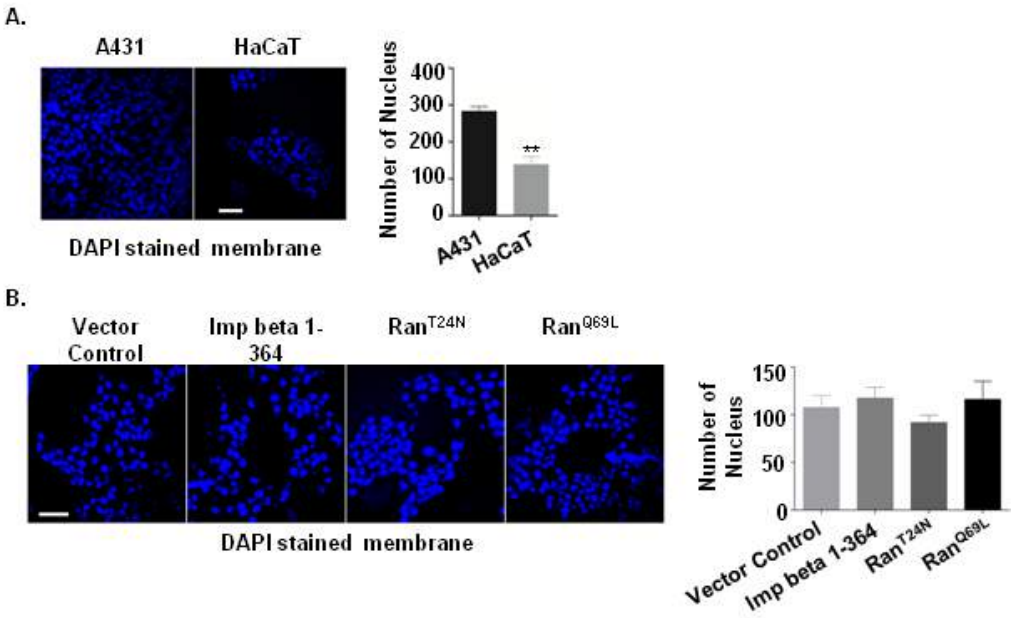

Figure 5.6: Invasiveness is not affected when N/C ratio is increased by dominant negative Importin beta and/ or Ran over expression in immortalized cell line HaCaT

.

(A) In the control experiment, only HaCaT and A431 cells were seeded for invasion assay. Cells that adhered to the lower surface were fixed, and the nuclei were stained with DAPI. Images of the DAPI staining membranes were captured using fluorescence microscopy HaCaT cells are significantly less invasive compared to A431 cells (B) Immortalized cells (HaCaT) were transfected with either dominant negative proteins. The result shows a field of one membrane per condition in one representative experiment out of three independent experiments. The DAPI-stained nuclei were counted in five fields per membrane in triplicates in one representative experiment out of three independent experiments.

To test this we performed invasion assay in immortalized cell line (HaCaT) after overexpressing either Importin beta 1-364 or Ran^{T24N} or Ran^{Q69L}. We found no significant difference in invasiveness compared to control cells (**Figure 5.6B**). MTT assay was performed at the same time to confirm efficiency of cell seeding for invasion assay. This result showed that forcefully increased N/C ratio by perturbation of nuclear transport could not alter the invasiveness of the immortalized cell line.

5.2.5: Effect of wild type ran and importin beta over expression over dominant negative Importin beta 1-364 and Ran^{T24N} and Ran^{Q69L} protein

We have over expressed wild type Ran and wild type Importin beta in transformed cell line A431. We hypothesized if wild type ran or importin beta over expression can bring down the N/C ratio in the transformed cell line similar to N/C ratio of immortalized cell line. We have cloned wild type ran and importin beta in pCMV-3X flag vector (appendix 1.4 and 1.5). Wild type ran or wild type importin beta is over expressed along with nuclear membrane marker Lamin-GFP and cell membrane marker F-mCherry. 48 hours post transfection images were captured in confocal microscope. 3D reconstruction of confocal images (**Figure 5.7A**) gave quantitative measurements of N/C ratio in A431 cells.

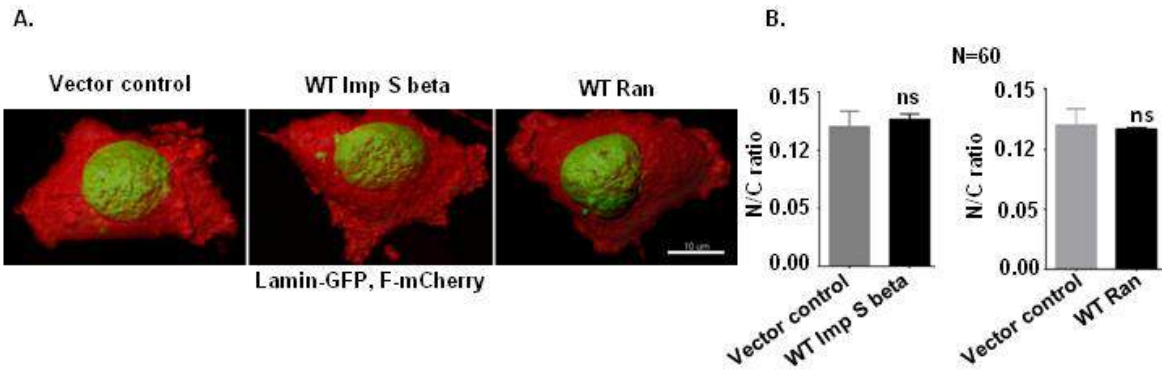

Figure 5.7: Wild type Importin beta or Ran has no effect on N/C ratio in skin transformed cells

Either of wild type Ran or wild type Importin beta along with GFP-Lamin and F-mCherry were transfected in A431 (Skin transformed) cells (A.) Overlay 3d reconstruction images of live cells obtained from Imaris. Scale Bar is 10 µm. (B) N/C ratios were quantified from 3d images in Imaris software for 60 cells from 3 different experiments. N/C ratio remained unchanged in both the cases as compared to control cells as represented in column graph). Error bars represent standard error mean (SEM).

Total 60 cells were captured in 3 different experiments. What is also fascinating is wild type Importin beta or Ran over expression in skin transformed cell line (A431) did not alter the N/C ratio as shown by the quantitative measurements (**Figure 5.7B**).

5.2.6: The nucleolus number and volume alters in transformed cells

The nucleus is host of several other sub nuclear compartments. An intriguing question to solve was whether the size and number of such compartments also changes as the nuclear size changes in transformed cell lines. Nucleolus hypertrophy is very common in cancer cells. We decided to quantitatively measure the alteration in size and number of nucleolus in transformed cell lines as compared to their immortalized counterparts. Therefore, we quantified the nucleolus number and volume with respect to nucleus volume in all four pair of immortalized and transformed cell lines used in this study. In live cells, nucleolus and nucleus volumes were measured in individual cells using GFP-Fibrillarin as nucleolus marker and RFP-Lamin as nuclear membrane marker. Quantitative measurements for nucleolar spots and nuclear volumes were done by the 3D reconstruction of confocal images (**Figure 5.8A**). The BrightR mode in the Leica-STED microscope was used during image capture, in which every nucleolus spot was evenly and optimally captured.

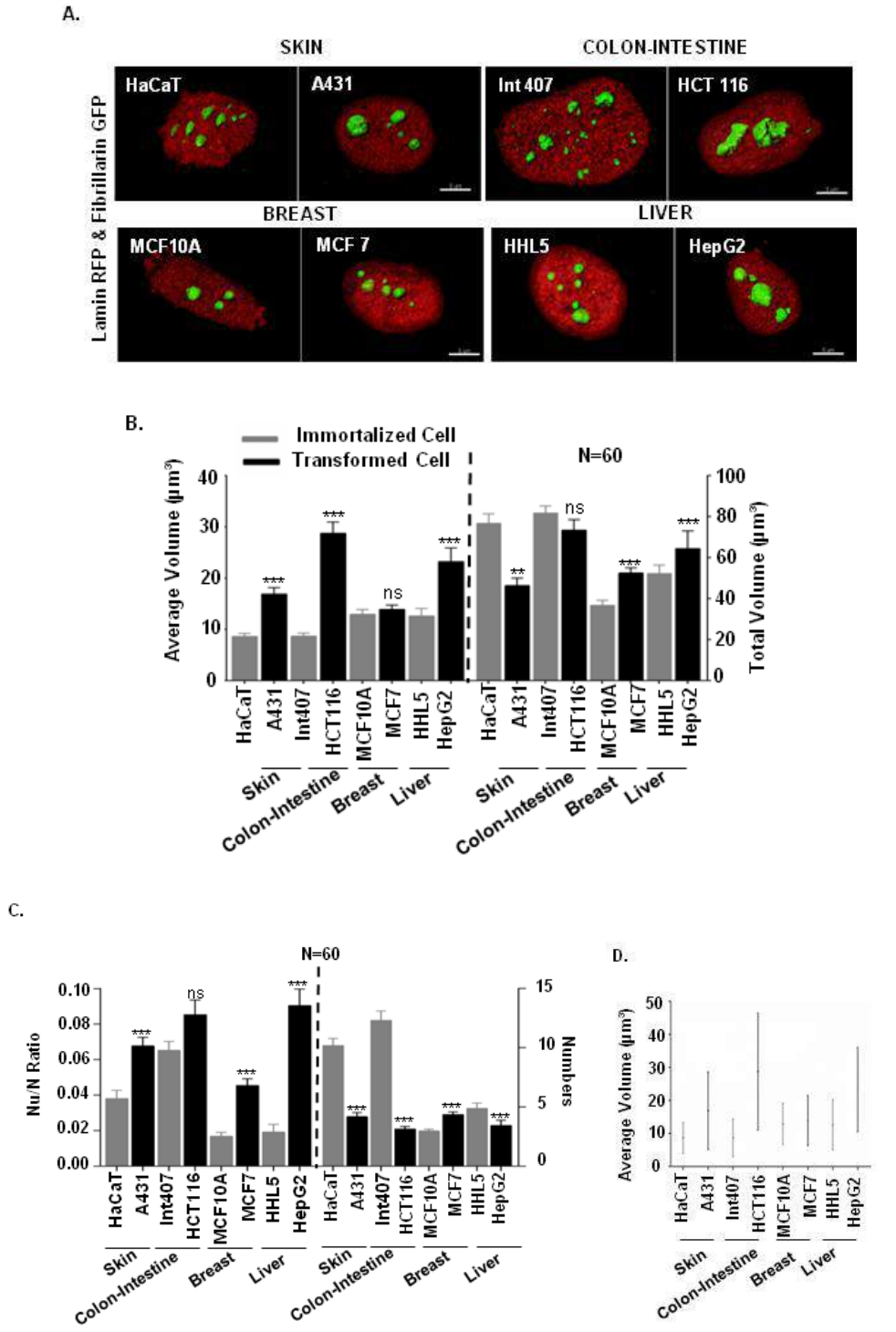

Figure 5.8: Nucleolus size and number alters in transformed cell lines compared to immortalized counterpart

(A) Cells were transfected with GFP-Fibrillarin and RFP-Lamin; Overlay 3D reconstruction images of live cell obtained from Imaris. Scale bar is 5 µm. (B) Nucleolus and nucleus volumes of each cell line were quantified from 3D reconstruction images (as represented in A) for 60 such nucleus in three different experiments. Average nucleolus volume and total nucleolus volume were calculated

*per nuclei. Error bars represent standard error mean (SEM). (C) Numbers of nucleolus spots and Nu/N ratio are altered in transformed cell lines. (D) In transformed cells, average nucleolus volume greatly varies compared to immortalized counterpart. Error bars represent standard error mean (SEM). ns, P > 0.05; *P ≤ 0.05; **P ≤ 0.01; ***P ≤ 0.001; ****P ≤ 0.0001*

Depending on tissue origin, we found that size and number of nucleolus spots altered differently from immortalized cell line to corresponding transformed cell lines (**Figure 5.8B, 5.8C**). To address this complexity in quantitative manner, we have measured two parameters, 'average volume' and 'total volume' of nucleolus. For the first parameter the average volume of all nucleolus spot's per nucleus was calculated and for the second parameter, the volumes of all nucleolus spots per nucleus were summed. In most of the cases, the first parameter alters in incremental fashion; if it does not alter then always the second parameter increases. To be precise, the average nucleolar spot volume mostly increases in transformed cells; when average nucleolus spot volume remained unchanged then the total nucleolar volume increases. In the former case, nucleolar spot number decreases while the same increases for the latter case. For example in case of skin, colon-intestine and liver cell lines (A431, HCT116, and HepG2 respectively) average volume of nucleolus spots were found to be significantly higher ($p<0.001$; Mann-Whitney Test) and numbers of nucleolus spots were significantly reduced compared to their immortalized counterparts (HaCaT, INT407, HHL5 respectively) (**Figure 5.8B, 5.8C**). On the other hand, in breast cell lines, both number and total volume of nucleolus spots were increased significantly in transformed cell lines (MCF7) compared to immortalized cell line (MCF10A) although average volume of nucleolus spots remained unchanged (**Figure 5.8B, 5.8C**). We have also observed, in transformed cells lines, average volume of

nucleolus spots per nucleus varies greatly compared to their immortalized counterparts (**Figure 5.8D**).

Although the N/C ratio was invariably found to be increased in all the transformed cell lines, but to address consistent nucleolus size alteration in transformed cells, we calculated another parameter, the total nucleolus volume to nucleus volume (Nu/N) ratio by dividing total volume of nucleolus spots per nucleus and volume of the nucleus. We found Nu/N ratio to be significantly increased in all the transformed cell lines (**Figure 5.8C**) except that of colon-intestine origin in which the increase was not statistically significant. Increase in Nu/N ratio (in most of the transformed cell lines) certainly indicate that the nucleolus size also scale with respect to nucleus in transformed cells. Nucleolus size is very dynamic and numbers and volume of nucleolus varies greatly in cell lines of different tissue.

5.2.7: The nucleolus number and volume alters upon blockade of nucleo-cytoplasmic transport

It is evident from the data shown in previous sections that the size of nucleus and the nucleolus are similarly altered in transformed cells compare to corresponding immortalized counterparts used in this study. This prompted us to explore whether the nucleolus size is also controlled by nuclear transport perturbation.

5.2.7.1: Effect of over expression of importin beta 1-364

To test the effect of importin beta 1-364 on nucleolus size, we transfected the same along with GFP-Fibrillarin and RFP- Lamin, 48 hours post transfection imaging was done as described previously for total 60 nucleuses in 3 different experiments. Post live cell imaging, immunofluorescence against Flag-Importin beta 1-364 was done to

show the cytoplasmic and nuclear pore localization of Importin beta 1-364. Over expression of importin beta 1-364 in immortalized cell line INT407 causes an increase of the average & total nucleolus spot volumes significantly ($p<0.001$; Mann-Whitney Test) (**Figure 5.9A, C**); while number of nucleolar spots were decreased in this condition($p<0.05$). Immunoflurescence experiment showed nuclear pore and cytoplasmic localization for importin beta 1-364 cells (**Figure 5.9B**).

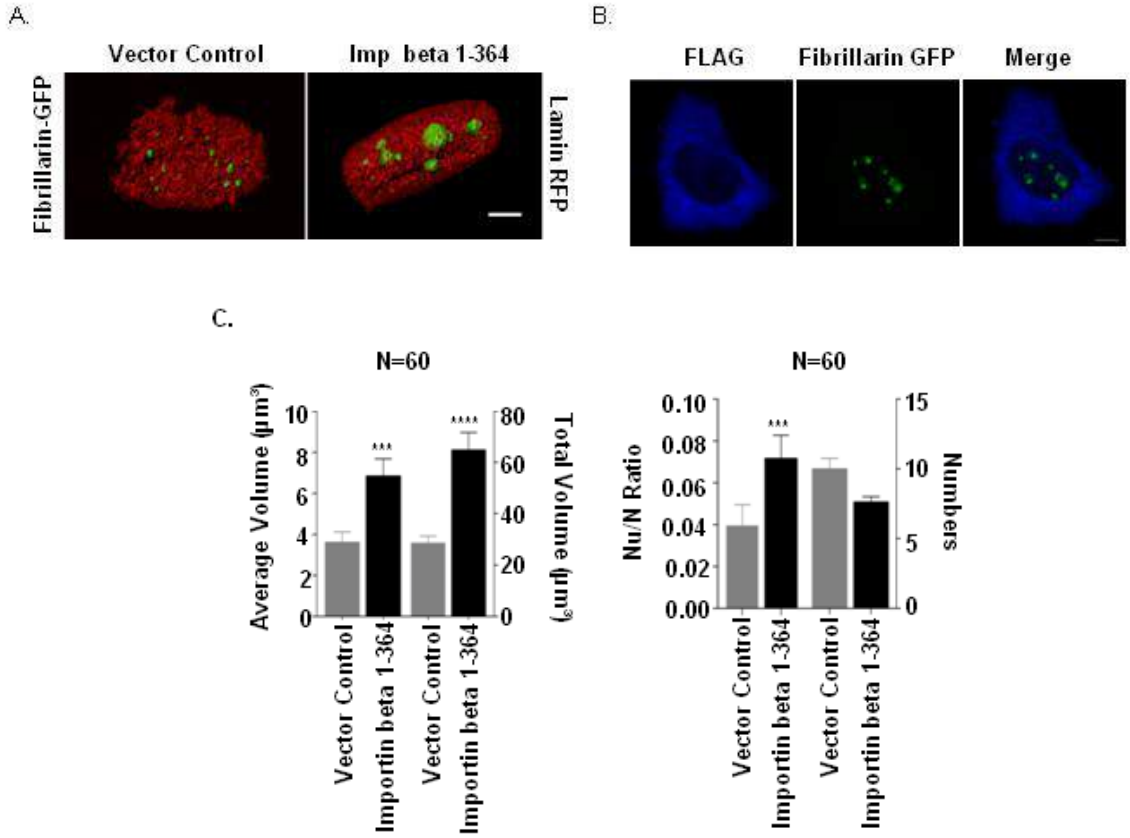

Figure 5.9: The nucleolus number and volume alters upon perturbation of nucleo-cytoplasmic transport.

INT 407 (Colon-intestine immortalized) cells were transfected with GFP-Fibrillarin, Lamin RFP, and Importin beta 1-364.(A) Overlay 3D reconstruction images of live cell obtained from Imaris. Scale bar is 5 lm. (B) Importin beta 1-364 is visualized by immunofluorescence against mAb Flag which is tagged with the former protein post live cell imaging. Fibrillarin-GFP images are live cell images. Scale bar is 5 lm. (C) Nucleus and nucleolus volumes were quantified from 3D reconstruction images (as represented in A) for 60 such nucleus in each case in three different experiments. Average nucleolus volume and total nucleolus volume per nuclei are increased significantly ($P < 0.001$) compared to vector control cells. Numbers of nucleolus

*spots and Nu/N ratio were calculated per nuclei. Error bars represent standard error mean (SEM). ***P ≤ 0.001; ****P ≤ 0.0001.*

We conclude that the over expression of importin beta 1-364 not only increases the N/C ratio, it also increases the size of nucleolus and Nu/N ratio as compared to vector control cell.

5.2.7.2: Effect of over expression of RanT24N and RanQ69L

We over expressed Ran^{T24N} or Ran^{Q69L} in the same way as described above.

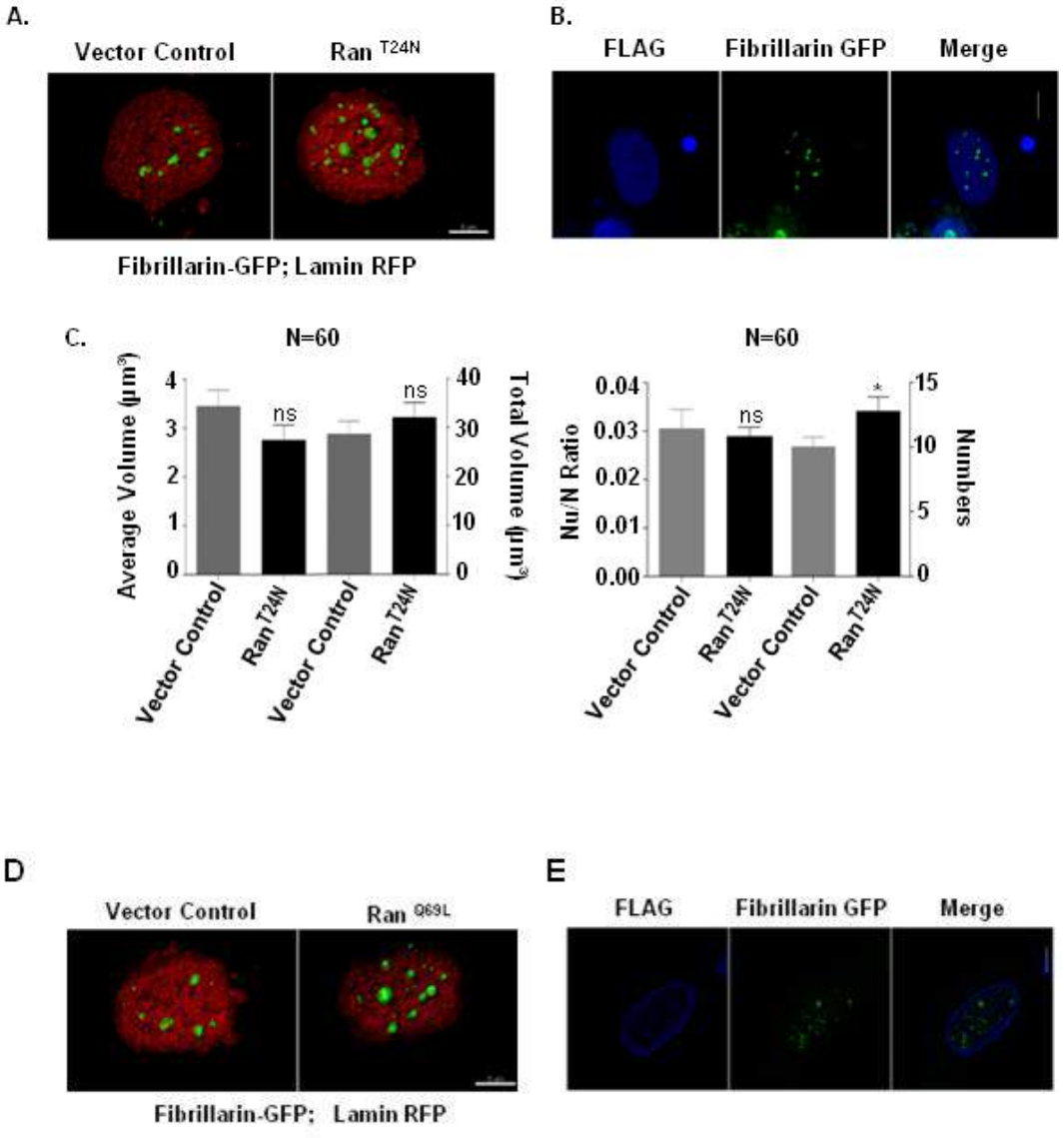

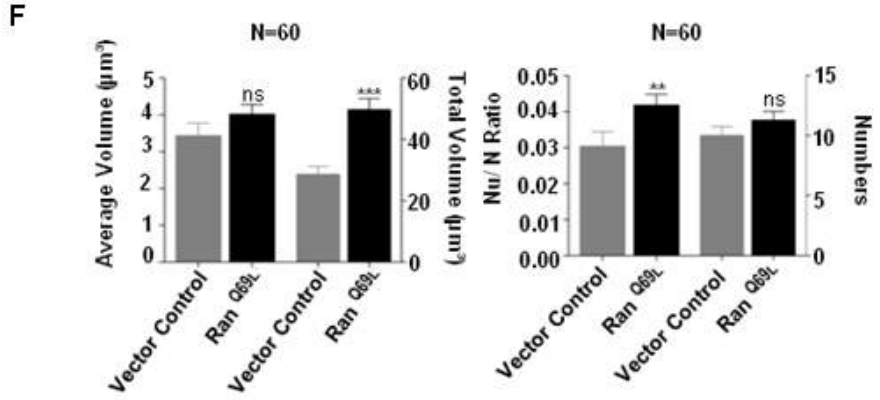

Figure 5.10: The Nucleolus number and volume alteration upon perturbation of nucleo-cytoplasmic transport by Ran dominant negative proteins.

*INT 407 (Colon-intestine immortalized) cells were transfected with GFP-Fibrillarin, Lamin RFP, and Ran ^{T24N} or Ran ^{Q69L}. (A) Overlay 3D reconstruction images of live cell obtained from Imaris, Scale bar is 5µm. (B) Ran^{T24N} and (E) Ran ^{Q69L} is visualized by immunofluorescence against mAb Flag which is tagged with the former protein post live cell imaging. Fibrillarin-GFP images are live cell images. Scale bar is 5 µm. (C) and (F) Nucleus and nucleolus volumes were quantified from 3D reconstruction images (as represented in A and D) for 60 such nucleus in each case in three different experiments. Average nucleolus volume, total nucleolus volume per nuclei, and Nu/N ratio remain unchanged (ns, P > 0.05) in Ran ^{T24N} over expressed cells compared to vector control cells. Numbers of nucleolus spots increased significantly (*P ≤ 0.05) in this case. In Ran Q69L over expressed cells, only number of nucleolus volume and total nucleolus volume increased significantly compared to vector control transfected cells.*
*Error bars represent standard error mean (SEM). **P ≤ 0.01; ***P ≤ 0.001.*

When we over expressed Ran^{T24N}, no significant difference were observed in nucleolus size or in Nu/N ratio but number of nucleolus spots increased significantly (**Figure 5.10A, C**). Interestingly, when we over expressed Ran^{Q69L}, although the average volume and numbers of nucleolar spots did not increase significantly, but the total nucleolus volume and Nu/N ratio increased significantly (**Figure 5.10 D, E, F**)
Post live cell imaging, immunofluorescence against Flag- Ran^{T24N} or Ran^{Q69L}, was done which showed complete nuclear localization for Ran^{T24N} and nuclear pore localization for Ran^{Q69L} as reported elsewhere.

Nucleo-cytoplasmic transport perturbation affects size of mammalian nucleus

We found similar results in over expression studies of dominant negative importin beta and ran performed in another immortalized cell line HaCaT.

5.2.8: Cytosolic component determines the size of nucleolus

From our previous results it was evident that importin beta 1-364 over expression leads to increase in nucleus size as well as nucleolus size. We can speculate that import block might play an important role in controlling nucleus and nucleolus size in mammalian system. To study this in detail, we have developed an 'in vitro' assay system in which intact nucleus isolated was incubated with cytosolic fraction isolated from a cell with different expression background.

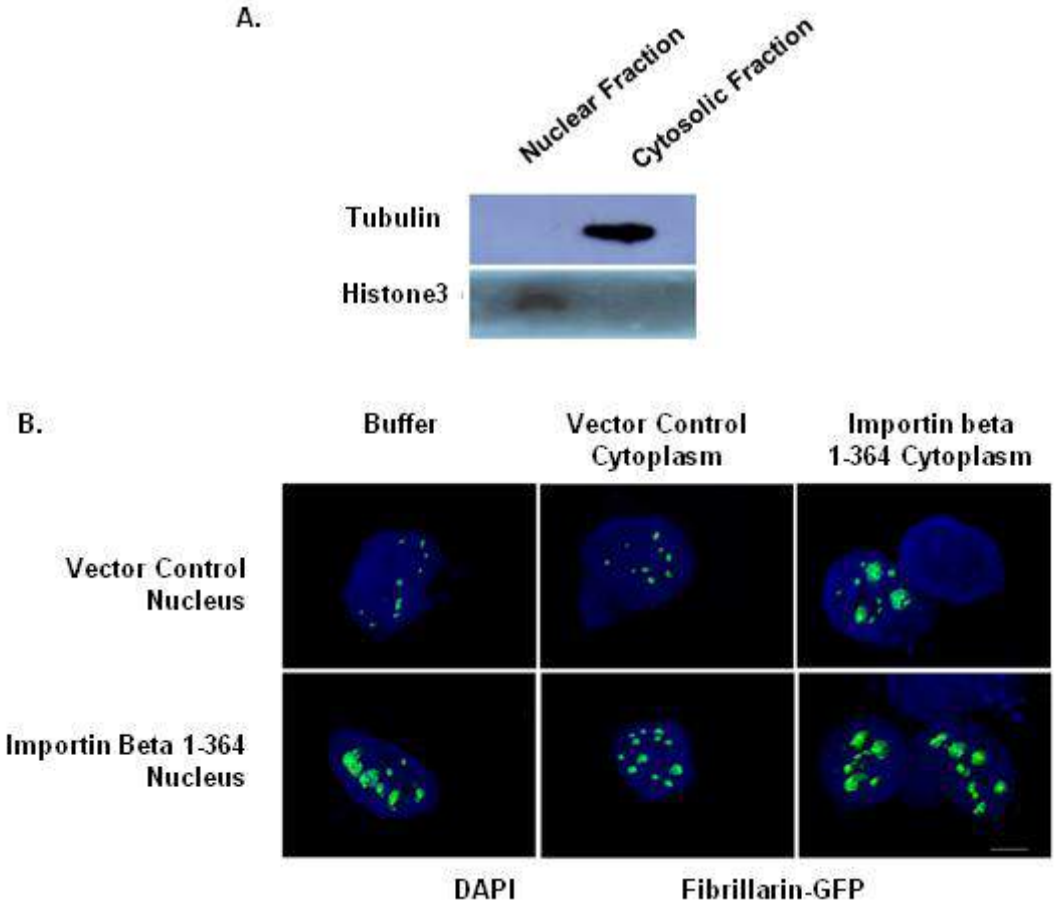

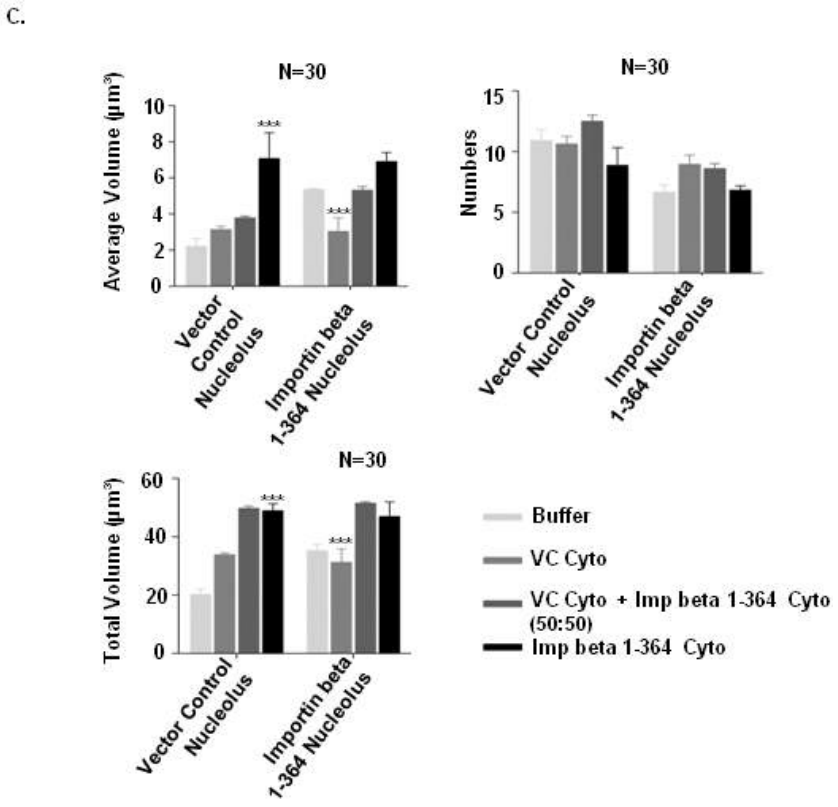

Figure 5.11: Cytosolic components determine morphological changes of nucleolus

*An in vitro assay combining intact nucleus and cytosolic fractions from different sources has been established to determine changes of nucleolus size. (A) Western blot showing purity of cytoplasmic and nuclear fraction (B) INT 407 cells were transfected with Fibrillarin-GFP and Importin beta 1-364 or vector control constructs and nuclei were isolated. Overlay 3D reconstruction images were obtained from Imaris. Scale bar represents 5 µm. (C) Nucleolus volume (Average and total volume) and numbers in each case were quantified from 3D reconstruction images (as represented in B) for total 30 such nucleus in each case from three different experiments. Average nucleolus volume of vector control nucleus significantly increased ($P < 0.001$) when incubated with cytosolic fraction of Importin beta 1-364 transfected cells. The same of Importin beta 1-364 transfected nucleus reduced significantly ($P < 0.001$) when incubated with cytosolic fraction of vector control transfected cells. When both the cytosolic fractions were incubated (1: 1 ratio) with either of the nucleus pool, average nucleolus volume scaled up or down respectively by ~ 50%. Error bars represent standard error mean (SEM). ns, $P > 0.05$; ***$P \leq 0.001$.*

We incubated the isolated pure nuclei with different cytosolic fractions in 1:2 ratios at 22°C for 30 minutes. Confocal imaging was done in different conditions; and volume

of nucleolus and numbers were calculated from 3d reconstruction images (**Figure 5.11A**).

When Cytosolic fraction of vector control transfected cells was incubated with pure nucleus population of Importin beta 1-364 transfected cells, nucleoli volume was scaled back to its normal size and vice versa (**Figure 5.11B**) whereas the number of nucleoli of Importin beta 1-364 transfected cells were increased although not significantly. When the cytosolic fraction of two different sources (vector control transfected cells and that for importin beta 1-364 transfected cells) were combined in a 50-50 ratio approximately 50% scaling of nucleolus size was observed.

These results suggest the following conclusions:

1. Cytosol of vector control transfected cell can scale down the increased size of nucleolus in a nucleus isolated from cells in which nucleo-cytoplasmic import is blocked.

2. Cytosol of cells in which nucleo-cytoplasmic import is blocked can scale up the smaller size of nucleolus in a nucleus isolated from a vector control transfected cell.

The results also indicate the importance of nuclear transport for size regulation of nucleus and nucleolus and underlay the possible role of unknown cytosolic factors in such regulation.

5.3: Discussion

We can hypothesize that redistribution of biomolecules from different cellular sub-compartments determine their relative size increases. Our comparative analysis resulted an insight of N/C ratio variation in different immortalized and transformed cell lines with powerful microscopic and image processing techniques. Such

knowledge would help to determine the biological relevance of alteration in N/C ratio in immortalized cells. In most of the cases such increase in N/C ratio contributed by the reduction in the cell volume of the transformed cell lines. However such increase is contributed mainly by nuclear volume increase in breast origin transformed cell lines while the cell volumes remained comparable. This actual nuclear volume increase in breast cell line and relative nuclear volume increase in others are probably reflection of a same mechanism, which is simply a redistribution of cytosolic and nuclear content. One of the key questions that we have asked that whether nuclear volume increase (relative or actual) is associated with any synchronous increase in nuclear sub-compartments such as nucleolus.

Our results show that total nucleolar volume changes in synchrony with nucleus volume. We have observed increase in Nu/N ratio in almost every case but changes in nucleolar spot numbers are widely variable. This variation in nucleolar spot numbers has been supported by another recent study [51]. It is possible that nucleolar spot number variation is related to variation in total nucleolar volume. Once again this indicates that such variations are result of redistribution nuclear and nucleolar components.

We for the first time have shown the importance of nucleo-cytoplasmic transport in human nuclear size regulations. However, previously such role was shown in different model organisms. Now one may ask why we get differences in degrees of N/C ratio increase between the cases where we have over expressed importin beta or Ran^{T24N}/Ran^{Q69L}. The reason for this is most likely due to the degrees of effectiveness of attenuation of the nucleo-cytoplasmic transport by over expressions of these different factors. It is to be noted, that both the nuclear import and the nuclear export block resulted the alteration of the N/C ratio. These suggest that not only the

incoming flux of biomolecules towards nucleus is important, but the outgoing flux has equal importance. In other words, the process of redistribution of nucleo-cytoplasmic components maintains the N/C ratio. Moreover, we established that the nucleo-cytplasmic transport plays an important role in the nucleolus size and number regulation in human cells.

According to our results, the nuclear import is probably more important than nuclear export in maintaining relative nucleolar structures. The over expression RanQ69L or importin beta causes a nuclear import blockade while over expression of RanT24N effectively perturbs the nuclear export pathway. We get high degree of Nu/N ratio change both for RanQ69L or importin beta over expression while we did not get any appreciable alteration of Nu/N ratio upon over expression of RanT24N. In short, if we block nuclear import we get dramatic alteration of relative the nucleolar volume but if we do block nuclear export there is no effect on relative nucleolar volume.

Now if we assume these blockades are directional specific, then we can assume during nuclear import block the nuclear size will shrink due to existing nuclear export. Yet during the effective nuclear export block the nuclear size will continue to increase. Such conditions can help us to make a simplistic deduction that probably a threshold nuclear volume is required for maintaining the balance of Nucleolus-to-nucleus bio-molecular distribution and Nu/N ratio. Any reduction of such threshold volume will disturb the equilibrium and in turn dramatically alter the relative nucleolar volume; while any increase of the nuclear volume is probably permissible to some extent. It is possible that the rule of requirement of threshold nuclear volume will apply to the relative size regulations for all nuclear sub-compartments. It is true though that blockade of nuclear export also causes N/C ratio to increase while it has no effect on Nu/N ratio. This may be contributed by a combination of alteration of

cell volume and nuclear volume through some unknown process which yet to be discovered.

Our in vitro assay shows that the cytosolic factors are determinant of nucleolar spot size and number. This is supported by the fact that even intact nucleus isolated from vector control transfected cells display enlarged nucleolus upon incubation with cytosol from cells undergoing nuclear import blockade by over expression of importin beta. Stoichiometry of these cytosolic factors are important as when the cytosolic fractions are diluted by half the extent of alteration of nucleolar spot size was reduced by half (**Figure 5.13**). It is very much possible that the dominant negative form of importin beta 1-364 themselves directly responsible for such phenotype as the factor is present in cytosol only. However it is also possible there are other unknown cytosolic factors expression of which probably get induced when importin beta is over expressed; It is very much possible these unknown factors are the determinant of nucleolar size. Known or unknown the fact that the factors are cytosolic, this alone indicates that the mechanism that control nucleolar size, can be regulated from outside of nucleus. In near future we expect to see the unraveling of these networks that control the nucleolar size from cytosol.

Chapter 6:

Study to investigate size and shape control mechanism of nucleus in yeast system

6.1: Introduction

How the nuclear shape is maintained in interphase cells as well as during mitosis, is poorly understood in budding yeast. Although some genes had been discovered recently but the underlying molecular mechanism is not well understood. The nucleus is a very dynamic structure containing various sub compartments [2, 3, 5]. Alteration in nuclear shape is often associated with different pathophysiological conditions in metazoans, of which mostly studied are in different forms of cancer, different muscular dystrophy etc [5, 7, 30]. In budding yeasts, the nucleus is mostly spherical or round [22]. During closed mitosis of yeast cells, the nucleus undergoes a dumbbell/ hourglass shape [121, 122]. Mutation in lamin is often associated with premature aging disease in which nuclear shape becomes very aberrant in metazoans [30, 31]. But, in yeast lamin is not present. In budding yeasts, nuclear shape changes upon certain cues, for example in the presence of mating pheromones nuclear shape is reformed [123] . Upon alteration of certain growth conditions, for example, reduced levels of acetyl co-A carboxylase activity reported showing nuclear membrane expansion [124]. Budding yeast mutants of early secretory pathway genes [38, 125], or some nuclear pore mutants (Nup84) [126], nuclear envelope extensions had been documented. Nem1p or Spo7 null mutant expands both nuclear and ER membrane in budding yeast [39, 122]. Nem1 and Spo7 basically form an ER-associated phosphatase complex which negatively regulates phospholipid biosynthesis [39, 122]. Interestingly, nuclear expansion in those mutants is devoid of chromatin but stay attached to a crescent shaped nucleolus [39, 41]. Under such membrane proliferating condition, if vesicular trafficking is disrupted, the nucleus becomes more irregularly shaped with increased nuclear surface area although N/C ratio remains unaltered [41].

In the closed mitosis of budding yeast, the nuclear shape becomes dumbbell/ hourglass shaped and again becomes round [121, 127, 128]. How the nuclear shape is controlled during these events is not known. Recently few groups studied nucleus shape in mitotic cells. Genes involved in DNA recombination and repair are reported to have nuclear extensions [122] . It has been suggested that due to mitotic delay in those mutants cells show such nuclear extensions by increasing phospholipid synthesis. In short, nuclear extensions observed in mitotic cells are due to mitotic delay followed by checkpoint activation and subsequent phopholipid synthesis activation [122]. Nuclear extension in all the cases is associated with nucleolus, suggesting uneven addition or expansion of nuclear membrane around the nucleus [122]. Nuclear extensions also observed in wild type mitotic cells are always not due to checkpoint activation in mitotic delayed cells. They showed that nuclear membrane protrudes ahead of mitotic spindles in pre anaphase cells [121]. It was believed that dynein mediated spindle oscillations help to traverse the spindle and nucleus across the bud. Surprisingly, the nuclear protrusions or nucleopodia formation does not depend on dynein/ Kar9 mediated spindle oscillation pathway[121]. Such nuclear extensions are mostly observed in cells delayed in mitosis and require actin, phospholipid synthesis and exocyst complex and independent of Kar9/ Dynein pathway [121]. These nuclear protrusions are also shown to be devoid of (contain very little amount) chromatin/ DNA [121]. It can be speculated that prior nuclear membrane expansion might be required for spindle oscillations. Microtubules are one of the important factors for chromosome segregation and it was believed cell division exclusively requires the presence of microtubules [129, 130] . Spindle pole body is embedded in the nuclear envelope, changes in the nuclear envelope environment affect SPB duplication, and as a result spindle formation [131]. However, the opposite

has not been shown. Very recently, it has been shown that in the absence of spindle microtubules, cells can divide via an unknown alternative method that requires spindle pole body separation, sister chromatid separation and actin polymerization [129].

Here we used an unbiased approach to find out genes responsible for strange nuclear shape in yeast. We exploited the information from a mammalian database called mitocheck, in which human genes were screened for impaired mitosis and in the same database genes responsible for strange nuclear shape are enlisted [132]. With this available information, we could directly assess the conservation of gene function at the level of nuclear shape phenotype. We screened the yeast homologues responsible for altered nuclear size and shape.

In this study, we report that most of the nuclear kinesins play an important role in maintaining nuclear shape. Amongst all, Kar3 and Cin8, minus and plus end motor proteins respectively [133-135], play an important role controlling nuclear shape throughout the cell cycle. One of the major findings is the identification of Prp45 gene, which is mainly responsible for pre-mRNA splicing [136, 137]. Nuclear shape alteration in Kar3, Cin8 null mutants, and prp45 1-169 ts mutant are not solely due to mitotic delay since we showed the nuclear shape alteration is present in all stages of cell cycle. Although chromatin volume or surface area is not significantly altered in kinesin mutants, but significantly altered in the prp45 1-169 mutant, suggesting that nuclear membrane expansion or alteration can affect the sub nuclear environment in various manners. We conclude that, kinesins like kar3, cin8 and pre mRNA splicing protein prp45 1-169 play important roles maintaining nuclear shape from yeast to mammalian system.

6.2 Results:

6.2.1: To develop an assay system to monitor Nucleus Size and shape in budding yeast (*S.cerevisiae*) system

To monitor the size and shape of the yeast nucleus we have developed an assay system, in which nuclear core, as well as overall cell, is tagged with two different colored fluorescent proteins. Initially, we used Histone **H2B** (HTB2) GFP fusion as a nuclear core marker and HDEL-E2-Crimson to label the nuclear as well as cell periphery, HDEL is the ER retention signal while E2-Crimson is a unique fluorescent protein of far red excitation region. In this dual color strain, live cell imaging was done (**Figure 6.1A**). Histones are present in euchromatin and heterochromatin but not in the entire nucleus throughout the cell cycle. It was reported recently that budding yeast nuclear envelope can expand or alter without affecting the chromatin [39].

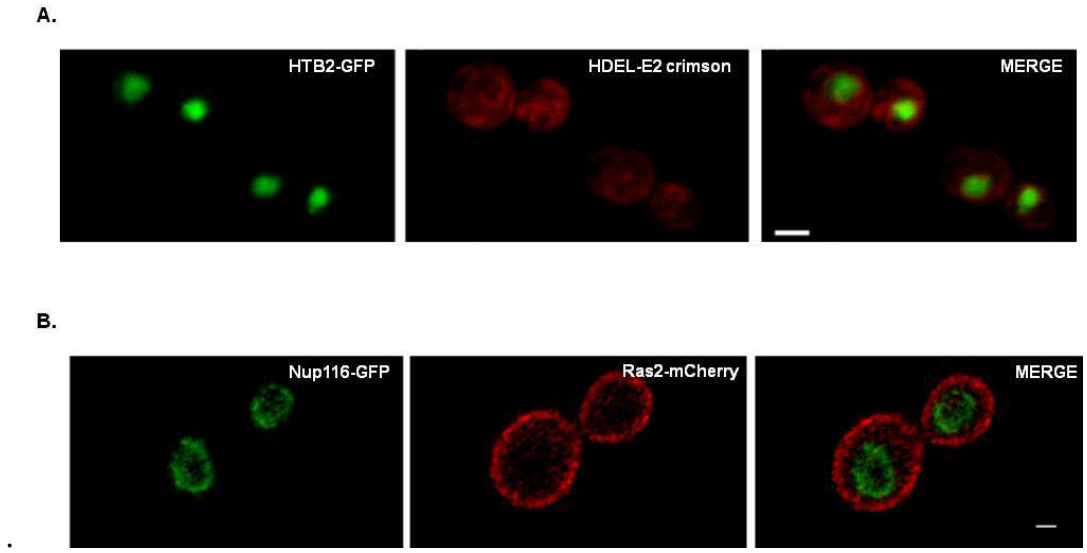

Figure 6.1: Assay Systems to monitor the nucleus size and shape in yeast

(A) Histone HTB2 is tagged with GFP and expressed as an episomal plasmid (YEplac195-HTB2) while HDEL-E2Crimson is integrated in the genome endogenously. Scale bar is 2µm. (B) Nuclear membrane is labeled with Nup116-GFP endogenously by PCR mediated epitope tagging and Cell membrane is labeled with mCherry Ras2 and integrated in the genome of S. cerevisiae. Scale Bar is 1µm.

To have a better idea of entire nucleus size and shape at any given condition, any nuclear membrane protein is a good candidate marker. We have developed a different assay system, in which nuclear envelope marker Nup116 is tagged endogenously with mGFP by PCR-mediated epitope tagging. The map of the vector used for epitope tagging is shown in appendix 1.7. In the same strain, mCherry is tagged with cell membrane marker Ras2 endogenously (**Figure 6.1B**). mCherry-Ras2 cloning strategy is shown in the appendix (appendix 1.6). This particular assay system with Nup116-GFP and mCherry-Ras2 is used in all the following study.

6.2.2: Directed mutagenesis to study Nucleus size and shape in budding yeast system

Regulation of nucleus size and shape is one of the very primary processes inside the cell which is strongly selected during evolution. In a database, also known as "Mitocheck", 22,000 human genes were analyzed for defective cellular phenotypes during mitosis using siRNA & high-throughput live cell imaging in HeLa cells [132]. In this database, 200 genes, responsible for strange nuclear shape are also enlisted. We searched for yeast orthologues of all such genes through Ensemble Genome Browser. 44 yeast orthologuess then listed in two categories as essential genes (20) and non essential genes (24) using Saccharomyces Genome Database (SGD). Null mutation of any gene if viable makes that particular gene as nonessential gene and if any null mutation is inviable, that mutant gene is an essential gene. To make null mutants for the nonessential genes, first the genomic loci were simulated in Snapgene database using SGD to design specific primers. A very well-known strategy is available in which the gene of interest is removed by homologous recombination through a PCR selection cassette. Using two different vectors, namely, pUG6 (with

G418 selection) and pUG72 (with URA3 selection) different genes' deletion cassettes were PCR amplified. The map of the vectors pUG6 and pUG72 are shown in figure 6.2. PCR amplicons with respective genes are transformed in the assay system strain (Nup116-GFP and mCherry Ras2) to visualize the nucleus size and shape in live cell condition upon deletion of any particular gene.

Null mutants were first confirmed by PCR using two primers in which one primer is approximately 500bp upstream of the gene of interest and another primer in the PCR deletion cassette, strategy shown in Figure 6.3.

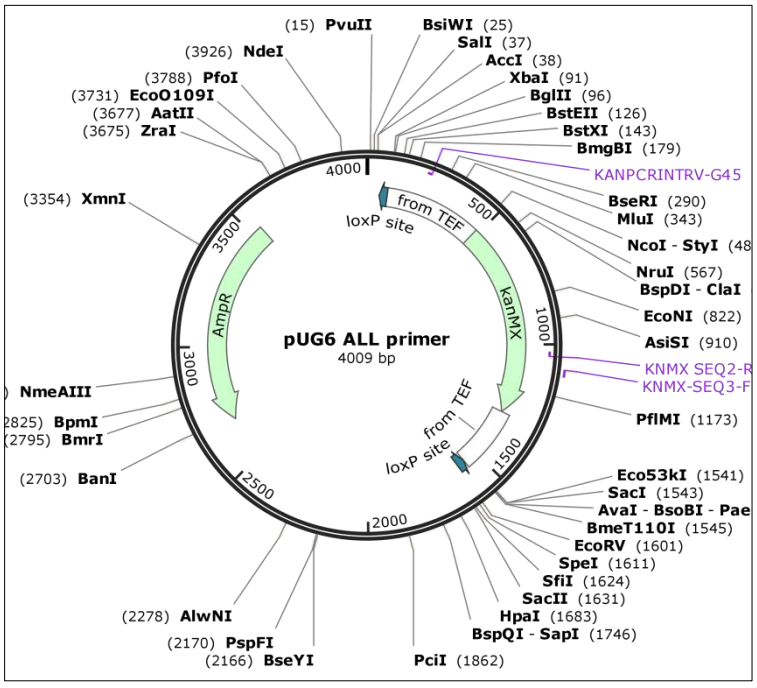

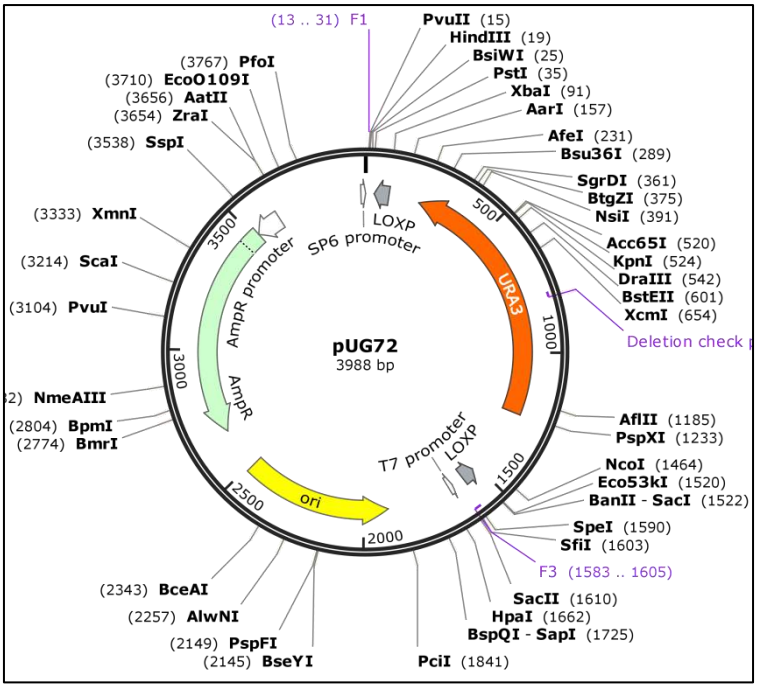

Figure 6.2: Map of pUG6 and pUG72

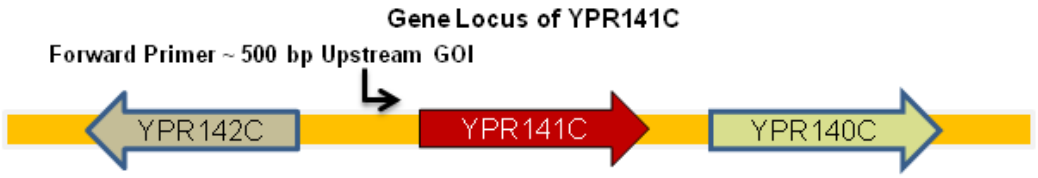

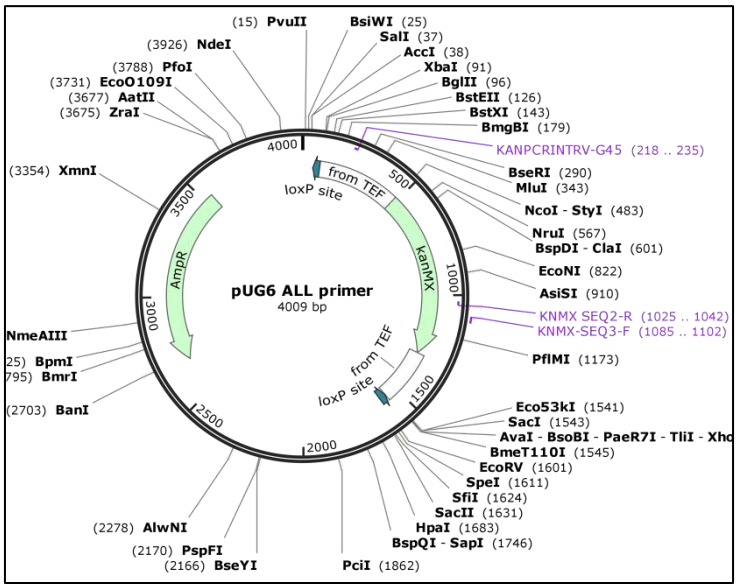

Reverse Primer in the URA3 or G418 locus in the respective vectors

Figure1 6.3: Strategy to confirm deletion of gene of interest

Null mutants were confirmed by PCR (**Figure 6.4A**).

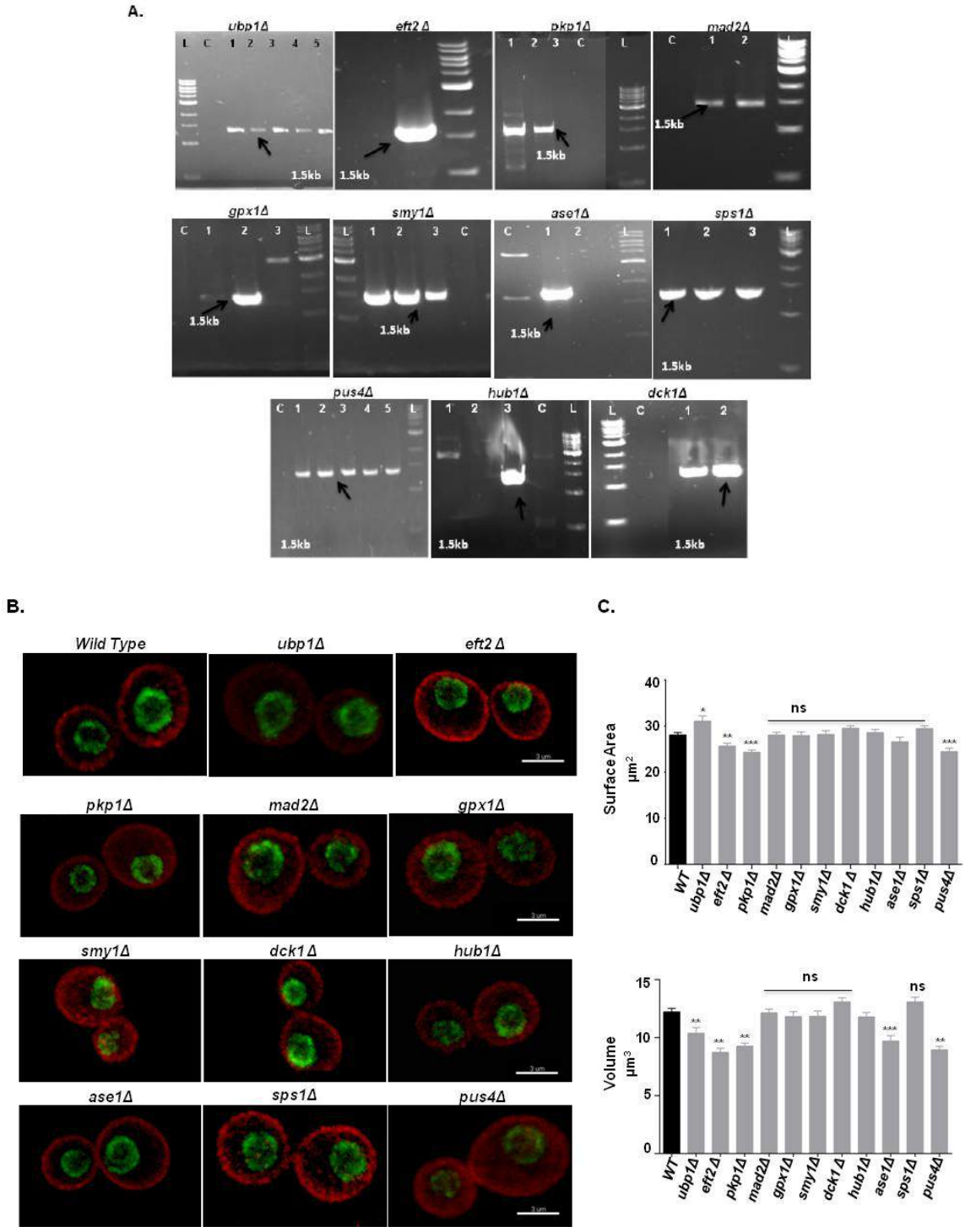

Figure 6.4: Analysis of mitocheck yeast homologues responsible for strange nuclear shape

(A) Gel pictures of respective null mutants showing correct PCR amplification of size 1.5 kb.(B) Overlay confocal live cell images of null muatants labelled with NUP116-GFP and mCherry-Ras2; deletion of the respective genes were performed in the background strain (nup116-GFP, mCherry-Ras2). Scale Bar is 3µm.(C) Quantification of nuclear surface area and volume in the yeast null mutants.Column graph showing nuclear surface area or volumes was quantified from 3D reconstruction images of confocal images as representated in figure B, in 100 cells in

*3 different experiments. Error bar represents standard error mean. ns, P > 0.05; *P ≤ 0.05; **P ≤ 0.01; ***P≤ 0.001*

Cells of different deletion mutants were grown up to log phase (OD_{600}= 0.5) and then immobilized on a cover slip bottom plate. We have performed live cell imaging of the deletion mutants 100 cells each in 3 different experiments. Confocal images were captured including entire z stack (**Figure 6.4B**). 3D reconstruction of confocal images of the mutants' nucleus resulted in the nuclear surface area and volume estimations. We found several genes showed significantly increased nuclear surface area and volume while some genes showed decreased nuclear surface area and volume compared to wild type cells (**Figure 6.4C**). In the *mitocheck* data base, all these genes showed strange nuclear shape. In our result, we find many of the genes depletion resulted in a reduction in nucleus size (*eft2Δ, pkp1Δ, pus4Δ*) as quantified by nuclear surface area and volume while few gene showed increased nucleus size and shape (*ubp1Δ*) and rest of the genes showed no effect on nucleus size and shape in yeast system. We infer that all the genes which showed strange nuclear shape in HeLa cells are not functionally conserved from yeast to mammal with respect to nuclear shape regulation. In this study, we focused on few selective genes, which showed distinctive phenotypes as described below.

6.2.2.1: Nuclear kinesins play important role controlling nuclear shape:

From the *in silico* screen, we found all six nuclear kinesins in yeast are present in the yeast homologues list [138]. All of the kinesins are nothing but motor proteins, kar3 is the only minus end motor protein while all other nuclear kinesins (Cin8, Kip1, Kip2, Kip3, Smy1) in *S. cerevisiae* are plus end motor proteins [138].

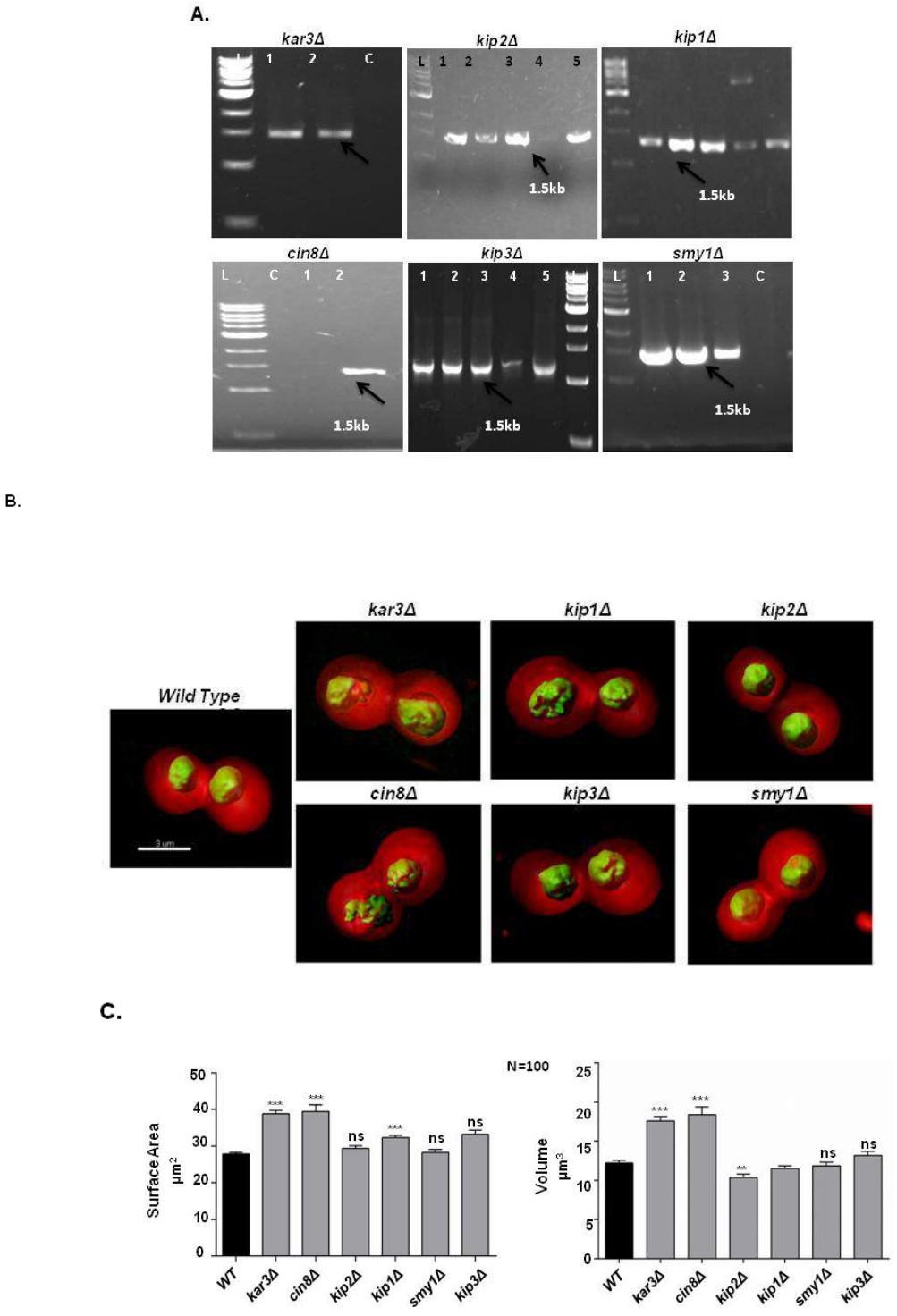

Figure 6.5: Effect of nuclear kinesins on nuclear size and shape

kar3 and cin8 null mutants exhibit significantly increased nuclear surface area and volume (A) Gel pictures of different nuclear kinesins showing correct PCR amplification of size 1.5 kb. (B) Overlay 3d reconstruction images of respective genes labelled with Nup116-GFP and mCherry-Ras2; deletion of the respective genes were performed in the background strain (nup116-GFP, mCherry-Ras2). Scale Bar is 3µm. (C) Quantification of nuclear surface area and volume of nuclear kinesin null

*mutants.Column graph showing nuclear surface area or volumes, quantified from 3D reconstruction images as representated in figure B, in 100 cells in 3 different experiments. Error bar represents standard error mean. ns, P > 0.05; ***P≤ 0.001.*

We have created null mutations of all the kinesins. Null mutants were first confirmed by PCR using two primers in which one primer is 500bp upstream of the gene of interest and

another primer in the PCR deletion vector as described before. Representative gel pictures are shown in (**Figure 6.5A**). Deletion mutants were grown up to log phase (OD_{600}= 0.5), and then immobilized on a cover slip bottom plate. We have performed live cell imaging of those mutants, 100 cells each in 3 different experiments. 3D reconstruction of confocal images of each nucleus resulted surface area and volume estimations (**Figure 6.5B**). *kar3Δ* and *cin8Δ* showed significantly increased nuclear surface area and volume. *kip1Δ* and *kip2Δ* also showed alteration in nuclear shape but to a lesser extent while *kip3Δ* and *smy1Δ* showed no significant effect on the nuclear shape (**Figure 6.5C**). To confirm that null mutant of kar3 and cin8 caused the altered nuclear phenotype; wild type kar3 and cin8 are cloned in YCplac33 vector (appendix 1.9 & 1.10) and transformed in the respective null mutant strains. A single copy of kar3 and cin8 rescued the altered nuclear phenotype in those mutants (appendix 3).

Of interest, amongst the splicing genes, we checked the phenotype for one of the essential gene *Prp45*; the temperature sensitive (Ts) mutant prp45 1-169, were grown up to log phase (OD_{600}=0.4) and then shifted to 37°C for 2 hours. Live cell imaging was performed at both 25°C as well as 37°C temperature in an incubator equipped with the microscope. 100 cells were imaged in 3 different experiments in each case. 3D reconstruction of confocal images of Prp45 1-169 ts mutant showed significantly altered nuclear shape in terms of increased nuclear surface area and volume when shifted to 37°C compared to the wild type cells (**Figure 6.6A and 6.6B**)

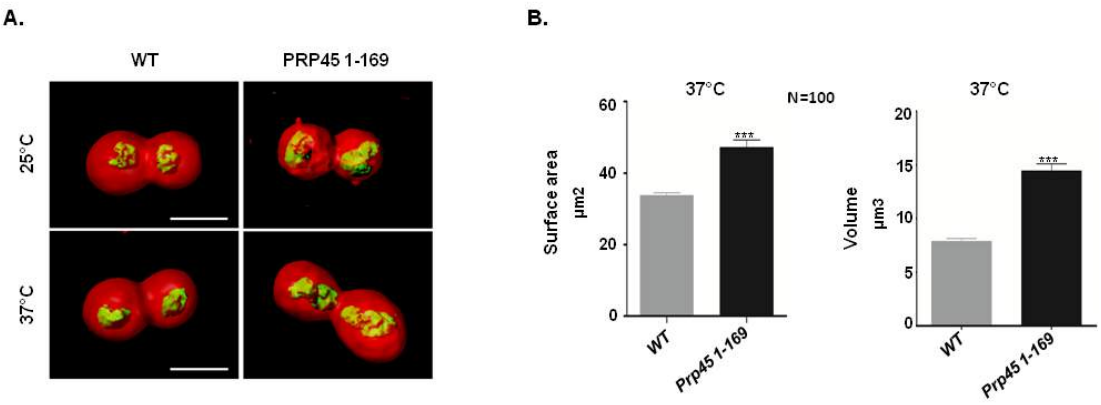

Figure 6.6: Prp45 1-169 Ts mutant exhibit significantly increased nuclear surface area and volume at non permissive temperature

*(A) Overlay 3d reconstruction images of prp45 1-169ts mutants captured in both 25°C and 37°C labelled with Nup116-GFP and mCherry-Ras2. Scale Bar is 3µm.(B) Quantification of nuclear surface area and volume in the prp45 1-169 mutants at 37°C.Column graphs showing nuclear surface area or volumes, quantified from 3D reconstruction images as representated in figure B, in 100 cells in 3 different experiments. Error bar represents standard error mean..***P≤ 0.001.*

6.2.3: Nuclear shape mutants showed abnormal nuclear morphology throughout cell cycle:

The flawless execution of cell division is fundamental to the formation and survival of living organisms. Budding yeast has a closed mitosis and during cell division yeast nucleus goes through from round to dumbbell nuclear shape [139]. However, the mechanism by which it does is poorly understood. To have an unbiased estimation of nucleus size, we have checked nuclear shape phenotype in telophase cells, with two buds each containing one nucleus, for all the screening. So, next obvious question was to check whether an altered nuclear shape in *kar3Δ, cin8Δ*, and prp45 1-169 ts mutants are specific to any cell cycle stage. Mutants were grown as described before, and live cell imaging of the mutants was performed in cells, with different stages of cell cycle based on different bud size in 3 independent experiments.

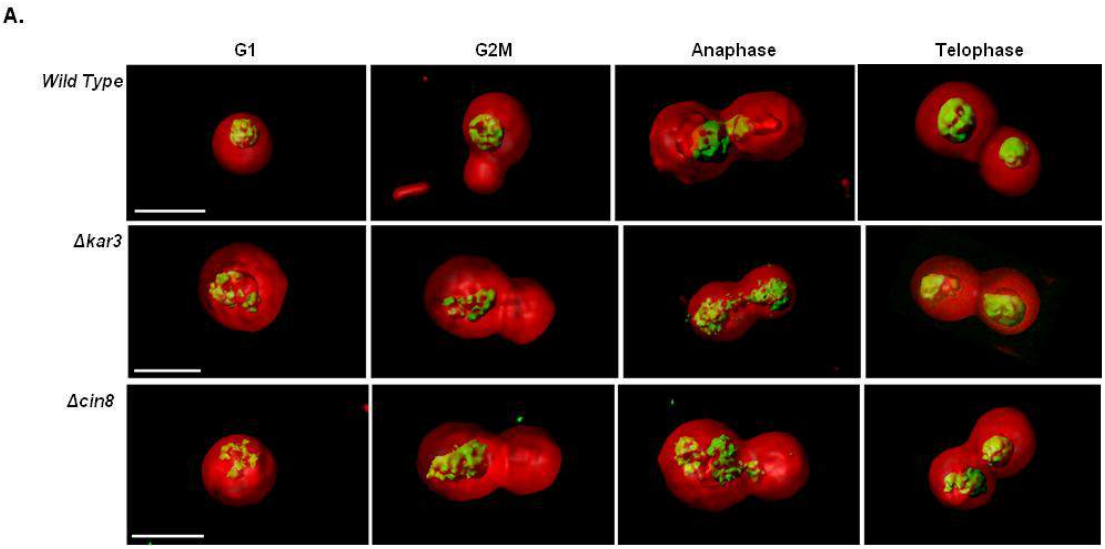
A.
G1
G2M
Anaphase
Telophase
Wild Type
Δkar3
Δcin8

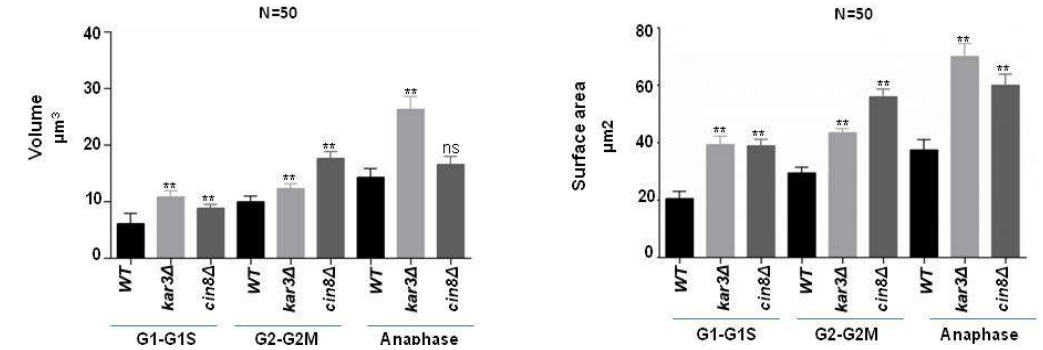
B.
N=50
Volume µm3
40
30
20
10
0
**
ns
WT
kar3Δ
cin8Δ
G1-G1S
G2-G2M
Anaphase
N=50
Surface area µm2
80
60
40
20
0
**

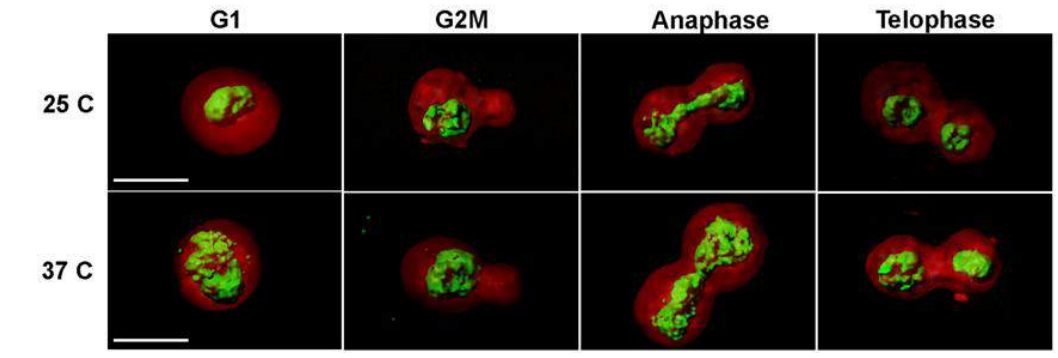
A.
G1
G2M
Anaphase
Telophase
25 C
37 C

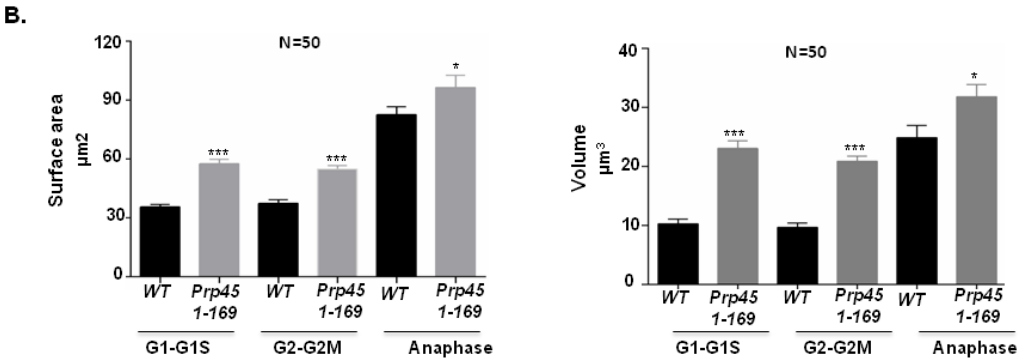

Figure 6.7: *kar3Δ, cin8Δ* and prp45 1-169 Ts mutants showed altered nuclear shape in each stage of cell cycle

*(A) Overlay 3d reconstruction images of kar3Δ and cin8Δ in different stages of cell cycle. Scale Bar is 5µm. (B) & (D)Quantification of nuclear surface area and volume in kar3Δ, cin8Δ and prp45 1-169 Ts mutants.Column graph showing nuclear surface area or volumes was quantified from 3D images of confocal images as representated in figure A and C, in 60 cells for each stages of cell cycle in 3 different experiments. Error bar represents standard error mean. *P ≤ 0.05; **P ≤ 0.01; ***P≤ 0.001 (C) Overlay 3d reconstruction images of prp45 1-169ts mutants captured in both 25°C and 37°C in different stages of cell cycle. Scale Bar is 5µm.*

For, prp45 -169 strain, images were captured both at 25°C and after the cells were shifted to 37°C to obtain the mutant phenotype. 3D reconstruction of confocal images resulted in an estimation of nuclear surface area and volume. Our results show that *kar3Δ, cin8Δ* and prp45 1-169 ts mutant, nuclear surface area and volume are significantly increased in G1/G1-S, G2/ G2M and anaphase cells compared to respective wild type cells (**Figure 6.7 A-D**). However, in *cin8Δ*, during anaphase, nuclear surface area is increased significantly but nuclear volume remained unchanged compared to wild type cell. *kar3Δ and cin8Δ* null mutants are reported to be delayed in mitosis [138]. Therefore, we have also confirmed the nuclear shape alteration by electron microscopy in different stages of cell cycle in kar3Δ and cin8Δ mutants (**Figure 6.8**).

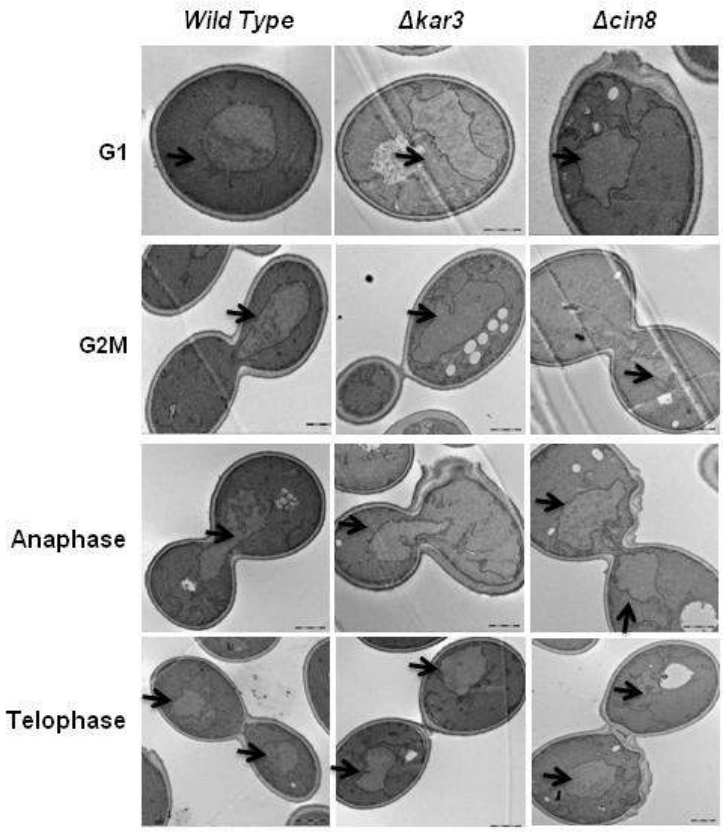

Figure 6.8 EM micrographs of *kar3Δ and cin8Δ* mutants showing altered nuclear shape in different stages of cell cycle

It is previously reported that abnormal nuclei are observed in the case of cin8 mutants, and most of them were in mitotic phase [122]. Our results rule out the possibility that nuclear surface area alteration in kar3 and cin8 null mutants are not solely due to mitotic delay. Kar3 deletion leads to syntelic attachment [140] and Cin8 is a chromosome segregation protein [135], in both the cases, spindle checkpoint pathway is activated which is reported to delay cell cycle in mitosis. We suggest that although those mutants exhibit a delay in mitosis, but altered nuclear shape is not solely due to mitotic delay.

6.2.4: Microtubules are required for maintenance of abnormal nuclear shape in kinesin mutants

Microtubules are important for chromosome segregation and it was believed cell division exclusively requires the presence of microtubules [129, 130]. Motor proteins are mostly present on the microtubules. Microtubule depolymerizing agent nocodazole treatment leads to mitotic delay in and shows nuclear extension. We checked if microtubules are required in *Δkar3 and Cin8Δ* mutants to maintain the abnormal nuclear shape.

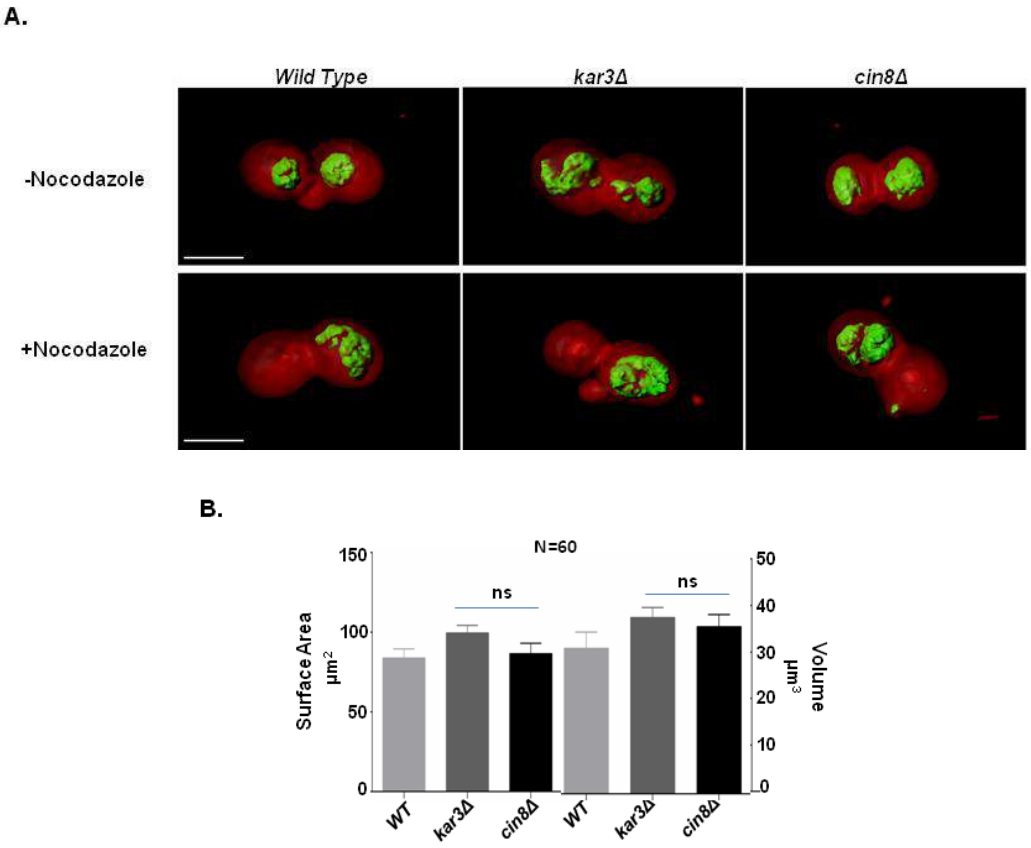

Figure 6.9: Microtubules maintain the altered nuclear shape in kar3 and cin8 null mutants *(A) Overlay 3D reconstruction images of nucleus and cell in the kar3 and cin8 mutants upon nocodazole treatment (B) Quantification of nuclear surface area, volume in the same mutants upon nocodazole treatment. 60 cells were imaged in 3 different experiments. Error bar represents standard error mean. ns P > 0.05*

kar3Δ and cin8Δ cells were synchronized with alpha factor followed by nocodazole treatment. Cells were imaged in confocal microscopes for 100 cells each in 3 different experiments for both the mutants. 3D reconstruction of confocal images of each nucleus resulted surface area and volume estimation (**Figure 6.9A & B**). We observed nuclear shape became near round and entangled upon nocodazole treatment in the mutants compare to wild type cells. However, in *kar3Δ and cin8Δ* mutants total surface area or volume did not change significantly upon nocodazole treatment. We conclude that intact microtubules are important in those mutants to maintain altered nuclear shape (**Figure 6.9A & B**).

6.2.5: Spindle lengths are altered in *kar3Δ and cin8Δ* mutants in different stages of cell cycle

In budding yeast spindle pole body is embedded in nuclear envelope [141]. Spindles are originated from SPB embedded in nuclear envelope [141].

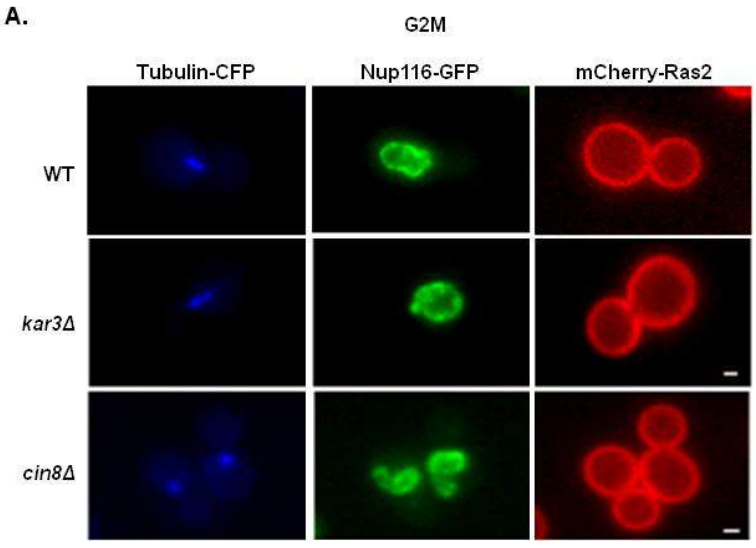

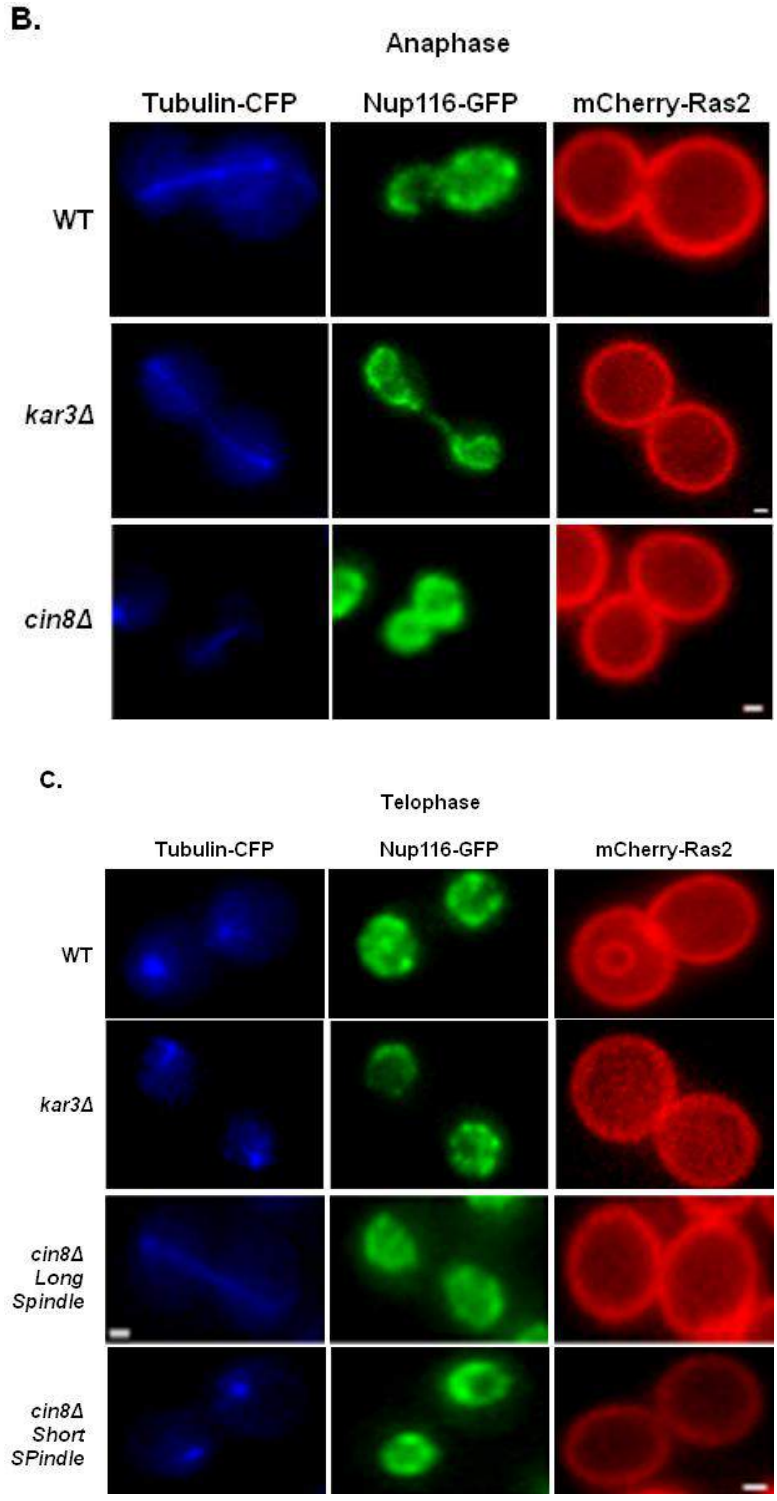
B.
Anaphase
Tubulin-CFP
Nup116-GFP
mCherry-Ras2
WT
kar3Δ
cin8Δ
C.
Telophase
Tubulin-CFP
Nup116-GFP
mCherry-Ras2
WT
kar3Δ
cin8Δ Long Spindle
cin8Δ Short SPindle

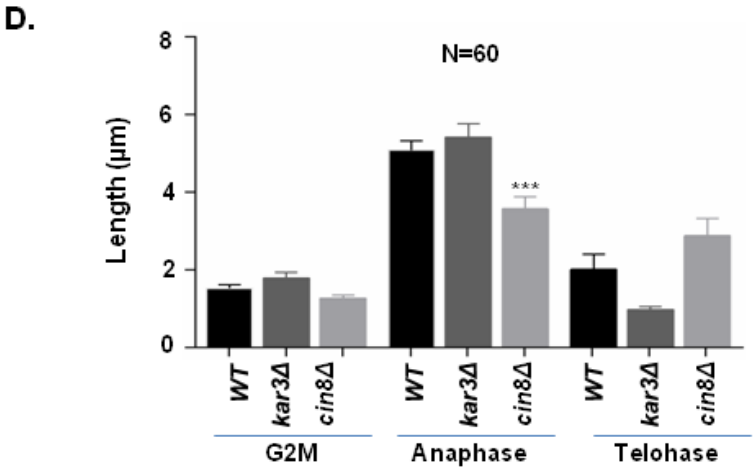

Figure 6.10: Spindle lengths in *kar3Δ and cin8Δ* mutants in different stages of cell cycle *Live cell images of wild type, kar3Δ and cin8Δ stably expressing α tubulin-CFP, Nup116-GFP and mCherry Ras2 in (A) G2M stage (B) Anaphse, and (C) Telophase stage of cell cycle. Scale bar is 1 µm. (D) Quantification of spindle lengths of wild type, kar3Δ, and cin8Δ mutants of 60 cells in 3 different experiments for each stage of cell cycle. Error bar represents standard error mean. ***P≤ 0.001*

One of the important roles of motor proteins is to form the spindle apparatus and to separate the chromosomes during cell division [142]. We checked next the spindle structure in *kar3Δ and cin8Δ* mutants in the different stage of cell cycle. For the same, first, we expressed alpha Tubulin-CFP endogenously in wt, *kar3Δ, and cin8Δ* mutants. Cells were grown up to log phase (OD_{600}= 0.5) and immobilized on a cover slip bottom plate. Live cell images were captured in a wide field microscope with entire z-stack with different fluorescent filters. Our result shows spindle length differs but not significantly in *kar3Δ and cin8Δ* mutants compare to wild type cells in g2m, anaphase and telophase cells (**Figure 6.10 A, B, C**). We measured the length of spindles in cells with different stage of cell cycle in the null mutants using imaris software (**Figure 6.10D**). We found that during anaphase, spindle length reduces significantly only in *cin8Δ* null mutant compared to wild type cells. In other conditions, no significant difference in spindle length is observed in the null mutants.

We observed in the *cin8Δ* mutant, during telophase, occurrence of cells with intact long spindle even after nuclei are separated, is very high compared to wild type cells (Figure 6.10C third row). We conclude that in the *kar3Δ and cin8Δ* mutants spindle length alters mainly during anaphase.

6.2.6: Cortical ER did not contribute in the increased nuclear surface area of *kar3Δ* and prp45 1-169 Ts mutants

We have shown that in *kar3Δ, cin8Δ* and prp45 1-169 mutants' nuclear shape is altered and such altered phenotype is observed in all stages of cell cycle. Since the nuclear membrane is continuous with ER, we checked the membrane of other ER domain (peripheral ER) if expanded in the mutants in *kar3Δ and cin8Δ* and prp45 1-169 ts mutants. To visualize the ER, we fluorescently labeled Sec63 with GFP. Sec63 is an abundant transmembrane protein, localizes to both sheets and tubules of ER [143, 144].

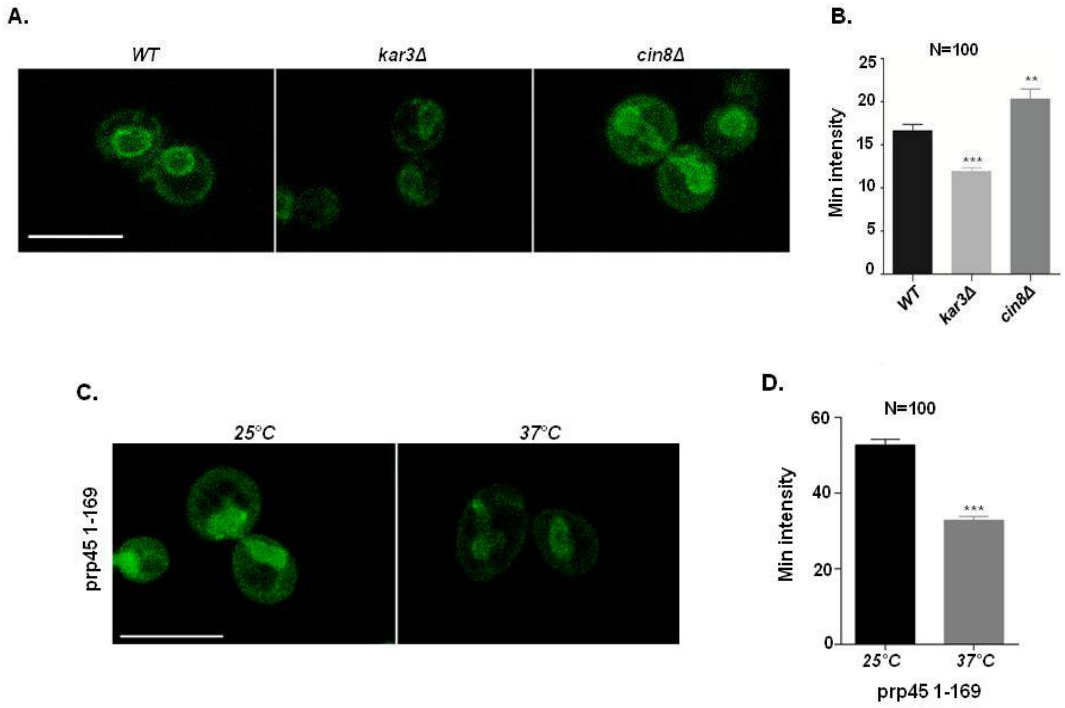

Figure 6.11: Peripheral ER expression in the *kar3Δ, cin8Δ* and prp45 1-169 Ts mutants

*(A) Confocal sections of wild type, kar3Δ and cin8Δ cells, expressing endogenously labeled Sec63-GFP. Scale bar is 5 µm. Right panel shows the min intensity of cortical ER GFP signal in all the strains calculated from Image J for 100 cells in 3 different experiments. (B) Confocal sections of prp45 1-169 Ts mutant at both 25°C and 37°C, expressing endogenously labeled Sec63-GFP (peripheral ER marker). Scale bar is 5 µm. Right panel shows the min intensity of cortical ER GFP signal calculated from Image J for 100 cells in 3 different experiments. Error bar represents standard error mean. **P ≤ 0.01; ***P≤ 0.001*

Cells were grown up to log phase (OD_{600}=0.5) and live cell confocal imaging was performed for 100 cells in 3 different experiments for *kar3Δ and cin8Δ* null mutants.

In prp45 1-169 ts mutants, cells were grown first up to log phase (OD_{600}=0.4) then shifted to non permissive temperature. Live cell imaging were performed both at 25°C and 37°C as described earlier. Optical sections through the middle of these cells showed the evenly labeled nuclear envelope and the peripheral ER, which in yeast lies just underneath the plasma membrane (**Figure 6.11A and C**). Peripheral and perinuclear ER are connected by a small number of tubules, which were only occasionally captured in single optical sections. In *cin8Δ* mutant, cortical ER expression was significantly increased while in *kar3Δ* mutant the same is decreased compared to wild type cells (**Figure 6.11 B**). In prp45 1-169 ts mutant, the cortical ER expression is significantly reduced when shifted to non-permissive temperature (**Figure 6.11D**). These results indicate that peripheral ER is only expanded in *cin8Δ* despite the fact that nuclear surface area is increased in both *kar3Δ* and prp45 1-169 ts mutants. Hence, the ER domain might have contributed in the nuclear surface area increase in *cin8Δ* null mutant but not in *kar3Δ* and prp45 1-169 ts mutants.

6.2.7: Effect of *Kar3Δ, Cin8Δ* and prp45 1-169 Ts mutants on sub nuclear DNA mass domain

To further understand the effect *kar3Δ, cin8Δ* and prp45 1-169 ts mutants on sub nuclear organization, we labeled chromatin marker histone (HTB2) with Ds-Red and expressed in all the mutant strains episomaly. Live cell imaging of log phase cells followed by 3D reconstruction of confocal images resulted in surface area and volume estimations of chromatin. Cells were grown and imaging experiments were performed as described earlier.

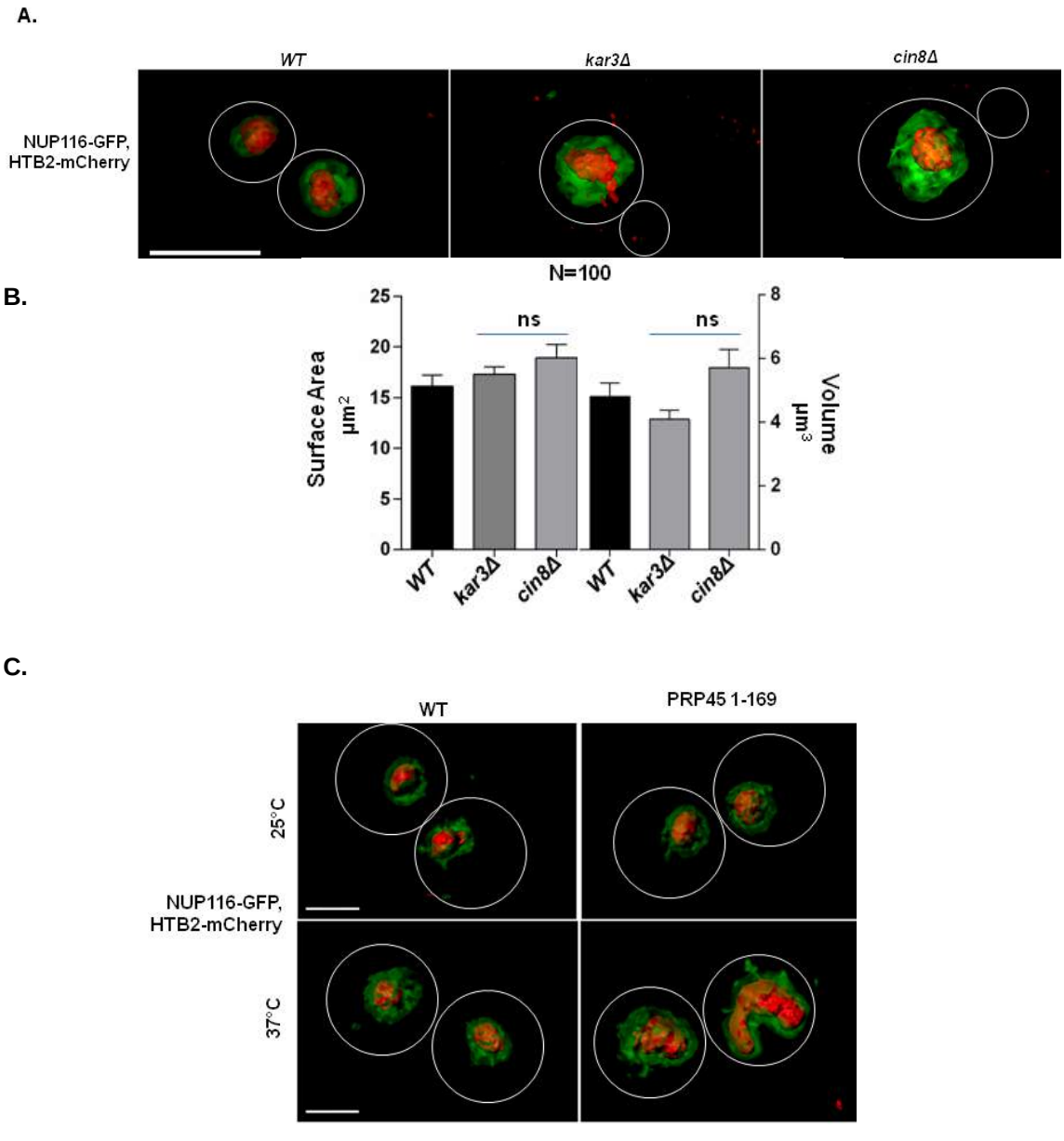

D.

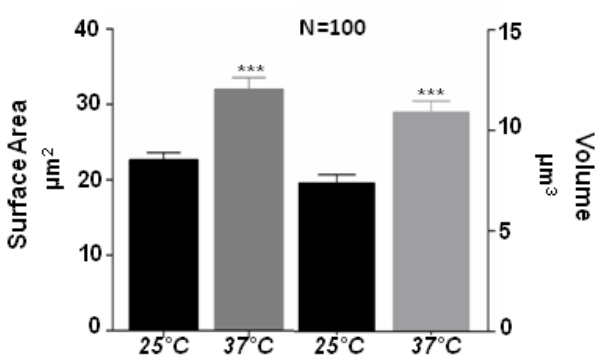

Figure 6.11 Chromatin size and shape in *kar3Δ*, *cin8Δ* and prp45 1-169 Ts mutants. *(A) Overlay 3D reconstruction images live cells of wild type, kar3Δ and cin8Δ cells labeled with Nup116-GFP (nuclear membrane marker) and HTB2- DsRed (chromatin marker).Scale bar is 5μm. (B) Quantification of the chromatin surface area and volume from the images represented in (A), of 100 cells in 3 different experiments. Error bar represents standard error mean (C) Overlay 3D reconstruction images of wild type, and prp45 1-169 Ts cells at both 25°C and 37°C, labeled same as above. (D) Quantification of the chromatin surface area and volume from the images represented in C of 100 cells in 3 different experiments. Error bar represents standard error mean.*

We found that in *kar3Δ and cin8Δ* mutants, there is no significant difference in the chromatin surface area or volume compared to wild type cells **(Figure 6.11 A, B).** Most of the cells, nuclear membrane expansion is limited to the other side where chromatin is not present. However, in very few cells, 3D images revealed that nuclear envelope expanded around the chromatin. Previous reports demonstrated that nuclear envelop expansion is restricted around DNA in different mutants as well as in wild type cells with nuclear protrusions [39, 121]. Consistent with these, we find that nuclear membrane expansion in *Kar3Δ and Cin8Δ* mutants are restricted to the region where DNA is not present. To our surprise, we found that in prp45 1-169 cells, when shifted to 37°C chromatin shape is also changed with a significantly increased surface area and volume. All these results prompted us to believe that nuclear shape alteration phenotypes arise by different mechanisms and the downstream effects are also different in different mutants.

6.3: Discussion

Size is tightly regulated in different level of organization, for example at cells as well as at the sub cellular level [14, 145]. Simply the reason is size is critical to biological function. The fact that size is tightly regulated demonstrates that this property strongly selected during evolution. To directly assess the conservation of gene function at the level of nuclear shape phenotype, in this part of our study, we used an unbiased approach to find out genes responsible for strange nuclear shape in yeast. We exploited the information from a mammalian database called mitocheck [132]. We screened the yeast homologues responsible for altered nuclear size and shape.

We quantitatively demonstrated the phenotype "Strange nuclear shape" in yeast system as nuclear surface area and volume. To our surprise, we found many of such genes are not conserved with respect to control nuclear shape. Moreover, we found that, strange nuclear shape sometimes could result in decreased nuclear surface area and volume (*eft2Δ, pkp1Δ, pus4Δ*). In the *mitocheck* data base, all the genes used in this study showed strange nuclear shape. It is noteworthy that HeLa cells (adenocarcinoma origin), which are already expected to exhibit altered nuclear shape due to several unknown mutations, were used in the mitocheck database [132]. The genes that did not show any effect in yeast, might show effect if some other gene/ s are also altered at the same time, which possibly happened in HeLa cells. Once again, some of the genes were found to be conserved from yeast to mammal to control nuclear shape.

Amongst the conserved genes which are responsible for maintaining nuclear shape, we report that most of the nuclear kinesins and pre mRNA splicing protein PRP45 play an important role in maintaining the nuclear shape.

kar3Δ and *cin8Δ* showed the most altered nuclear shape amongst nuclear kinesins. Function of Kip1 is similar with Cin8, so deletion of Kip1 showed almost similar effect as shown by Cin8 deletion [134, 146]. Kar3 and Cin8 mainly function in spindle microtubules. Amongst all the kinesins, only smy1 is not linked to spindle functions [146]. Kip3 and Kip2 both are reported to be present throughout the cell cycle and mainly observed in cytoplasmic microtubules and spindle pole bodies [146].

We observed significant alteration of nuclear surface area and volume in *kar3Δ and cin8Δ* in G1/G1-S, G2/ G2M, anaphase and telophase cells compared to respective wild type cells. Our results show that *cin8Δ*, during anaphase, nuclear surface area is increased significantly but nuclear volume remained unchanged compared to wild type cell. In the same mutant, spindle length is significantly reduced and varying during anaphase. Since Kar3 is a minus end motor protein and Cin8 is a plus end motor protein, deletion of Kar3 and Cin8 is expected to result in increased and decreased spindle lengths respectively in wild type cells, and the similar result we observed in spindle lengths of these two mutants. However, our result shows alteration in spindle length but not significantly in *kar3Δ and cin8Δ* mutants compare to wild type cells in g2m, and telophase cells. We can hypothesize that during anaphase, kar3 and cin8 both balance the length and tension of spindles in budding yeast cells, therefore maintaining a proper nuclear shape. In either deletion, due to loss of tension, the nuclear shape becomes aberrant in mitotic cells.

We have observed the expression of cortical ER is significantly increased in Cin8 deletion while the same is significantly reduced in Kar3 deletion strains. This is very strange. In the former case, we can propose that membrane expansion in ER is accompanied with nuclear surface area increase in Cin8 deletion mutant. However, we at this point have no idea the reason behind the reduction of cortical ER

expression in kar3 deletion strain. DNA mass in both the mutants remain unaffected, the same phenomenon also observed in many other nuclear shape mutants.

In this study, we found one of the novel protein prp45 controlling nuclear shapes in yeast system. Prp45 1-169 ts mutant when shifted to non permissible temperature, it showed significantly increased nuclear surface area and volume compared to its wild type. We showed that alteration in the nuclear shape in Prp45 1-169 mutant is not specific in any cell cycle stage rather it is observed in all stages of cell cycle. In Prp45 1-169 ts mutant, nuclear surface area and volume are significantly increased in G1/G1-S, G2/ G2M and anaphase cells compared to respective wild type cells. Moreover, the chromatin shape becomes significantly altered (surface area and volume) in this mutants at non permissive temperature. We have also observed significant reduction in cortical ER expression in this mutant. This is might be due to the fact that cells are about to die at non permissible temperature, leading to cortical ER disruption.

Our results indicate that Prp45 is one of the important gene that controls nuclear shape as well as sub nuclear domain like DNA mass unlike Kar3 and Cin8 null mutants. Prp45 is involved mainly in pre-mRNA splicing. In the absence of prp45 splicing, many different genes are unable to be spliced properly and these genes might control nuclear shape. It is also possible that nuclear shape is controlled by global splicing defect. We can also presume, Prp45 itself has some novel role to control nucleus size and shape which is completely unknown.

Chapter 7:

Summary

In this study, we investigated two model organisms to understand nucleus size and shape control mechanism. We have demonstrated alteration in both N/C ratio and size of nucleolus in different transformed cell lines compared to the immortalized cell lines of same tissue origin. For the first time we showed perturbation of nucleo cytoplasmic transport can alter both N/C ratio and nucleolus size and number in immortalized cells. However, this increased N/C ratio could not change the invasion potential further of the same immortalized cells. Using an in vitro assay system, it has been demonstrated that cytosolic factors control size of nucleolus. All these results indicate the importance of nuclear transport for size regulation of nucleus and nucleolus. We conclude that in mammalian system, communication between nucleus and cytoplasm is very important to maintain the N/C ratio in immortalized cells.

In yeast system, we focused mainly on nuclear shape. Using an unbiased approach, we found that motor proteins (Kar3, Cin8) and pre mRNA splicing protein (Prp45) control nuclear size and shape. In motor proteins Kar3, Cin8 and pre mRNA splicing protein Prp45 1-169, nuclear shape is altered in all stages of cell cycle. Our results indicate that prp45 is one of the important gene that controls nuclear shape as well as sub nuclear domain like chromatin unlike Kar3 and Cin8 null mutants. We conclude that in yeast, nucleus size and shape alteration phenotype can be achieved through many different genes/ pathways. Alteration in nuclear surface area or volume does not necessarily alter the chromatin inside the nucleus always.

Chapter 8:

Bibliography

1. Chan, Y.H. and W.F. Marshall, *How cells know the size of their organelles.* Science, 2012. **337**(6099): p. 1186-9.
2. Huber, M.D. and L. Gerace, *The size-wise nucleus: nuclear volume control in eukaryotes.* J Cell Biol, 2007. **179**(4): p. 583-4.
3. Lamond, A.I. and W.C. Earnshaw, *Structure and function in the nucleus.* Science, 1998. **280**(5363): p. 547-53.
4. Newport, J.W. and D.J. Forbes, *The nucleus: structure, function, and dynamics.* Annu Rev Biochem, 1987. **56**: p. 535-65.
5. Webster, M., K.L. Witkin, and O. Cohen-Fix, *Sizing up the nucleus: nuclear shape, size and nuclear-envelope assembly.* J Cell Sci, 2009. **122**(Pt 10): p. 1477-86.
6. Campisi, J., *Aging, cellular senescence, and cancer.* Annu Rev Physiol, 2013. **75**: p. 685-705.
7. Zink, D., A.H. Fischer, and J.A. Nickerson, *Nuclear structure in cancer cells.* Nat Rev Cancer, 2004. **4**(9): p. 677-87.
8. Wang, X., et al., *Rapid hepatocyte nuclear translocation of the Forkhead Box M1B (FoxM1B) transcription factor caused a transient increase in size of regenerating transgenic hepatocytes.* Gene Expr, 2003. **11**(3-4): p. 149-62.
9. Neumann, F.R. and P. Nurse, *Nuclear size control in fission yeast.* J Cell Biol, 2007. **179**(4): p. 593-600.
10. Gest, H., *The discovery of microorganisms by Robert Hooke and Antoni Van Leeuwenhoek, fellows of the Royal Society.* Notes Rec R Soc Lond, 2004. **58**(2): p. 187-201.
11. Schwann, T.H., *Microscopial researches into the accordance in the structure and growth of animals and plants. 1847.* Obes Res, 1993. **1**(5): p. 408-18.
12. Marshall, W.F., et al., *What determines cell size?* BMC Biol, 2012. **10**: p. 101.
13. Marshall, W.F., *Organelle size control systems: from cell geometry to organelle-directed medicine.* Bioessays, 2012. **34**(9): p. 721-4.
14. Chan, Y.H. and W.F. Marshall, *Scaling properties of cell and organelle size.* Organogenesis, 2010. **6**(2): p. 88-96.
15. Edens, L.J., et al., *Nuclear size regulation: from single cells to development and disease.* Trends Cell Biol, 2013. **23**(4): p. 151-9.
16. Marshall, W.F., *Engineering design principles for organelle size control systems.* Semin Cell Dev Biol, 2008. **19**(6): p. 520-4.
17. Iwamoto, M., et al., *Two distinct repeat sequences of Nup98 nucleoporins characterize dual nuclei in the binucleated ciliate tetrahymena.* Curr Biol, 2009. **19**(10): p. 843-7.
18. Kaczanowski, A., *Mitosis and polyploidy in nuclei of Opalina ranarum.* Experientia, 1968. **24**(8): p. 846-7.
19. Pederson, T., *The nucleus introduced.* Cold Spring Harb Perspect Biol, 2011. **3**(5).
20. Shiels, C., et al., *Quantitative analysis of cell nucleus organisation.* PLoS Comput Biol, 2007. **3**(7): p. e138.
21. Maeshima, K., et al., *Nuclear size, nuclear pore number and cell cycle.* Nucleus, 2011. **2**(2): p. 113-8.
22. Jorgensen, P., et al., *The size of the nucleus increases as yeast cells grow.* Mol Biol Cell, 2007. **18**(9): p. 3523-32.
23. Simon, D.N. and K.L. Wilson, *The nucleoskeleton as a genome-associated dynamic 'network of networks'.* Nat Rev Mol Cell Biol, 2011. **12**(11): p. 695-708.
24. Levy, D.L. and R. Heald, *Mechanisms of intracellular scaling.* Annu Rev Cell Dev Biol, 2012. **28**: p. 113-35.

25. Levy, D.L. and R. Heald, *Nuclear size is regulated by importin alpha and Ntf2 in Xenopus.* Cell, 2010. **143**(2): p. 288-98.
26. Harris, H., *The reactivation of the red cell nucleus.* J Cell Sci, 1967. **2**(1): p. 23-32.
27. Brandt, A., et al., *Developmental control of nuclear size and shape by Kugelkern and Kurzkern.* Curr Biol, 2006. **16**(6): p. 543-52.
28. Anderson, D.J. and M.W. Hetzer, *Reshaping of the endoplasmic reticulum limits the rate for nuclear envelope formation.* J Cell Biol, 2008. **182**(5): p. 911-24.
29. Shen, X., et al., *Linker histones are not essential and affect chromatin condensation in vivo.* Cell, 1995. **82**(1): p. 47-56.
30. Zwerger, M., C.Y. Ho, and J. Lammerding, *Nuclear mechanics in disease.* Annu Rev Biomed Eng, 2011. **13**: p. 397-428.
31. Scaffidi, P. and T. Misteli, *Lamin A-dependent nuclear defects in human aging.* Science, 2006. **312**(5776): p. 1059-63.
32. Olins, D.E. and A.L. Olins, *Granulocyte heterochromatin: defining the epigenome.* BMC Cell Biol, 2005. **6**: p. 39.
33. Hoffmann, K., et al., *The granulocyte nucleus and lamin B receptor: avoiding the ovoid.* Chromosoma, 2007. **116**(3): p. 227-35.
34. Hampoelz, B., et al., *Microtubule-induced nuclear envelope fluctuations control chromatin dynamics in Drosophila embryos.* Development, 2011. **138**(16): p. 3377-86.
35. King, M.C., T.G. Drivas, and G. Blobel, *A network of nuclear envelope membrane proteins linking centromeres to microtubules.* Cell, 2008. **134**(3): p. 427-38.
36. Dahl, K.N., A.J. Ribeiro, and J. Lammerding, *Nuclear shape, mechanics, and mechanotransduction.* Circ Res, 2008. **102**(11): p. 1307-18.
37. Higashio, H., et al., *Sfb2p, a yeast protein related to Sec24p, can function as a constituent of COPII coats required for vesicle budding from the endoplasmic reticulum.* J Biol Chem, 2000. **275**(23): p. 17900-8.
38. Matynia, A., S.S. Salus, and S. Sazer, *Three proteins required for early steps in the protein secretory pathway also affect nuclear envelope structure and cell cycle progression in fission yeast.* J Cell Sci, 2002. **115**(Pt 2): p. 421-31.
39. Campbell, J.L., et al., *Yeast nuclear envelope subdomains with distinct abilities to resist membrane expansion.* Mol Biol Cell, 2006. **17**(4): p. 1768-78.
40. Golden, A., J. Liu, and O. Cohen-Fix, *Inactivation of the C. elegans lipin homolog leads to ER disorganization and to defects in the breakdown and reassembly of the nuclear envelope.* J Cell Sci, 2009. **122**(Pt 12): p. 1970-8.
41. Webster, M.T., J.M. McCaffery, and O. Cohen-Fix, *Vesicle trafficking maintains nuclear shape in Saccharomyces cerevisiae during membrane proliferation.* J Cell Biol, 2010. **191**(6): p. 1079-88.
42. Sehgal, N., et al., *Gene density and chromosome territory shape.* Chromosoma, 2014. **123**(5): p. 499-513.
43. Reddy, K.L. and A.P. Feinberg, *Higher order chromatin organization in cancer.* Semin Cancer Biol, 2013. **23**(2): p. 109-15.
44. Sirri, V., et al., *Nucleolus: the fascinating nuclear body.* Histochem Cell Biol, 2008. **129**(1): p. 13-31.
45. Maggi, L.B., Jr. and J.D. Weber, *Nucleolar adaptation in human cancer.* Cancer Invest, 2005. **23**(7): p. 599-608.
46. Hernandez-Verdun, D., *Nucleolus: from structure to dynamics.* Histochem Cell Biol, 2006. **125**(1-2): p. 127-37.
47. Pederson, T., *The nucleolus.* Cold Spring Harb Perspect Biol, 2011. **3**(3).

48. Zatsepina, O.V., P.V. Chelidze, and S. Chentsov Iu, *[Changes in the number and size of fibrillar centers in nucleolus inactivation during erythropoiesis].* Ontogenez, 1989. **20**(1): p. 40-6.
49. Caudron-Herger, M., et al., *Alu element-containing RNAs maintain nucleolar structure and function.* EMBO J, 2015. **34**(22): p. 2758-74.
50. Carmo-Fonseca, M., *Assembly of the nucleolus: in need of revision.* EMBO J, 2015. **34**(22): p. 2731-2.
51. Farley, K.I., et al., *Determinants of mammalian nucleolar architecture.* Chromosoma, 2015. **124**(3): p. 323-31.
52. Smirnov, E., et al., *Nucleolar DNA: the host and the guests.* Histochem Cell Biol, 2016.
53. van Koningsbruggen, S., et al., *High-resolution whole-genome sequencing reveals that specific chromatin domains from most human chromosomes associate with nucleoli.* Mol Biol Cell, 2010. **21**(21): p. 3735-48.
54. Handwerger, K.E. and J.G. Gall, *Subnuclear organelles: new insights into form and function.* Trends Cell Biol, 2006. **16**(1): p. 19-26.
55. Lam, Y.W. and L. Trinkle-Mulcahy, *New insights into nucleolar structure and function.* F1000Prime Rep, 2015. **7**: p. 48.
56. Rieker, C., et al., *Nucleolar disruption in dopaminergic neurons leads to oxidative damage and parkinsonism through repression of mammalian target of rapamycin signaling.* J Neurosci, 2011. **31**(2): p. 453-60.
57. Sia, P.I., et al., *Role of the nucleolus in neurodegenerative disease with particular reference to the retina: a review.* Clin Experiment Ophthalmol, 2015.
58. Akahori, T., et al., *[Cytologic studies of cervical adenocarcinoma].* Nihon Sanka Fujinka Gakkai Zasshi, 1987. **39**(1): p. 70-8.
59. Derenzini, M., L. Montanaro, and D. Trere, *What the nucleolus says to a tumour pathologist.* Histopathology, 2009. **54**(6): p. 753-62.
60. van Diest, P.J., G. Brugal, and J.P. Baak, *Proliferation markers in tumours: interpretation and clinical value.* J Clin Pathol, 1998. **51**(10): p. 716-24.
61. Brighenti, E., D. Trere, and M. Derenzini, *Targeted cancer therapy with ribosome biogenesis inhibitors: a real possibility?* Oncotarget, 2015. **6**(36): p. 38617-27.
62. Derenzini, M., et al., *Nucleolar function and size in cancer cells.* Am J Pathol, 1998. **152**(5): p. 1291-7.
63. Orsolic, I., et al., *The relationship between the nucleolus and cancer: Current evidence and emerging paradigms.* Semin Cancer Biol, 2015.
64. Burger, K., et al., *Chemotherapeutic drugs inhibit ribosome biogenesis at various levels.* J Biol Chem, 2010. **285**(16): p. 12416-25.
65. Quin, J.E., et al., *Targeting the nucleolus for cancer intervention.* Biochim Biophys Acta, 2014. **1842**(6): p. 802-16.
66. Brangwynne, C.P., T.J. Mitchison, and A.A. Hyman, *Active liquid-like behavior of nucleoli determines their size and shape in Xenopus laevis oocytes.* Proc Natl Acad Sci U S A, 2011. **108**(11): p. 4334-9.
67. Weber, S.C. and C.P. Brangwynne, *Inverse size scaling of the nucleolus by a concentration-dependent phase transition.* Curr Biol, 2015. **25**(5): p. 641-6.
68. Ganguly, A., et al., *Perturbation of nucleo-cytoplasmic transport affects size of nucleus and nucleolus in human cells.* FEBS Lett, 2016. **590**(5): p. 631-43.
69. Harris, B., et al., *Cohesion promotes nucleolar structure and function.* Mol Biol Cell, 2014. **25**(3): p. 337-46.
70. Kitamura, H., et al., *The actin family protein ARP6 contributes to the structure and the function of the nucleolus.* Biochem Biophys Res Commun, 2015. **464**(2): p. 554-60.

71. Neumuller, R.A., et al., *Conserved regulators of nucleolar size revealed by global phenotypic analyses.* Sci Signal, 2013. **6**(289): p. ra70.
72. Carmo-Fonseca, M., L. Mendes-Soares, and I. Campos, *To be or not to be in the nucleolus.* Nat Cell Biol, 2000. **2**(6): p. E107-12.
73. Kuersten, S., M. Ohno, and I.W. Mattaj, *Nucleocytoplasmic transport: Ran, beta and beyond.* Trends Cell Biol, 2001. **11**(12): p. 497-503.
74. Sorokin, A.V., E.R. Kim, and L.P. Ovchinnikov, *Nucleocytoplasmic transport of proteins.* Biochemistry (Mosc), 2007. **72**(13): p. 1439-57.
75. Gorlich, D., *Transport into and out of the cell nucleus.* EMBO J, 1998. **17**(10): p. 2721-7.
76. Avis, J.M. and P.R. Clarke, *Ran, a GTPase involved in nuclear processes: its regulators and effectors.* J Cell Sci, 1996. **109 (Pt 10)**: p. 2423-7.
77. Kunzler, M. and E. Hurt, *Targeting of Ran: variation on a common theme?* J Cell Sci, 2001. **114**(Pt 18): p. 3233-41.
78. Kimura, M. and N. Imamoto, *Biological significance of the importin-beta family-dependent nucleocytoplasmic transport pathways.* Traffic, 2014. **15**(7): p. 727-48.
79. Inoue, H., H. Nojima, and H. Okayama, *High efficiency transformation of Escherichia coli with plasmids.* Gene, 1990. **96**(1): p. 23-8.
80. Liu, H. and J.H. Naismith, *An efficient one-step site-directed deletion, insertion, single and multiple-site plasmid mutagenesis protocol.* BMC Biotechnol, 2008. **8**: p. 91.
81. Higuchi, R., et al., *A general method for cloning eukaryotic structural gene sequences.* Proc Natl Acad Sci U S A, 1976. **73**(9): p. 3146-50.
82. Nath, S., et al., *Deregulation of Rb-E2F1 axis causes chromosomal instability by engaging the transactivation function of Cdc20-anaphase-promoting complex/cyclosome.* Mol Cell Biol, 2015. **35**(2): p. 356-69.
83. Ibrahim, S.F. and G. van den Engh, *Flow cytometry and cell sorting.* Adv Biochem Eng Biotechnol, 2007. **106**: p. 19-39.
84. Basu, S., et al., *Purification of specific cell population by fluorescence activated cell sorting (FACS).* J Vis Exp, 2010(41).
85. Lamouille, S. and R. Derynck, *Cell size and invasion in TGF-beta-induced epithelial to mesenchymal transition is regulated by activation of the mTOR pathway.* J Cell Biol, 2007. **178**(3): p. 437-51.
86. Nabbi, A. and K. Riabowol, *Isolation of Nuclei.* Cold Spring Harb Protoc, 2015. **2015**(8): p. 731-4.
87. Sambrook, J. and D.W. Russell, *SDS-Polyacrylamide Gel Electrophoresis of Proteins.* CSH Protoc, 2006. **2006**(4).
88. Mahmood, T. and P.C. Yang, *Western blot: technique, theory, and trouble shooting.* N Am J Med Sci, 2012. **4**(9): p. 429-34.
89. Bhattacharyya, D., A.T. Hammond, and B.S. Glick, *High-quality immunofluorescence of cultured cells.* Methods Mol Biol, 2010. **619**: p. 403-10.
90. Ettinger, A. and T. Wittmann, *Fluorescence live cell imaging.* Methods Cell Biol, 2014. **123**: p. 77-94.
91. Sherman, F., *Getting started with yeast.* Methods Enzymol, 2002. **350**: p. 3-41.
92. Kunz, J., et al., *Target of rapamycin in yeast, TOR2, is an essential phosphatidylinositol kinase homolog required for G1 progression.* Cell, 1993. **73**(3): p. 585-96.
93. Kawai, S., W. Hashimoto, and K. Murata, *Transformation of Saccharomyces cerevisiae and other fungi: methods and possible underlying mechanism.* Bioeng Bugs, 2010. **1**(6): p. 395-403.
94. Looke, M., K. Kristjuhan, and A. Kristjuhan, *Extraction of genomic DNA from yeasts for PCR-based applications.* Biotechniques, 2011. **50**(5): p. 325-8.

95. Harju, S., H. Fedosyuk, and K.R. Peterson, *Rapid isolation of yeast genomic DNA: Bust n' Grab.* BMC Biotechnol, 2004. **4**: p. 8.
96. Gardner, J.M. and S.L. Jaspersen, *Manipulating the yeast genome: deletion, mutation, and tagging by PCR.* Methods Mol Biol, 2014. **1205**: p. 45-78.
97. Knop, M., et al., *Epitope tagging of yeast genes using a PCR-based strategy: more tags and improved practical routines.* Yeast, 1999. **15**(10B): p. 963-72.
98. Boeke, J.D., F. LaCroute, and G.R. Fink, *A positive selection for mutants lacking orotidine-5'-phosphate decarboxylase activity in yeast: 5-fluoro-orotic acid resistance.* Mol Gen Genet, 1984. **197**(2): p. 345-6.
99. Breeden, L.L., *Alpha-factor synchronization of budding yeast.* Methods Enzymol, 1997. **283**: p. 332-41.
100. Amberg, D.C., D.J. Burke, and J.N. Strathern, *Inducing yeast cell synchrony: nocodazole arrest.* CSH Protoc, 2006. **2006**(1).
101. Wright, R. and J. Rine, *Transmission electron microscopy and immunocytochemical studies of yeast: analysis of HMG-CoA reductase overproduction by electron microscopy.* Methods Cell Biol, 1989. **31**: p. 473-512.
102. Pianese, G., *Beitrag zur Histologie und Aetiologie des Carcinoms.* Histologische und experimentelle Untersuchungen. Beitr Pathol Anat., 1896. **142**.
103. Lever, E. and D. Sheer, *The role of nuclear organization in cancer.* J Pathol, 2010. **220**(2): p. 114-25.
104. Nickerson, J.A., *Nuclear dreams: the malignant alteration of nuclear architecture.* J Cell Biochem, 1998. **70**(2): p. 172-80.
105. Busch, H., P. Byvoet, and K. Smetana, *The nucleolus of the cancer cell: a review.* Cancer Res, 1963. **23**: p. 313-39.
106. Cavalier-Smith, T., *Skeletal DNA and the evolution of genome size.* Annu Rev Biophys Bioeng, 1982. **11**: p. 273-302.
107. Jovtchev, G., et al., *Nuclear DNA content and nuclear and cell volume are positively correlated in angiosperms.* Cytogenet Genome Res, 2006. **114**(1): p. 77-82.
108. Orgel, L.E. and F.H. Crick, *Selfish DNA: the ultimate parasite.* Nature, 1980. **284**(5757): p. 604-7.
109. Kau, T.R., J.C. Way, and P.A. Silver, *Nuclear transport and cancer: from mechanism to intervention.* Nat Rev Cancer, 2004. **4**(2): p. 106-17.
110. Bai, S.W., et al., *The fission yeast Nup107-120 complex functionally interacts with the small GTPase Ran/Spi1 and is required for mRNA export, nuclear pore distribution, and proper cell division.* Mol Cell Biol, 2004. **24**(14): p. 6379-92.
111. Maeshima, K., et al., *Nuclear pore formation but not nuclear growth is governed by cyclin-dependent kinases (Cdks) during interphase.* Nat Struct Mol Biol, 2010. **17**(9): p. 1065-71.
112. Hancock, R., *The crowded nucleus.* Int Rev Cell Mol Biol, 2014. **307**: p. 15-26.
113. Sato, S., S.B. Burgess, and D.L. McIlwain, *Transcription and motoneuron size.* J Neurochem, 1994. **63**(5): p. 1609-15.
114. Schmidt, E.E. and U. Schibler, *Cell size regulation, a mechanism that controls cellular RNA accumulation: consequences on regulation of the ubiquitous transcription factors Oct1 and NF-Y and the liver-enriched transcription factor DBP.* J Cell Biol, 1995. **128**(4): p. 467-83.
115. Kutay, U., et al., *Dominant-negative mutants of importin-beta block multiple pathways of import and export through the nuclear pore complex.* EMBO J, 1997. **16**(6): p. 1153-63.
116. Izaurralde, E., et al., *The asymmetric distribution of the constituents of the Ran system is essential for transport into and out of the nucleus.* EMBO J, 1997. **16**(21): p. 6535-47.

117. Ribbeck, K., et al., *NTF2 mediates nuclear import of Ran.* EMBO J, 1998. **17**(22): p. 6587-98.
118. Cushman, I., D. Stenoien, and M.S. Moore, *The dynamic association of RCC1 with chromatin is modulated by Ran-dependent nuclear transport.* Mol Biol Cell, 2004. **15**(1): p. 245-55.
119. Dasso, M., et al., *A mutant form of the Ran/TC4 protein disrupts nuclear function in Xenopus laevis egg extracts by inhibiting the RCC1 protein, a regulator of chromosome condensation.* EMBO J, 1994. **13**(23): p. 5732-44.
120. Hutchins, J.R., W.J. Moore, and P.R. Clarke, *Dynamic localisation of Ran GTPase during the cell cycle.* BMC Cell Biol, 2009. **10**: p. 66.
121. Kirchenbauer, M. and D. Liakopoulos, *An auxiliary, membrane-based mechanism for nuclear migration in budding yeast.* Mol Biol Cell, 2013. **24**(9): p. 1434-43.
122. Witkin, K.L., et al., *The budding yeast nuclear envelope adjacent to the nucleolus serves as a membrane sink during mitotic delay.* Curr Biol, 2012. **22**(12): p. 1128-33.
123. Stone, E.M., et al., *MAP kinase signaling induces nuclear reorganization in budding yeast.* Curr Biol, 2000. **10**(7): p. 373-82.
124. Schneiter, R., et al., *A yeast acetyl coenzyme A carboxylase mutant links very-long-chain fatty acid synthesis to the structure and function of the nuclear membrane-pore complex.* Mol Cell Biol, 1996. **16**(12): p. 7161-72.
125. Kimata, Y., et al., *Mutation of the yeast epsilon-COP gene ANU2 causes abnormal nuclear morphology and defects in intracellular vesicular transport.* Cell Struct Funct, 1999. **24**(4): p. 197-208.
126. Fabre, E. and E. Hurt, *Yeast genetics to dissect the nuclear pore complex and nucleocytoplasmic trafficking.* Annu Rev Genet, 1997. **31**: p. 277-313.
127. Takemoto, A., et al., *Nuclear envelope expansion is critical for proper chromosomal segregation during a closed mitosis.* J Cell Sci, 2016.
128. Walters, A.D., A. Bommakanti, and O. Cohen-Fix, *Shaping the nucleus: factors and forces.* J Cell Biochem, 2012. **113**(9): p. 2813-21.
129. Castagnetti, S., S. Oliferenko, and P. Nurse, *Fission yeast cells undergo nuclear division in the absence of spindle microtubules.* PLoS Biol, 2010. **8**(10): p. e1000512.
130. Troxell, C.L., et al., *pkl1(+)and klp2(+): Two kinesins of the Kar3 subfamily in fission yeast perform different functions in both mitosis and meiosis.* Mol Biol Cell, 2001. **12**(11): p. 3476-88.
131. Witkin, K.L., et al., *Changes in the nuclear envelope environment affect spindle pole body duplication in Saccharomyces cerevisiae.* Genetics, 2010. **186**(3): p. 867-83.
132. Neumann, B., et al., *Phenotypic profiling of the human genome by time-lapse microscopy reveals cell division genes.* Nature, 2010. **464**(7289): p. 721-7.
133. Endow, S.A., et al., *Yeast Kar3 is a minus-end microtubule motor protein that destabilizes microtubules preferentially at the minus ends.* EMBO J, 1994. **13**(11): p. 2708-13.
134. Hirokawa, N. and Y. Noda, *Intracellular transport and kinesin superfamily proteins, KIFs: structure, function, and dynamics.* Physiol Rev, 2008. **88**(3): p. 1089-118.
135. Fridman, V., et al., *Midzone organization restricts interpolar microtubule plus-end dynamics during spindle elongation.* EMBO Rep, 2009. **10**(4): p. 387-93.
136. Gahura, O., et al., *Prp45 affects Prp22 partition in spliceosomal complexes and splicing efficiency of non-consensus substrates.* J Cell Biochem, 2009. **106**(1): p. 139-51.
137. Martinkova, K., et al., *Functional mapping of Saccharomyces cerevisiae Prp45 identifies the SNW domain as essential for viability.* J Biochem, 2002. **132**(4): p. 557-63.

138. Hildebrandt, E.R. and M.A. Hoyt, *Mitotic motors in Saccharomyces cerevisiae.* Biochim Biophys Acta, 2000. **1496**(1): p. 99-116.
139. Boettcher, B. and Y. Barral, *The cell biology of open and closed mitosis.* Nucleus, 2013. **4**(3): p. 160-5.
140. Jin, F., et al., *Loss of function of the Cik1/Kar3 motor complex results in chromosomes with syntelic attachment that are sensed by the tension checkpoint.* PLoS Genet, 2012. **8**(2): p. e1002492.
141. Jaspersen, S.L. and M. Winey, *The budding yeast spindle pole body: structure, duplication, and function.* Annu Rev Cell Dev Biol, 2004. **20**: p. 1-28.
142. Winey, M. and K. Bloom, *Mitotic spindle form and function.* Genetics, 2012. **190**(4): p. 1197-224.
143. Voeltz, G.K., et al., *A class of membrane proteins shaping the tubular endoplasmic reticulum.* Cell, 2006. **124**(3): p. 573-86.
144. Prinz, W.A., et al., *Mutants affecting the structure of the cortical endoplasmic reticulum in Saccharomyces cerevisiae.* J Cell Biol, 2000. **150**(3): p. 461-74.
145. Goehring, N.W. and A.A. Hyman, *Organelle growth control through limiting pools of cytoplasmic components.* Curr Biol, 2012. **22**(9): p. R330-9.
146. Cottingham, F.R., et al., *Novel roles for saccharomyces cerevisiae mitotic spindle motors.* J Cell Biol, 1999. **147**(2): p. 335-50.

Appendix

Appendix 1: Cloning strategies and Different vector maps

Appendix 1.1: Cloning Strategy of pmCherry-F

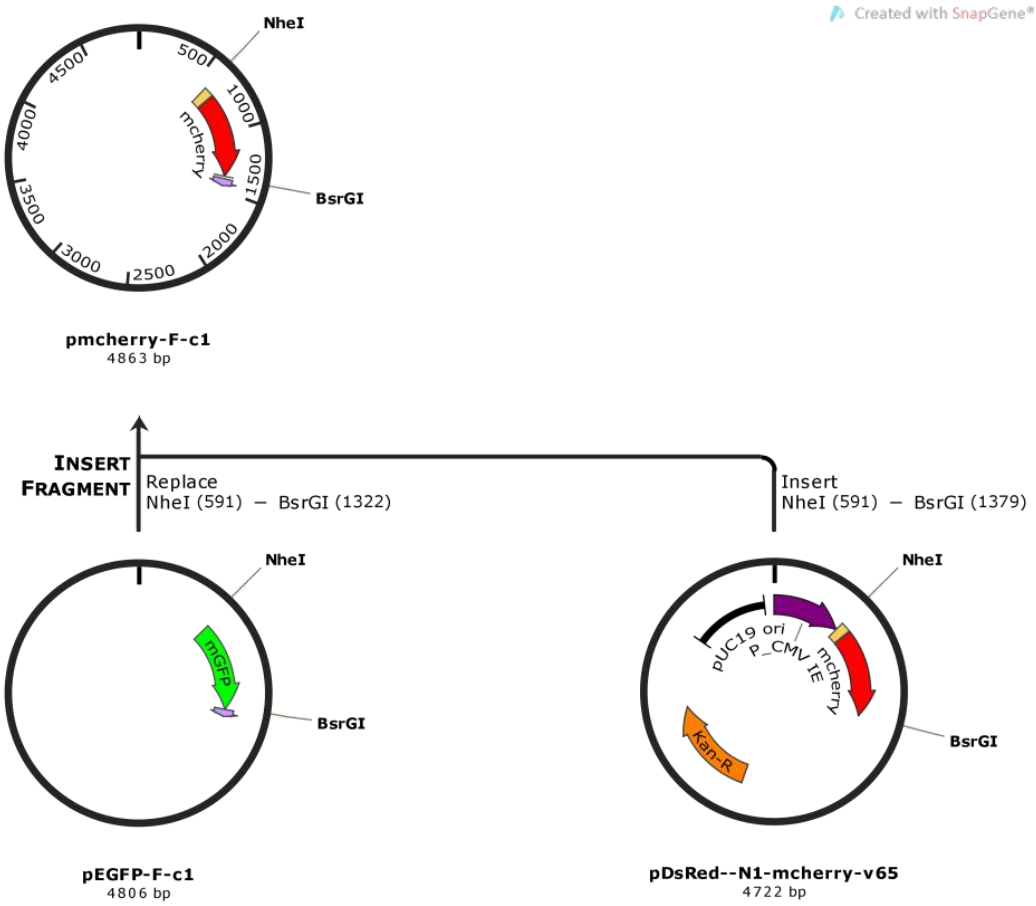

Appendix 1.2: Cloning strategy of pmGFP-LaminA

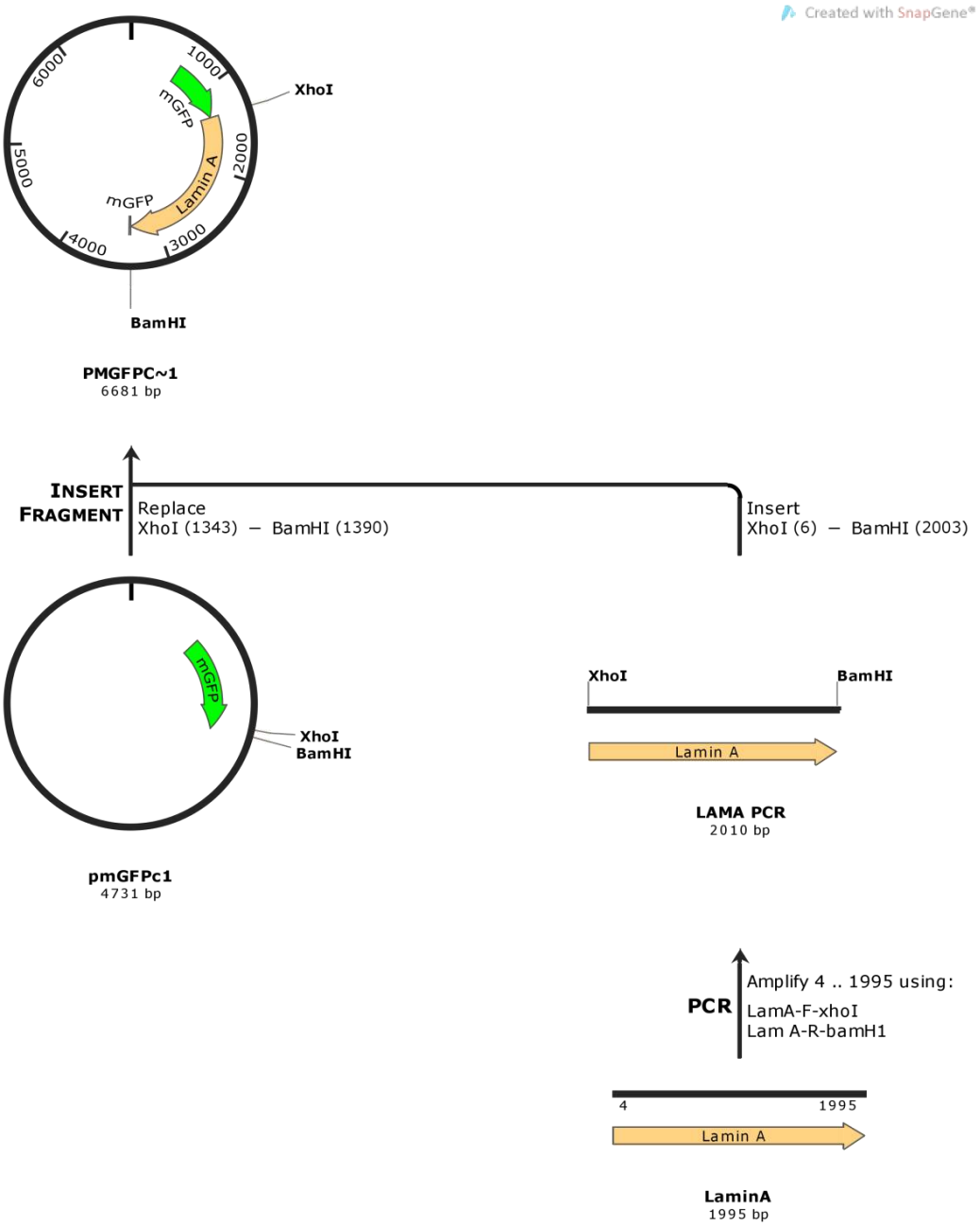

Appendix 1.3: Cloning strategy of pcmv3X Flag-Importin S beta 1-364

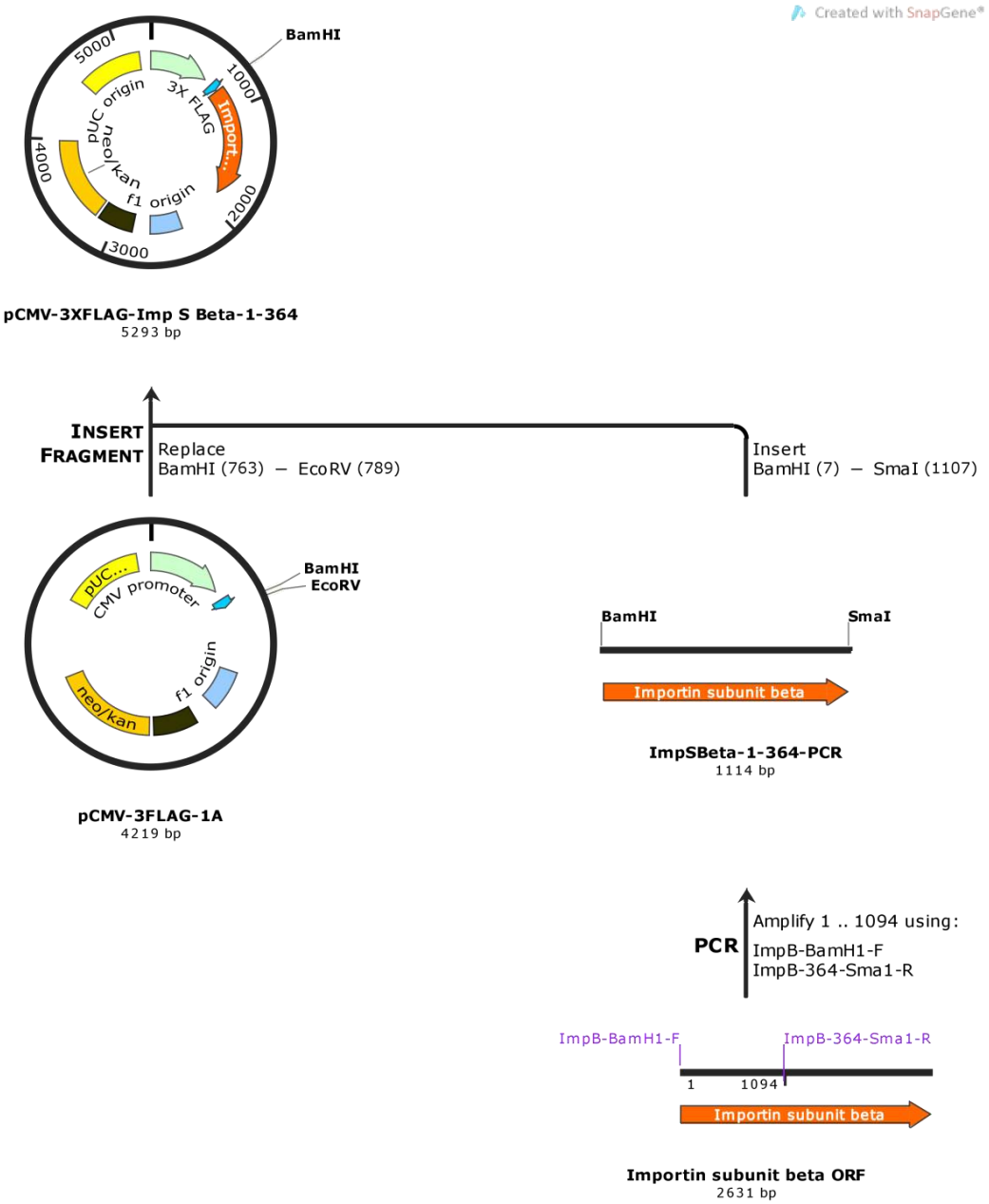

Appendix 1.4: Cloning strategy of pcmv3X Flag-Importin S beta

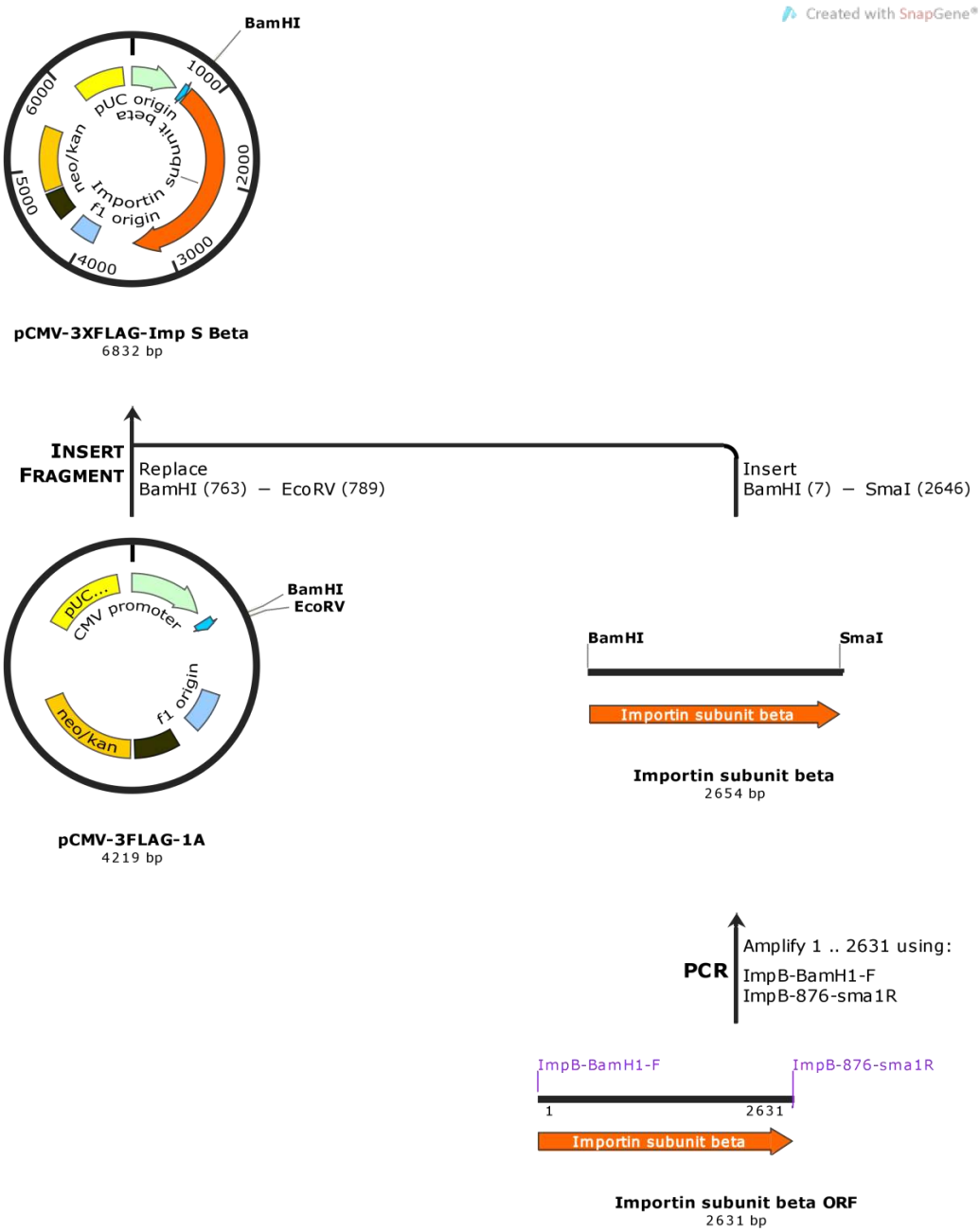

Appendix 1.5: Cloning strategy of pcmv3X Flag-Ran, pcmv3X Flag-Ran^{T24N} and pcmv3X Flag-Ran^{Q69L}

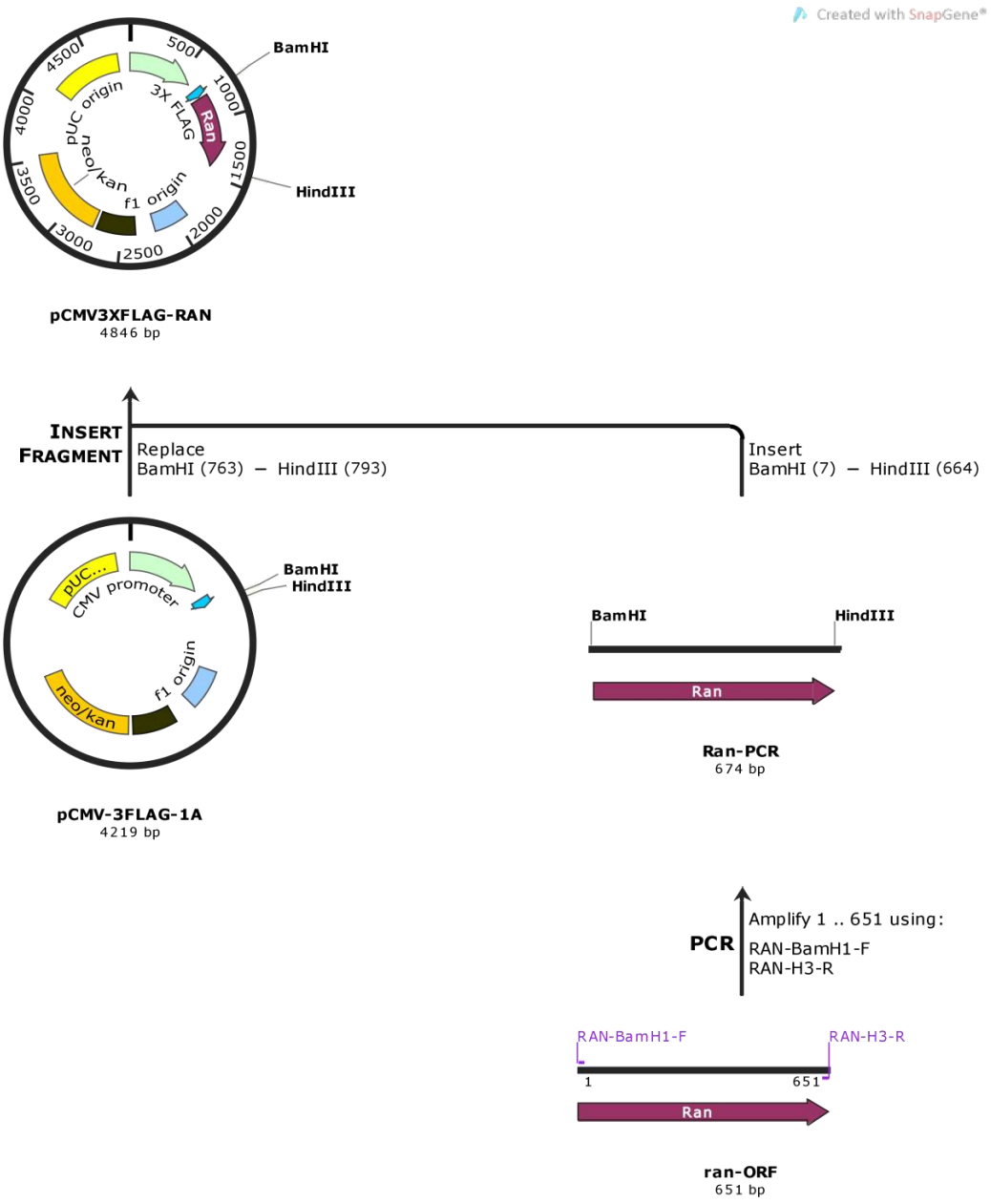

Site directed mutagenesis of pcmv3X Flag-Ran^{T24N} & pcmv3X Flag-Ran^{Q69L}

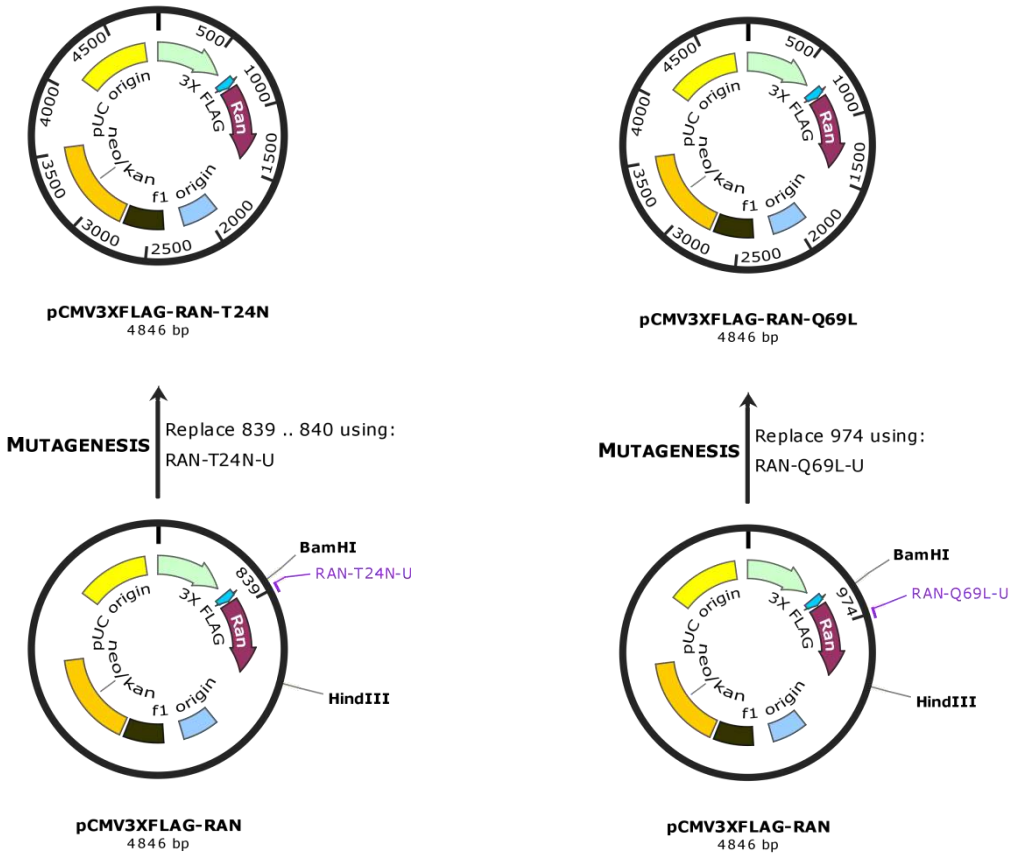

Appendix 1.6: Cloning strategy of pmCherry-128-Ras2

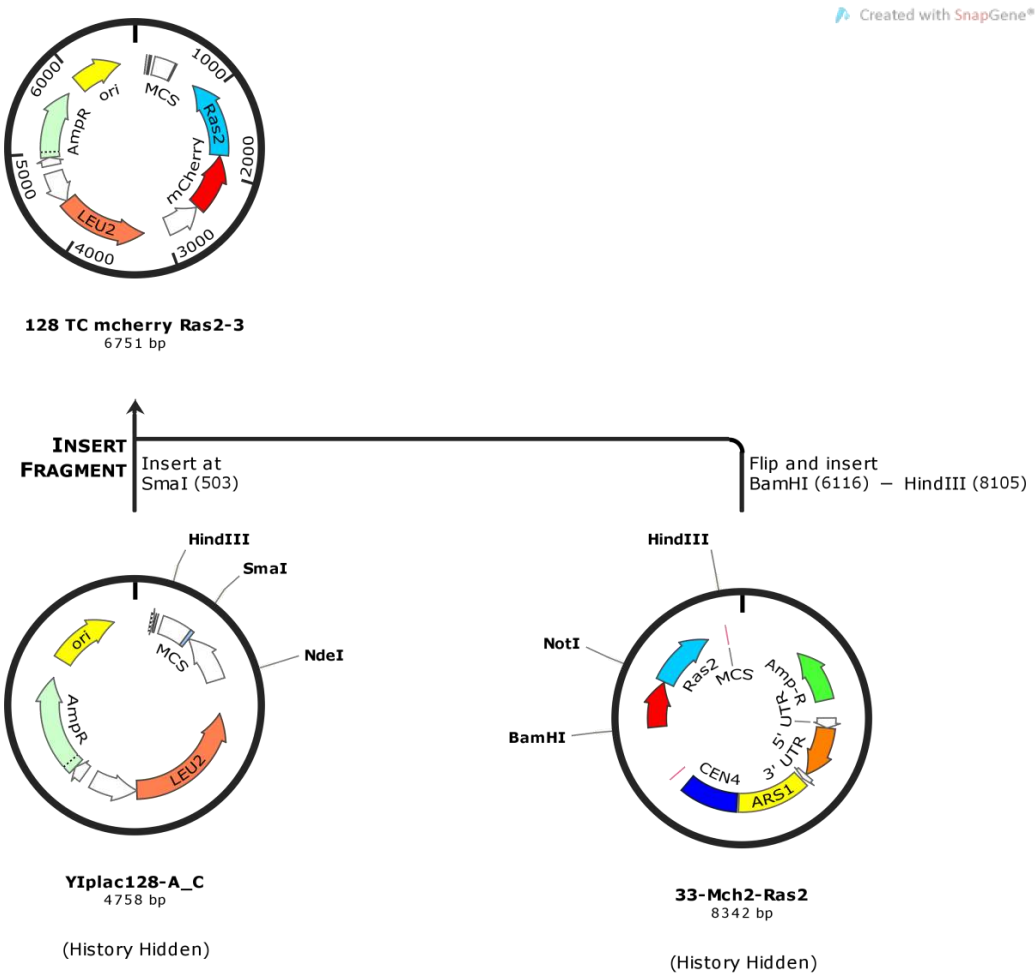

Appendix 1.7: Map of pFA6a-GFP-TRP for PCR mediated epitope tagging
(For example Nup116-GFP Tagging)

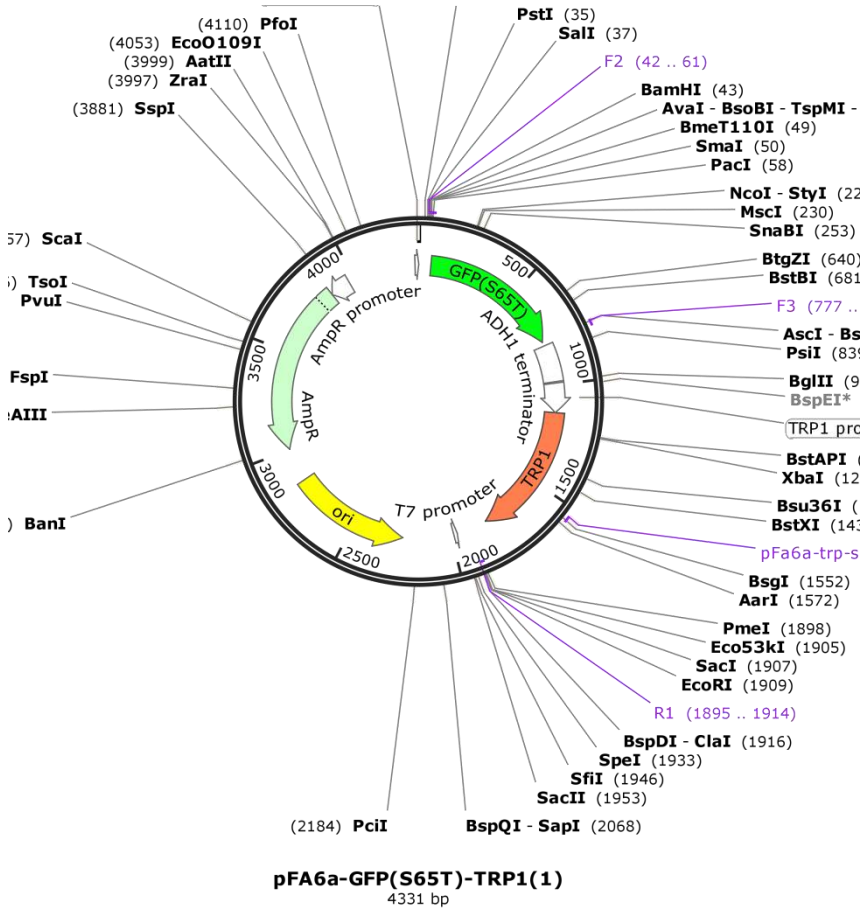

Appendix 1.8: Cloning strategy of yCplac33-Kar3

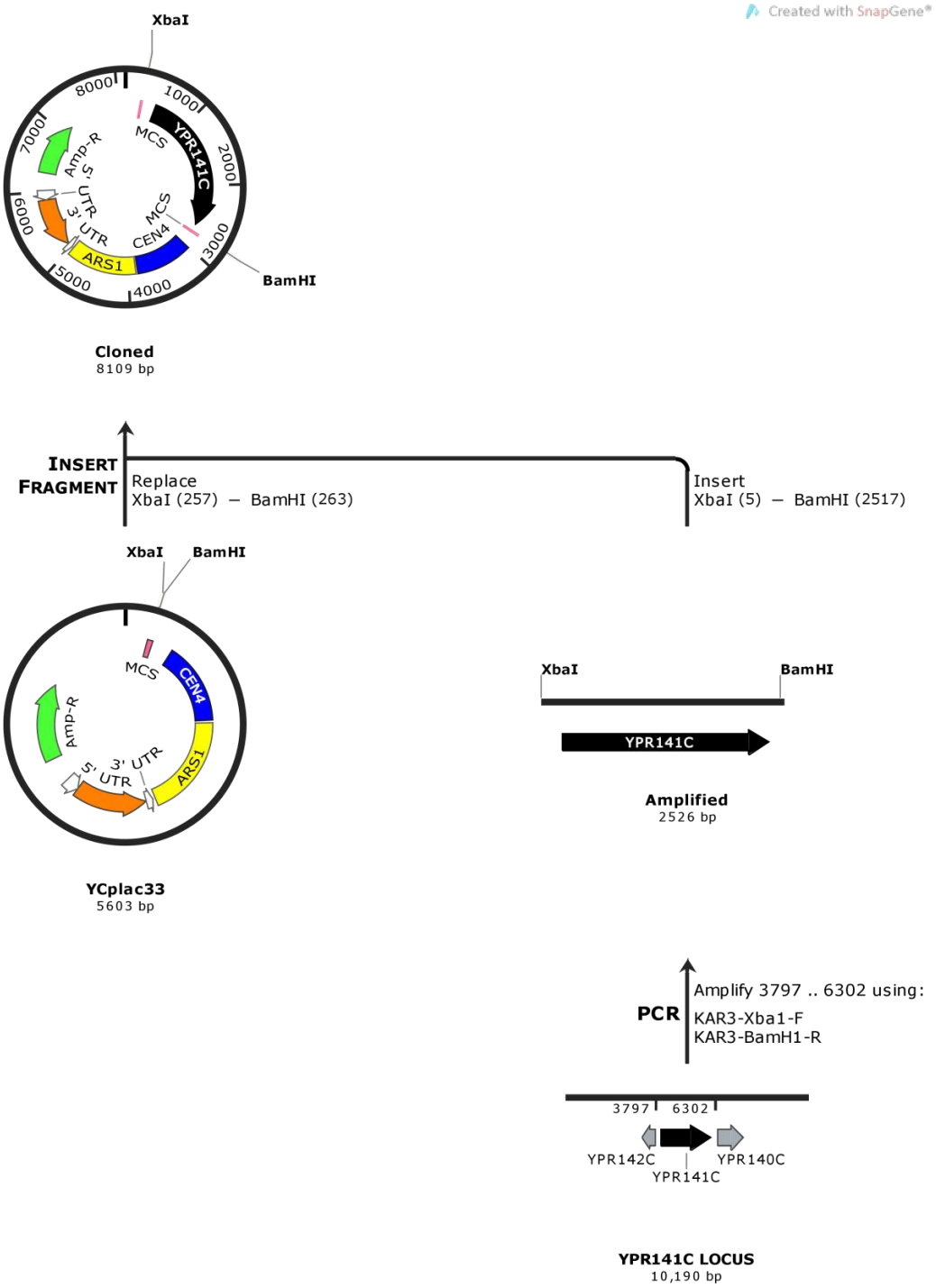

Appendix 1.9: Cloning strategy of yCplac33-cin8

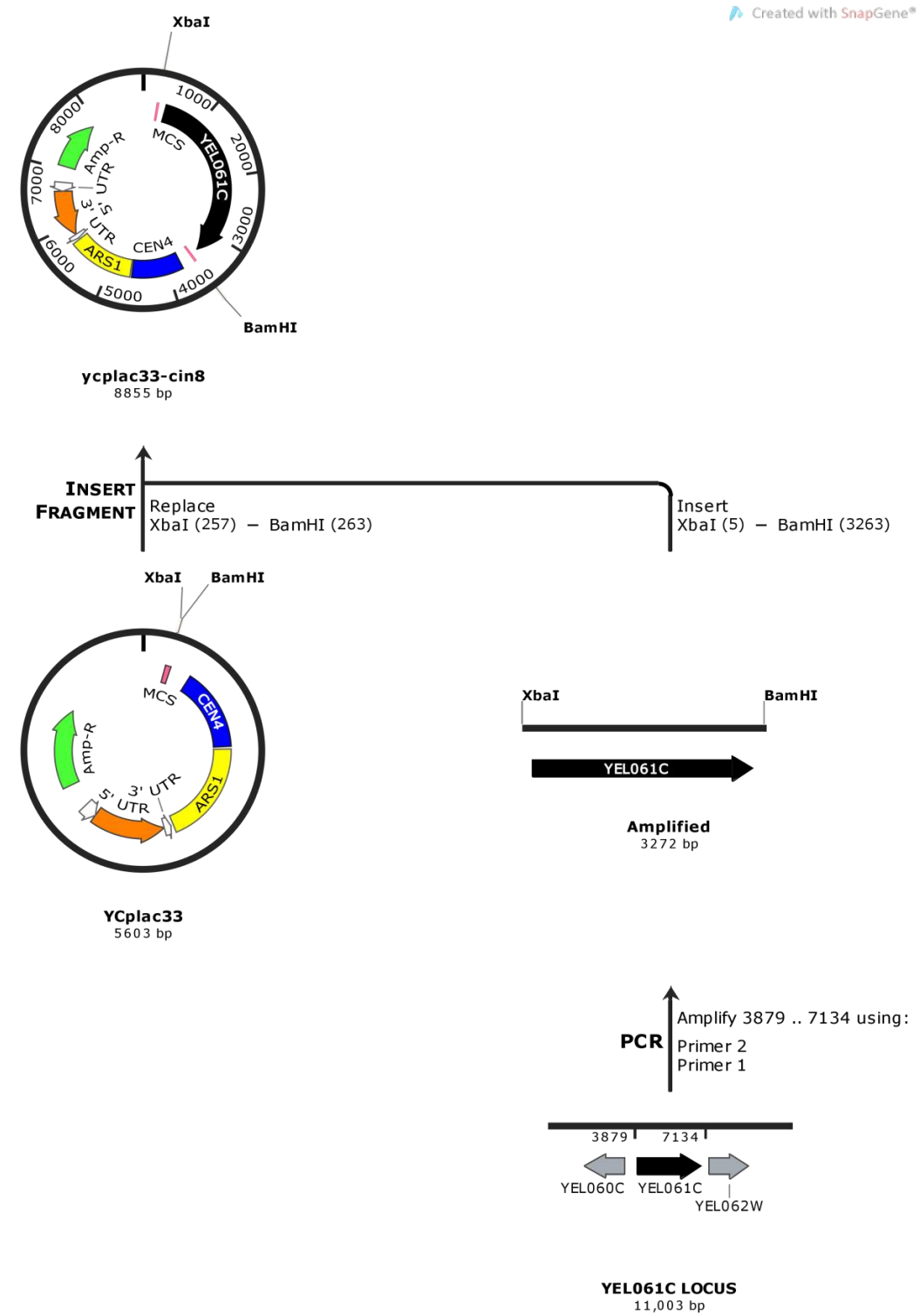

Appendix 1.10: Cloning strategy of yeplac195-kar3

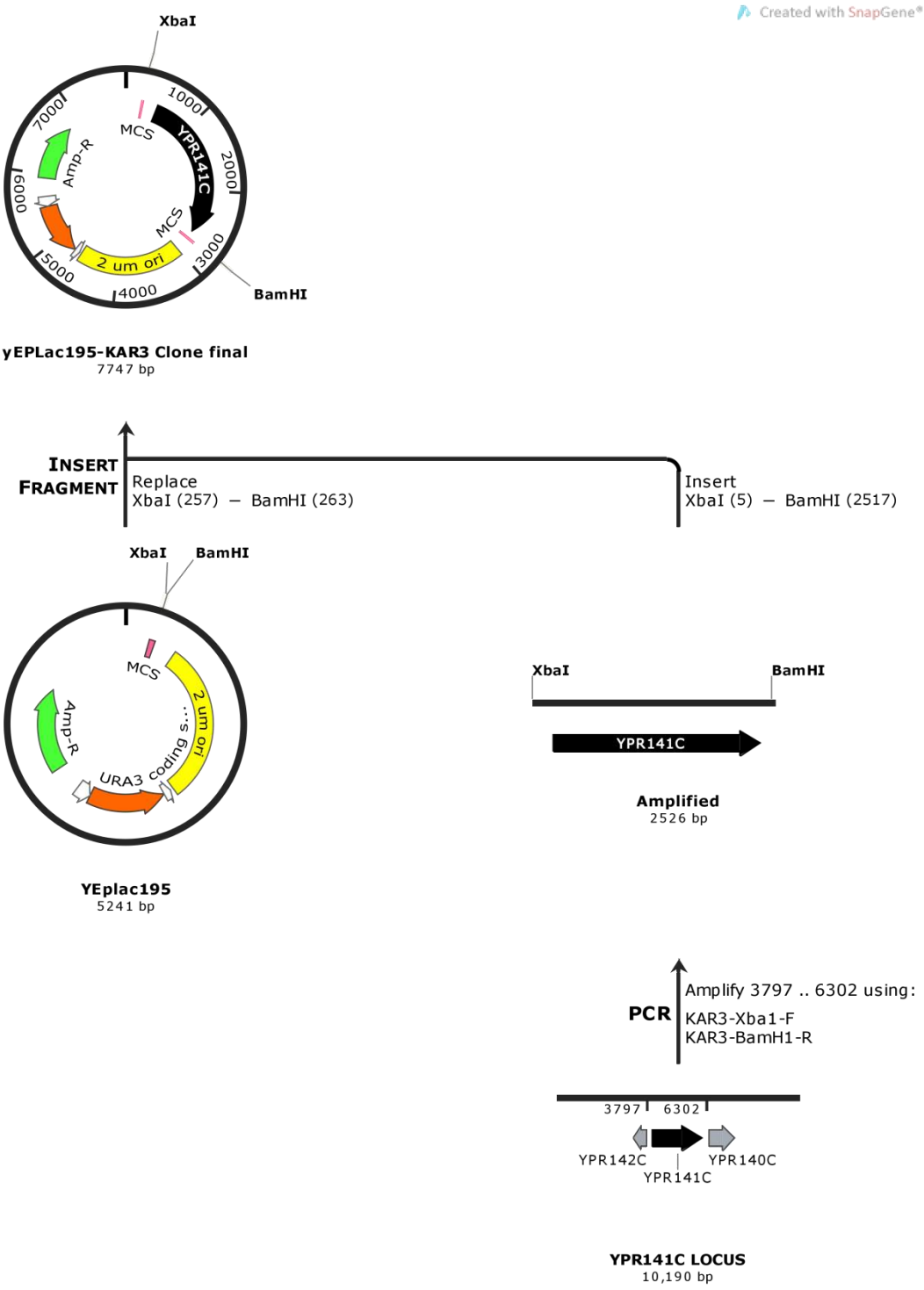

Appendix 1.11: Cloning strategy of yeplac195-cin8

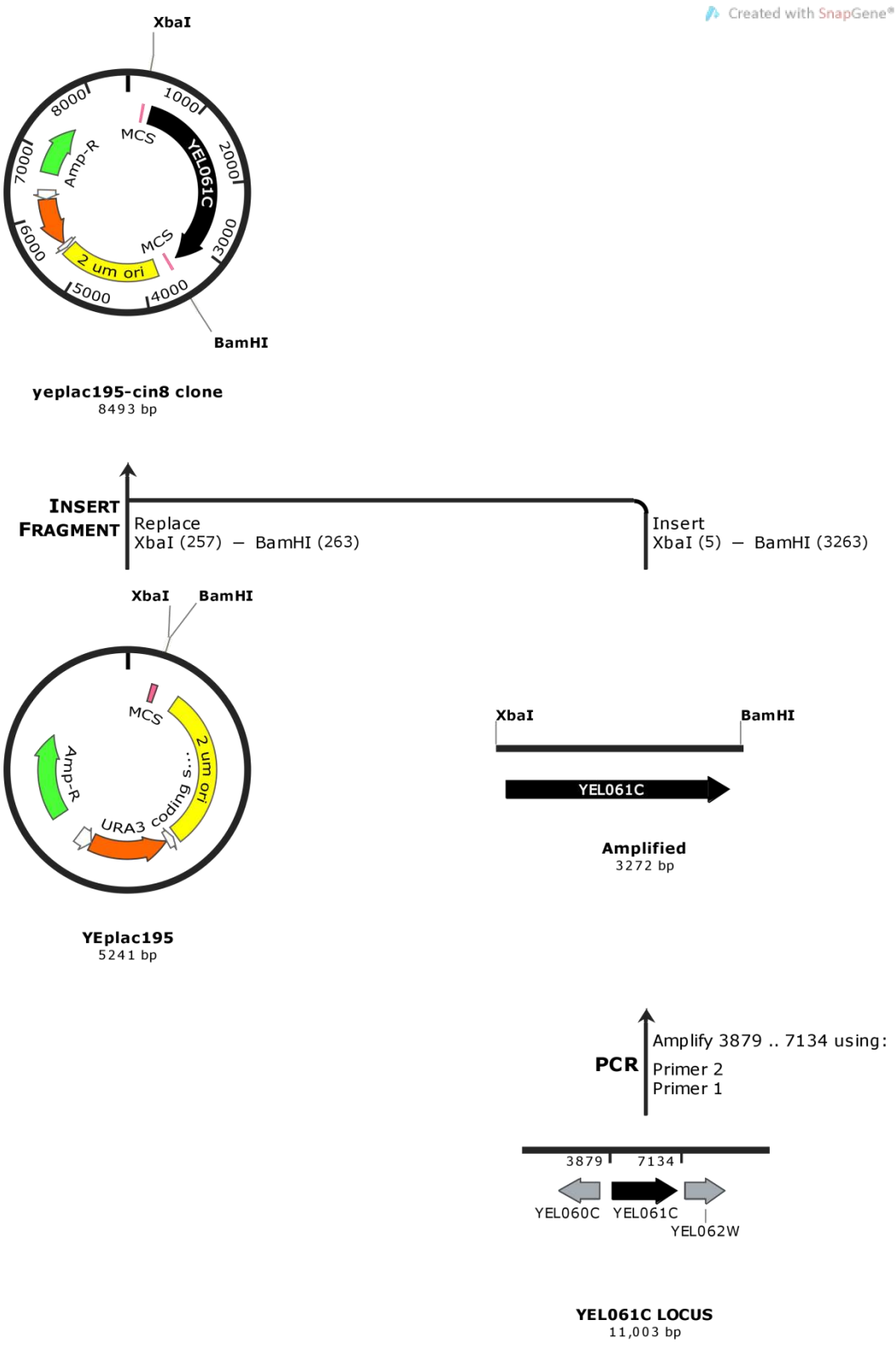

Appendix 2: List of yeast strains used in the study

Serial No.	Strain Name	Genotype
1	*JK9-3d*	*Mat a leu2-3,112 ura3-52 rme1 trp1 his4*
2	*JK9-Nup116 GFP*	*Mat a leu2-3,112 ura3-52 rme1 his4 Nup116-GFP::TRP*
3	*JK9-Nup116 GFP-mCherry Ras2*	*Mat a 112 ura3-52 rme1 his4 Nup116-GFP::TRP mCherry-Ras2:: LEU2*
4	*JK9-Nup116 GFP-mCherry Ras2-kar3Δ*	*Mat a 112 ura3-52 rme1 his4 Nup116-GFP::TRP mCherry-Ras2:: LEU2 kar3Δ::kanMX6*
5	*JK9-Nup116 GFP-mCherry Ras2-cin8Δ*	*Mat a 112 rme1 his4 Nup116-GFP::TRP mCherry-Ras2:: LEU2 cin8Δ :: URA3*
6	*JK9-Nup116 GFP-mCherry Ras2-kip1Δ*	*Mat a 112 rme1 his4 Nup116-GFP::TRP mCherry-Ras2:: LEU2 kip1Δ ::URA3*
7	*JK9-Nup116 GFP-mCherry Ras2-kip2Δ*	*Mat a 112 rme1 his4 Nup116-GFP::TRP mCherry-Ras2:: LEU2 kip2Δ ::URA3*
8	*JK9-Nup116 GFP-mCherry Ras2-kip3Δ*	*Mat a 112 rme1 his4 Nup116-GFP::TRP mCherry-Ras2:: LEU2 kip3Δ ::URA3*
9	*JK9-Nup116 GFP-mCherry Ras2-smy1*	*Mat a 112 rme1 his4 Nup116-GFP::TRP mCherry-Ras2:: LEU2 smy1Δ ::URA3*
10	*JK9-Nup116 GFP-mCherry Ras2-ubf1*	*Mat a 112 rme1 his4 Nup116-GFP::TRP mCherry-Ras2:: LEU2 ubf1Δ ::URA3*
11	*JK9-Nup116 GFP-mCherry Ras2-pkp1Δ*	*Mat a 112 rme1 his4 Nup116-GFP::TRP mCherry-Ras2:: LEU2 pkp1Δ ::URA3*
12	*JK9-Nup116 GFP-mCherry Ras2-eft2Δ*	*Mat a 112 rme1 his4 Nup116-GFP::TRP mCherry-Ras2:: LEU2 eft2Δ ::URA3*

Serial No.	Strain Name	Genotype
13	*JK9-Nup116 GFP-mCherry Ras2-mad2Δ*	*Mat a 112 rme1 his4 Nup116-GFP::TRP mCherry-Ras2:: LEU2 mad2Δ ::URA3*
14	*JK9-Nup116 GFP-mCherry Ras2-gpx1Δ*	*Mat a 112 rme1 his4 Nup116-GFP::TRP mCherry-Ras2:: LEU2 gpx1Δ ::URA3*
15	*JK9-Nup116 GFP-mCherry Ras2-dck1Δ*	*Mat a 112 rme1 his4 Nup116-GFP::TRP mCherry-Ras2:: LEU2 dck1Δ ::URA3*
16	*JK9-Nup116 GFP-mCherry Ras2-hub1Δ*	*Mat a 112 rme1 his4 Nup116-GFP::TRP mCherry-Ras2:: LEU2 hub1Δ ::URA3*
17	*JK9-Nup116 GFP-mCherry Ras2-ase1Δ*	*Mat a 112 rme1 his4 Nup116-GFP::TRP mCherry-Ras2:: LEU2 ase1Δ ::URA3*
18	*JK9-Nup116 GFP-mCherry Ras2-sps1Δ*	*Mat a 112 rme1 his4 Nup116-GFP::TRP mCherry-Ras2:: LEU2 sps1Δ ::URA3*
19	*JK9-Nup116 GFP-mCherry Ras2-pus4Δ*	*Mat a 112 rme1 his4 Nup116-GFP::TRP mCherry-Ras2:: LEU2 pus4Δ ::URA3*
20	*JK9-Nup116-GFP-mCherry Ras2 -kar3Δ cre pop out*	*Mat a 112 rme1 ura3-52 his4 Nup116-GFP::TRP mCherry-Ras2:: LEU2 kar3Δ [pSH62]*
21	*JK9-Nup116-GFP-mCherry Ras2 cin8Δ pop out*	*Mat a 112 rme1 ura3-52 his4 Nup116-GFP::TRP mCherry-Ras2:: LEU2 cin8Δ*
22	*JK9-Nup116-GFP-mCherry Ras2 -kar3Δ-YCplac33-KAR3*	*Mat a 112 rme1 his4 Nup116-GFP::TRP mCherry-Ras2:: LEU2 kar3Δ [YCplac33-KAR3]*
23	*JK9-Nup116-GFP-mCherry Ras2 -cin8Δ-YCplac33-CIN8*	*Mat a 112 rme1 his4 Nup116-GFP::TRP mCherry-Ras2:: LEU2 cin8Δ [YCplac33-CIN8]*
24	*JK9-Nup116-GFP-mCherry Ras2 -kar3Δ-Yeplac 195-KAR3*	*Mat a 112 rme1 his4 Nup116-GFP::TRP mCherry-Ras2:: LEU2 kar3Δ [YEplac195-KAR3]*
25	*JK9-Nup116-GFP-mCherry Ras2 -cin8Δ-YEplac195-CIN8*	*Mat a 112 rme1 his4 Nup116-GFP::TRP mCherry-Ras2:: LEU2 cin8Δ [YEplac195-CIN8]*

26	*JK9-Nup116-GFP-mCherry Ras2 -YEplac195-CIN8*	*Mat a 112 rme1 his4 Nup116-GFP::TRP mCherry-Ras2:: LEU2 [YEplac195-CIN8]*
27	*JK9-Nup116-GFP-mCherry Ras2 -kar3Δ-Yeplac 195-CIN8*	*Mat a 112 rme1 his4 Nup116-GFP::TRP mCherry-Ras2:: LEU2 kar3Δ [YEplac195-CIN8]*
28	*JK9-Nup116-GFP-mCherry Ras2 -kar3Δ-HTB2-Dsred*	*Mat a 112 rme1 his4 Nup116-GFP::TRP mCherry-Ras2:: LEU2 kar3Δ [YEplac195-HTB2-DsRed]*
29	*JK9-Nup116-GFP-mCherry Ras2 -cin8Δ-HTB2-Dsred*	*Mat a 112 rme1 his4 Nup116-GFP::TRP mCherry-Ras2:: LEU2 cin8Δ [YEplac195-HTB2-DsRed]*
30	*JK9-Nup116-GFP-mCherry Ras2 -kar3Δ-Sec63-GFP*	*Mat a 112 rme1 his4 Nup116-GFP::TRP mCherry-Ras2:: LEU2 kar3Δ sec63GFP:: URA3*
31	*JK9-Nup116-GFP-mCherry Ras2 -cin8Δ-Sec63-GFP*	*Mat a 112 rme1 his4 Nup116-GFP::TRP mCherry-Ras2:: LEU2 cin8Δ sec63GFP:: URA3*
32	*JK9-Nup116 GFP-mCherry Ras2-prp45 1-190*	*Mat a 112 rme1 his4 Nup116-GFP::TRP mCherry-Ras2:: LEU2 prp45 1-190 ::URA3*
33	*JK9-Nup116-GFP-mCherry Ras2 -kar3Δ-αTbulin-CFP*	*Mat a 112 rme1 his4 Nup116-GFP::TRP mCherry-Ras2:: LEU2 kar3Δ α tubulin:: URA3*
34	*JK9-Nup116-GFP-mCherry Ras2 -cin8Δ-αTbulin-CFP*	*Mat a 112 rme1 his4 Nup116-GFP::TRP mCherry-Ras2:: LEU2 cin8Δα tubulin:: URA3*
35	*JK9-Nup116-GFP-mCherry Ras2 -HTB2-DsRed*	*Mat a 112 rme1 his4 Nup116-GFP::TRP mCherry-Ras2:: LEU2 [YEplac195-HTB2-DsRed]*
36	*JK9-Nup116-GFP-mCherry Ras2 -Sec63-GFP*	*Mat a 112 rme1 his4 Nup116-GFP::TRP mCherry-Ras2:: LEU2 sec63GFP:: URA3*
37	*JK9-Nup116-GFP-mCherry Ras2 -αTubulin-CFP*	*Mat a 112 rme1 his4 Nup116-GFP::TRP mCherry-Ras2:: LEU2 α tubulin:: URA3*
38	*Prp45-Wild Type*	*ura3 his3 trp1 LexA (6XOP)-leu2*

39	*Prp45-1-169*	*ura3 his3 trp1 LexA (6XOP)-LEU2 prp45(1-169) HA::kanMX6*
40	*Prp45 Wild Type Nup116 GFP-mCherry-Ras2*	*ura3 LexA (6XOP)-leu2 Nup116-GFP::HIS3 mCherry-Ras2:: TRP*
41	*Prp45 Wild Type Nup116 GFP-mCherry-Ras2-Sec63-GFP*	*Nup116-GFP::HIS3 mCherry-Ras2:: TRP LexA (6XOP)-leu2 sec63GFP:: URA3*
42	*Prp45 Wild Type Nup116 GFP-mCherry-Ras2-HTB2-Ds-Red*	*Nup116-GFP::HIS3 mCherry-Ras2:: TRP LexA (6XOP)-leu2 [YEplac195-HTB2-DsRed :: URA3]*
43	*Prp45-1-169-Nup116 GFP-mCherry-Ras2*	*ura3 LexA (6XOP)-LEU2 prp45(1-169) HA::kanMX6 Nup116-GFP::HIS3 mCherry-Ras2:: TRP*
44	*Prp45-1-169-Nup116 GFP-mCherry-Ras2-HTB2-Ds-Red*	*LexA (6XOP)-LEU2 prp45(1-169) HA::kanMX6 Nup116-GFP::HIS3 mCherry-Ras2:: TRP [YEplac195-HTB2-DsRed]*
45	*Prp45-1-169-Nup116 GFP-mCherry-Ras2-Sec63-GFP*	*LexA (6XOP)-LEU2 prp45(1-169) HA::kanMX6 Nup116-GFP::HIS3 mCherry-Ras2:: TRP sec63GFP:: URA3*
46	*JK9-HTB2-GFP-HEDL-E2Crimson*	*Mat a leu2-3,112 rme1 his4 HDEL E2Crimson::TRP [YEplac195-HTB2-URA3]*

Appendix 3: Supportive data

A. Single copy kar3 can rescue the phenotype for *kar3* deletion

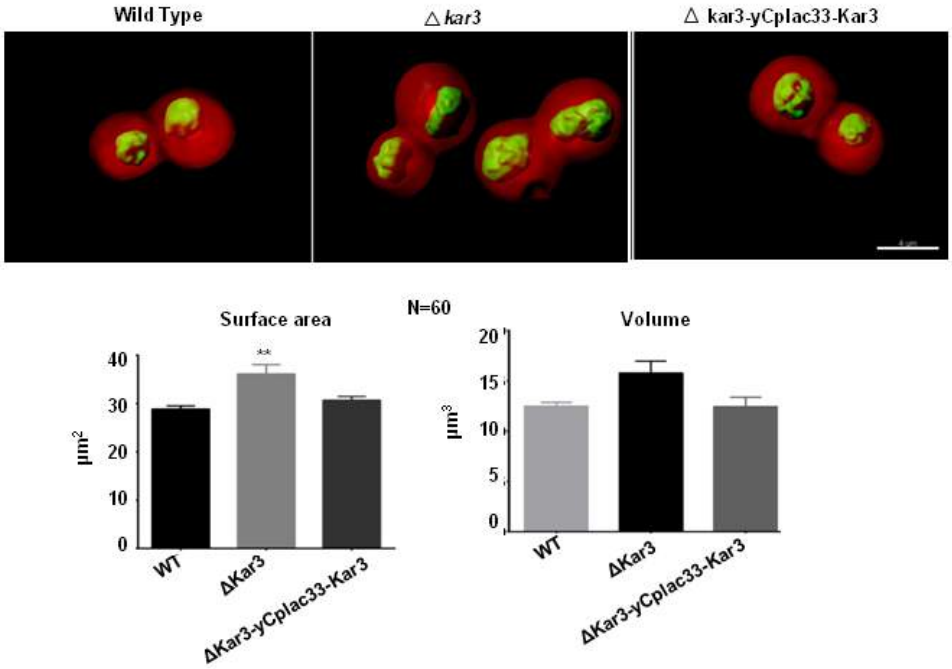

B. Single copy cin8 can rescue the phenotype for cin8 deletion

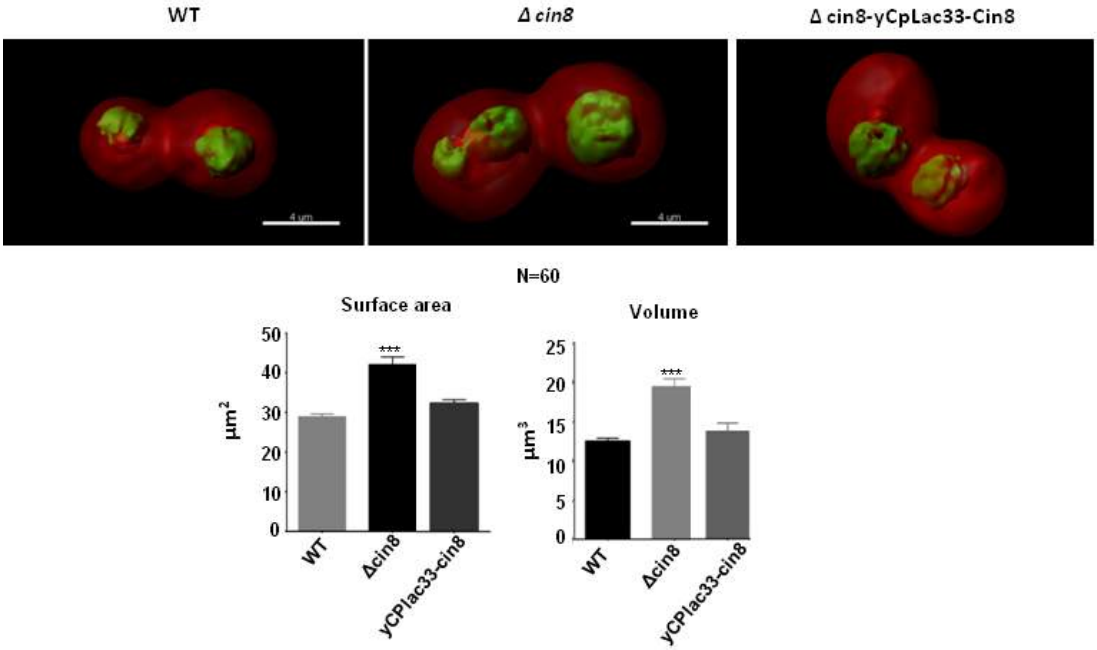

Publication

FEBS Letters

FEBS PRESS science publishing by scientists

Perturbation of nucleo-cytoplasmic transport affects size of nucleus and nucleolus in human cells

Abira Ganguly[1], Chumki Bhattacharjee[1], Madhura Bhave[1], Vaishali Kailaje[1], Bhawik K. Jain[1], Isha Sengupta[1], Annapoorni Rangarajan[2] and Dibyendu Bhattacharyya[1]

1 Advanced Centre for Treatment Research & Education in Cancer (ACTREC), Tata Memorial Centre, Navi Mumbai, Maharashtra, India
2 Department of Molecular Reproduction, Development and Genetics, Indian Institute of Science Bangalore, India

Correspondence
D. Bhattacharyya, Advanced Centre for Treatment Research & Education in Cancer (ACTREC), Tata Memorial Centre, Sector 22, Kharghar, Navi Mumbai 410210 MH, India
Fax: +91 22 2740 5085
Tel: +91 22 2740 5025
E-mail: dbhattacharyya@actrec.gov.in

(Received 19 October 2015, revised 2 January 2016, accepted 18 January 2016)

doi:10.1002/1873-3468.12077

Edited by Quan Chen

Size regulation of human cell nucleus and nucleolus are poorly understood subjects. 3D reconstruction of live image shows that the karyoplasmic ratio (KR) increases by 30–80% in transformed cell lines compared to their immortalized counterpart. The attenuation of nucleo-cytoplasmic transport causes the KR value to increase by 30–50% in immortalized cell lines. Nucleolus volumes are significantly increased in transformed cell lines and the attenuation of nucleo-cytoplasmic transport causes a significant increase in the nucleolus volume of immortalized cell lines. A cytosol and nuclear fraction swapping experiment emphasizes the potential role of unknown cytosolic factors in nuclear and nucleolar size regulation.

Keywords: cancer; importin beta; karyoplasmic ratio; nuclear transport; nucleolus size; nucleus size; organelle size; Ran

Highlights

- 3D reconstruction of live image shows that the karyoplasmic ratio (KR) and nucleolar volume increases significantly in cancer cells.
- Attenuation of nucleo-cytoplasmic transport alters the size of human cell nucleus and nucleolus.
- Unknown cytosolic factors play roles in regulating the nucleus and nucleolus size in human cells.
- Learning how organelle sizes are regulated will contribute to basic cell biology and may help organelle directed medicines for diseases.

One of the very fundamental questions in cell biology is how distinct morphologies of different organelles are maintained to accommodate cell size differences and to execute different metabolic functions [1,2]. The nucleus, the largest of all organelles, is the evident candidate for these kinds of studies to answer this question. It contains several membraneless subcompartments, nucleolus being the prominent example [3]. The nuclear to cell volume ratio or 'karyoplasmic ratio' (KR) remains a roughly constant value in cells with widely different DNA contents, ranging from single-celled eukaryote to mammalian cells [4,5]. Moreover, abnormal organelle architecture, primarily altered nuclear size or nucleolus morphology, have been considered for more than a hundred years a diagnostic hallmark for cancer [6–10]. In spite of such an early knowledge of association with several forms of cancers, the regulation of nuclear or nucleolar size, especially in human cells, still remains a poorly understood field. However, a few groups have shown recent interests in the field and several studies in

Abbreviations
KR, karyoplasmic ratio; N/C, nucleus to cytoplasmic volume ratio; Nu/N, nucleolus to nucleus volume ratio.

different model organisms have been reported over last few years [5,11].

It was thought for a long time that nuclear size increases in cancer cells simply to accommodate the higher DNA content as a result of aneuploidy [12–14]. However, ploidy had been shown to have no direct effect on the nuclear size of both budding and fission yeast [4,5] suggesting the existence of active regulation of nuclear size in synchrony with cell size. Disruption of the cytoskeleton did not affect N/C ratio in fission yeasts [5]. In fact, it exemplified that in yeast almost no genetic or physiological modification can alter the N/C ratio except a blockade in nucleo-cytoplasmic transport [5]. In metazoans, the nuclear envelope is perforated by the nuclear pore complex (NPC) which mediates nucleo-cytoplasmic transport [15]. In other organisms, namely *S. pombe*, and mammalian cells, the NPC has shown to have no direct role in regulating nuclear size [16,17]. Nucleo-cytoplasmic transport factors Importin alpha2 and NTF2 are responsible for interspecies nuclear scaling in two related but different-sized frog species and also during Xenopus development [11]. Nuclear scaling acts mainly through the import pathway, with a much higher level of importin α and also of importin α1, importin α3, and importin β [11]. Different studies in *Tetrahymena thermophile*, *Drosophila melanogaster*, and in *C. elegans* showed that different import factors are what most likely play a role in controlling their respective nuclear size [18]. Altered nuclear transport is frequently observed in transformed cells [15,18]. These coinciding results from different organisms suggest that nucleo-cytoplasmic transport most likely directly or indirectly controls nuclear size in human cells.

Although many similar characteristics exist between the nucleus and nucleolus, it is unknown whether the sizes of the nucleus and the nucleolus are controlled by same or different active mechanisms. Nucleus size and cell size are shown to correlate with RNA transcription level [19,20]. Genes regulating rRNA biosynthesis, ER–Golgi transport, nucleosome assembly are shown to be responsible for decreased nucleolar size in yeast and fruit fly while genes involved in cell cycle regulation are shown to be responsible for increased nucleolus size [21]. Considering these facts, we can postulate that the size and shape of the nucleus and nucleolus are carefully controlled by similar or different mechanisms, which are normally disrupted in transformed cells.

Very few studies so far focused on the size control mechanism of the nucleus and the nucleolus of human cells. In the present study, we have determined the range of variation of nuclear size in terms of N/C ratio and nucleolus size with respect to nucleus size in different immortalized and transformed cell lines of same human tissue origin. Upon nuclear transport perturbation, it is found that N/C ratio and nucleolus size are increased significantly in immortalized cell lines. In an *in vitro* assay system, combining intact nucleus and cytosolic fractions from different sources has been established to determine regulation of morphogenic changes of nucleolus. The analysis of the results from the nuclear transport perturbation have led to the verdict that nucleolar size is indeed correlated with nucleus size.

Material & Methods

Plasmids and cloning

Lamin A, Ran, Importin beta, and Importin beta 1-364 were PCR amplified from cDNA made from human mRNA with site-specific primers (Table S2). Lamin A was cloned in pmGFPC1 vector in XhoI and BamHI sites. Ran was cloned in pCMV3X-Flag1A (Clonetech, Mountain View, CA, USA) vector using BamHI and HindIII sites. pCMV3X-Flag1A-Ran was used for site-directed mutagenesis at Ran T24N and Ran Q69L with site-specific primers (Table S2). Importin beta and Importin beta 1-364 were cloned in pCMV3X-Flag1A (Clonetech) vector using BamHI and SmaI sites. pmCherry-F plasmid was created by subcloning mCherry from vector pDS-Red-N1-mCherry (Glick Lab, University of Chicago, Chicago, IL, USA) vector in pEGFP-F (Clonetech) vector, in which EGFP was replaced with using Nhe1 and BsrG1 sites. pEGFPC1-Fibrillarin construct was obtained from Addgene.

Cell culture and transfection

HaCaT, A431, HHL5, and MCF7 cell lines were cultured in Dulbecco's modified Eagle's medium (DMEM) media (HiMedia) and HepG2 cell line was cultured in RPMI media (Himedia) supplemented with 10% fetal bovine serum (Invitrogen) and antibiotics (1% Pen-Strep glutamine and 0.006% gentamicin, Invitrogen) in a 37 °C incubator under a 5% CO_2 atmosphere. MCF10A cells were cultured in DMEM/F12 (1 : 1) (Himedia) media supplemented with cholera toxin, epidermal growth factor, insulin, and hydrocortisone, and with 10% FBS and 1% Pen-streptomycin. HHL5 was gift from Arvind Patel, University of Glasgow and INT 407 was kind gift from S. R. Chowdhury, IICB, India. In all experiments, X-tremeGENE HP DNA transfection reagent (Roche, Mumbai, India) was used for transient transfections as per manufacturer's protocol. All transient transfections were analyzed after 48 h (expression analysis).

Live cell imaging followed by immunofluorescence

Zeiss (LSM510-Meta or Zeiss780) confocal microscopes were used for imaging nucleus and cells using 63X 1.4 N.A

oil immersion objectives. Eight-bit images of 512 × 512 pixels were acquired with one airy-unit pinhole aperture size and a z-step size of 500 nm. Live cell images were captured, with stage temperature maintained at 37 °C and CO_2 concentration maintained at 5%. For nucleolus imaging, GFP-Fibrillarin-labeled nucleolus signal was not even in every nucleolus, making it difficult to have images with evenly distributed unsaturated signal. BrighteR mode in Leica-STED microscope was used in which every nucleolus spots were evenly and optimally captured using high dynamic range imaging. Cells were always seeded in glass bottom Petri dishes (Cell E&G, Houston, TX, USA); 48 h post transfection, live cell imaging was performed while cells were kept in Phenol red-free media (Himedia, Mumbai, India). For live cell followed by immunofluorescence, post live cell image capture, cells were fixed with 100% chilled methanol for 4 min and then incubated in blocking (1% horse serum) solution for 1 h in moisture chamber at room temperature. Cells were then sequentially incubated with primary antibody (mouse monoclonal anti-flag) (1 : 100) and secondary antibody (goat anti-mouse alexa 405) (1 : 100) (adopted from [22]).

Image processing

For quantification, each confocal 3D dataset were opened with IMARIS 7.6.4 software (Bitplane, Zurich, Switzerland). Images were processed by smoothing using 'Median filter 3 × 3 × 1.' A surface was then created using a threshold of absolute intensity. Radii were determined by taking half of the longest diameters for each cell/ nucleus/ nucleolus spot as measured in an individual stack using the 'slice' view in Imaris. Measurements were taken from 20 cells of each set and total 60–100 samples from three such sets were analyzed. The nucleolus, nucleus, and cell volumes were obtained in statistics of processed images and from those volumes the N/C ratio and the Nu/N ratio were calculated.

Statistical analysis

Values of cell volumes, nuclear volumes, nucleolus volumes, and N/C ratio or Nu/N ratio were incorporated in the GRAPH PAD PRISM 6 software, and graphs were plotted in column type mean with standard error mean. Normal distributions of dataset were checked in column statistics in GRAPH PAD PRISM 6 and as datasets were non-Gaussian distribution, Mann–Whitney test was performed to calculate the statistical significance.

Preparation of intact nuclei and cytoplasmic fraction

Cells were trypsinized and harvested in cold PBS followed by addition of 500 μL of ice cold isotonic buffer (0.25 M sucrose, 50 mM Tris-Cl pH7.5, 25 mM KCl, 5 mM MgCl2, 0.1% Triton X-100, 0.2 mM PMSF, 0.2 mM protease cocktail inhibitor) and incubated on ice for 30 min with intermittent mixing. Cells were then treated with 0.1% NP40 followed by vortexing for 10 s. Nuclei were pelleted by centrifugation at 4193 ***g*** for 10 min and supernatant was collected as cytoplasmic fraction. Nuclear pellet was resuspended in 200 μL of nuclei buffer (0.34 M sucrose, 15 mM Tris-Cl pH7.5, 60 mM KCL, 15 mM NaCl, 2 mM EDTA, 0.5 mM EGTA, 0.15 mM βME, 0.15 mM spermine, 0.15 mM spermidine). Two measures were taken to isolate intact nuclei, in first case, pure nuclei pool were first checked under phase contrast microscope for their integrity before proceeding further and cells were incubated in lysis buffer until only intact nuclei were observed under the microscope. Secondly, western blot against β-tubulin (Sigma, St. Louis, MO, USA) and Histone 3 (Abcam, Cambridge Science Park, Cambridge, UK) was performed against cytoplasmic fraction and nuclear fraction (Fig. S8) as β-tubulin is only present in cytoplasm and histone 3 is only present in nucleus. The protocol was standardized as the blot showed presence of β-tubulin only in cytoplasmic fraction and histone 3 is only present in nuclear fraction.

In vitro assay

Different cytoplasmic fractions were incubated with pure nuclei of different conditions in 1 : 2 ratios for 30 min at 22 °C. Nuclei were immobilized on a glass bottom dishes (Cell E & G, Houston, TX, USA) using concanavalin A (Sigma-Aldrich) and were imaged at same temperature.

Invasion assay

We used a standard *in vitro* invasion assay [23] in which cells migrate through matrigel toward 10% serum. Cells were trypsinized and 50 000 cells resuspended in DMEM with 0.2% FBS were seeded to rehydrated matrigel-coated inserts (8 μm pore size inserts, BD Pharmingen, San Diego, CA, USA) and placed in 24-well companion plates with DMEM and 10% FBS. After 24 h, the noninvading cells in the upper surface of the membrane were removed using a cotton tip. The filters were fixed in methanol for 4 min at −20 °C, incubated in DAPI (1 : 5000; Sigma-Aldrich) for 10 min, and mounted. The invading cells were counted at room temperature using a fluorescence microscope (Leica DMI 6000) with a 20 × air objective, and images were analyzed using IMAGE J software.

Results & Discussions

Transformed cells exhibit increase in nuclear to cytoplasmic volume (N/C) ratio by 30–80%

At first, we wanted to determine the range of variation of N/C ratio in mammalian cell lines as the size and shape

of both nucleus as well as cell from different tissue types are very heterogeneous. For the same, we have selected four pairs of immortalized and transformed cell lines of similar tissue origins, namely skin, colon-intestine, breast and liver (Table 1) comparative measurements of N/C ratio. We have transfected each of the cell lines with constructs expressing GFP-Lamin and F-mCherry for subsequent measurements of nuclear volume and cell volume, respectively (Fig. S1). 3D reconstruction (Fig. 1A) of confocal images of each cell as well as their corresponding nucleus resulted near accurate respective volume estimations. Using these volume estimation results, we have calculated the nuclear to cell volume (N/C) ratio for each cell line. Our analysis shows that N/C ratio is significantly higher ($P < 0.001$) in transformed cell lines (A431, HCT116, MCF7, and HepG2) compared to their respective immortalized counterparts (HaCaT, INT 407, MCF10A, and HHL5) (Fig. 1B). N/C ratio is ~ 80% higher in transformed cell lines from colon-intestine, ~ 45% higher in breast cell lines, 40% higher in skin cell lines, and 30% higher in liver cell lines (Fig. 1C). The N/C ratio varies widely (Fig. 1D) in all the transformed cell lines compared to their immortalized counterparts in which it maintains primarily a constant value of (0.10 ± 0.04) which is similar in range to the highly constant value of N/C ratio of budding yeast (0.09 ± 0.01) (Fig. S2, Fig. 1D). Previous reports have shown that fission yeast also has a similar constant value of N/C ratio [5]. It was noted that nuclear volume may not have always increased in a transformed cell line. Rather the reduction of cell volume in transformed cell lines is what contributed to the effective increase of N/C ratio in the same (Fig. 1E). However in case of breast origin, cell volumes are comparable, but the nucleus volume is higher in the transformed cell line (MCF7) compared to its immortalized counterpart (MCF 10A) (Fig. 1E). It is evident from these observations that increase in N/C ratio is variable in different transformed cell lines. All measurements were done in an unsynchronized condition. We have repeated the measurements in G1/S-enriched conditions and found similar results (Fig. S3).

Perturbation of nucleo-cytoplasmic transport in immortalized cells causes (N/C) ratio to increase by 30–50%

As we have validated the phenomenon of the N/C ratio increase in transformed cells, we wanted to further investigate whether the N/C ratio could be altered by perturbation of any physiological or cellular process in immortalized cell lines. Previously it had been reported that nucleo-cytoplasmic transport played an important role in regulating nuclear size and nuclear scaling in yeast and *Xenopus* systems, respectively [5,11]. However, no such studies have been reported in mammalian cells. For this reason, we decided to attenuate the nuclear transport in immortalized cells and study the effect of this on the N/C ratio. We used an overexpression of dominant negative forms of Importin beta and Ran to create such attenuation of nuclear transport [24–26]. Nucleo-cytoplasmic transport attenuation was first confirmed by cotransfecting NLS-YFP along with dominant negative form of Importin beta or Ran^{Q69L} in which NLS-YFP is restricted in the cytoplasm compared to vector control cells (Fig. S4).

Table 1. Cell lines used in the present study.

Origin	Immortalized	Transformed
Skin	HaCaT	A431
Colon-Intestine	INT 407	HCT116
Breast	MCF10A	MCF7
Liver	HHL5	HepG2

Effect of overexpression of Importin beta 1-364

The dominant negative form of Importin beta blocks multiple pathways of nucleo-cytoplasmic transport [25]. We overexpressed Importin beta 1-364 fragment along with GFP-Lamin and F-mCherry in HaCaT (skin immortalized) cells. Live cell imaging were done for total of a hundred cells in five different experiments, after 48 h of transfection. Post live cell imaging, immunofluorescence against Flag-Imp-beta 1-364 was done to identify Importin beta 1-364 positive cells that should show nuclear pore localization and cytoplasmic localization (Fig. 2A; left panel). 3D reconstruction of confocal images (Fig. 2B) results quantitative measurement of N/C ratio as described earlier. N/C ratio was increased significantly ($P < 0.0001$), when we overexpressed Importin beta 1-364, in the immortalized cell line HaCaT (Fig. 2D top). The N/C ratio increased by almost 50% as compared to the vector control transfected same cells (2D bottom).

Effect of Overexpression of Ran^{T24N} and Ran^{Q69L} on immortalized cell

Ran is one of the key players of classical nuclear transport pathway [27]. An over expression of any of the two mutant forms, Ran^{T24N} or Ran^{Q69L}, can effectively perturb the nucleo-cytoplasmic transport pathway [28,29]. Once again we overexpressed dominant negative pCMV 3X Flag-Ran^{T24N} or pCMV 3X Flag-Ran^{Q69L} in HaCaT cells along with GFP-Lamin and F-mCherry as described earlier. Post live cell imaging, immunofluorescence against Flag-Ran^{Q69L} showed

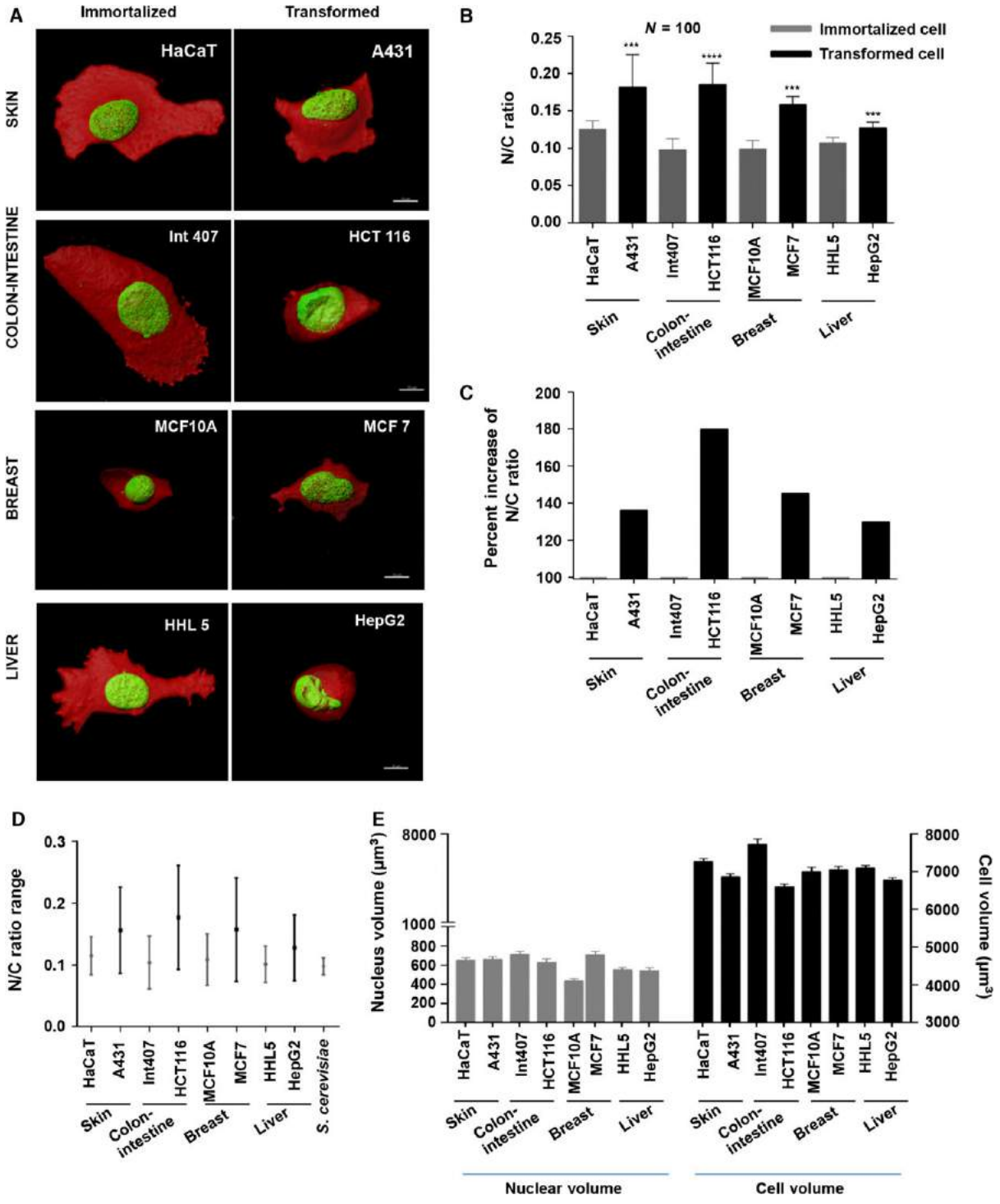

Fig. 1. Transformed cell lines exhibit increase in nuclear to cytoplasmic volume (N/C) ratio by 30–80% compared to their immortalized counterpart of same tissue origin. (A) Overlay of 3D reconstruction images of live cells; cell membrane (F-mCherry) and nuclear envelope (GFP-Lamin). Scale bar is 10 μm. (B) N/C ratio is significantly higher ($P < 0.0001$, $P < 0.001$) in all transformed cell lines compared to the corresponding immortalized cell lines as represented in column graph. Error bars represent standard error mean (SEM). (C) About 30–80% increase in N/C ratio in different transformed cell lines were observed compared to immortalized counterpart. (D)The range of N/C ratio varies more in all transformed cell lines compared to immortalized counterparts (Table S1). (E) Column graph showing nucleus volumes and cell volumes was quantified from images (as represented in A) in IMARIS software for 100 cells in each case in five different experiments. ns, $P > 0.05$; $*P \leq 0.05$; $**P \leq 0.01$; $***P \leq 0.001$; $****P \leq 0.0001$.

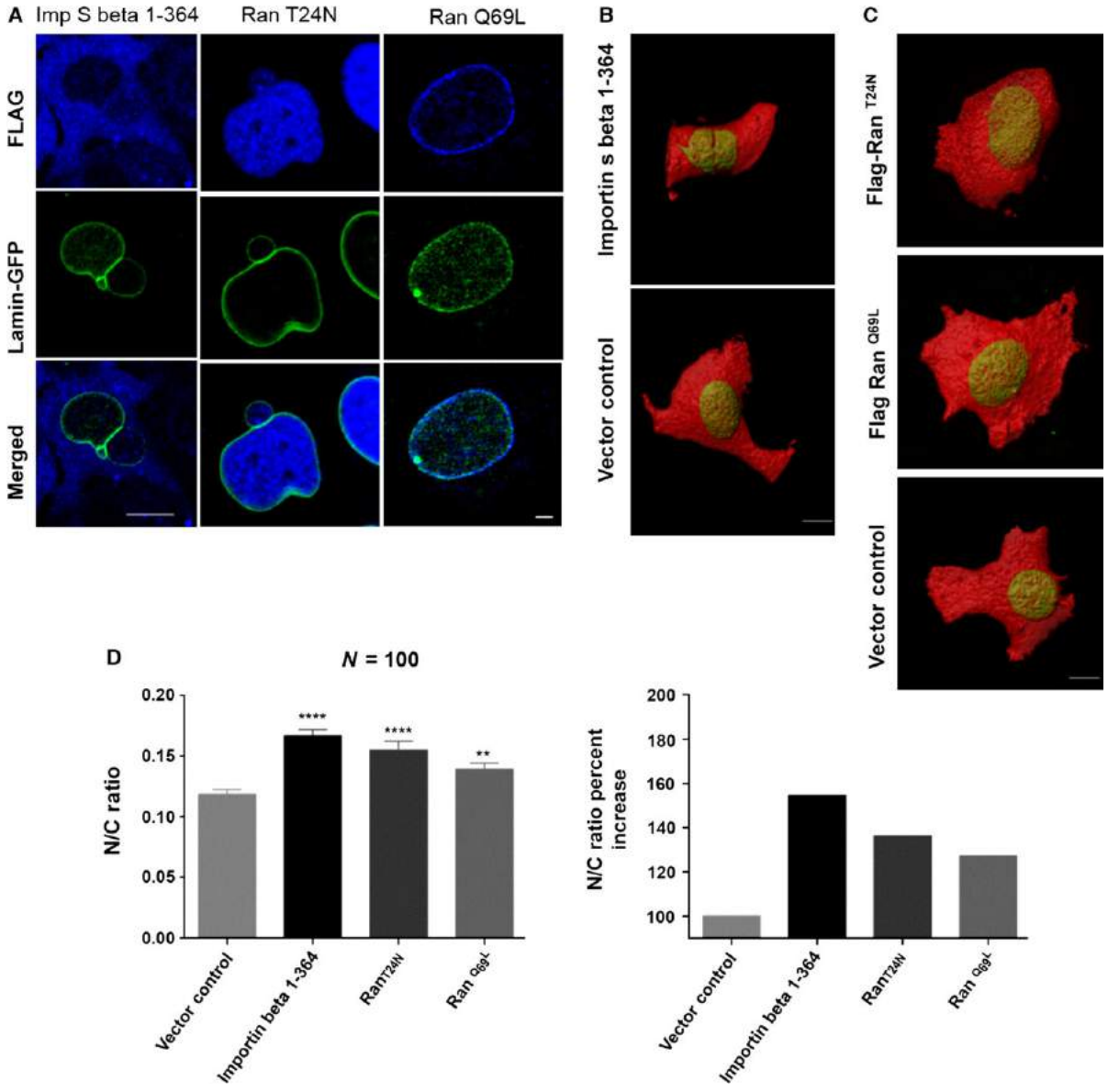

Fig. 2. Nucleo-cytoplasmic transport perturbation in immortalized cells causes (N/C) ratio to increase by 30–50%. Either of dominant negative proteins (Importin beta 1-364 or Ran^{T24N} or Ran^{Q69L}) along with GFP-Lamin, F-mCherry were transfected in HaCaT (Skin immortalized). Live cell images were captured 48 h post-transfection in confocal microscope (as described in materials & methods). (A) Dominant negative proteins in the cells were visualized by immunofluorescence against mAb Flag. GFP-Lamin images are live cell images. Scale bar is 5 μm. (B) Overlay 3D reconstruction images of live cells transfected with Importin beta 1-364 along with GFP-Lamin, F-mCherry in HaCaT (skin immortalized), cell membrane (F-mCherry), and nuclear envelope (GFP-Lamin). Scale bar is 10 μm. (C) Overlay 3D reconstruction images of live cells transfected with Ran^{T24N} or Ran^{Q69L} along with GFP-Lamin, F-mCherry in HaCaT (skin immortalized), cell membrane (F-mCherry), and nuclear envelope (GFP-Lamin). Scale bar is 10 μm. (D) N/C ratios were quantified from images (as represented in 2B, 2C) in IMARIS software for 100 cells from five different experiments. N/C ratio is significantly higher ($P < 0.001$, $P < 0.05$) in either case of Importin beta 1-364 or Ran^{T24N} or Ran^{Q69L} transfected cells compare to vector control represented in column graph. Error bars represent standard error mean (SEM). About 30–50% increase was observed when nucleo-cytoplasmic transport perturbation condition created by dominant negative proteins overexpression in the same cells. ns, $P > 0.05$; $*P \leq 0.05$; $**P \leq 0.01$; $***P \leq 0.001$; $****P \leq 0.0001$.

localization on nuclear pore complex (Fig. 2A right panel) while Flag-Ran^{T24N} showed overall nuclear localization (Fig. 2A middle panel) suggesting successful nuclear transport perturbation as described in reference [30]. 3D reconstruction of live cell images results in quantitative measurements. Dominant

negative Ran^{T24N} or Ran^{Q69L} overexpression also increased N/C ratio significantly ($P < 0.0001$, $P < 0.0027$, respectively) in immortalized cells compared to vector control transfected cells (Fig. 2D top) by ~ 30% and 20%, respectively (Fig. 2D bottom). This increase in the N/C ratio is mainly due to the increase in nuclear volume of the cell as nuclear volume and cell volume were also compared separately.

We found similar results in the overexpression studies of dominant negative Importin beta and Ran performed in another immortalized cell line INT 407 (Fig. S5). We conclude that perturbation of nuclear transport pathway by overexpressing dominant negative Importin beta and Ran leads to increase in N/C ratio in immortalized cells. Such perturbation of nucleo-cytoplasmic transport does not affect the transformed cells though (Fig. S10).

Next obvious question was to check if there is any property associated with malignancy such as invasiveness is changed when N/C ratio is increased in immortalized cell lines. To test this we performed invasion assay in immortalized cell line (HaCaT) after overexpressing either Importin beta 1-364 or Ran^{T24N} or Ran^{Q69L}. We found that there was no significant change in invasiveness compared to control cells (Fig. S6A). As a control experiment, invasiveness was also checked between A431 (transformed) and HaCaT (immortalized) and found to be significantly more in case of A431 (Fig. S6A). What is also fascinating is when wild-type Importin beta or Ran is overexpressed in skin transformed cell line (A431), the N/C ratio remains unchanged (Fig. S6B).

The nucleolus number and volume alters in transformed cells

The nucleus is host of several other subnuclear compartments. An intriguing question to solve was whether the size and number of such compartments also changes as the nuclear size changes in transformed cell lines. Nucleolus hypertrophy is very common in cancer cells [10,31]. We wanted to quantitatively measure the alteration in size and number of nucleolus in transformed cell lines as compared to their immortalized counterparts. Therefore, we quantified the nucleolus number and volume with respect to nucleus volume in all four pair of immortalized and transformed cell lines used in this study. In live cells, nucleolus and nucleus volumes were measured in individual cells using GFP-Fibrillarin as nucleolus marker and RFP-Lamin as nuclear membrane marker. Quantitative measurements for nucleolar spots and nuclear volumes were done by the 3D reconstruction of confocal images (Fig. 3A). The BrightR mode in the Leica-STED microscope was used during image capture, in which every nucleolus spot was evenly and optimally captured.

Depending on tissue origin, we found that size and number of nucleolus spots altered differently from immortalized cell line to corresponding transformed cell lines (Fig. 3B–D). To address this complexity in quantitative manner, we have measured two parameters, 'average volume' and 'total volume' of nucleolus. For the first parameter, the average volume of all nucleolus spots per nucleus was calculated and for the second parameter, the volume of all nucleolus spots per nucleus was summed. In most of the cases, the first parameter alters in incremental fashion; if it does not alter then always the second parameter increases. To be precise, the average nucleolar spot volume mostly increases in transformed cells; when average nucleolus spot volume remained unchanged then the total nucleolar volume increases. In the former case, nucleolar spot number decreases while the same increases for the latter case. For example in case of skin, colon-intestine and liver cell lines (A431, HCT116, and HepG2, respectively) average volume of nucleolus spots were found to be significantly higher ($P < 0.001$) and numbers of nucleolus spots were significantly reduced compared to their immortalized counterparts (HaCaT, INT407, HHL5, respectively) (Fig. 3B,D). On the other hand, in breast cell lines, both number and total volume of nucleolus spots were increased significantly in transformed cell lines (MCF7) compared to immortalized cell line (MCF10A) although average volume of nucleolus spots remained unchanged (Fig. 3B,D). We have also observed, in transformed cells lines, average volume of nucleolus spots per nucleus varies greatly compared to their immortalized counterparts (Fig. 3C).

Although the N/C ratio was invariably found to be increased in all the transformed cell lines, but to address consistent nucleolus size alteration in transformed cells, we calculated another parameter, the total nucleolus volume to nucleus volume (Nu/N) ratio by dividing total volume of nucleolus spots per nucleus and volume of the nucleus. We found Nu/N ratio to be significantly increased in all the transformed cell lines (Fig. 3D) except that of colon-intestine origin in which the increase was not statistically significant. Increase in Nu/N ratio (in most of the transformed cell lines) certainly indicate that the nucleolus size also scale with respect to nucleus in transformed cells.

The nucleolus number and volume alters upon blockade of nucleo-cytoplasmic transport

It is evident from the data shown in previous sections that the size of nucleus and the nucleolus are corre-

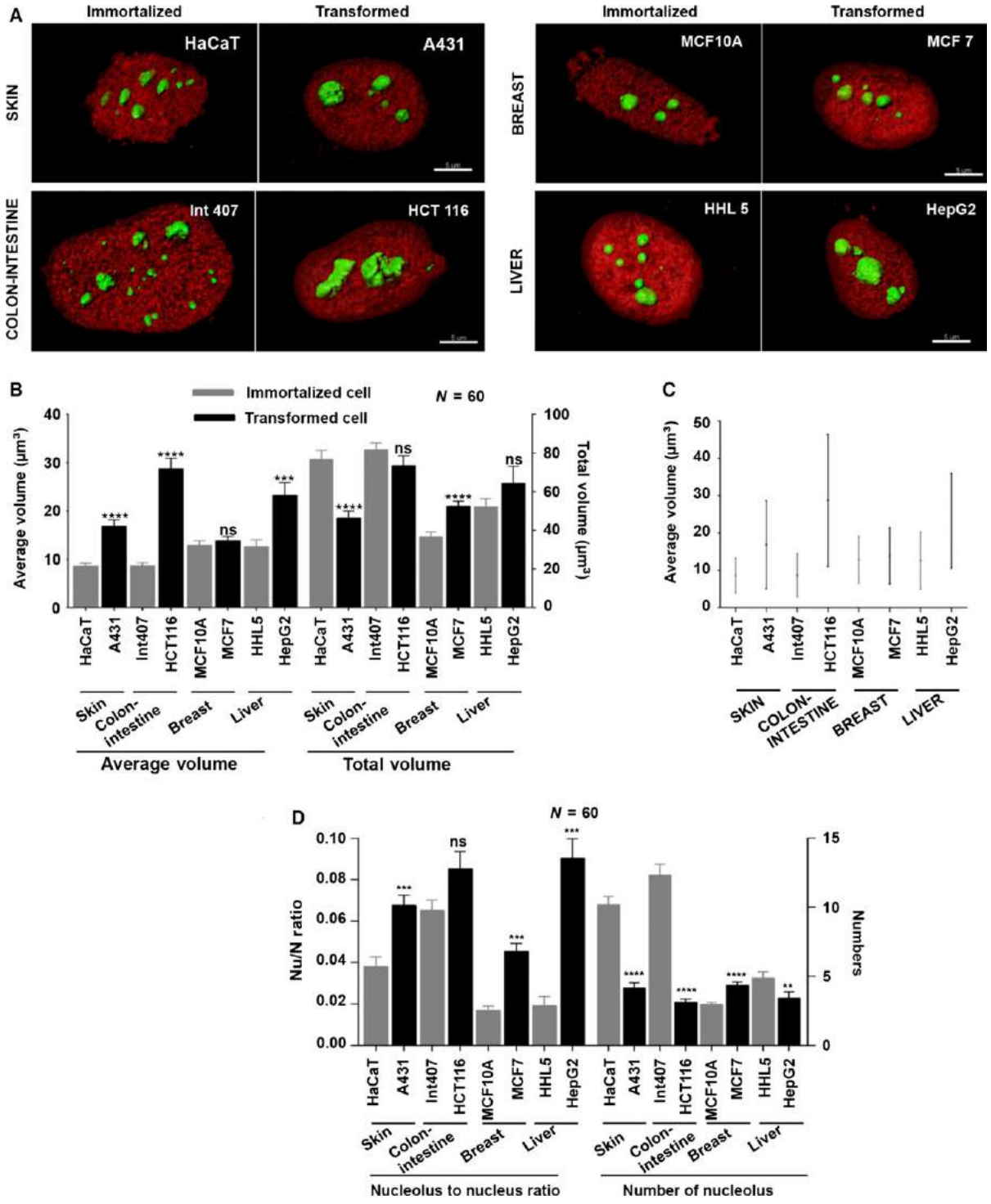

Fig. 3. Nucleolus size and number alters in transformed cell lines compared to immortalized counterpart. (A) Cells were transfected GFP-Fibrillarin and RFP-Lamin; 48 h post-transfection images were captured in confocal microscope. Overlay 3D reconstruction images of live cell obtained from Imaris. Scale bar is 5 μm. (B) Nucleolus and nucleus volumes of each cell line were quantified from 3D reconstruction images (as represented in 3A) for 60 such nucleus in three different experiments. Average nucleolus volume and total nucleolus volume were calculated per nuclei. Error bars represent standard error mean (SEM). (C) In transformed cells, average nucleolus volume greatly varies compared to immortalized counterpart. (D) Numbers of nucleolus spots and Nu/N ratio are altered in transformed cell lines. Error bars represent standard error mean (SEM). ns, $P > 0.05$; *$P \leq 0.05$; **$P \leq 0.01$; ***$P \leq 0.001$; ****$P \leq 0.0001$.

lated. This prompted us to explore whether the nucleolus size is also controlled by nuclear transport perturbation. To test that, we transfected the same dominant negative constructs (used earlier) along with GFP-Fibrillarin and RFP- Lamin; 48 h post-transfection imaging was done as described previously for total 60 nuclei in three different experiments. Post live cell imaging, immunofluorescence against Flag-Importin beta 1-364 was done to show the cytoplasmic and nuclear pore localization of Importin beta 1-364 (Fig. 4A). Overexpression of Importin beta 1-364 in immortalized cell line INT 407 causes an increase of the average and total nucleolus spot volumes significantly ($P < 0.001$) (Fig. 4B,C), while number of nucleolar spots were decreased in this condition ($P < 0.05$) (Fig. 4B,D). The Nu/N ratio is significantly higher in Importin beta 1-364 overexpressed cells compare to vector control transfected cells (Fig. 4D). We conclude that the overexpression of Flag-importin beta 1-364 not only increases the N/C ratio, it also increases the size of nucleolus and Nu/N ratio as compared to vector control cell.

We overexpressed Flag-Ran^{T24N}or Flag-Ran^{Q69L} in the same way as described above. When we overexpressed Flag-Ran^{T24N}, no significant difference was observed in nucleolus size or in Nu/N ratio (Fig. S7A) but number of nucleolus spots increased significantly. Interestingly, when we overexpressed Flag-Ran^{Q69L}, although the average volume of nucleolar spots did not increase significantly, the total nucleolus volume and Nu/N ratio increased significantly (Fig. S7B). Post live cell imaging, immunofluorescence against Flag-Ran^{T24N} or Ran^{Q69L} was done to show the localization of the respective dominant negative form of Ran. We found similar results of nucleolus volume and number in overexpression studies of dominant negative Importin beta and Ran performed in another immortalized cell line HaCaT (Fig. S9).

Cytosolic component determines the size of nucleolus

It is now evident that Importin beta 1-364 overexpression leads to increase in nucleus size as well as nucleolus size. We can speculate that import block might play an important role in controlling nucleus and nucleolus size in mammalian system. To study this in detail, we have developed an '*in vitro*' assay system in which intact nucleus isolated was incubated with cytosolic fraction isolated from a cell with different expression background. (See Materials Methods section) We incubated the isolated pure nuclei with different cytosolic fractions in 1 : 2 ratios at 22 °C for 30 min. Confocal imaging was done in different conditions; and volume of nucleolus and numbers were calculated from 3D reconstruction images (Fig. 5A).

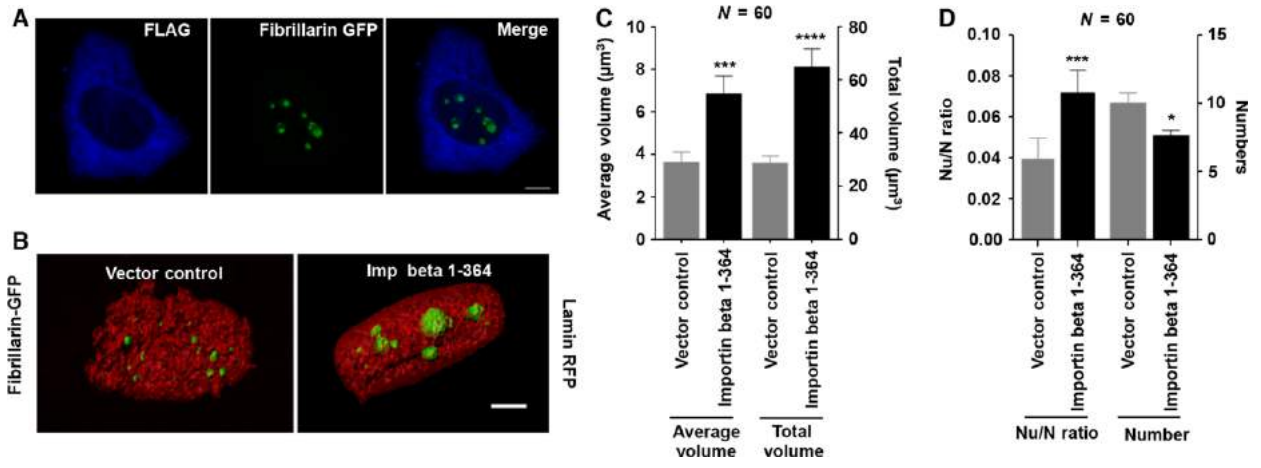

Fig. 4. The nucleolus number and volume alters upon perturbation of nucleo-cytoplasmic transport. INT 407 (Colon-intestine immortalized) cells were transfected with GFP-Fibrillarin, Lamin RFP, and Importin beta 1-364. Forty-eight hours post-transfection, live cell images were captured in confocal microscope (Leice-STED-BrightR mode). (A) Importin beta 1-364 is visualized by immunofluorescence against mAb Flag which is tagged with the former protein post live cell imaging. Fibrillarin-GFP images are live cell images. Scale bar is 5 μm. (B) Overlay 3D reconstruction images of live cell obtained from Imaris. Scale bar is 5 μm. (C) Nucleus and nucleolus volumes were quantified from 3D reconstruction images (as represented in 4B) for 60 such nucleus in each case in three different experiments. Average nucleolus volume and total nucleolus volume per nuclei are increased significantly ($P < 0.001$) compared to vector control cells. (D) Numbers of nucleolus spots and Nu/N ratio were calculated per nuclei. Error bars represent standard error mean (SEM). ns, $P > 0.05$; *$P \leq 0.05$; **$P \leq 0.01$; ***$P \leq 0.001$; ****$P \leq 0.0001$.

When cytosolic fraction of vector control transfected cells was incubated with pure nucleus population of Importin beta 1-364 transfected cells, nucleoli volume was scaled back to its normal size and vice versa (Fig. 5B), whereas the number of nucleoli of Importin beta 1-364 transfected cells were increased although not significantly. When the cytosolic fraction of two different sources (vector control transfected cells and that for importin beta 1-364 transfected cells) were combined in a 50–50 ratio, ~ 50% scaling of nucleolus size was observed.

These results suggest the following conclusions:

1 Cytosol of vector control transfected cell can scale down the increased size of nucleolus in a nucleus isolated from cells in which nucleo-cytoplasmic import is blocked.
2 Cytosol of cells in which nucleo-cytoplasmic import is blocked can scale up the smaller size of nucleolus in a nucleus isolated from a vector control transfected cell.

The results also indicate the importance of nuclear transport for size regulation of nucleus and nucleolus and underlay the possible role of unknown cytosolic factors in such regulation.

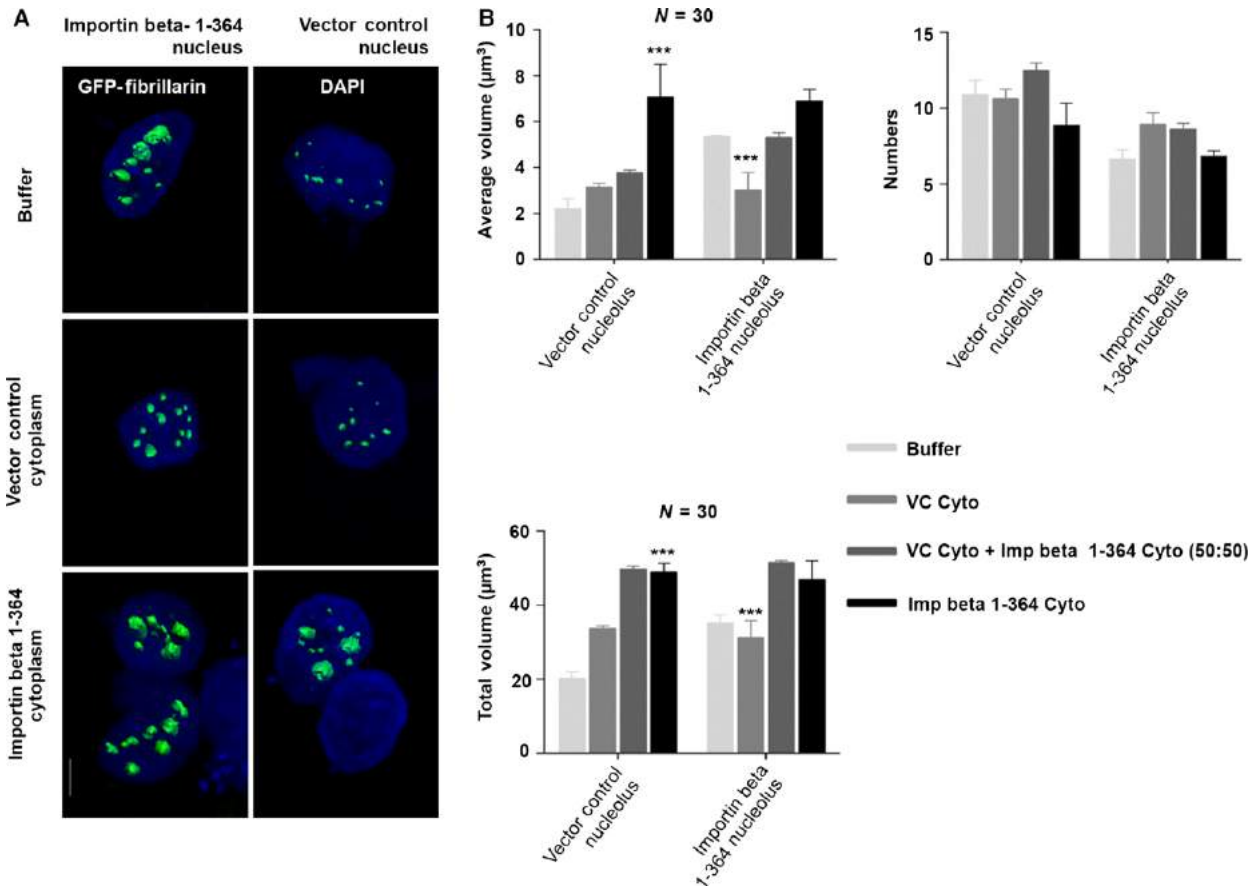

Fig. 5. An *in vitro* assay combining intact nucleus and cytosolic fractions from different sources has been established to determine changes of nucleolus size. (A) INT 407 cells were transfected with Fibrillarin-GFP and Importin beta 1-364 or vector control constructs. Forty-eight hours post-transfection, DAPI (1 : 1000 dilutions) was added to the cells and incubated for 30 min. Nuclei were isolated from each condition (See Materials & Methods). Overlay 3D reconstruction images were obtained from Imaris. Scale bar represents 5 µm. (B) Nucleolus volume (Average and total volume) and numbers in each case were quantified from 3D reconstruction images (as represented in 5A) for total 30 such nucleus in each case from three different experiments. Average nucleolus volume of vector control nucleus significantly increased ($P < 0.001$) when incubated with cytosolic fraction of Importin beta 1-364 transfected cells. The same of Importin beta 1-364 transfected nucleus reduced significantly ($P < 0.001$) when incubated with cytosolic fraction of vector control transfected cells. When both the cytosolic fractions were incubated (1 : 1 ratio) with either of the nucleus pool, average nucleolus volume scaled up or down respectively by ~ 50% (5B). Error bars represent standard error mean (SEM). Although not significantly, numbers of nucleolus spots were reduced in vector control nucleus when incubated with cytoplasmic fraction of Importin beta 1-364 transfected cells and vice versa. ns, $P > 0.05$; $*P \leq 0.05$; $**P \leq 0.01$; $***P \leq 0.001$; $****P \leq 0.0001$.

Conclusions

We can hypothesize that redistribution of biomolecules from different cellular subcompartments determine their relative size increases. Our comparative analysis resulted an insight of N/C ratio variation in different immortalized and transformed cell lines. The increase in N/C ratio contributed either by the reduction in the cell volume or by the increase of nuclear volume. Such variations are probably reflection of a same mechanism, which is simply a redistribution of cytosolic and nuclear content. Such a redistribution of organelle content probably also happens during oncogene-mediated cellular transformation [32–34] (Fig. S11). One of the key questions that we have asked that whether nuclear volume increase (relative or actual) is associated with any synchronous increase in nuclear subcompartments such as nucleolus. Our results show that total nucleolar volume changes in synchrony with nucleus volume. We have observed increase in Nu/N ratio in almost every case but changes in nucleolar spot numbers are widely variable. This variation in nucleolar spot numbers has been supported by another recent study [35]. It is possible that nucleolar spot number variation is related to variation in total nucleolar volume. Once again this indicates that such variations are result of redistribution nuclear and nucleolar components.

We for the first time have shown the importance of nucleo-cytoplasmic transport in human nuclear size regulations. Now one may ask why we get differences in degrees of N/C ratio increase between the cases where we have overexpressed importin beta or Ran^{T24N}/Ran^{Q69L}. The reason for this is most likely due to the degrees of effectiveness of attenuation of the nucleo-cytoplasmic transport by overexpressions of these different factors. It is to be noted that both the nuclear import and the nuclear export block resulted in the alteration of the N/C ratio. These suggest that not only the incoming flux of biomolecules toward nucleus is important but the outgoing flux also has equal importance. This once again support that the process of redistribution of nucleo-cytoplasmic components maintains the N/C ratio. Moreover, we established that the nucleo-cytoplasmic transport plays an important role in the nucleolus size and number regulation in human cells. In a recent genome-wide screen implicated several nuclear transport genes for alteration of nucleolar structure in *S. cerevisiae* and *D. melanogaster* [21]. In contrast to the budding yeast and fruit fly where the nucleolus follows a bipartite architecture, the nucleolus can be divided into three subcompartments in human. In spite of such major structural differences, the role of nucleo-cytoplasmic transport apparently has remained very much conserved in maintaining relative nucleolar volume to nucleus.

According to our results, the nuclear import is probably more important than nuclear export in maintaining relative nucleolar structures. The overexpression of Ran^{Q69L} or importin beta causes a nuclear import blockade, while overexpression of Ran^{T24N} effectively perturbs the nuclear export pathway [23,25,36]. We get high degree of Nu/N ratio change both for Ran^{Q69L} or importin beta overexpression, while we did not get any appreciable alteration of Nu/N ratio upon overexpression of Ran^{T24N}. In short, if we block nuclear import, we get dramatic alteration of relative nucleolar volume but if we do block nuclear export, there is no effect on relative nucleolar volume. Now if we assume these blockades are directional specific, then we can assume during nuclear import block, the nuclear size will shrink due to existing nuclear export. Yet during the effective nuclear export block, the nuclear size will continue to increase. Such conditions can help us to make a simplistic deduction that probably a threshold nuclear volume is required for maintaining the balance of nucleolus-to-nucleus biomolecular distribution and Nu/N ratio. Any reduction of such threshold volume will disturb the equilibrium and in turn dramatically alter the relative nucleolar volume, while any increase of the nuclear volume is permissible to some extent. It is possible that the rule of requirement of threshold nuclear volume will apply to the relative size regulations for all nuclear subcompartments. It is true though that blockade of nuclear export also causes N/C ratio to increase while it has no effect on Nu/N ratio. This may be contributed by alteration of nuclear volume through some unknown process which yet to be discovered. Our *in vitro* assay shows that the cytosolic factors are determinant of nucleolar spot size and number. This is supported by the fact that even intact nucleus isolated from vector control transfected cells display enlarged nucleolus upon incubation with cytosol from cells undergoing nuclear import blockade by overexpression of importin beta. Stoichiometry of these cytosolic factors are important as when the cytosolic fractions are diluted by half the extent of alteration of nucleolar spot size was reduced by half (Fig. 5). It is very much possible that the dominant negative form of importin beta 1-364 themselves directly responsible for such phenotype as the factor is present in cytosol only. However it is also possible there are other unknown cytosolic factors expression of which probably get induced when importin beta is overexpressed. It is very much possible these unknown factors are the determinant of nucleolar size. Known or unknown the fact that the factors are cytosolic, this alone

indicates that the mechanism that control nucleolar size, can be regulated from outside of nucleus. In near future, we expect to see the unraveling of these networks that control the nucleolar size from cytosol.

Author contributions

AG did majority of the experimental works and contributed intellectually for experimental designs. CB and BKJ helped in analysis of data. VK helped in acquiring images. MB and IS made two DNA constructs. AR provided the expertise for oncogene-mediated transformation experiment and provided the hf-hTERT (human fibroblast immortalized) and hf-hTERT-Ras cell lines. DB intellectually contributed to all the experimental designs and prepared the manuscript.

Acknowledgement

We thank Bhattacharyya lab members for critical review of the manuscripts and providing valuable input. We also thank Prof. Benjamin Glick for critical comments and Diganto Bhattacharyya for editing. The research was funded by DBT research grant (102/IFD/SAN/2282/2O12-2O13). A.G and B.K.J were funded by ACTREC doctoral fellowship. C.B is funded by U.G.C postdoctoral fellowship.

References

1 Marshall W (2002) Size control in dynamic organelles. *Trends Cell Biol* **12**, 414–419.
2 Marshall WF (2008) Engineering design principles for organelle size control systems. *Semin Cell Dev Biol* **19**, 520–524.
3 Handwerger KE and Gall JG (2006) Subnuclear organelles: new insights into form and function. *Trends Cell Biol* **16**, 19–26.
4 Jorgensen P, Edgington NP, Schneider BL, Rupes I, Tyers M and Futcher B (2007) The size of the nucleus increases as yeast cells grow. *Mol Biol Cell* **18**, 3523–3532.
5 Neumann FR and Nurse P (2007) Nuclear size control in fission yeast. *J Cell Biol* **179**, 593–600.
6 Pianese G (1896) Beitrag zur histologie und aetiologie des carcinoms. Histologische und experimentelle untersuchungen. *Beitr Pathol Anat* **142**
7 Lever E and Sheer D (2010) The role of nuclear organization in cancer. *J Pathol* **220**, 114–125.
8 Nickerson JA (1998) Nuclear dreams: the malignant alteration of nuclear architecture. *J Cell Biochem* **70**, 172–180.
9 Zink D, Fischer AH and Nickerson JA (2004) Nuclear structure in cancer cells. *Nat Rev Cancer* **4**, 677–687.
10 Busch H, Byvoet P and Smetana K (1963) The nucleolus of the cancer cell: a review. *Cancer Res* **23**, 313–339.
11 Levy DL and Heald R (2010) Nuclear size is regulated by importin alpha and Ntf2 in Xenopus. *Cell* **143**, 288–298.
12 Cavalier-Smith T (1982) Skeletal DNA and the evolution of genome size. *Annu Rev Biophys Bioeng* **11**, 273–302.
13 Jovtchev G, Schubert V, Meister A, Barow M and Schubert I (2006) Nuclear DNA content and nuclear and cell volume are positively correlated in angiosperms. *Cytogenet Genome Res* **114**, 77–82.
14 Orgel LE and Crick FH (1980) Selfish DNA: the ultimate parasite. *Nature* **284**, 604–607.
15 Kau TR, Way JC and Silver PA (2004) Nuclear transport and cancer: from mechanism to intervention. *Nat Rev Cancer* **4**, 106–117.
16 Bai SW, Rouquette J, Umeda M, Faigle W, Loew D, Sazer S and Doye V (2004) The fission yeast Nup107-120 complex functionally interacts with the small GTPase Ran/Spi1 and is required for mRNA export, nuclear pore distribution, and proper cell division. *Mol Cell Biol* **24**, 6379–6392.
17 Maeshima K, Iino H, Hihara S, Funakoshi T, Watanabe A, Nishimura M, Nakatomi R, Yahata K, Imamoto F, Hashikawa T *et al.* (2010) Nuclear pore formation but not nuclear growth is governed by cyclin-dependent kinases (Cdks) during interphase. *Nat Struct Mol Biol* **17**, 1065–1071.
18 Edens LJ, White KH, Jevtic P, Li X and Levy DL (2013) Nuclear size regulation: from single cells to development and disease. *Trends Cell Biol* **23**, 151–159.
19 Sato S, Burgess SB and McIlwain DL (1994) Transcription and motoneuron size. *J Neurochem* **63**, 1609–1615.
20 Schmidt EE and Schibler U (1995) Cell size regulation, a mechanism that controls cellular RNA accumulation: consequences on regulation of the ubiquitous transcription factors Oct1 and NF-Y and the liver-enriched transcription factor DBP. *J Cell Biol* **128**, 467–483.
21 Neumuller RA, Gross T, Samsonova AA, Vinayagam A, Buckner M, Founk K, Hu Y, Sharifpoor S, Rosebrock AP, Andrews B *et al.* (2013) Conserved regulators of nucleolar size revealed by global phenotypic analyses. *Sci Signal* **6**, ra70.
22 Bhattacharyya D, Hammond AT and Glick BS (2010) High-quality immunofluorescence of cultured cells. *Methods Mol Biol* **619**, 403–410.
23 Holaska JM, Black BE, Rastinejad F and Paschal BM (2002) Ca2+-dependent nuclear export mediated by calreticulin. *Mol Cell Biol* **22**, 6286–6297.
24 Izaurralde E, Kutay U, von Kobbe C, Mattaj IW and Gorlich D (1997) The asymmetric distribution of the

constituents of the Ran system is essential for transport into and out of the nucleus. *EMBO J* **16**, 6535–6547.
25 Kutay U, Izaurralde E, Bischoff FR, Mattaj IW and Gorlich D (1997) Dominant-negative mutants of importin-beta block multiple pathways of import and export through the nuclear pore complex. *EMBO J* **16**, 1153–1163.
26 Ribbeck K, Lipowsky G, Kent HM, Stewart M and Gorlich D (1998) NTF2 mediates nuclear import of Ran. *EMBO J* **17**, 6587–6598.
27 Sazer S and Dasso M (2000) The ran decathlon: multiple roles of Ran. *J Cell Sci* **113** (Pt 7), 1111–1118.
28 Klebe C, Bischoff FR, Ponstingl H and Wittinghofer A (1995) Interaction of the nuclear GTP-binding protein Ran with its regulatory proteins RCC1 and RanGAP1. *Biochemistry* **34**, 639–647.
29 Bischoff FR, Klebe C, Kretschmer J, Wittinghofer A and Ponstingl H (1994) RanGAP1 induces GTPase activity of nuclear Ras-related Ran. *Proc Natl Acad Sci USA* **91**, 2587–2591.
30 Hutchins JR, Moore WJ and Clarke PR (2009) Dynamic localisation of Ran GTPase during the cell cycle. *BMC Cell Biol* **10**, 66.
31 Derenzini M, Trere D, Pession A, Govoni M, Sirri V and Chieco P (2000) Nucleolar size indicates the rapidity of cell proliferation in cancer tissues. *J Pathol* **191**, 181–186.
32 Hahn WC, Counter CM, Lundberg AS, Beijersbergen RL, Brooks MW and Weinberg RA (1999) Creation of human tumour cells with defined genetic elements. *Nature* **400**, 464–468.
33 Hahn WC, Dessain SK, Brooks MW, King JE, Elenbaas B, Sabatini DM, DeCaprio JA and Weinberg RA (2002) Enumeration of the simian virus 40 early region elements necessary for human cell transformation. *Mol Cell Biol* **22**, 2111–2123.
34 Rangarajan A, Hong SJ, Gifford A and Weinberg RA (2004) Species- and cell type-specific requirements for cellular transformation. *Cancer Cell* **6**, 171–183.
35 Farley KI, Surovtseva Y, Merkel J and Baserga SJ (2015) Determinants of mammalian nucleolar architecture. *Chromosoma* **124**, 323–331.
36 Weis K, Dingwall C and Lamond AI (1996) Characterization of the nuclear protein import mechanism using Ran mutants with altered nucleotide binding specificities. *EMBO J* **15**, 7120–7128.

Supporting information

Additional supporting information may be found in the online version of this article at the publisher's web site:
Table S1. List of oligo primers used in the present study.
Fig. S1. Development of assay system to monitor size and shape of nucleus in live cell condition under the microscope.
Fig. S2. Measurement of N/C ratio in budding yeast.
Fig. S3. Transformed cells have significantly high N/C ratio compare to immortalized cells.
Fig. S4. Overexpression of dominant negative Importin beta 1-364 and Ran^{Q69L} perturbs nucleo-cytoplasmic import.
Fig. S5. Nucleo-cytoplasmic transport perturbation in immortalized cells INT 407 causes (N/C) ratio to increase significantly.
Fig. S6. Invasiveness is not changed when N/C ratio is increased by dominant negative Importin beta and Ran overexpressed in immortalized cell line HaCaT, and overexpression of wild-type Ran and Importin beta has no effect on skin transformed cell A431.
Fig. S7. Effect of nucleo-cytoplasmic transport perturbation by Ran^{Q69L} or Ran^{T24N} on nucleolus volume, number, and Nu/N ratio in immortalized cells INT 407.
Fig. S8. Quality control experiment to confirm that isolated nuclei are intact and nonpermeabilized.
Fig. S9. The nucleolus number and volume alters upon perturbation of nucleo-cytoplasmic transport in immortalized cells HaCaT.
Fig. S10. Nucleo-cytoplasmic transport perturbation in transformed cells (A431) did not alter the N/C ratio.
Fig. S11. hf-hTERT-Ras transformed cells exhibit significant increase in N/C ratio compared to hf-hTERT immortalized cells.